5-2019

Design and Analysis of Fiber Reinforced Concrete Structure for Transportation Infrastructures

Salam Adil Mutlag Wtaife

Design and Analysis of Fiber Reinforced Concrete Structure for Transportation Infrastructures

by

Salam Adil Mutlag Wtaife

Bachelor Degree in Civil Engineering

Babylon University, 2006

Master of Science in Civil Engineering

Babylon University, 2009

A dissertation submitted to the college of Engineering at

Florida Institute of Technology

in partial fulfillment of the requirements for the degree of

Doctor of Philosophy
in
Civil Engineering

Melbourne, Florida
May, 2019

We the undersigned committee hereby recommend that the attached document be accepted as fulfilling in part the requirements for the degree of
Doctoral of Philosophy of Civil Engineering

Design and Analysis of Fiber-reinforced Concrete Structure for Transportation Infrastructures

by

Salam Adil Mutlag Wtaife

_____

Nakin Suksawang, Ph.D.,P.E
Associate Professor of Civil Engineering
Department of Mechanical and Civil Engineering
Committee Chair

_____

Albert Bleakley, Ph.D., P.E.
Associate Professor of Civil Engineering
Department of Mechanical and Civil Engineering
Committee Member

_____

Paul J. Cosentino, Ph.D., P.E.
Professor of Civil Engineering
Department of Mechanical and Civil Engineering
Committee Member

_____

Razvan Rusovici, Ph.D., P.E.
Associate Professor of Aerospace and Biomedical Engineering; Associate Professor of Aviation Science, Aerospace, Physics and Space Sciences
Outside Committee Member

_____

Ashok Pandit, Ph.D., P.E.
Professor of Civil Engineering
Department of Mechanical and Civil Engineering
Department Head

Abstract

Title: Design and Analysis of Fiber-reinforced Concrete Structure for Transportation Infrastructures

Author: Salam Adil Mutlag Wtaife

Advisor: Nakin Suksawang, Ph. D.

Concrete is one of the most popular materials in superstructures (buildings), substructures (foundation) and infrastructure facilities (bridges, pavements, and tunnels). However, concrete is a brittle material that cracks easily under tension.

Fiber may be used as reinforcement to impede the concrete from cracking as well as to increase the concrete flexural strength. Nevertheless, current design codes do not include this design enhancement. Furthermore, there are discrepancies in the design methodology concerning the inclusion of discrete fibers in concrete structures. Therefore; there is a need to develop new analysis methodology and design methodology for fiber reinforced concrete (FRC) and fiber reinforced cement composite (FRCC).

The aim of this study is to deepen the knowledge to analyze and design the fiber-reinforced concrete by developing a novel method to predict the stress compression and tension blocks at the design ultimate limit state.

To accomplish this, an experimental program was developed to characterize FRC and FRCC using common test methods. Three group of fibers were investigated: steel, PVA, and synthetic fiber with volume fractions ranging from 0 to 2%. The experimental program consisted of compression tests, flexural tests, and direct tensile tests which were used to assess the fibers' usefulness as reinforcement components and to compare to the assumptions of current design methods. Experimental results of this research, combined with an additional 1,120 data points obtained from other researchers, were statistically analyzed to develop a new model to predict the design stress block of FRC and FRCC so that their design.

This dissertation is divided into four parts:1) development of stress block in compression, 2) development of stress block in tension, 3) development of analysis, and 4) development of design of the new FRC and FRCC components.

First, the development of stress block in compression requires the yield and ultimate strains to be know.

A new equation for yield strain was developed by modifying the American Concrete Institute (ACI) Committee 544, fiber reinforced concrete and Rilem equations that depend on the compressive strength. An ultimate strain of 0.0035 and 0.005 at the extreme concrete compression fiber for the volume fraction of less than 1% and for a volume fraction of more than or equal to 1%, respectively, are proposed. New parameters are also introduced to account for different fiber types.

Steel, PVA, basalt and synthetic fibers, two compresive stress block shapes are proposed. The two shapes consist of a rectangular stress block commonly used in regular concrete and a tapezoid stress block.

For the rectangular compressive stress block, two constants, $K_1$and K_2, are proposed. These constants are affected by the volume fraction (V_f) of FRC and FRCC. For $V_f \geq 1\%$, K_1 and K_2 are constant value of 0.75 and 0.375 for FRC and FRCC, respectively, while for $V_f < 1\%$, they depend on the concrete compressive strength of FRC and FRCC. To this end, there are two additional parameters, β and $\propto$, which depend on the strain at the elastic, yield, and the ultimate stages. For the ultimate stage, β, which is also affected by the volume fraction of fiber, is proposed to be the same as the ACI 318 Code value for $V_f < 1\%$. While for $V_f \geq 1\%$, β depends on the FRC and FRCC concrete compressive strength. On the other hand, $\propto$ depends on the FRC and FRCC concrete compressive strength for $V_f < 1\%$. While for $V_f \geq 1\%$, it may be observed that it becomes approximately a constant value of 1.0.

For the trapezoid stress block in compression, an idealized constitutive model which is a bilinear, elastic-perfectly plastic stress-strain response, has been a proposed. It is ssumed in compression that the linear portion of the response terminates at a yield point ($\propto$fc',ε_{cy}) and remains perfectly plastic at the compressive yield stress until the ultimate compressive strain $\varepsilon_{Ult.}$. $\propto$ of fiber-

reinforced concrete for ultimate design is taken to be 0.85, which is the same as the $\propto$ of ACI 318 for volume fraction less than 1%, and 1 for $f_c' \geq 69\ Mpa$, $\propto = 1$.

The proposed models were compared to six design codes using 250 data points obtained from previous studies.

The evaluation for an area of the database which used the other codes more than twice underestimated the lower bond of the database. Therefore, the other codes do not give a valid evaluation for compressive strength due to neglecting the effect of fiber. For volume fraction of fiber more than 1, the rectangular and trapezoid area of stress blocks are almost matches. While for volume fraction less than 1 and compressive strength more than 40 MPa, there is a small difference between the rectangular and trapezoid stress blocks. For K_2 value, the rectangular of stress block is in the lower bond of the database, while the trapezoid stress block model is near to the average of the database. As a result, the rectangular stress block is underestimated by the database and also is easy for a designer to use. Therefore, it will be used in the new design and analysis proposal model.

Second, determining tension stress block by knowing the first crack strength, first crack strain, elastic modulus, and ultimate strain in tension is necessary. More than 250 points of data are used to evaluate the first crack strength. The new empirical relations developed ACI 318 equation by multiple factor λ.

Factor λ depends on the length of the fiber. In this dissertation, factor λ is determined by the average and lower bond of the database.

Third, analysis of the new model for the ultimate stage is assumed to have a rectangular stress block with an average uniform stress. Also, this model adopts $\emptyset$ equal to 0.75 because of safe.

Comparing the proposal model with a moment of ACI 544 model shows that the proposed model is safer and more accurate than the ACI 544 model because the ACI 544 model has overestimated moment value for more than 3.5 Kn.m.

Finally, in the design of the new model for the ultimate stage, the majority of the design volume fraction for a proposal is more than the measurement volume fraction for the database. According to the database, this model works for volume fraction ≤ 2. It is necessary for the designer to know what kind of behavior is appropriate for each design. Through that, it is possible to precisely estimate the volume fraction of the requirement of each behavior as will be explained below. The volume fraction of fiber is critical for the response of strain-softening (hardening deflection). In the case of the strain of softening, the internal moment provided by FRC and FRCC is to resist the external moment more than the first crack moment. In addition to that, the volume fraction of fiber is critical for the response of strain-hardening. In the case of the strain hardening for FRC and

FRCC, the strength of tension is defined for the stress block model as a constant value. FRC and FRCC strengths in tension are more than the first crack strength.

In conclusion of this dissertation, twelve equations were evaluated:

1. yield strain in compression,
2. ultimte strain in compression,
3. first crack strength in tension,
4. first crack strain in tension,
5. the elastic modulus in tension,
6. neutral axis for the elastic stage in tension,
7. ultimate strain in tension,
8. moment capacity for analysis and design model,
9. tensile strength for analysis and design model,
10. volume fraction equation of fiber for the design model,
11. volume fraction equation as a minimum requirement for deflection-hardening, and
12. volume fraction equation as a minimum requirement for strain-hardening.

In addition, there were the five parameters, in which $K_1 and\ K_2$ factor for stress block in compression and β factor for rectangular stress block in compression and α factor for rectangular and trapezoid stress block in compression.

In summary, this dissertation proposes new design and analysis for fiber-reinforced concrete and fiber-reinforced cement in order to increase safety and to provide an easier process method for the designer.

Table of Contents

Table of Figures

Table of Tables

Table of Flowcharts

Acknowledgement

First and foremost, I have to thank and praise God for giving me the health and the necessary strength to carry out the present dissertation.

I am deeply grateful for being mentored by Dr. Nakin Suksawang, a role model of excellence and dedication. He has encouraged me always to give the best in both personal and professional activities. I am thankful for his support, constructive criticism, and countless development opportunities. By giving me research freedom and debating my ideas, he nurtured my creative and independent thinking.

I would thank you Ms. Halah Adnan kadhim who lecture in University of Misan to support me throughout my years of study of Ph.D.

I would like to express my sincere gratitude with my committee members: Prof. Paul J. Cosentino, Dr. Albert M. Bleakley, and Dr. Razvan Rusovici. I appreciate their time reviewing my work and providing meaningful comments to improve it.

None of this work would be possible without the financial and academic support of my sponsor, Ministry of Higher Education and Scientific Research (MOHESR) in Iraq.

I would like to thank Laboratory System Analyst E. Martin at the Florida Institute of Technology, and graduate student Ahmed Alsabbagh and the

undergraduate students D. Lucca, A. E. D. Canali, M. T. Silva, and L. A. Argenta and for their help in this study.

There would be no sufficient space to describe the appreciation that I feel for my wife, so I am not writing it here. I will say thank you for your love and support throughout my years of study, and she has played an extremely important role in supporting my goals. Also, thank you to my mother and father, family, and my friends.

To my beloved wife

Marwa

To my son

Abd Allah

To My son

Saden

To my daughter

Ellen

1 Chapter 1 Introduction

1.1 Overview of Fiber-reinforced Concrete

Concrete is one of the most popular materials in superstructures, such as buildings, and infrastructure facilities, such as the bridges, in addition to pavements, tunnels et al. It is used included in structures and sub-structures because it has high strength in compression. It is readily a available and cheap material, and it has high durability. However, concrete is a brittle material in tension. The tensile strength of concrete is about 8% to 12% of its compressive strength. Conventional reinforcement is used to improve the behavior of concrete structural components in tension.

The rapid progress of architectural and structural concrete applications with more complex geometries, the high cost in labor and time for preparing the rebar, and the heavy weight of rebar led to the appearance of new techniques for reinforced materials, such as fiber-reinforced cement or concrete (FRCC or FRC).

Fiber-reinforced concrete is a composite material. It is a type of concrete that includes discrete fibers with uniform distribution and random orientation. FRC is used in most common concrete structures due to the possibility of molding it into virtually any shape and geometry, thereby supplementing the physical properties of concrete. Despite the fact that fibers are not as proficient as rebar in withstanding high tension stress, they are better at controlling cracking because they are more

closely spaced than conventional reinforcement. Fiber can be combined with used or instead of conventional reinforcement in some applications.

1.2 History FRC

The idea of fiber reinforcement was not new (Abbas, 2013). Over 3500 years ago, Babylonia used sunbaked bricks of clay reinforced with straw to build the town of Aqar Quf (ancient: Dur Kurigalzu) to hight of 187 ft, see Figure 1-1. In the early 1900s, asbestos fibers were used in concrete. At the beginning of the 1950s, new design methods were developed for FRC but no general design code existed. In 1978, synthetic fibers were used in concrete.

Figure 1-1: The Ziggurat of Dur-Kurigalzu(1).

1.3 Advantages FRC

Fibers are uniformly distributed, discontinuous, and random. These features of fibers improve structural behavior. Depending on the level of property improvement, fiber-reinforced concretes are subdivided into two groups: softening

strain and hardening strain. With low fiber volume fraction, fibers mainly contribute to crack-arresting capacity and post-crack ductility (Jiang, 2003).

There are several advantages in the use of FRC. They can be classified from a structural or economic viewpoint (MartÍnez, 2006), (Löfgren, 2005) (Jiang, 2003) and (Jansson, 2008).

1. From the structural viewpoint: the fibers' ability to bridge cracks improves:
    a. Serviceability limit states: by controllong crack propagation
        i. Reduced the crack spacing and crack width
        ii. Increased flexural stiffness by the Improved post-peak response
        iii. Increased moment resistance
        iv. Enhanced durability for bridge decks
        v. Improved corrosion resistance especially for synthetic, carbon, or amorphous metal fibers
        vi. Reduced constraints on concrete element shape as curvilinear-shaped wall panels
        vii. Reduced the number of cut-joints in large continuous structures such as containers
    b. Ultimate limit states:
        i. Increased load resistance

ii. Increased toughness in compression and tension by improving the energy absorption capacity

iii. Increased ductility in compression and tension

iv. Improved Fatigue life and impact resistance

2. From the economic viewpoint

One of the goals of any building project is to minimize the construction costs. Rroughly 10 % of total construction costs for a concrete building can be related to the reinforcement work (Löfgren, 2005). Placing the steel bars takes many person-hours. Costs can be reduced considerably by eliminating the reinforcement part of the construction work. Fibers will reduce some cost by the following:

a. Reducing cost of some of the labor activities at the construction site, such as reinforcing, casting and finishing of concrete.

b. Eliminating overly extensive, structural dimensions and weight in order to make space for all the steel

c. Reducing or avoiding secondary reinforcement for designing bridge decks by improved serviceability performance and fatigue resistance (Massicotte, 2000 and Moffatt and Massicotte 2004)

d. Reducing or avoiding transverse reinforcement by improving the toughness in compression due to the pull-out of fibers from the concrete matrix (Ou, 2011)

1.4 Application of FRC:

FRC has several structural applications in fields. The significant applications of FRC are shotcrete, rock slope stabilization, airport runways, and pavements, overlays of existing pavement, precast concrete, slab-on-grade construction, and tunneling because the fibers improve the toughness in compression and control shrinkage cracks (Li, 2002). FRC is also used in buildup and repair bridge applications, such as decks, piers, girder, approach slab and parapets.

Fiber-reinforced concrete parapets showed a reduction of conventional reinforcement while keeping its thickness and improving its load-carry capacity and ultimate residual strength under dynamic loadings (Charron, 2012). Using FRC in bridge piers reduces transverse reinforcement and post-earthquake repair costs by increasing damage tolerance, shear strength, and energy dissipation under cyclic loading compared without fibers (Aviram, 2014). Also, FRC could be used to replace all secondary reinforcement in the anchorage zone of girders that cause congestion and pose difficulty in the placement of concrete (Yazdani, 2002). Using FRC in bridge decks reduces the amount of reinforcement and improves their durability with roughly the same safety and reliability level of conventional decks (Massicotte, 2000).

The Horikoshi C ramp bridge in Japan was designed and constructed as the first road bridge with ultra-high strength fiber-reinforced concrete girders with

conventional concrete deck slab and cross beams to reduce superstructure dead load and to improve durability (Resplendino and Toulemonde, 2013).

Figure 1-2: The Horikoshi C ramp bridge in Japan (Resplendino and Toulemonde, 2013).

1.5 Problem

Despite these advantages, the lack of design specifications make FRC less attractive to engineers, preventing it from being widely used. The current rectangular stress block specified by ACI 318 and AASHTO LRFD Bridge Design Specifications (2004) is based on normal-strength concrete (without fiber). Currently, only the European Codes and ACI 544.4R-18 Guideline address the fibers' contribution to the ultimate limit state of FRC. These codes only address steel fibers and, in most cases, the strain-softening behavior of FRC. Also, these codes were built on several possibilities like deflection and elastic modulus. They

do not affect the volume fraction of fibers (V_f), which plays a significant role with newer fiber types. As the improvement of the concrete compressive strength encourages the designers to use FRC and FRCC in design, the rectangular stress block parameters must be evaluated for the use of FRC and FRCC, and if necessary, new rectangular stress block parameters must be introduced for FRC and FRCC design. For these reasons, there is a need to develop new design equations to consider the various fibers and their contribution to the behavior of FRC.

1.6 Aim

This dissertation aims at the development of new analysis and design equations for computing the moment resistance at the ultimate limit state for FRC with both strain-softening and strain-hardening behavior. The objectives of the study are as follows:

1. The first objective is to determine the compressive and tensile stress-strain relationships for FRC using various fibers and volume fractions.
2. The second objective is to modify the ACI code equations that are used to analyze and design.

In pursuit of this objective, an experimental program. One will be the investigation and evaluation of the softening and hardening behavior of FRC beams in flexure and compression state for fiber concrete reinforced with five types and four contents of fibers. The fiber used in this dissertation will be end-hooked steel,

polypropylene, PVA, basalt, and polyolefin. A comparison between types of fibers will be taken to find which of these fiber types gives the better overall performance.

For the softening and hardening behavior of FRC, stress block distribution will be evaluated from the tensile strength at cracking and at a modulus of rupture and ultimate stress from the height of the beam. From the load-deflection $F-\varepsilon$ curves, the tensile strength in cracked parts will be determined by residual flexural tensile strength at a modulus of rupture and ultimate stress from the net height of the beam.

Another investigation will be the evaluation of the FRC compression behavior by finding the parameters of stress block distribution. This evaluation depends on the same concept of Hognestad (1955) that developed rectangular stress block parameters which are used in the current codes for flexure analysis and design. This will also evaluate the data published by other researchers related to stress block parameters, ultimate compressive strain, yield compression strain, modulus of rupture, first crack strength, strain at a modulus of rupture and first crack strength and ultimate tensile strain of FRC. The netural axis will calculate the ultimate of compression and tensile strains.

Also, a database gathered from experimental results from various publications will also be used to widen the range of applicability for the proposed equations.

The final step is to modify the analysis and design equations of ACI code.

1.7 Dissertation layout

This dissertation is divided into six chapters. Chapter 1 provides an introduction to the definition of FRC, as well as the history and the advantages of fiber-reinforced concrete and its applications. The aim and problem of the dissertation are defined in this chapter. The literature review on the stress-stress relationship and stress block parameters in compression and tension of FRC is presented in Chapter 2. Proposed stress-strain models for FRC and proposed rectangular stress block parameters by different researchers are presented. The literature includes a comprehensive review of the stress block parameters in different design codes from all over the world. Chapter 3 discusses the materials used in this study and the database of other studies of the stress-stress relationship in compression and tension of FRC. Chapter 4 explains the methodology followed in experimental studies and the database of other studies. Also, the experimental program and testing methods are described further in detail. Chapter 5 deals with design and analysis methods for flexural members based on fracture mechanics. A comparison is made between analytical approaches. The measured response including; the behavior of the specimens, is also illustrated. The test results are compiled, analyzed, evaluated, and compared with the test data presented in Chapter 2. Chapter 5 also includes the proposed relationships for FRC stress block parameters. Statistical and parametric analyses are carried out to justify the proposed relationships.

Finally, a summary of the testing program and analytical work is presented in Chapter 6. Based on the research, conclusions and recommendations are made.

2 Chapter 2 Literature Review

2.1 Introduction

Fiber reinforced concrete (FRC) has become increasingly popular as more and more owners rely on it to improve the service life of their concrete structures. FRC provides many advantages over normal concrete, particularly in minimizing early-age cracking, increasing toughness, and enhancing post-crack load carrying capacity by improving the energy absorption (Grzybowski et al., 1990, Islam et al., 2016 and Saje et al., 2011). Also, the fibers increase the flexural stiffness of concrete by improving post-peak response and increasing moment resistance since stresses carried by fibers across a tensile crack in the concrete act as a function of the crack opening. Overall, fiber enhances durability, fatigue life, and impact resistance of concrete (Löfgren, 2005, Martínez, 2006, Jansson, 2008 and Jiang 2003). The use of fibers also helps save time and the overall cost of the construction, which leads to their growing use in a concrete application for structural and repair material for old structures (Moffatt and Massicotte, 2004 and Massicotte.et al., 2000).

Despite these advantages, the lack of design specifications make FRC less attractive to engineers, preventing it from being widely used. Currently, only the European Codes address the fibers' contribution to the ultimate limit state of FRC. The problem with these codes is they address only steel fibers and, in most cases, the strain-softening behavior of FRC. In addition, these codes were built on several

possibilities, such as deflection and elastic modulus. They do not affect the volume fraction of fibers (V_f), which plays a significant role with newer fiber types. For these reasons, there is a need to develop new design equations to consider the various fibers and their contribution to the behavior of FRC.

2.2 Compression Stress Block Parameters

The stress distribution behavior in concrete is non-linear. Simplified, it is defined by three parameters, K_1, K_2 and K_3. K_1 is the ratio of average stress f_{av} over the compression area to maximum stress developed under flexure f_{max} ; K_2 is the ratio of distance between the extreme compressive fiber and the resultant force of the stress block (Pc) to that between the same fiber to the neutral axis (c); K_3 is the ratio of f_{max} to uniaxial concrete strength f_c' (Yi, 2002).

ParametersK_1, K_2 and K_3 have been used in the strength-based design method to account for the shape of the compressive stress-strain diagram; see Figure.2.1

$$f_{average} = K_1.K_3.f_c' \qquad \textit{Equation 2-1}$$

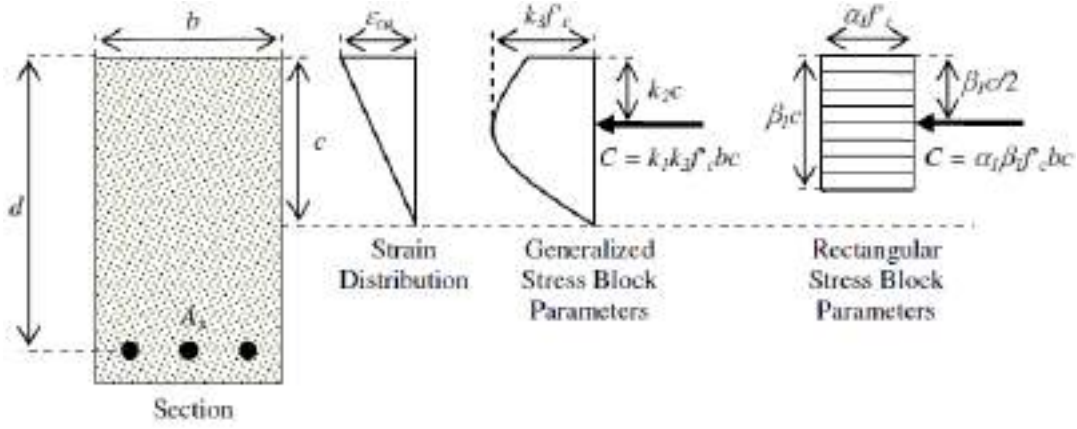

Figure 2.1: Equivalent rectangular compressive stress blocks that have been adopted by some codes (Mertol, 2006).

However, the behavior of concrete in flexure is not the same as that of the concrete cylinder in pure compression. The primary reason is the distribution of stresses in concrete; the strain gradient effect in flexure helps concrete to achieve higher strains than that in pure compression. Other reasons are the shape and size that affects the concrete cylinder compared to the real reinforced concrete structural member. Furthermore, the rate of loading of a structural member is always much slower than that of a concrete cylinder. However, the stress distribution of concrete in flexure may still be represented adequately by the stress-strain relationship of the concrete cylinder using an empirical constant (K_3) to account for all of these differences (Mertol 2006). However, the ACI Code does not refer to the use of $K_3 f'_c$ except for column sections subjected to pure axial load (no

bending).Figure2.2 shows that the value of K_3 varies between 0.80 and 1.20 with an average of about 1(Mansur and Wee 1997).

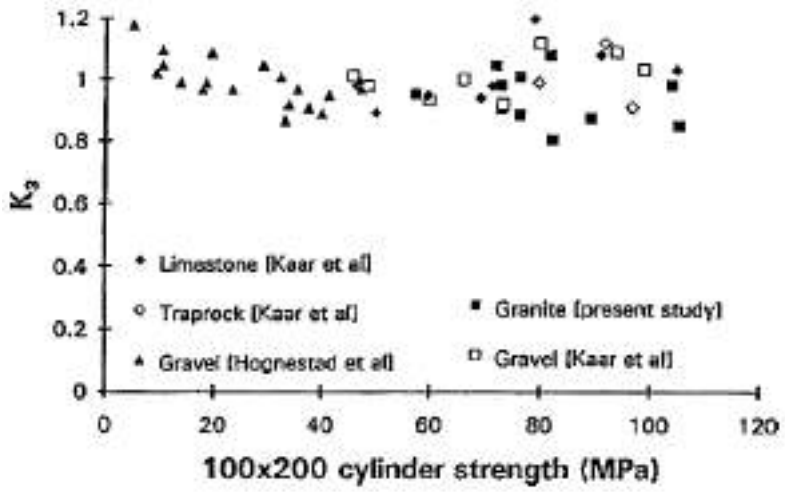

Figure 2.2: K3 values for concrete without fiber (cylinder size 100x200 mm) (Mansur and Wee 1997).

The resultant is assumed in the middle of the rectangle. Under ultimate load, Hooke's Law and the theory of elasticity have no significance as far as the internal stresses are concerned (Whitney 1937). The ACI 318 Code states that an equivalent rectangular stress block coefficient α1 is a constant value, but the coefficient β1 changes based on concrete compressive strength.

When $\boldsymbol{\alpha}$ and $\boldsymbol{\beta}$ that are combined and derived from K_1, $K_2$and K_3, they are the parameters of the equivalent rectangular concrete stress block that are adopted in various design codes to simplify the stress strain curve in compression (ACI, 2014; CEN, 2004; SNZ, 2006):

$$Area\ under\ curve = K_1.K_3.f_c'.\varepsilon_{ult} = \alpha.\beta.f_c'.\varepsilon_{ult} \qquad \textit{Equation 2-2}$$

$$\alpha.\beta = K_1.K_3 \qquad \textit{Equation 2-3}$$

$$\beta = 2.K_2 \qquad \textit{Equation 2-4}$$

$$\alpha = \frac{K_1.K_3}{\beta} \qquad \alpha = \frac{K_1.K_3}{2.K_2} \qquad \textit{Equation 2-5}$$

Where $\boldsymbol{\alpha}$ is the ratio of equivalent concrete compressive stress in flexure to concrete cylinder strength f_c' and $\boldsymbol{\beta}$ is the ratio of the height of average rectangular concrete compressive stress block to neutral axis depth (c).

For FRC, α and β are conversion factors that simplify the designed compression stress distribution that a rectangular stress block generates from parabolic stress distribution to a rectangular stress distribution.

In Figure 2.3, a lower-bound line corresponding to a rectangular stress block with a height of 0.85 f_c', and by using $\boldsymbol{\beta}$, that is represented by the dashed line. The value for $\beta_1$was determined as a lower bound on the results data, which are shown as a dashed line in Figure. 2.3. The moment of the compression force in the concrete at the centroid axis of a rectangular stress block is $\left(C - \frac{\beta_1.C}{2}\right)$where c is the depth of the neutral axis. If β_1 is too small, the moment will be too large, and the moment capacity will be overestimated (Wight and MacGregor 2009).

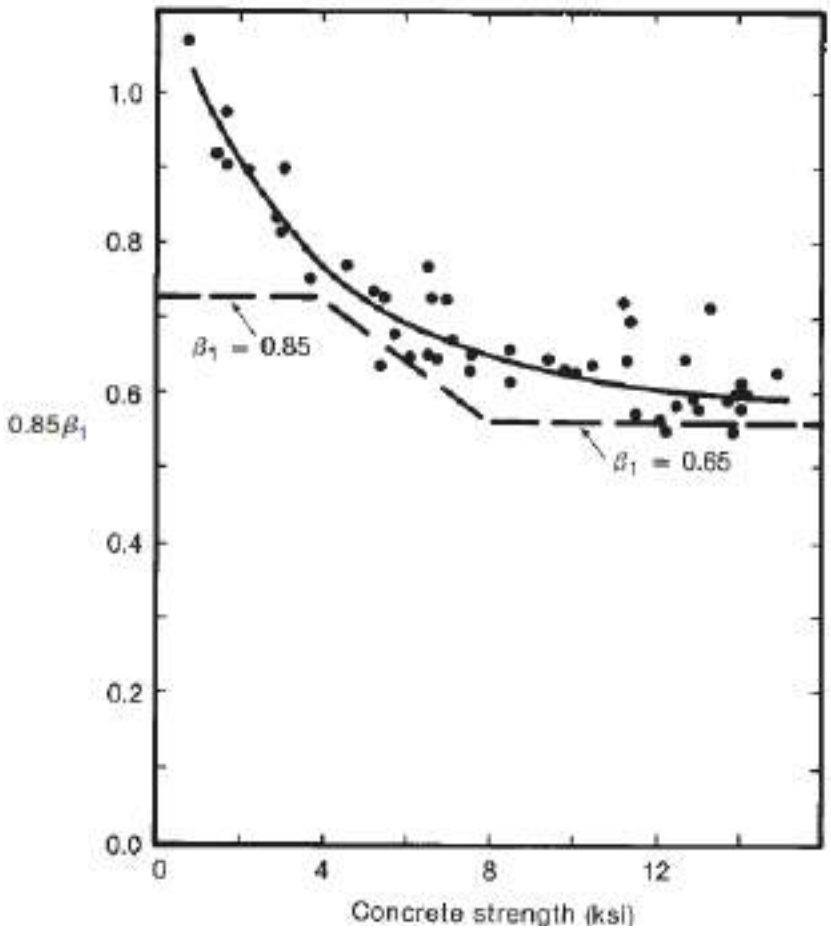

Figure 2.3: Values of B from tests of concrete prisms (Paul et al. 1976).

The β value defines the fraction of the neutral axis depth that can be used for the rectangular-stress-block depth. The fraction β shall be taken as 0.85 for strength, f_c' less than 4,000 psi, and shall be reduced continuously at a rate of 0.45 for each 1,000 psi of strength more than 4,000 psi, but β1 shall not be taken as less than 0.65. The values of $\boldsymbol{\alpha}$ and $\boldsymbol{\beta}$ are dependent only on one parameter, which is the concrete strength (Whitney 1937).

2.2.1 Stress Block Parameters of Compression in Design Codes

2.2.1.1 ACI 318 (2014) and AASHTO LRFD Bridge Design Specifications (2004)

ACI 318 (2014) and AASHTO LRFD Bridge Design Specifications (2004) use rectangular stress block as simplified for the stress-strain curve for a flexural design that depends on the concept of Mattock et al. (1961). The upper limit of concrete compressive strength for AASHTO LRFD Bridge Design Specifications (2004) is ten *ksi*. ACI 318 (2005) has no upper limit. The ultimate strain of concrete compression is assumed to be 0.003. The parameters of equivalent stress block are explained as follows:

The factor $\alpha = 0.85$

$$\beta = \begin{cases} 0.85 & f_c^{'} \leq 4000 \\ 0.85 - 0.05\dfrac{f_c^{'} - 4000\ psi}{1000\ psi} & 4000 < f_c^{'} \leq 8000 \\ 0.65 & f_c^{'} \geq 8000 \end{cases} \qquad \textit{Equation 2-6}$$

2.2.1.2 CSA S6 (2001)

Rectangular stress block parameters were introduced by Canadian Standards Association, Standard S6 (2001), "Canadian Highway Bridge Design Code." This model was mainly the modified version of the equations proposed by Ibrahim and MacGregor (1997). These equations are the triangular distribution of the higher strengths of concrete. The provisions specified by CSA S6 (2001) apply to concrete with a compressive strength ranging from 4.4 ksi to 12.3 ksi.

The upper limits in both codes are established due to the lack of knowledge in the behavior of structural elements with HSC. In the calculation of the rectangular stress block, the ultimate strain of concrete compression is assumed to be 0.0035. The parameters of equivalent stress block are explained as follows:

$$\alpha = 0.85 - 0.0015 f_c' \geq 0.67 \qquad \textit{Equation 2-7}$$

$$\beta = 0.97 - 0.0025 f_c' \geq 0.67 \qquad \textit{Equation 2-8}$$

2.2.1.3 NS 3473 (1995)

The Norwegian Concrete Structures Code 3473 (1995) provides discrete values for various concrete compressive strength, as presented in Table 2.1.

Table 2.1: Stress Block Parameters for the Norwegian Code NS 3473 (1995).

Concrete Compressive Strength (ksi)	**3.6**	**5.1**	**6.5**	**8.0**	**9.4**	**10.9**	**12.3**
α_1	0.0035	0.0035	0.0035	0.0035	0.0032	0.00305	0.0029
β_1	0.80	0.80	0.80	0.80	0.80	0.78	0.76
ε_{ult}	1	1	1	1	0.97	0.96	0.95

2.2.1.4 NZS 3101 (1995)

For New Zealand Concrete Structures Code 3101 (1995), the stress block parameters specified were based on concepts performed by Li (1993). The model provided a tri-linear shape for both α_1 and β_1 as follows:

$\alpha_1 = 0.85 - 0.004(f_c' - 55)$ $\quad 0.85 \geq \alpha_1 \geq 0.75$ *Equation 2-9*

$\beta_1 = 0.85\text{-}0.008(f_c' - 30)$ $\quad 0.85 \geq \beta_1 \geq 0.65$ *Equation 2-10*

$$\varepsilon_{ult} = 0.003$$

2.2.1.5 EC2 (2004)

In Eurocode 2 (2004), the rectangular stress block is used for concrete compressive strengths more than 13 ksi. For compressive strengths, more than 7.25 ksi, stress block parameters and ultimate compressive strain of concrete were constant. In EC 2 (2004), the concrete compressive strength is based on the cylinder strength test. The following stress block parameters and ultimate strain of concrete are proposed:

$$\alpha_1 = 0.85\left(1 - \frac{f_c' - 50}{200}\right) \quad 50 \leq f_c' \leq 90 \qquad \textit{Equation 2-11}$$

$$\beta_1 = 0.8\left(1 - \frac{f_c' - 50}{320}\right) \quad 50 \leq f_c' \leq 90 \qquad \textit{Equation 2-12}$$

$$\varepsilon_{ult} = 0.0026 - 0.035\left(\frac{90 - f_c'}{100}\right)^4 \; 50 \leq f_c' \leq 90 \qquad \textit{Equation 2-13}$$

The α_1 is recommended to be 1.0 by EC 2 (2004). However, this factor may be changed, depending on an individual country. Many countries in Europe have adopted the value of α_1 as 0.85.

2.2.1.6 CEB-FIB Model Code (1990)

For CEB-FIB Model Code (1990), the rectangular stress block specified has the following parameters:

$$\alpha_1 = 0.85\left(1 - \frac{f_c'}{250}\right), \beta_1 = 1.0, \qquad \textit{Equation 2-14}$$

$$\varepsilon_{ult} = 0.004 - 0.002\frac{f_c'}{100} \qquad \textit{Equation 2-15}$$

2.2.1.7 AS3600 -06 code provisions (2006)

In AS3600-06, the Australian code provisions for the stress block parameters are derived from the stress-strain curves for concrete with strengths up to 50 MPa. The value of the ultimate concrete strain is taken as 0.003; see Figure 2.4.

$$\alpha_1 = 0.85$$

$$\beta_1 = 0.85\text{-}0.007(f_c' - 28) \qquad 0.85 \geq \beta_1 \geq 0.65 \qquad \textit{Equation 2-16}$$

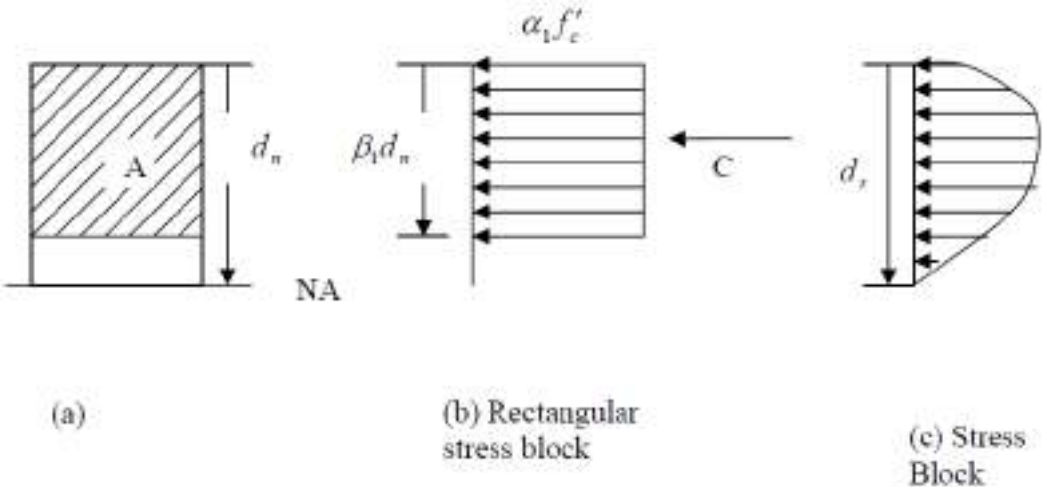

Figure 2.4: AS 3600 Rectangular Stress Block (AS 3600, 2006).

2.2.1.8 ACI 544

The design procedures of ACI 544 are based on theoretical derivations of Soranakom and Mobasher 2007, Rilem and ACI 318. This theory depends on the trapezoidal shape to design the FRC. They found that $f_{cy}\ is\ (0.6-0.9)f_c'$. Therefore, they assumed $as\ 0.85.\ f_c'$ to minimize the number of parameters that assume ε_{ult} is limited as 0.0035 as the lower bound value of SFRC and $\varepsilon_{cy}\ is\ 0.00018\sqrt{f_c'}$.

2.2.1.9 Rilem

The theory depends on a parabolic shape to design FRC. They assume the ε_{ult} as 0.0035 and $\varepsilon_o equal\ to\ 0.002.\ f_{cy}$ adopted as $0.85f_c'$

2.2.2 Stress Block Parameters for FRC in Other Research

2.2.2.1 Henager and Doherty, 1976 and Craig, 1987

They used the equivalent rectangular concrete stress distribution for fiber reinforced concrete, the same as initially proposed by Whitney. This rectangular stress block is shown in Figure 2-5 with nominal flexural strength calculations. The factor α shall be taken 0.85. The factor β shall be taken as follows:

$$\beta = \begin{cases} 0.85 & f_c^{'} \le 4000 \\ 0.85 - 0.05\dfrac{f_c^{'} - 4000\ psi}{1000\ psi} & 4000 < f_c^{'} \le 8000 \\ 0.65 & f_c^{'} \ge 8000 \end{cases} \qquad \textit{Equation 2-17}$$

2.2.2.2 Zijl and Mbewe, 2013

Based on force equilibrium and equivalent moment resistance with the bilinear compressive stress-strain model shown in Figure 2.5, factors, λ_c and η_c , converting bilinear compression stress-strain distribution to an equivalent rectangular stress block can be derived as follows:

$$\lambda_c = \frac{2(\omega^2 - 3.\omega + 3)}{3(2 - \omega)} \qquad \textit{Equation 2-18}$$

$$\eta_c = \frac{3(2 - \omega)^2}{4(\omega^2 - 3.\omega + 3)} \qquad \textit{Equation 2-19}$$

$$\beta_c = \lambda_c.\eta_c = \frac{2 - \omega}{2} \qquad \textit{Equation 2-20}$$

$$\omega = \frac{\varepsilon_{cy}}{\varepsilon_{ult}} \qquad \textit{Equation 2-21}$$

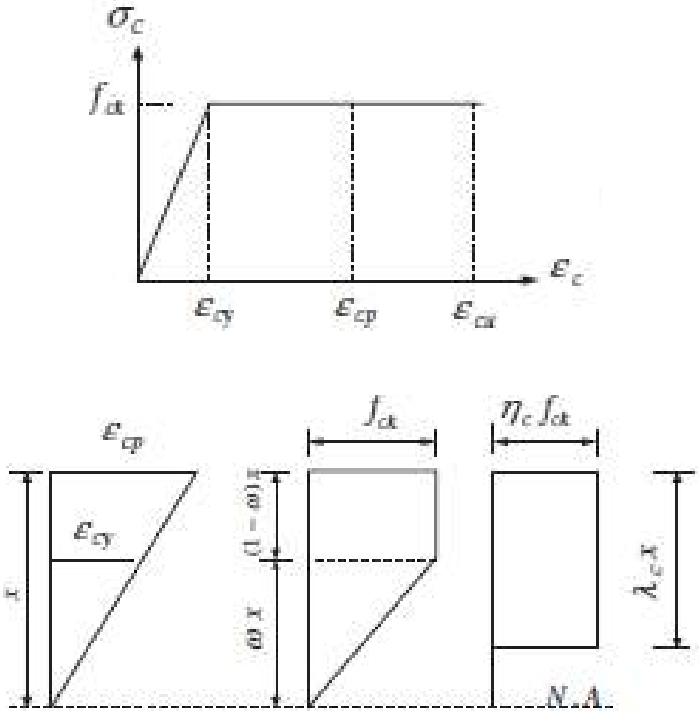

Figure 2.5: Definition of rectangular stress block from a bilinear compressive stress-strain model (Zijl and Mbewe 2013).

With the yield compressive strain to post-yield compressive strain ratio represented as using appropriate strain limits, the conversion factors at ultimate compression strength, λ_c andη_c, are similar to the conversion factors given in Eurocode 2 (Eurocode 2, 2004).

2.2.2.3 (Singh, 2014)

The contribution of the fibers is most apparent in the post-peak region, where the response is described by a relatively less steep decaying stress-strain response. Accordingly, the maximum design flexural stress of fiber-RC can be taken as $0.5f_c'$ by applying a partial safety factor of 1.5, and the corresponding ultimate strain can be taken as 0.004. The design stress corresponding to any strain ε_{ult},0.004 can be taken from Eq. (1).

$$f_c = \begin{cases} 0.5f_c'[2\left(\frac{\varepsilon}{0.002}\right) - \left(\frac{\varepsilon}{0.002}\right)^2] & \varepsilon < 0.002 \\ 0.5f_c' & 0.002 \leq \varepsilon \leq 0.004 \end{cases} \qquad \textit{Equation 2-22}$$

The area under the curve, represented by Eq. (1), can be determined by integration, and it indicates the total compressive resistance offered by the concrete mass above the neutral axis of the beam. The magnitude of this force C is determined to be $0.4167f_c'\ h\ B$.

2.3 Tension Stress Block Parameters

There are three common existing design codes and guidelines for the analysis and design of FRC, namely the ACI 544.4R, FIB model code, RILEM TC-162-TDF (2003) and the Spanish EHE-08, shown in Table 2.2.

2.3.1 Design according to Rilem code

The Rilem TC-162-TDF guideline is based on the Eurocode2 that takes only the pre-peak behavior of concrete in tension because the primary post-peak behavior depends on the presence of steel fibers. This method needs various parameters, which are used to evaluate the post-cracking behavior for fiber, including the compressive strength, modulus of elasticity, compression stress-strain to get the ultimate strain, and flexural test.

Rilem TC-162-TDF explained two approaches of design methods for steel fiber reinforced concrete. These approaches consisted of 1) stress-crack opening ($\sigma - w$) , and 2) stress-deflection ($\sigma - \varepsilon$).

Table 2.2: constitutive models proposed by the three European standards.

Diagram	Parameters	Characterization test	Ref.
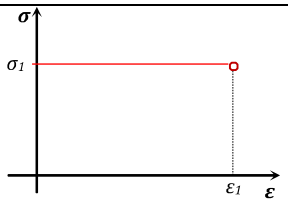	$\sigma_1 = f_{ctkd} = 0.33 f_{fk,3,d}$ $\varepsilon_1 = \varepsilon_u$=[20‰ bending; 10‰ ten	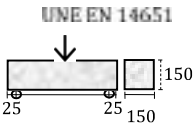	Spanish
	$\sigma_1 = f_{Fts} = f_{R1}/3$ $\varepsilon_1 = \varepsilon_u$= [20‰ softening ; 10‰ hard		FIB
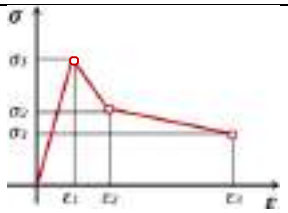	$\sigma_1 = 0.7\, f_{ctm,fl}$ $\sigma_2 = 0.45 \cdot \kappa_1 \cdot f_{R,1}$ $\sigma_3 = 0.37 \cdot \kappa_1 \cdot f_{R,4}$ $\varepsilon_1 = \sigma_1 / E_{ctm}$; $\varepsilon_2 = \varepsilon_1 + 0.1$‰; $\varepsilon_3 = \varepsilon_4 = 25$‰	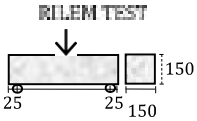	Rilem TC-162
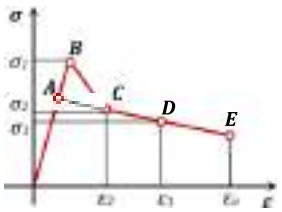	$\sigma_1 = f_{Ctd} = 0.6\, f_{ctk,0,d}$ $\sigma_2 = f_{ctR1,d} = 0.45 f_{fk,1,d}$ $\sigma_3 = f_{ctR3,d} = k_1[0.5 f_{fk,3,d}$ $-0.2 f_{fk,1,d}]$ $\varepsilon_2 = 0.1 + 1000 \cdot f_{ctd}$ / : characteristic length) ε_u=[20‰ bending; 10‰ pure tension	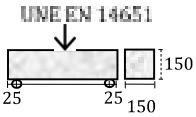	Spanish EHE-08
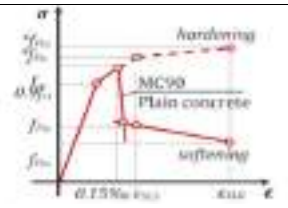	$f_{Ftu} = k[f_{Ft}$ $f_{ctm} = f_{ctk0,05} \cdot (f_{ck}/f_{ck0})^{2/3}$ $f_{Ft1} = 0.45 f_{R1}$ $-(w_u/CMOD_3)[f_{Ft1} - 0.5 f_{Ft3} + 0.2 f_{Ft2}]$ $\varepsilon_{SLS} = CMOD_1 / l_{cs}$ $= 2$ ε_{Fu} = [20‰ softening; 10‰ hard		FIB model code
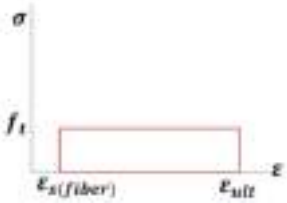	f_t = tensile strength in fiber $= 1.2 \frac{l}{d_f \cdot \rho_f \cdot F_{be}}$ ρ_f = volume fraction of fiber F_{be} = bond efficiency of fiber $\varepsilon_{s(fiber)} = \sigma_f / E_{steel}$ ε_{ult} = ultimate strain σ_f = *fiber stress* =333 psi	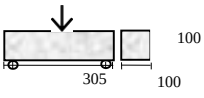	ACI 544.4R

2.3.1.1 $\boldsymbol{\sigma - w}$ ***approach***

The σ − w approach is based on a mechanical fracture approach (fictitious crack model) that depends on a stress-crack opening relationship $[\sigma(w)]$ (Hillerborg 1980). This method is used in combination with the finite elements method. A crack formation can be modelled by two zones that have a traction free crack and fictitious crack. The traction free crack zone does not transfer stresses (the stress on it is zero), whereas the fictitious crack zone does transfer stresses. Therefore, the fictitious crack zone is considered significant in this approach. The fictitious crack is divided into process zone and aggregate interlock for plain concrete. For FRC, the fictitious crack is divided into the process zone aggregate interlock and fiber interlock; see Figure2.6.

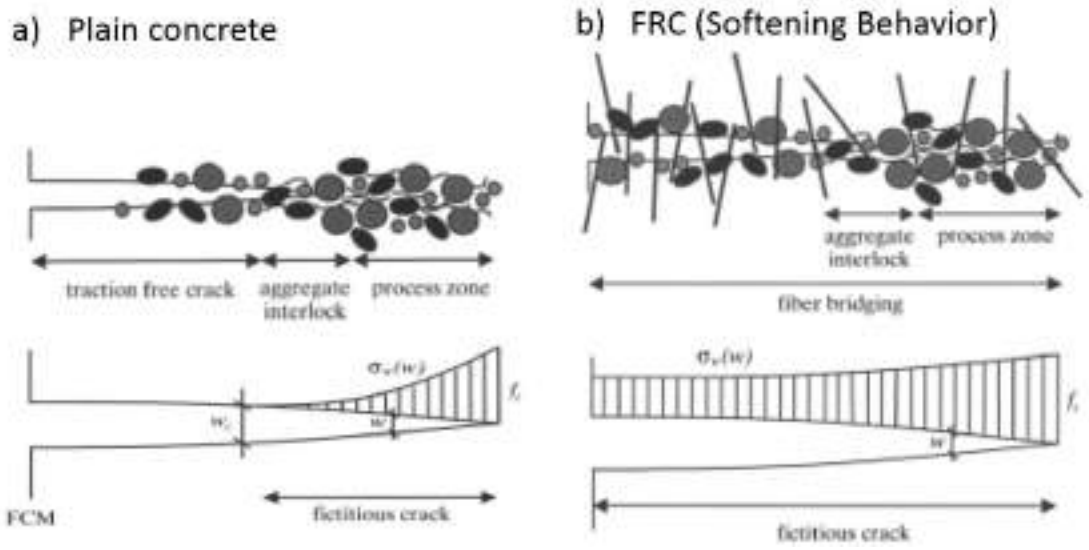

Figure 2.6: Fictitious crack model (Vandewalle,2000).

In the un-cracked zone, the behavior is assumed as linear elastic. If the stress is higher than tensile strength, it is considered as a cracked zone. In this state, stresses within the fictitious crack are related to crack opening (w), and the stresses outside the fictitious crack are related to the strain (ε).

To determine flexure and axial forces, Rilem TC 162 uses a non-linear hinge model to analyze the cracked section. The basis of the cracked hinge model beam consists of considering the element as being divided into two zones. The first zone is the cracked part, which is modeled as a non-linear hinge with length(s). In comparison, the second zone is the non-cracked part, which maintains the elastic behavior, according to Olesen (2001). Therefore, it can be assumed that the rest of the structure behaves in a linear elastic fashion. Also, it can be assumed that the end faces of the non-linear hinge are plane; see Figure2.7.

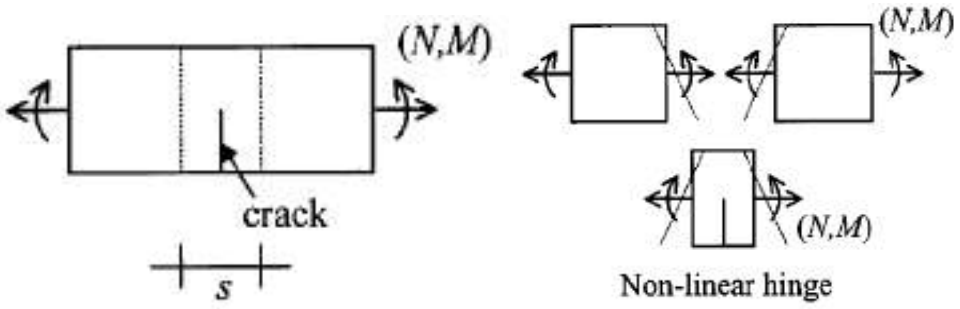

Figure 2.7: Non-linear hinge model (Vandewalle, 2000).

The stress block can be evaluated by the crack opening angle φ^*. There are different kinematic assumptions, such as Pedersen's approach and Casanova's approach.

2.3.1.1.1 Pedersen's approach

It is assumed that the cracked surface remains plane and the φ^* equates to the overall angular deformation (φ); see Figure 2.8.

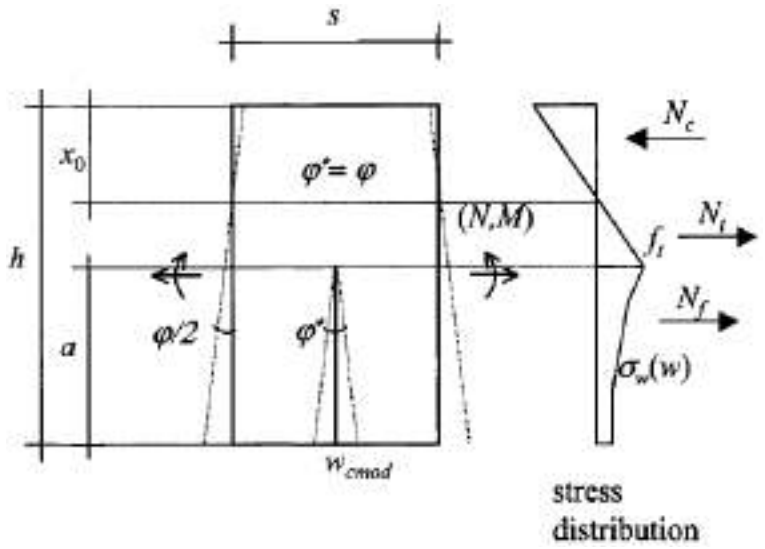

Figure 2.8: Non-linear hinge model (Pedersen's and Casanova's approach) (Vandewalle,2000).

The average curvature of the non-linear hinge is

$$k_m = \frac{\varphi}{s} \qquad \textit{Equation 2-23}$$

The crack mouth opening displacement, $w_{comd} = \varphi^*$ a

Therefore,

$$N_f = \frac{1}{\varphi^*} \int_0^{w_{comd}} \sigma_w(u)du \qquad \textit{Equation 2-24}$$

$$N_c = \frac{\varphi E x_0^2}{2s} \qquad \textit{Equation 2-25}$$

$$N_t = \frac{f_t^2 s}{2\varphi E} \qquad \textit{Equation 2-26}$$

$$M_f = \frac{1}{(\varphi^*)^2} \int_0^{w_{comd}} \sigma_w(u)udu \qquad \textit{Equation 2-27}$$

$$N = N_t + N_f - N_c \qquad \textit{Equation 2-28}$$

2.3.1.1.2 Casanova's approach

It is assumed that the cracked surface remains plane and the φ* equates to the overall angular deformation (φ). Curvature variation is based on an assumption of parabolic variation.

$$w_{comd} = 2k_m a^2 \qquad \textit{Equation 2-29}$$

Where

$$k_m = \frac{2k_1 + k_2}{3}, \quad k_1 = \frac{2M}{Eh^3}, \quad k_2 = \frac{\varepsilon_c}{x_0} \quad , \quad s = 2\,a,$$

Then, ε_c is the strain at the extreme fiber in compression.

M is the moment per unit width in the beam.

All equations for Pedersen's approach apply to Casanova's approach when $\frac{\varphi}{s}$ is replaced with k_m.

2.3.1.1.3 Olesen's approach

It is assumed that the cracked surface does not remain plane, with the φ determined by σ(w); see Figure 2.9.

The average curvature of the non-linear hinge is

$$k_m = \frac{\varphi}{s}$$ *Equation 2-30*

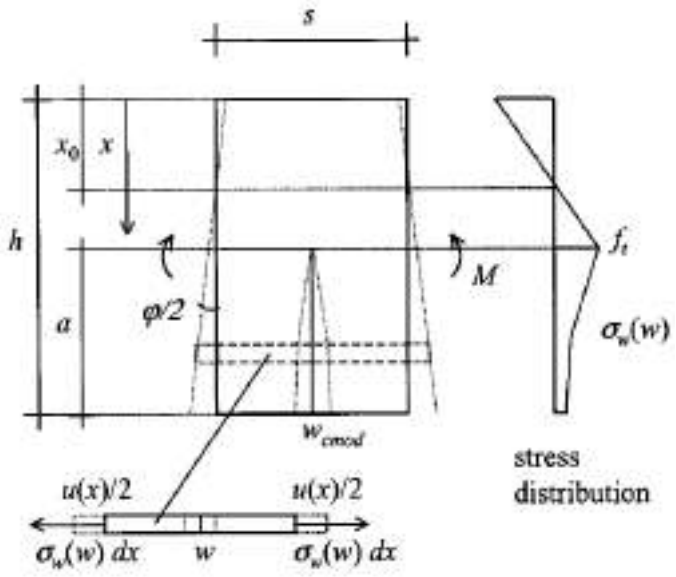

Figure 2.9: Non-linear hinge model (2) Olesen's approach) (Vandewalle, 2000).

2.3.1.2 σ−ε ***approach***

Second, the σ−ε approach is based on the same fundamentals that are used for normal reinforced concrete. It used the load-deflection $(F - \delta)$ curve in flexural beam to evaluate the force $\boldsymbol{F_{0.65}}$ and $\boldsymbol{F_{0.9}}$ at $0.65\boldsymbol{h_{sp}}$ and $0.9\boldsymbol{h_{sp}}$ crack length, respectively, as follows:

$$\boldsymbol{F_{0.65}} = \frac{area\ 1}{0.5}\ (\mathrm{N}) \qquad \textit{Equation 2-31}$$

$$\boldsymbol{F_{0.9}} = \frac{area\ 2}{2.5}\ (\mathrm{N}) \qquad \textit{Equation 2-32}$$

Rilem TC 162 assumed the ultimate deflection of plain concrete, according to Eurocode2, was 0.3 mm from the deflection of the first crack (δ_L). Moreover, it assumed the deflection at 0.65$\boldsymbol{h_{sp}}$ and 0.9$\boldsymbol{h_{sp}}$ crack length were 0.65 and 2.65 mm from the deflection of first crack (δ_L), as illustrated in Figure 2.10.

After determining the force, the stress was calculated based on a simplified assumption regarding the shape of the stress block. $f_{0.65}\ and\ f_{0.9}$ were calculated assuming linear elastic behavior, as shown in the figure to the left. However, in reality, the stress distribution is different. The flexural tensile strength cannot be used as an alternative to tensile strength in the cracked part because it represents an equivalent form of stress and not material properties. Figure 2.11(a) shows elastic material with a natural axis at mid depth and tensile strength equal to modulus of rupture. Rilem suggested assumptions that the tensile stress in the cracked part of the steel fiber concrete section is constant.

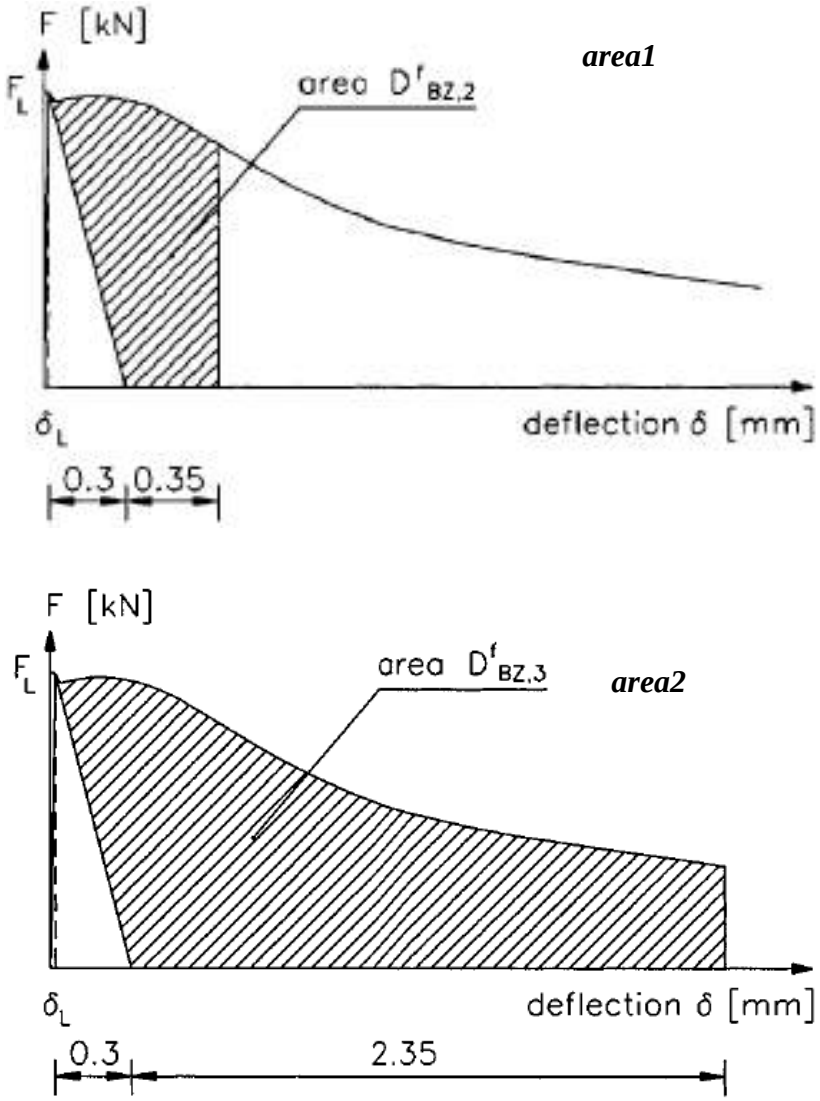

*Figure 2.10: Load- Deflection curve according to Rilem TC 162 (*Vandewalle, 2003).

While Figure 2.11(b) explains that plastic material with a natural axis moves toward the compression zone, tensile strength depends on the ability of the fiber to bridge the cracks. The tensile strength in the cracked part for FRC, as shown in Figure 2.11(b), can be evaluated for the case where the moment of

resistance of tensile strength in the cracked part is equal to the moment of resistance of flexural tensile strength.

The flexural tensile strength for $\boldsymbol{F_{0.65}}$ and $\boldsymbol{F_{0.9}}$ is

$$\boldsymbol{f_{0.65}} = \frac{3\ \boldsymbol{F_{0.65}}\ L}{2\ b\ h_{sp}^2}\ (N/mm^2) \qquad \textit{Equation 2-33}$$

$$\boldsymbol{f_{0.9}} = \frac{3\ \boldsymbol{F_{0.9}}\ L}{2\ b\ h_{sp}^2}\ (N/mm^2) \qquad \textit{Equation 2-34}$$

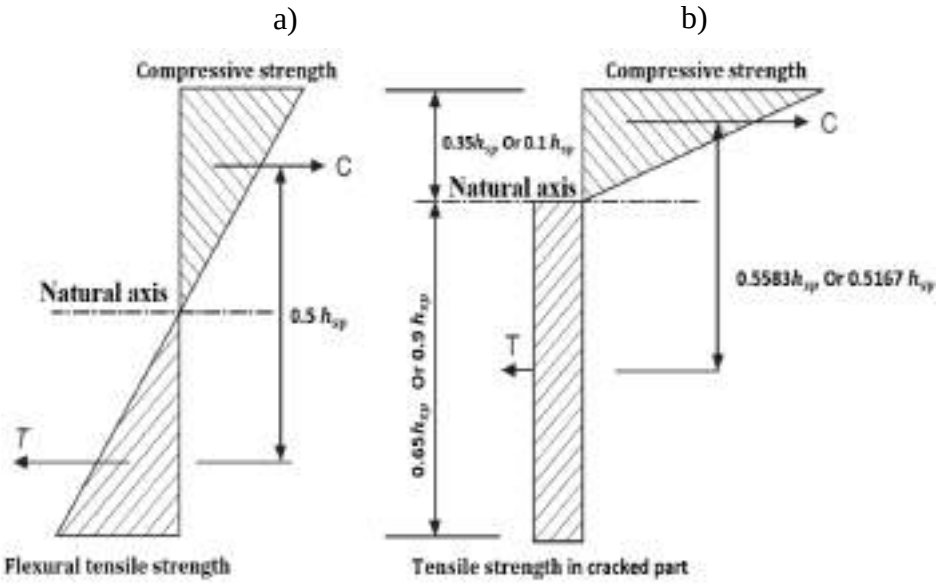

*Figure 2.11: Stress blocks in flexure. (a) Elastic in tension and compression. (b) Elastic in compression plastic in tension (*Vandewalle, 2000).

The tensile strength ($\sigma_{0.65}$) for 0.65$\boldsymbol{h_{sp}}$ crack length is

$$M_a = \frac{b.h_{sp}^2}{6} f_{0.65} \qquad \textit{Equation 2-35}$$

$$M_b = 0.65.h_{sp}^2.0.56.b.\sigma_{0.65} \quad \textit{Equation 2-36}$$

Where $M_a = M_b$, then,

$$\sigma_{0.65} = 0.45\, f_{0.65} \quad \textit{Equation 2-37}$$

The tensile strength ($\sigma_{0.9}$) for $0.9h_{sp}$ crack length is

$$M_a = \frac{b.h_{sp}^2}{6} f_{0.9} \quad \textit{Equation 2-38}$$

$$M_b = 0.9.h_{sp}^2.0.51.b.\sigma_{0.9} \quad \textit{Equation 2-39}$$

Where $M_a = M_b$, then,

$$\sigma_{0.9} = 0.37\, f_{0.9} \quad \textit{Equation 2-40}$$

The basic concept of RILEM specifications has been used to determine the values of the constants. In this dissertation, the second approach ($\sigma - \varepsilon$ approach) will be used to develop the design and analysis of FRC with various volume fractions and types of fibers. The second approach is easier and is the same concept that is currently used by engineers for analysis and design for normal reinforced concrete. The big difference between the designing of FRC and normal reinforced concrete is post-cracking behavior.

Post-cracking behavior

Fiber reinforced concrete can have a strain softening or hardening behavior. When the first crack generates, the presence of fiber will resist further crack openings and allow the load transfer across the crack. This state is called crack closing, or crack bridging, between the concrete textures to carry a tensile load

across the crack. For tension softening behavior, the fibers cannot carry more load after the first crack generates. The first cracking strength is larger than the strength of post-cracking. With strain hardening behavior, the fibers can carry more load after the formation of the first crack; see Figure 2.12.

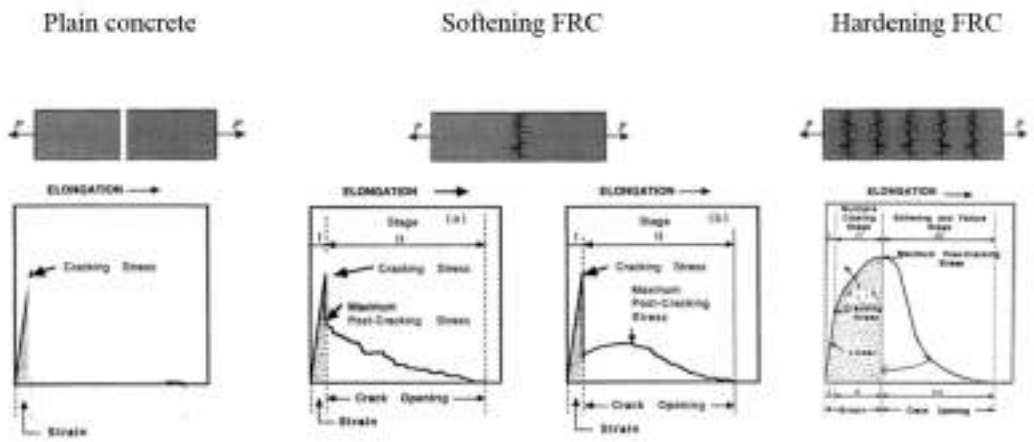

Figure 2.12: Post cracking stress stage.

This can be lead to the formation of multiple cracks in the weak part of the matrix of concrete. The post-cracking strength is larger than the strength of the first cracking. Also, some equilibrium equations are derived to obtain the value that can be obtained by hand calculations. Both ways of analysis are compared to decide the validity of the approaches.

2.3.2 Design according to Chote and Mobasher, 2009 Model

Chote and Mobasher, 2009, used a set of closed-form equations for the flexural design of fiber-reinforced concrete that were based on simplified tensile and compressive constitutive response. The design procedures of this model depend on the same concept of theoretical derivations in RILEM TC 162-TDF.16, ACI 318-0524 and Soranakom and Mobasher (Chote and Mobasher, 2009). This model determines the first crack strength and post-crack strength of tensile response and the yield strength of compression response, in addition to nominal moment capacity, short-term deflection calculations, and strain limit of strain-softening FRC. It can be simplified to idealized stress-strain models, as shown in Figure 2.13 (a) and (b). In this model, the contribution of these types of fibers is most apparent in a decaying stress-strain relationship, where the post-peak tensile region describes the response.

Chote and Mobasher method to develop material models has these assumptions:

1. Young's modulus E for compression and tension are equal.
2. Tension model (Figure 2.13 (a))
    a. consists of a linear stress-strain for elastic stage cracking tensile strain ε_{cr},

b. a constant post-crack tensile strength $\sigma_p = \mu E \varepsilon_{cr}$ with a parameter μ ($0 \leq \mu \leq 1$) representing the post-crack strength as a first cracking tensile strength $\sigma_{cr} = E\varepsilon_{cr}$; and

c. an average constant post-crack tensile strength σ_p for the softening response, which depends on the fiber volume fraction and their bond characteristics.

3. The compression model (Figure 2.13(b)) is defined by an elastic-perfectly plastic model using a yield compressive strain $\varepsilon_{cy} = \omega\varepsilon_{cr}$ with a parameter ω ($\omega \geq 1$) representing the compressive to cracking tensile strain ratio.

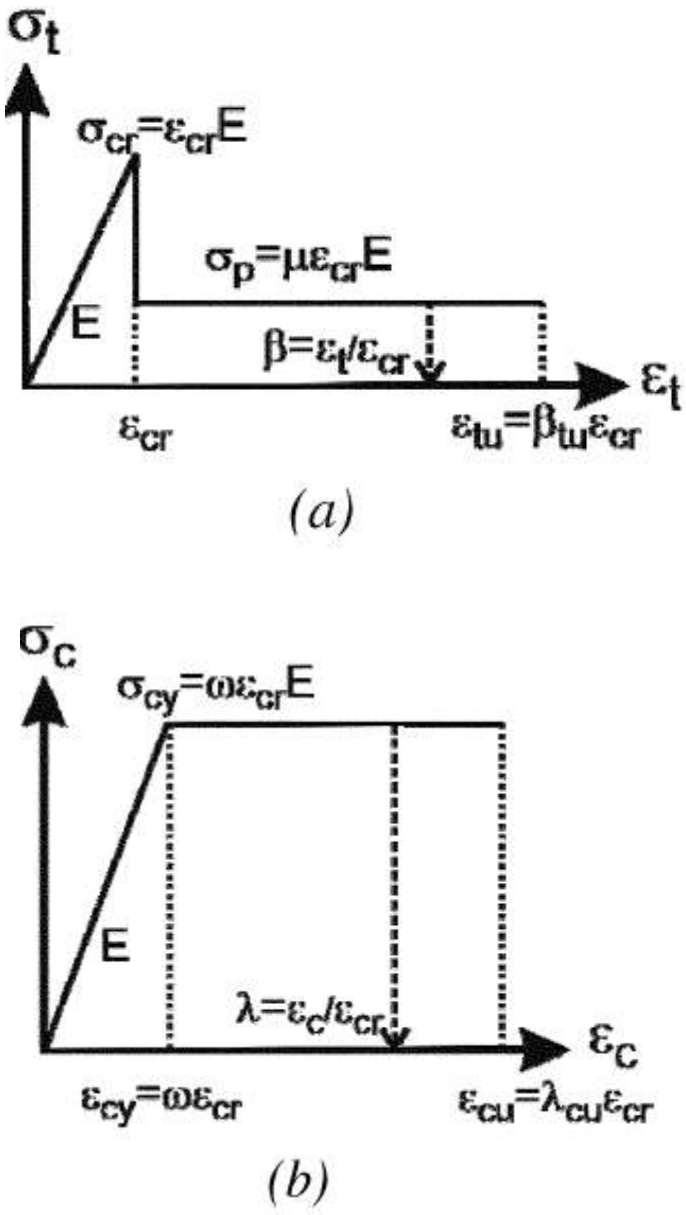

Figure 2.13: Idealized material models for strain-softening fiber-reinforced concrete: (a) tension model; and (b) compression model (*Soranakom and Mobasher, 2009)*.

To minimize the number of material parameters, Chote and Mobasher assumed the tensile strength and Young's modulus to be marginally affected by fiber type and content and to depend on the relationship governing normal concrete using ACI 318-05 Sections 11.2 and 8.5.1, respectively

$$\sigma_{cr} = E\varepsilon_{cr} = 0.56\, f_c' \text{ (MPa)}$$

$$\sigma_{cr} = E\varepsilon_{cr} = 6.7\ f_c' \text{ (psi)}$$

Equation 2-41

$$\text{E} = 4733\sqrt{f_c'} \text{ (MPa)}$$

$$\text{E} = 57{,}000\sqrt{f_c'} \text{ (psi)}$$

Equation 2-42

Where:

f_c' is the ultimate uniaxial cylinder compressive strength.

The first crack tensile strain for FRC can be calculated assuming Hooke's law as:

$$\varepsilon_{cr} = \frac{\sigma_{cr}}{E} = \frac{0.56\, f_c'}{4733\sqrt{f_c'}} = \frac{6.7\, f_c'}{57{,}000\sqrt{f_c'}} = 118 \textit{ micro-strain}$$

Equation 2-43

This model defined the ultimate tensile strain ε_3 as 0.025 and the ultimate compressive strain ε_{cu} as 0.0035 according to the RILEM model16 shown in Figure 2.14.

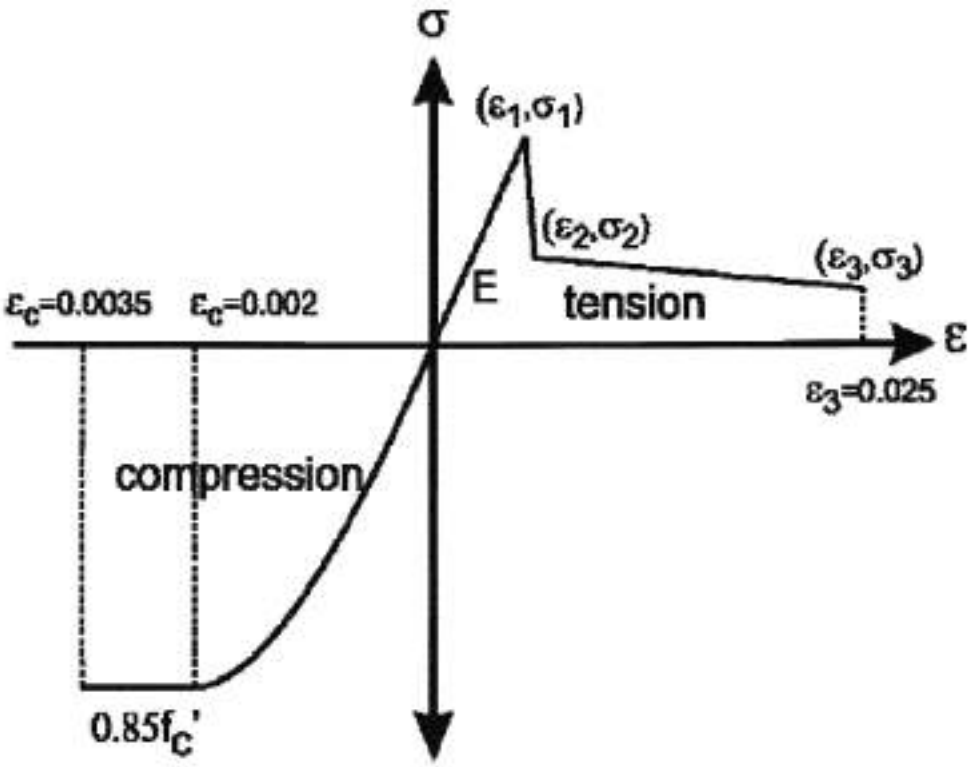

Figure 2.14: RILEM material model for steel fiber-reinforced concrete (Soranakom and Mobasher, 2009).

In addition, it adopted the yield compressive strength for FRC as

$$\sigma_{cy} = 0.85\, f_c' \text{ (MPa and psi)} \qquad \textit{Equation 2-44}$$

The parameter (μ) that is normalized post peak tensile strength and the parameter (ω) that is normalized yield compressive strain, is also a compressive-to-tensile strength ratio.

These two parameters are used in this model (Figure 2.13 (a) and (b)), and they are explained as follows:

$$\mu = \frac{\sigma_p}{E\varepsilon_{cr}} = \frac{\sigma_p}{\sigma_{cr}} \qquad \textit{Equation 2-45}$$

$$\omega = \frac{\varepsilon_{cy}}{\varepsilon_{cr}} = \frac{\sigma_{cy}}{E\varepsilon_{cr}} = \frac{\sigma_{cy}}{\sigma_{cr}} = 1.52\sqrt{f_c'} \text{ (SI units)}$$

$$\omega = 0.127\sqrt{f_c'} \text{ (U. S. customary units)} \qquad \textit{Equation 2-46}$$

ω varies between 6.8 and 12.8 for typical fc′ between 20 and 65 MPa (2900 and 9427 psi).

The parameter β is a normalized tensile strain (εt /εcr), and parameter λ refers to normalized compressive strain (εc /εcr). Therefore, the normalized ultimate tensile strain β_{tu} and compressive strain λ_{cu}, are summarized as follows:

$$\beta tu = \frac{\varepsilon tu}{\varepsilon cr} = \frac{0.025}{118 \times 10^{-6}} \approx 212$$

$$\lambda cu = \frac{\varepsilon cu}{\varepsilon cr} = \frac{0.0035}{118 \times 10^{-6}} \approx 30$$

As mentioned above, it can draw the stress block for compression and tension as:

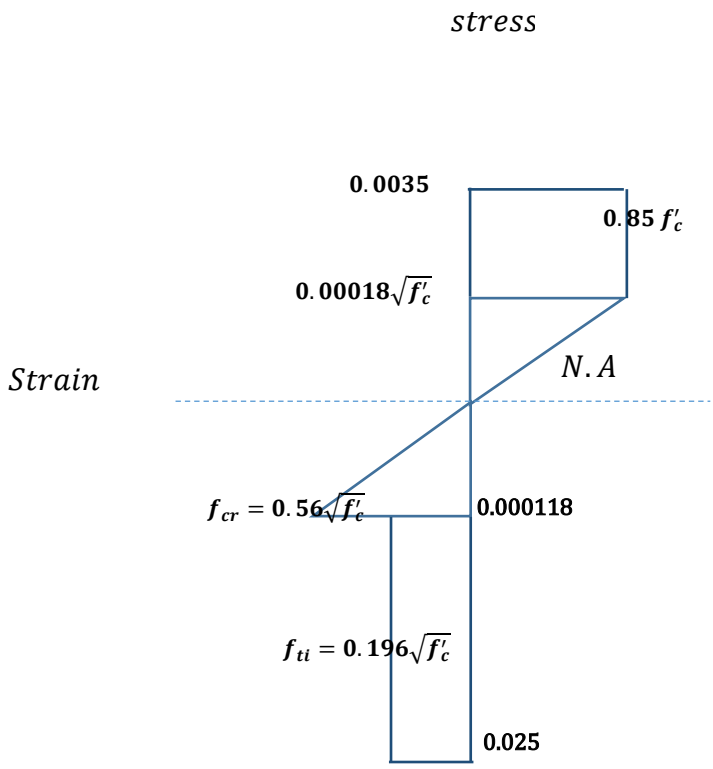

Figure 2.15: the stress block for compression and tension according to Chote and Mobasher, 2009.

2.3.3 Design according to Model ACI544-8R

For the back-calculation procedure of material properties from experimental data, a general strain softening and hardening uses a tri-linear model derived by Soranakom and Mobasher (Soranakom and Mobasher, 2007), (Soranakom and Mobasher, 2008,) and (Soranakom and Mobasher, 2009). This approach used closed-form equations of the load-deflection results of FRC that can be fitted to the experimental data. However, the ACI544 model explains the different features of the strength and ductility of strain FRC behavior.

Figure 2.16 presents the constitutive model for homogenized strain softening reinforced concrete.

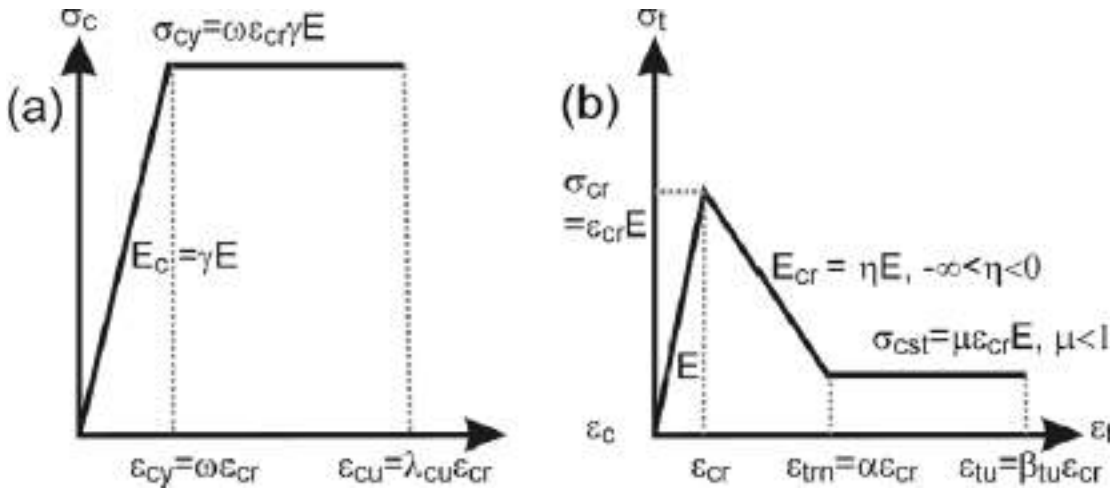

Figure 2.16: Strain softening material model for FRC materials: (a) compression, (b) tension (Barsby, 2011).

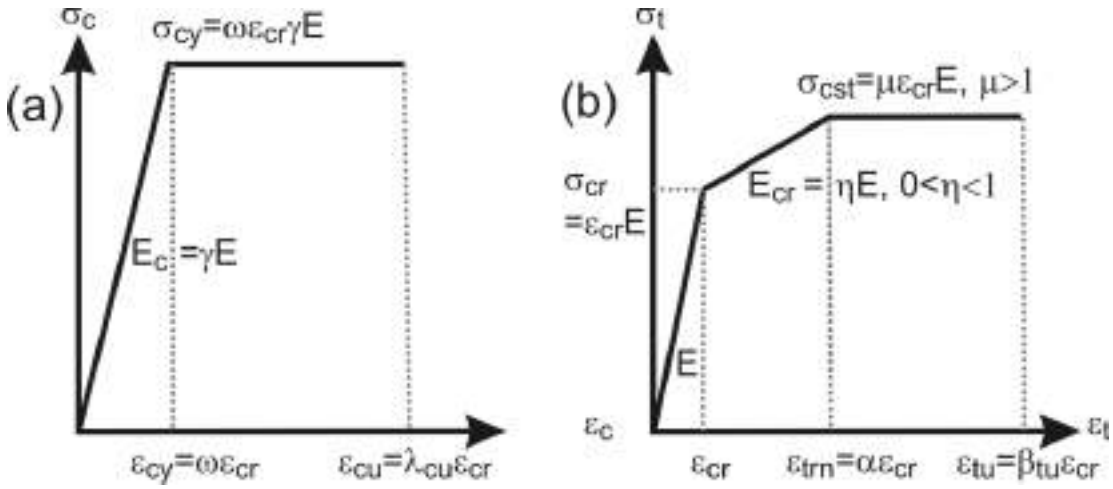

Figure 2.17: Strain hardening model for FRC materials: (a) compression, (b) tension (Barsby, 2011).

Figure 2.16 shows that a bi-linear model describes the compression model with an elastic range E. ACI544 assumed the linear portion of compressive stress-strain response terminates at yield point (ε_{cy}, σ_{cy}) and remaind constant at compressive yield stress σ_{cy} until the ultimate compressive strain ε_{cu}.

The tension model is a tri-linear model with three regions. The first region is explained by an elastic modulus E and first cracking (ε_{cr}). The second region is defined by transition strains (ε_{turn}) and post-cracking modulus Ecr which is assigned a negative or positive value to simulate the behavior of the softening and hardening strain. The third region in the tensile model is stress σ_{cst} in the post-crack region which is defined with a constant stress range, in addition to the ultimate tensile strain level of ε_{tu}. Using first cracking tensile strain ε_{cr} and tensile modulus *E* parameters to normalize the seven parameters is shown in the equation below in Figure 2.16 b

$$\omega = \frac{\varepsilon_{cy}}{\varepsilon_{cr}}; \propto = \frac{\varepsilon_{trn}}{\varepsilon_{cr}}; \beta_{tu} = \frac{\varepsilon_{tu}}{\varepsilon_{cr}}; \lambda cu = \frac{\varepsilon_{cu}}{\varepsilon_{cr}}; \gamma = \frac{E_c}{E}; \eta = \frac{E_{cr}}{E};\ \mu = \frac{\sigma_{cst}}{E\varepsilon_{cr}}$$

For a rectangular cross-section with dimensions width “b” and depth “d,” ACI 544 assumed that the maximum tensile strain β and maximum compressive strain λ are linearly related through the normalized neutral axis parameter, k.

$$\beta = \frac{\varepsilon tbot}{\varepsilon_{cr}};\ \lambda = \frac{\varepsilon_{ctop}}{\varepsilon_{cr}}; \frac{\lambda\varepsilon_{cr}}{kd} = \frac{\beta\varepsilon_{cr}}{d - kd}\ or\ \lambda = \frac{k}{1-k}\beta$$

ACI 544 made in the development of the material models by assumptions:

1- Linear strain distribution across the depth

2- Ignoring shear deformations,

3- Three stages of Stress distribution across the cross section at tensile strain: $0 \leq \beta \leq 1$, $1 < \beta \leq \alpha$ and $\alpha < \beta \leq \beta_{tu}$ obtained in closed form.

The internal moment is obtained using the force components and their distance from the neutral axis. The curvature is determined as the ratio of compressive strain ($\varepsilon_c = \lambda \varepsilon_{cr}$) to the depth of neutral axis kd. ACI 544 normalized the moment M_i and curvature ϕ_i at each stage i (which corresponds to an input tensile fiber strain, β) concerning the values at cracking μ_{cr} and ϕ_{cr}, and are presented in equations below. The transition from deflection softening to deflection hardening is defined by critical normalized post-peak tensile strength (μ_{crit}) as defined in the equation below; see Figure 2.18.

$$M_i = M' M_{cr};\ M_{cr} = \frac{1}{6} b d^2 E \varepsilon_{cr} \qquad \textit{Equation 2-47}$$

$$\phi_i = \phi_i' \phi_{cr};\ \phi_{cr} = \frac{2\varepsilon_{cr}}{d} \qquad \textit{Equation 2-48}$$

$$\mu_{crit} = \frac{\omega}{3\omega - 1} \qquad \textit{Equation 2-49}$$

The calculation of k, M', and ϕ' for the five stages of governing strain is presented in Table 2.3

1- Stage 1: the tensile and compressive zones are both elastic, and the neutral axis remains at the centroid of the test sample when elastic compression and tension are the same. This case continues to the point of first cracking.

2- Stage 2.1: tension cracking-elastic compression: when the elastic Stage 1 ends, the neutral axis moves toward the compression zone which remains elastic during early stages. While in the tension side, the strain is less than transition strains (ε_{trn}).

3- Stage 2.2: cracking tension- plastic compression is defined as the compression side enters the plastic range. While in the tension side, the strain is less than transition strains (ε_{trn})

4- Stage 3.1: the compression zone is already in the elastic range. While in the tension side, the strain is more than transition strains (ε_{trn}).

5- Stage 3.2: the compression zone has already entered the plastic range. While in the tension side, the strain is more than transition strains (ε_{trn}).

Table 2.3: Governing equations for the calculation of k, M' and φ' for each stage specified by strains at the top and bottom fibers (Barsby, 2011).

Stage	Parameters	k	$M' = M/M_{cr}$	$\phi' = \phi/\phi_{cr}$
1	$0 < \beta \leq 1$	$k_1 = \begin{cases} \frac{1}{2} & \text{for } \gamma = 1 \\ \frac{-1+\sqrt{\gamma}}{-1+\gamma} & \text{for } \gamma \neq 1 \end{cases}$	$M'_1 = \frac{2\beta\left[(\gamma-1)k_1^3 + 3k_1^2 - 3k_1 + 1\right]}{1-k_1}$	$\phi'_1 = \frac{\beta}{2(1-k_1)}$
2.1	$1 < \beta \leq \alpha$ $0 < \lambda \leq \omega$	$k_{21} = \frac{D_{21} - \sqrt{D_{21}\gamma\beta^2}}{D_{21} - \gamma\beta^2}$ $D_{21} = \eta\left(\beta^2 - 2\beta + 1\right) + 2\beta - 1$	$M'_{21} = \frac{\left(2\gamma\beta^3 - C_{21}\right)k_{21}^3 + 3C_{21}k_{21}^2 - 3C_{21}k_{21} + C_{21}}{1-k_{21}}$ $C_{21} = \frac{(2\beta^3 - 3\beta^2 + 1)\eta + 3\beta^2 - 1}{\beta^2}$	$\phi'_{21} = \frac{\beta}{2(1-k_{21})}$
2.2	$1 < \beta \leq \alpha$ $\omega < \lambda \leq \lambda_{cr}$	$k_{22} = \frac{D_{22}}{D_{22} + 2\omega\gamma\beta}$ $D_{22} = D_{21} + \gamma\omega^2$	$M'_{22} = \left(3\gamma\omega\beta^2 + C_{22}\right)k_{22}^2 - 2C_{22}k_{22} + C_{22}$ $C_{22} = C_{21} - \frac{\gamma\omega^3}{\beta^2}$	$\phi'_{22} = \frac{\beta}{2(1-k_{22})}$
3.1	$\alpha < \beta \leq \beta_{cr}$ $0 < \lambda \leq \omega$	$k_{31} = \frac{D_{31} - \sqrt{D_{31}\gamma\beta^2}}{D_{31} - \gamma\beta^2}$ $D_{31} = \eta\left(\alpha^2 - 2\alpha + 1\right) + 2\mu(\beta - \alpha) + 2\alpha - 1$	$M'_{31} = \frac{\left(2\gamma\beta^3 - C_{31}\right)k_{31}^3 + 3C_{31}k_{31}^2 - 3C_{31}k_{31} + C_{31}}{1-k_{31}}$ $C_{31} = \frac{(2\alpha^3 - 3\alpha^2 + 1)\eta - 3\mu\left(\alpha^2 - \beta^2\right) + 3\alpha^2 - 1}{\beta^2}$	$\phi'_{31} = \frac{\beta}{2(1-k_{31})}$
3.2	$\alpha < \beta \leq \beta_{cr}$ $\omega < \lambda \leq \lambda_{cr}$	$k_{32} = \frac{D_{32}}{D_{32} + 2\omega\gamma\beta}$ $D_{32} = D_{31} + \gamma\omega^2$	$M'_{32} = \left(3\gamma\omega\beta^2 + C_{32}\right)k_{32}^2 - 2C_{32}k_{32} + C_{32}$ $C_{32} = C_{31} - \frac{\gamma\omega^3}{\beta^2}$	$\phi'_{32} = \frac{\beta}{2(1-k_{32})}$

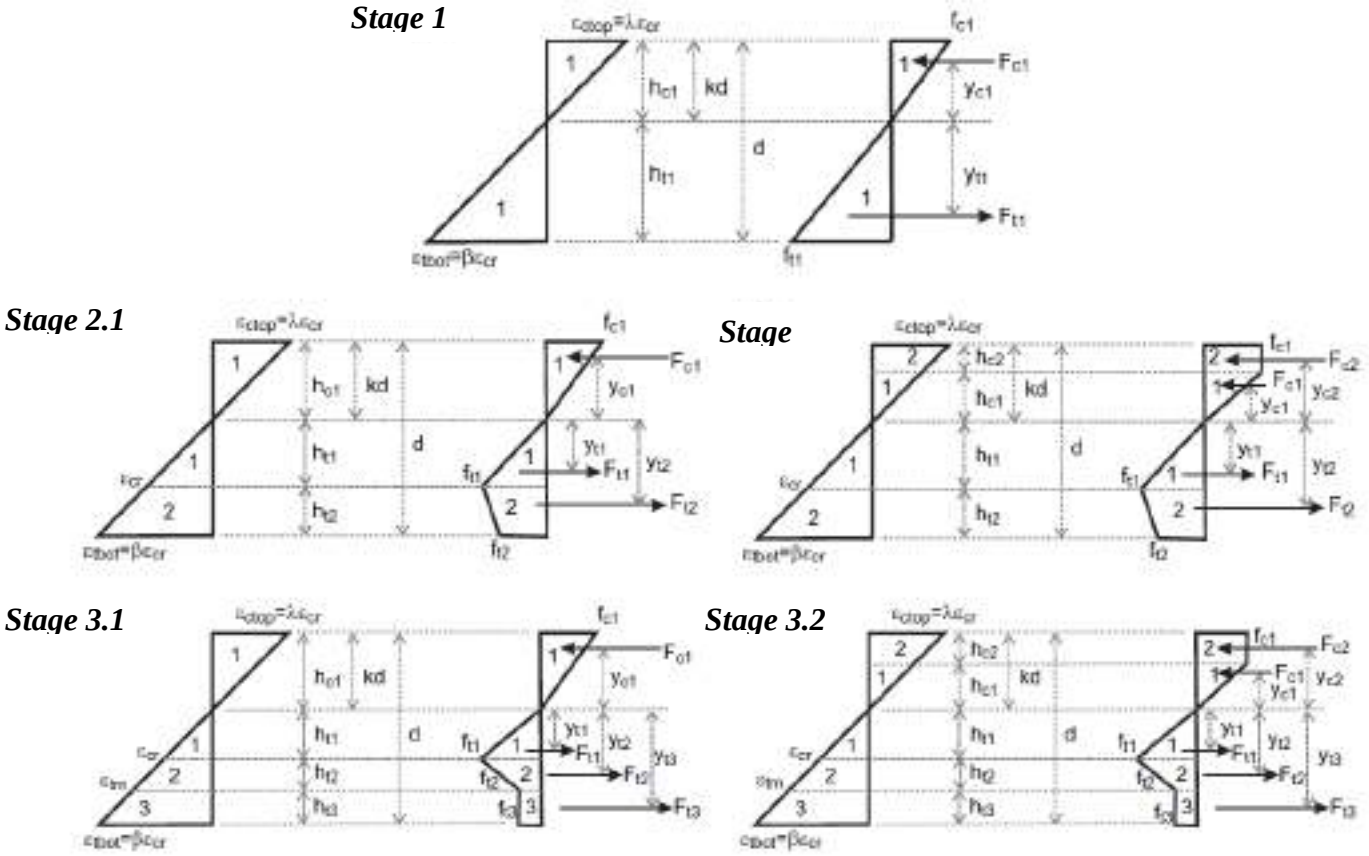

Figure 2.18: Stress–strain diagram at different stages of normalized tensile strain at the bottom fiber for different stages (Soranakom, and Mobasher, 2008).

Strain hardening and softening model spreadsheet by Mobasher

Mobasher uses a spreadsheet of Microsoft Excel as the platform opens the field in a format that is user-friendly to drive the software and perform the analysis. Data is then input it into a spreadsheet of experimental data of load-deflection from flexural beam test (4 or 3 points). The user inputs are material properties and model parameters. The output of the spreadsheet changes material parameters and updates the simulated curve, providing a fast and reliable way of data reduction.

Figure 2.19 shows the user inputs into the Mobasher spreadsheet, including the type of test, beam dimensions, the two material properties (E andε_{cr}) and the seven parameters of the tensile and compressive model (ω, λ_{cu} and α, γ, η, μ, β_{tu}).

As explained above, these parameters are normalized concerning (E andε_{cr}) so units must be consistent as noted (in, lbs, psi or mm, N, MPa). Figure 2.20 shows the experimental and simulated load deflection curves required to fit the simulation.

FRC_Back_Calculation_Spreadsheet_TENSION_v1.5

Model Parameters		
Use input should be in the green shaded cells		
Unit Convention (0 or 1)		
SI	1	
US Customary	0	
User Defined η (Y or N)?		
	Y	
User Defined η =	0.015	
Beam Size		
Test Method	4	Point Bending
b =	150	(mm)
d =	150	(mm)
L =	450	(mm)
Don't need Lp	1.00	(mm)
Material Model		
E =	23000	MPa
εcr =	0.0002	(mm/mm)
α =	27	
Tension		
γ =	0.95	
η =	0.015	
μ =	0.95	
βtu =	50	
Compression		
ω =	100	
λcu =	100	

Figure 2.19: User inputs to a back-calculation spreadsheet.

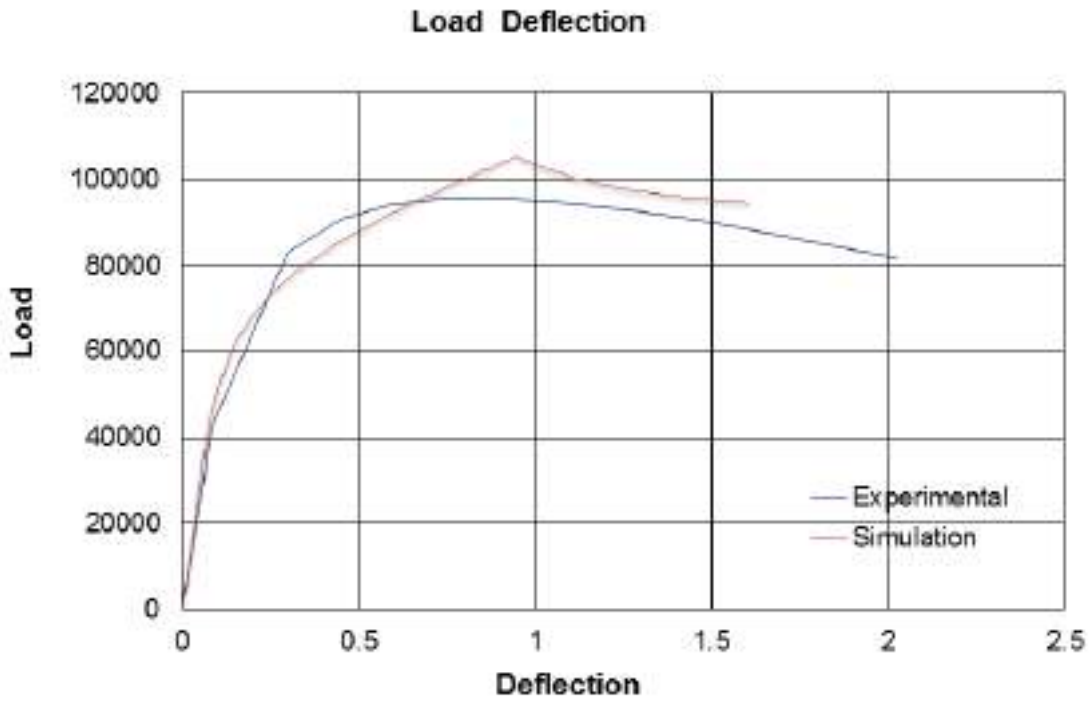

Figure 2.20: Experimental and simulated load-deflection curves.

Figure 2.21 shows the output of the type of data included. This spreadsheet was used to provide back-calculation analysis for all of the flexural tests as softening and hardening strain behavior. The model was implemented based on an incrementally imposed tensile strain (β), with the ultimate tensile strain being represented by βtu.

Output Data - Experimental

Flexural Toughness =	142240	(N-mm)
Bending Strength =	14.0461	(MPa)
Flexural Stiffness =	584712	(MPa)
Load @ 1st Crack =	34057.6	(N)
Defl @ 1st Crack =	0.05825	(mm)
Max Flex Load =	105346	(N)
Defl. @ Max Load =	0.9475	(mm)
Deflection Capacity =	1.60496	(mm)

Output Data - Back-Calc Parameters

Tensile Toughness =	0.04388	(MPa)
εcr (μstr) =	200	
E =	23000	(MPa)
σcr =	4.60	(MPa)
μ =	0.95	
α =	27	
εtrn (μstr) =	5400	
εtu (μstr) =	10000	
μσcr =	4.37	(MPa)

Figure 2.21: Output tab results are showing experimental and back-calculation parameters.

2.3.4 Design according to FIB model code

FIB (fédération Internationale du béton) is an international federation for the structural concrete model code. There are many assumptions made to determine the ultimate limit moment resistance of reinforced or prestressed concrete sections by FIB code.

1- Plane sections remain plane

2- In tension or compression, the strain in bonded reinforcement or bonded prestressing tendons is the same as that in the surrounding concrete (Full bond).

3- The tensile strength of the concrete is negleate except for fiber reinforced concrete.

4- The stresses in the concrete are derived from stress-strain relations for the design of cross-sections.

5- The stresses in the reinforcing and prestressing steel are derived from design curves given in subclause 7.2.3.2 and 7.2.3.3 in the FIB model code.

According to the FIB model code, the concrete tensile stresses, f_t (MPa) was used to derive,

$$f_t = 0.3(f_c')^{0.67} \qquad \textit{Equation 2-50}$$

With f_c' being the cylindrical compressive fiber reinforced concrete strength.

While modulus of elasticity,E_c were used to derive as ,

$$E_c = (\frac{f_c' + 8}{10})^{0.3} \qquad \textit{Equation 2-51}$$

It should, however, as the mean concrete modulus of elasticity, E_c , cannot be smaller than the mean compressive strength. So the modulus of elasticity,E_c, given by RILEM TC-162-TDF (2003), was used.

$$E_c = 9500(f_c')^{0.33} \qquad \textit{Equation 2-52}$$

According to the FIB model code, the strength of fibers is determined by performing crack mouth opening displacement (CMOD) tests that deformation controlled loading tests. This test requires a notched beam to prevent horizontal cracking, and deflection or strain gauge and load gauge for recording the applied load and the crack opening, which is measured as a horizontal deflection. The FIB model code proposes that the strength of fibers measured as a residual flexural tensile strength,$f_{R,j}$.

$$f_{R,j} = 3\frac{F_j l}{2bh_{sp}^2} \qquad \textit{Equation 2-53}$$

Where, $f_{R,j}$ is the residual flexural tensile strength corresponding to CMODj, with [j=1,2,3,4]

F_j is the load corresponding to

CMODj is the crack mouth opening displacement

l is the span of the specimen

b is the width of the specimen

h_{sp}^2 is the distance between the notch tip and the top of the specimen

The values $f_{R,1}$ and $f_{R,3}$ are obtained from the corresponding $f_{R,1}$- CMOD1 and $f_{R,3}$- CMOD3 values as shown in Figure 2.22. CMOD1 and CMOD3 are the crack mouth opening displacements and are equal to 0.5mm and 2.5mm, respectively. The FIB model code simplifies the stress-CMOD curve in tension into a linear post crack softening or hardening behavior and a plastic rigid behavior.

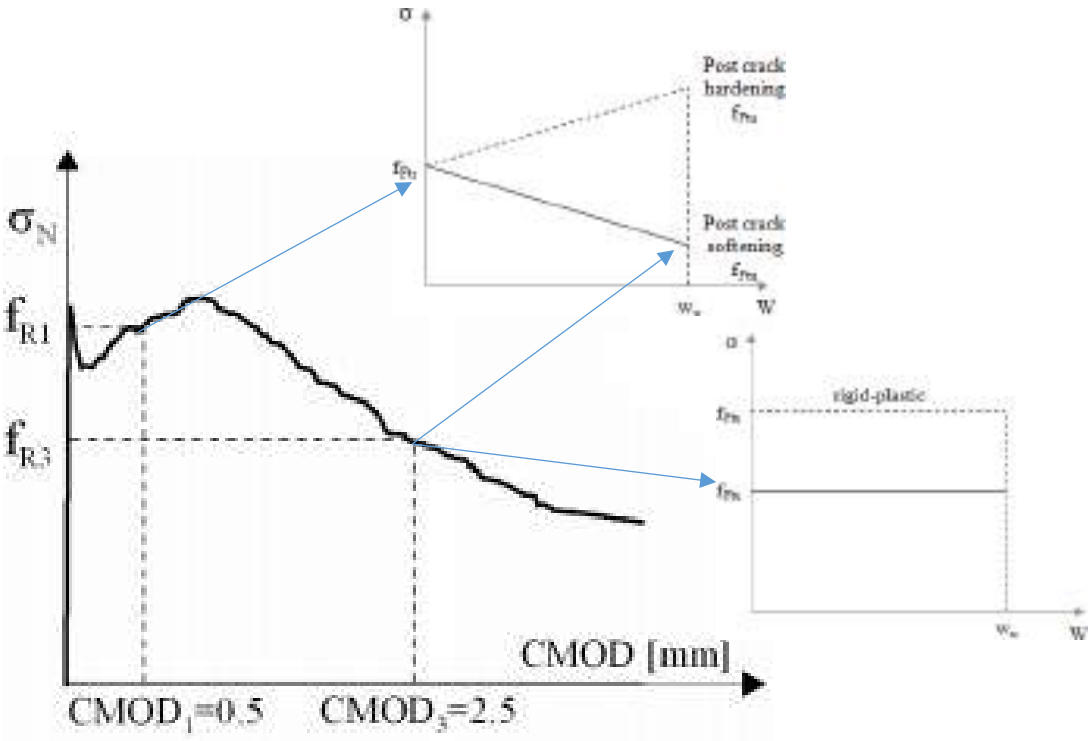

Figure 2.22: a softening and hardening material behaviour for FIB model code.

To determine the serviceability residual strength f_{Fts}:

$$f_{Fts} = 0.45 f_{R1} \qquad \textit{Equation 2-54}$$

To determine the ultimate residual strength f_{Ftu}:

$$f_{Ftu} = f_{Fts} - \frac{W_u}{CMOD3}(f_{Fts} - 0.5f_{R3} + 0.2f_{R1}) \geq 0 \qquad \textit{Equation 2-55}$$

Where

W_u is the ultimate crack opening accepted in structural design, can determine as:

$$W_u = \varepsilon_{Fu} l_{cs}$$

$\varepsilon_{Fu}$is assumed to be equal to 2% for variable strain distribution in cross section and 1% for only tensile strain distribution along the cross section

$l_{cs}$is the structural characteristic length, calculated as:

$$l_{cs} = min\{S_{rm}, y\}$$

$S_{rm}$is the mean crack spacin

y is the distance between the neutral axis and the tensile side of the cross-section.

According to the FIB model code, fiber reinforcement can partially or entirely substitute for the ordinary reinforcement in the ultimate limit state, when

$$f_{R1} > 0.4f_L,\ f_{R3} > 0.2f_L$$

Where, f_L is the limit of proportionality strength.

The FIB model code is a clear stress/strain relationship to determine bending moment and axial force in the ultimate limit state as a stress block as seen in Figure 2.23. The stress distribution compression is the linear post cracking stress

distribution, and in tension is the rigid plastic stress distribution, with η = 1 and λ = 0.8 for concrete with compressive strength $f_c' \leq 50$MPa.

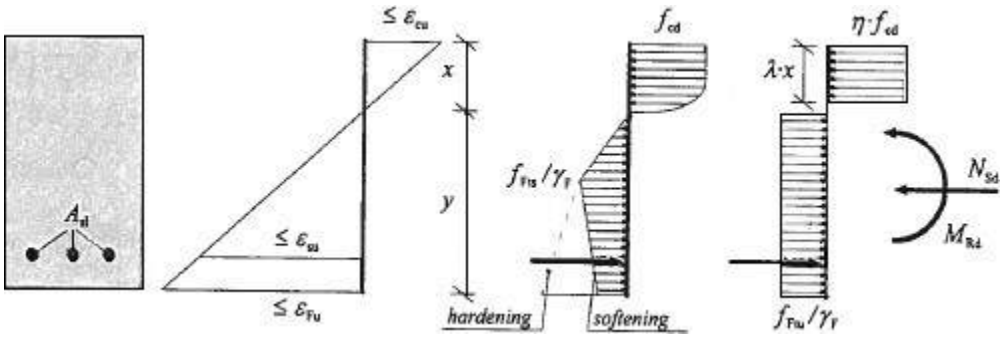

Figure 2.23: Stress block including the residual flexural tensile strength of fibers for FIB model code (CEB/FIP Model MC90, 1999).

According to FIB model code, the flexural cracking moment was calculated as:

$$M_{cr} = \frac{bh^2}{6} f_{ctm} \qquad \textit{Equation 2-56}$$

Where, M_{cr} is the cracking moment resistance and f_{ctm} is the mean tensile strength of the concrete mix with being the width of the cross section b, and the height of the cross section h.

The moments at yielding and ultimate stage were calculated using the simplified stress-strain relationship, according to FIB model code, see Figure 2.23.

By FIB model code, The yield moment M_{yield} was calculated using the concept of linear post cracking constitutive law.

$$M_{yield} = f_{sy} A_s (d - \beta x) + f_{Ft}(h - x) b[\beta x + x_{tot} y] \qquad \textit{Equation 2-57}$$

where

f_{sy} is the yield strength of the ordinary reinforcement

β is the distance from the top of the beam to the center of the concrete compressive zone

$A_s$is the area of the ordinary reinforcement bars

d is the effective depth

f_{Ft} is the total stress of the tensile stress block from the fiber contribution

h is the height of the beam

x is the distance from the top of the beam to the neutral axis

x_{tot} is the center of gravity for the tensile zone of fiber stress, given as a percentage of the total height

y is the height of the tensile stress block

The ultimate moment resistance $M_{ult}$was calculated as:

$$M_{ult} = f_{sy}A_s(d - \beta x) + f_{Ft}(h - x)b[\beta x + x_{tot}y]$$

The corresponding curvatures ∅ were calculated as:

$$\emptyset_c = \frac{\varepsilon_c}{x} \qquad \textit{Equation 2-58}$$

where x is h/2 for the elastic stage and ε_c is the strain in tenssion the concrete was calculated as:

$$\varepsilon_{cr} = \frac{f_t}{E_c} \qquad \textit{Equation 2-59}$$

$$\varepsilon_{c2} = \frac{\varepsilon_{sy}}{(\frac{d-x}{x})} \qquad \textit{Equation 2-60}$$

Where, $\varepsilon_{sy}$is the yield strain of the ordinary reinforcement and ε_{cr} is the strain at cracking concrete.

2.3.5 Design according to Spanish Guidelines (EHE-08)

EHE-08 is the Spanish code on structural concrete (the abbreviation for Instrucción de hormigón structure 2008). EHE-08 guidelines determine the moment and check the crack width in serviceability limit state.

The Spanish guideline EHE-08 have the same assumptions as FIB model code and RILEM TC-162 regarding the concept of linear post cracking distribution for the residual tensile strength. According to EHE-08, the design residual tensile strengths $f_{ctR1,d}$and $f_{ctR3,d}$ and their corresponding strains are determined using the multi-linear stress strain diagram shown in Figure 2.25.

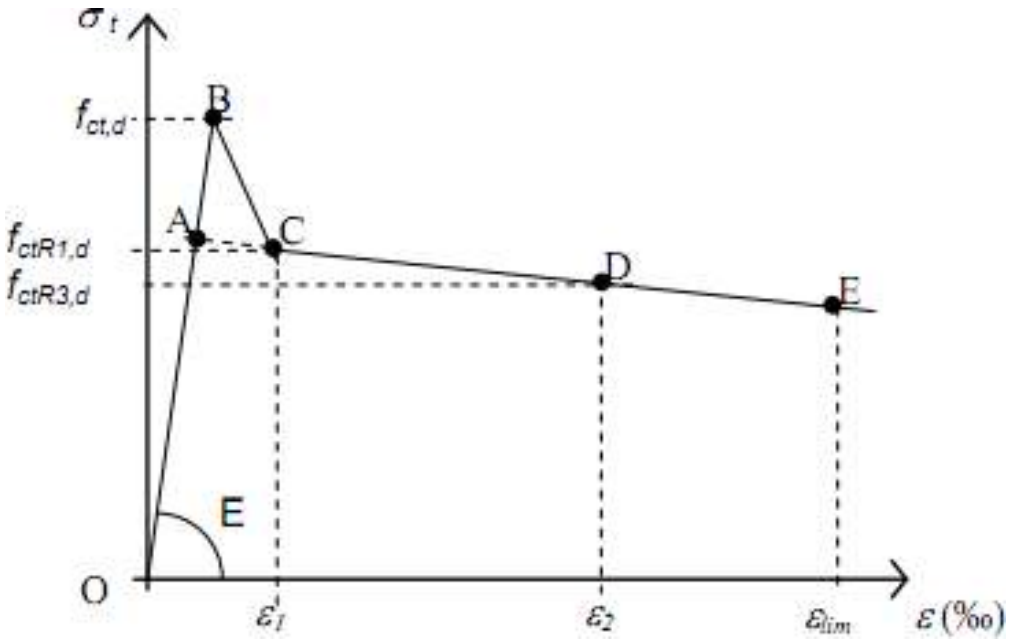

Figure 2.24: Multi-linear stress-strain diagram, from EHE-08 (EHE, 2008).

The values of residual tensile strengths are expressed as:

$$f_{ct,d} = 0.6 f_{ct,fl,d} \qquad \textit{Equation 2-61}$$

Where $f_{ct,fl,d}$is the design value of the flexural tensile strength.

The values of design residual tensile strength are expressed as:

$$f_{ctR1,d} = 0.45 f_{R1d} \qquad \textit{Equation 2-62}$$

$$f_{ctR3,d} = k_1(0.5 f_{R3d} - 0.2 f_{R1d}) \qquad \textit{Equation 2-63}$$

Where, f_{R1d} and f_{R3d} are the design residual flexural strength at$\varepsilon_1 and\ \varepsilon_2$, respectively and $k_1 = 1$ for sections subjected to bending and 0 for sections subjected to tension.

$$\varepsilon_1 = 0.1 + \frac{1000\, f_{ct,d}}{E_c} \qquad \textit{Equation 2-64}$$

$$\varepsilon_2 = \frac{2.5}{l_{cs}} \qquad \textit{Equation 2-65}$$

l_{cs} is the critical length of the element as:

$$l_{cs} = \min(s_m, h - x)$$

Where, s_m is the mean distance between cracks and h-x is the distance from the neutral axis to the highest tension end. In addition, $s_{lim} = 20 \times 10^{-3}$ for sections subjected to bending, and 10×10^{-3} for sections subjected to tension.

The Spanish guideline EHE-08 is calculated of the moment resistance as:

$$A_s f_{yd} + \frac{z_f}{z} A_{ct} f_{ctR,d} \geq \frac{w_1}{z} f_{ctm} \qquad \textit{Equation 2-66}$$

This equation guarantees that no brittle failure occurs.

So, $\frac{z_f}{z} A_{ct} f_{ctR,d}$ are the fiber contributions and $A_s f_{yd}$ are the reinforced contributions.

Where:

z_f is the lever arm for the tensile zone; A_{ct} is arean a of the tensile zone

$f_{ctR,d}$ is the design resi ofdual tensile strength; f_{yd} is the design value of the tensile strength of passive reinforcement; f_{ctm} is the mean flexural tensile strength.

A_s is the area of the passive reinforcement; z is the lever arm of the section

w_1 is the section modulus

3 Chapter 3 Experimental Work and Database of Other Researches

3.1 Introduction

Fiber reinforced concrete (FRC) has become increasingly popular as more and more owners rely on it to improve the service life of their concrete structures. In this dissertation, the data of new parameters, equations and design, and analysis models collected by experimental work and database of others researches are presented.

3.2 Experimental Investigation

Three main categories of tests characterized by different set-ups are used to evaluate the compression and tension behavior: Uni-axial compression tests, elastic modules test, compression strength test, and four-point loading flexural beam tests.

An experimental study had been conducted to improve the compression and tension behavior for FRC using five types of fiber, two-volume fractions, and two C/S ratios. The materials used, in addition to mixture and specimen preparation and test methods, are described in details below.

This investigation included 21 different mixes from which 4×8 inch cylinder specimens, 3×6 inch cylinder specimens, and 6×6×24 inch beam specimens were cast. Fresh concrete tests including slump tests were performed. Hardened concrete tests performed on cylinders at standard time intervals included

compression tests and modulus tests. Finally, a four-point bending test was performed on flexural beam specimens.

3.2.1 **Materials**

3.2.1.1 Fibers:

In this dissertation, five types of fiber were used to investigate their effects on mechanical properties of FRC consisting of steel end hooked, polypropylene, and polyolefin, two types of PVA and basalt fibers, see Figure 3-1. The fibers had varying diameters and length between 0.035 and 0.15 in. (1 to 4 mm), and 0.25 to 1.9 inch. (6 to 48 mm), respectively. Their tensile strengths ranged between 44 and 165 ksi (552 and 1655 MPa). Their physical properties are summarized in Table 3-1.

Figure 3-1: five types of fiber reinforced concrete.

Table 3-1: Physical properties of fibers.

Properties	Types of Fibers					
	Steel	**PVA150**	**PVA240**	**Polypropylene**	**Polyolefin**	**Basalt**
Specific Gravity	7.8	1.3	1.3	0.91	0.91	2.67
Cut Lengths in. (mm)	1.5 (38.1)	0.75 (19)	0.25 (6.35)	0.75 (19)	1.9 (48.26)	0.6 (15.24)
Diameter in. (mm)	0.035 (0.9)	0.0079 (0.2)	0.001 (0.25)	0.03 (0.762)	0.1 (2.54)	0.15 (3.81)
Tensile Strength ksi. (MPa)	165 (1138)	150 (1034)	240 (1655)	44 (303.4)	80 (552)	-
Flexural Strength ksi. (GPa)	29,000 (200)	4200 (29)	5500 (38)	700 (4.825)	1160 (8)	-
Color	Gray	White	White	White	Natural	Brown
Water Absorption	Nil	<1% by Weight	<1% by Weight	Nil	Nil	<1% by Weight

3.2.1.2 Cement:

A 3.15 a specific gravity of type I/II Portland cement was used in all mixtures depending on ASTM C18827.

3.2.1.3 Aggregate:

The crushed limestone of coarse aggregate with a relative density of 2.47 was used in all mixtures with one type of a maximum size of 0.75 in (19 mm) that conformed to the ASTM C 3328 specification. The absorption value for limestone was calculated using ASTM C127 and determined to be 1.27 percent. The bulk specific gravity calculated following ASTM C127 is 2.61 (ASTM 2012a), see Table 3-2.

Table 3-2: a sieve analysis of coarse aggregate.

Sieve #	ASTM #67 Average:	ASTM/FDOT Specs:
1"	100	100-100
3/4"	96.2	90-100
1/2"	68	
3/8"	33.7	20-55
#4	3	0-10
#8	1.8	0-5
FM	6.59	
-200	0.25	0 - 1.75
L.A.	35	Max. 45%

Natural sand with a relative density of 2.63 was used as the fine aggregate. The fineness modulus was calculated from a sieve analysis and was determined to be 2.23. The absorption value for sand was calculated using ASTM C128 at 0.2

percent. Bulk specific gravity was calculated following ASTM C128 and was determined 2.6 (ASTM 2012b). The specification is FLDOT Silica Sand, see Table 3-3.

Table 3-3: a sieve analysis of fine aggregates (sand).

Sieve #	
#4 (4.75mm)	100.00
#8 (2.36mm)	99.91
#16 (1.18mm)	94.12
#30 (0.6mm)	60.00
#50 (0.3mm)	20.28
#100 (0.15mm)	2.22
#200 (75μm)	0.18
Pan	0.00
-#200 (75um)	0.24
Color	2
Total Moisture	3.1
FM	2.23
Absorption (Fine)	0.2

3.2.2 Mixture

Two different mixtures consisting of ordinary concrete, FRC, and FCC were made. All mixtures had the same water-to-cement (w/c) ratio of 0.45. The mixture without any discrete fibers added was used the as a control concrete mixture. The controlled concrete mixture of FRC contained 28% natural sand and 40% crushed limestone with a C/S weight ratio of 1.35. In FRC mixtures the

portions of crushed limestone of the same controlled concrete mixture were replaced with discrete fibers. In the FRC, two fiber volume fractions were used in mixtures consisting of 0.5% and 0.8%. Crushed limestone was not used to enhance the strain-hardening property of the FRCC mixtures, but high volume fractions of fiber consisting of 1.5% and 2% were used instead. The mixture volume proportions of the FRC and FRCC are provided in Table 3-4.

Figure 3-2: Mixing of FRC and FRCC.

Table 3-4: mixing ratio for FRC and FRCC.

	FRC			FRCC		
	Control	**Mix (Vf=0.5%)**	**Mix (Vf=0.8%)**	**Control**	**Mix (Vf=1.5%)**	**Mix (Vf=2%)**
Fine Aggregate	28	27.9	27.8	33	32.5	32.4
Coarse Aggregate	40.1	39.9	39.7	----------	----------	----------
Cement	12.8	12.7	12.7	29.2	28.7	28.6
Water	18.1	18	18	36.8	36.3	36
Air content	1	1	1	1	1	1
Vf%	0	0.5	0.8	0	1.5	2

3.2.3 Specimens Preparation

The concrete was mixed by ASTM C19229 specification using a 1.7 ft3 (0.05 m3) laboratory mixer. First, all raw materials except the discrete fibers were added to the mixer and thoroughly mixed for about 3 minutes. Then, the mixture was rested for 3 minutes, followed by a 2-3 minutes final mixing where the fibers were added gradually to ensure even distribution into the mixture. Ten 4 × 8 in. (100 × 200 mm) Cylinders and two beams were cast in three layers using a vibrator to consolidate the concrete. All mixture of 21 beams were notched using a

conventional circular Table saw equipped with a diamond blade. The width of the notch was about 25 inch, and the depth was about 1/3 inch. A typical notched beam is shown Figure 3-3.

The plastic sheet membranes were used to cover concrete specimens and kept at room temperature (74°F (23°C)) for 24 hours, after which the specimens were removed from the molds and cured in water for seven days followed by air-dried curing at the same ambient temperature, see Figure 3-4.

Figure 3-3: notched beam.

Figure 3-4: Specimens preparation of FRC and FRCC.

3.2.4 Test Method

Fresh concrete tests including slump tests were performed. Then, the elastic modulus and compressive strength tests were performed by ASTM C469 and C39 specifications, respectively. Finally, a four-point bending test was performed on flexural beam specimens.

3.2.4.1 Slump test

Because discrete fibers impact the workability of FRC and FRCC, we evaluated their workability of fresh mixtures by using standard slump cone test by the ASTM C143 (ASTM 2012c) specification. The slump cone was filled with fresh FRC and FRCC by thirds of its volume by attaching the cone to the base plate. For each third of its volume, the FRC and FRCC were tamped 25 times. After that, excess concrete protruding from the top of the cone was scraped off. Then the slump cone was slowly raised to a vertical position over the fresh cone of FRC and FRCC.

The distance that evaluates from the top of the slump cone to the top of the center of the concrete on the base plate was determined as the slump value for FRC and FRCC mix. Superplasticizer was also used on some of the mixtures to ensure that all mixtures had a slump of approximately 2.75 inch (75 mm), see shown in Figure 3-5.

Figure 3-5: Slump cone test with the ASTM C143.

3.2.4.2 Compressive Strength Test

All cylinders were ground at both ends before testing to remove any surface irregularity as well as ensure both of ends to be perpendicular to the sides of the specimen. Compressive strength test on the 4 x 8 cylinders was measured using a Forney Automatic Testing Machine with a capacity of 325000 Ibs according to ASTM C39 [25], see Figure 3-6. The loading rate of the test was approximately 35 Psi/sec was applied to the cylinder until failure. For each of the 21 mixes conducted, three cylinders were tested in compression on 28 days.

Figure 3-6: Compressive strength test.

3.2.4.3 Elastic Modulus Test

The cylinders (150 by 300mm) were ground at both ends before testing to remove any surface irregularity to ensure the ends to be perpendicular to the sides of the specimen. Elastic modulus and compressive strength cylinders were

measured using a Forney Automatic Testing Machine with a capacity of 325000 Ibs according to ASTM C469. Tests were carried out at a loading rate of approximately 35 Psi/sec. Deformations were measured using one set of linear voltage differential transducers attached to two fixed rings (see Figure 3-7). The apparatus consisted of two aluminum rings with screws for attachment to the specimen. The spacing between screws on the top and bottom rings was (4 inch) 150mm for (4× 8inch) 150 by 300mm cylinders, which served as a gauge length for calculating axial strain from the measured deformations.

The elastic modulus is defined as a chord modulus from the stress-strain curve with a first point at a strain of 0.00005 ($\varepsilon 1$) and second point at 40% of the maximum stress as follows: Stress and strain must be simultaneously recorded at a constant loading rate in accordance with ASTM C 469. The loading/unloading cycles are carried out at 40 percent of the ultimate compressive strength; the modulus of elasticity of the tested concrete is calculated automatically by machine as the average of the slopes of the two ascendant parts of the 0.4 loadings. $Ec = \frac{0.4Fc - \sigma(\varepsilon 1)}{\varepsilon(0.4\ \mathrm{Fc}) - \varepsilon 1}\ (MPa)$. For each of the 21 mixes conducted, 2 cylinders were tested in elastic modulus on 28 days.

Figure 3-7: Elastic modulus test.

3.2.4.4 Stress-block stress test

Uni-axial compression tests that provide the compression stress-strain properties for strain softening and hardening FRC materials are shown in Figure 3-8. The most common tests to characterize FRC is a cylinder test. For achieving this test is MTESTQuattro device is used, see Figure 3-9. The MTESTQuattro device

consists of load, crosshead position, axial strain, transverse strain and auxiliary input channels with options for four additional auxiliary input channels and servo control. The MTESTQuattro is an advanced material testing system for servo-hydraulic and electromechanical testing machines that consists of the application program. It features a state-of-the-art digital controller for carrying out accurate and repea Table tests according to ASTM standards. The MTESTQuattro is capable of performing many types of tests including tension, compression, and flexure tests, see Figure 3-10. For each of the 21 mixes conducted, two cylinders were tested in elastic modulus on 28 days.

Figure 3-8: Stress -block stress test

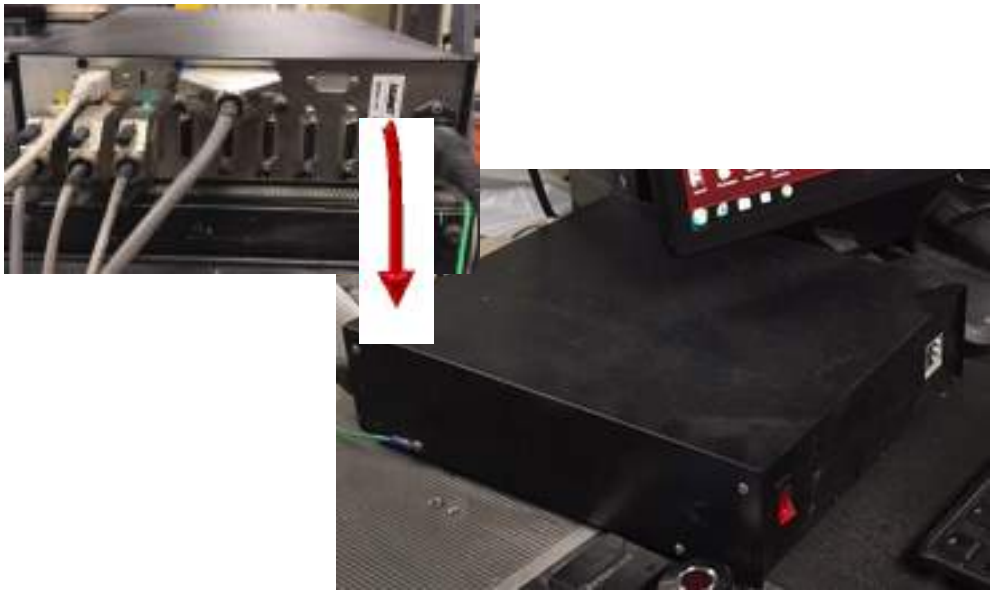

Figure 3-9: MTESTQuattro device.

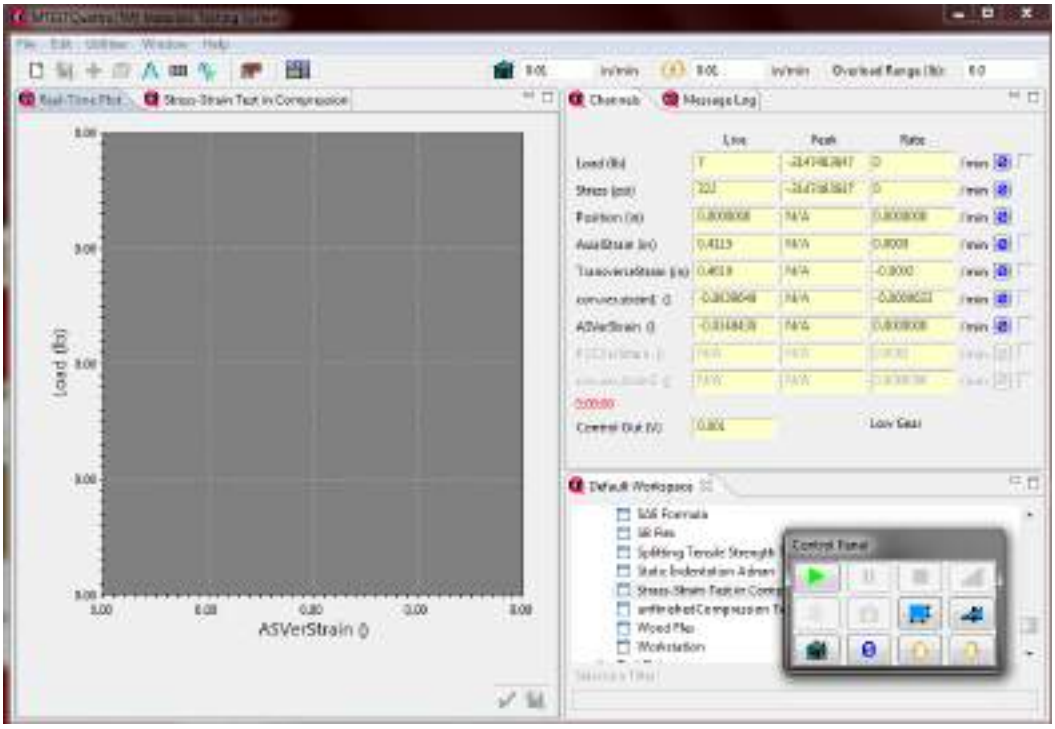

Figure 3-10: MTESTQuattro program for stress-strain block.

3.2.4.5 Flexural beam test

Flexural beam tests are the most commonly used standard test methods to determine the behavior of FRC. However, standard test methods used four-point bending loading notch configuration. Therefore, ASTM 1609 the suitability of commonly used standard flexural beam test methods is analyzed. In order to measure the displacement at mid-span of the beam specimens, the flexure test frame was used for the measurement of deflection during the flexure test on 150x150x550 mm beams. It was built in the Florida Institute of Technology workshop, and consisted of two sections: head and base, see Figure 3-11.

The average of two LVDT that represent the net mid-span deflection were mounted on a flexure test frame. Finally, a notched four-point bending test is described in the Rilem T-162 guidelines for design, construction and production control of FRC structures. In addition to that, there were two strain gauges placed on the top and bottom fiber of beams. These strain gauges were used to determine the strain in compression and tension of beams to evaluate the neutral axis and parameters of the new model.

As explained before, the MTESTQuattro program and device were used in stress-strain block test. Also, they were used in this test, as shown in Figure 3-12.

Figure 3-11: Flexural beam test.

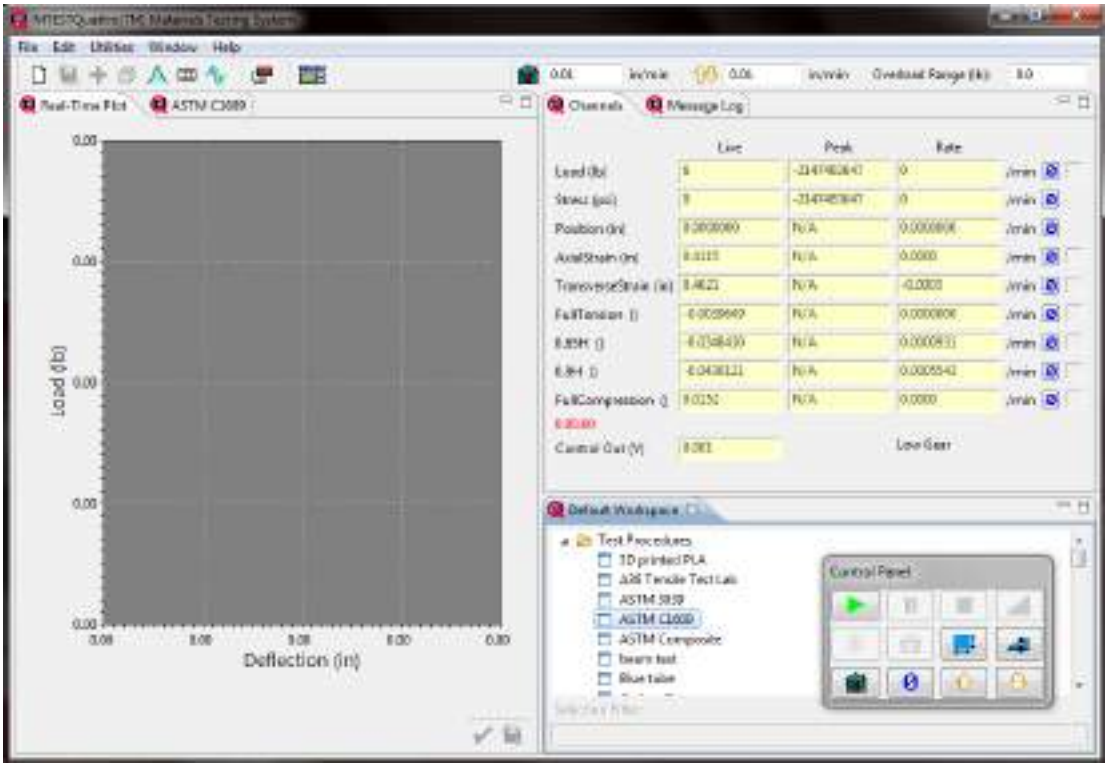

Figure 3-12: MTESTQuattro program for the flexural test.

As a summary of experimental tests, 3x6 and 4x8 inches cylinders were tested 69 and 230, respectively. For flexural tests, the number of beams that were tested was 46. The total number of tests were 345, see Table 3-5.

Table 3-5: summary of experimental tests.

	Type of Test	Time of tests		Number of cases	Sum
		7 days	28 days		
1	**Compression test for 4×8 inches**	3	3	23	138
2	**Compression test for 3×6 inches**		3		69
3	**Elastic modulus test 4×8 inches**	2	2		92
4	**Fracture test 6×6×24 inches**		2		46

3.3 Database of experimental data

For more accuracy in evaluating the impact of discrete fibers on parameters of the new analysis and design model, comprehensive stress-strain carvers and load-deflection curves database were collected using experimental results obtained from various literature listed in Tables 3-6, 3-7 and 3-8. A total of 45 kinds of literature consisting of over 1120 data points using steel, PVA, polypropylene, polyolefin, and basalt fibers were collected.

3.3.1 Database of load-deflection curves (flexural test) experimental data

Based on the experimental database results for load-deflection curves obtained from various literature listed in Table 3-6, were gathered.

This Table mentions some details as Type, aspect ratio, the volume of fraction and compressive strength of Fiber. A total of 19 sourced research consisting of over 230 data points using steel, PVA, polypropylene, and basalt fibers were collected for both FRC and FRCC mixtures. The length and volume fractions of fiber ranged from 0.12 in (3 mm) to 2.36 in (60 mm) and 0.1% to as high as 2.0%, respectively. The concrete compressive strengths were between 2,900 psi (20 MPa) and 14,500 psi (100 MPa). By these curves and experimental work of this dissertation, it is possible to determine the first crack parameters and identify the maximum load that carries the beam. This database led to checking the new analysis model, also, determining the volume fraction for the new design model.

Table 3-6: Database of load-deflection curves (flexural test).

	Reference	Type of Fiber						L_f (mm)[a]	V_f%		C/S		Strength (MPa)[b]	
		Steel	PVA	Polypropylene	Polyolefin	Polyethylene	Basalt		<1	≥1	<1	>1	f_c<50	f_c≥50
1	Mobasher et al. 2014			●				3	●			●	●	
		●						13-39	●			●	●	
2	Kanda et al. 2006	●						30,35 & 50	●	●	●		●	●
3	Kim et al. 2010	●						30		●	●			●
4	Liao et al. 2006	●						30		●	●		●	
5	Roesler et al. 2008	●						38,50&60	●			●	●	
						●		40,50&54	●			●	●	
6	Banthia et al. 1992	●						25-32.5	●		●		●	
7	Abbass et al. 2018	●						40,50&60	●	●		●	●	●
8	Jamsawang et al. 2014			●				58-75	●	●	●			
9	Sasmal et al. 2016		●					8&12		●	●		●	
10	Han et al. 2017	●						35	●	●	●		●	
11	Soutsos et al. 2017	●						50&60	●		●		●	
						●		40	●		●		●	
12	Carnovale et al. 2013	●						30,35&50	●	●	●		●	●
				●				54	●	●	●		●	●
13	Bei-Xing et al. 2004			●				13-32	●		●		●	
14	Yang et al. 2011	●						30,35&60	●	●	●		●	
			●					8 to 19	●		●		●	
15	Yoo et al. 2015	●						30	●	●		●	●	●
16	Hsie et al. 2008			●				60	●		●		●	
17	Noushini et al. 2014		●					6&12	●		●			●
18	Pliya et al. 2011	●						30		●		●		●
				●				6		●		●		●
19	Jiang et al. 2003	●						26	●			●	●	●
			●					12	●			●	●	●

3.3.2 Database of stress-strain curves (direct tension test) experimental data

The database information gathered using experimental results for tension stress-strain curves obtained from the various literature were listed in Table 3-7.

This Table mentions some details as Type, aspect ratio, the volume of fraction and compressive strength of Fiber. A total of 13 kinds of research consisting of over 155 data points using steel, PVA, polypropylene, and basalt fibers were collected for both FRC and FRCC mixtures. The length and volume fractions of fiber ranged from 0.12 in (3 mm) to 2.36 in (60 mm) and 0.1% to as high as 2.0%, respectively. The concrete compressive strengths ranged between 2,900 psi (20 MPa) and 14,500 psi (100 MPa).

By these curves and experimental work of this dissertation, it is possible to determine the first crack and ultimate strain with different types of fiber. In addition, it will easy to evaluate the neutral axis and moment capacity. This database led to checking the new analysis model, to determine the volume fraction for the new design model.

Table 3-7: Database of stress –strain curves (direct tension test).

	Reference	Type of Fiber						L_f (mm)[a]	V_f%		C/S		Strength (MPa)[b]	
		Steel	PVA	Polypropyle	Polyolefin	Polyethylen	Basalt		<1	≥1	<1	>1	f_c<50	f_c≥50
1	Kanda et al. 2006		●					6,12		●	●		●	
						●		6		●	●		●	
2	Kim et al. 2010	●						30		●	●			●
3	Liao et al. 2006	●						30		●	●		●	
4	Meng et al. 2006	●						30-32	●	●		●		
5	Choun et al. 2015	●						30		●	●	●	●	
6	Kanda et al. 1998		●					4&12		●	●			
7	Li et al. 1995					●		12.7		●	●		●	●
8	Ahmed et al. 2009	●						13		●	●			
						●		12		●	●			
9	Kim et al. 2008	●						30		●	●			
10	Ayub et al. 2018		●					30		●	●	●		●
							●	25		●	●	●		●
11	Wang et al. 1990					●		5-12.7		●	●			
12		●						30						
						●		38		●	●			
13	Carnovale et al. 2013	●						30,35&50	●	●	●		●	●
				●				54	●	●	●		●	●

3.3.3 Database of stress-strain curves (stress block test) experimental data

Based on the database gathered using experimental results for compressive stress-strain curves obtained from the various literature were listed in Table 3-8.

Table 3-8: Database of experimental data.

	Reference	Type of Fiber				Sp	$V_{f'_0}$		Strength (MPa)[b]		
		Steel	PVA	Polypropylene	Basalt		<1	≥1	f_c<50	50≤f_c<100	f_c≥100
1	Altun et al. 2007	*				80	*		*		
2	Mansur et al. 1999	*				50 and 60	*	*		*	*
3	Yang 2011	*				35, 60 and 82	*	*	*		
			*			533,800,1000,and 1267	*		*		
4	Yoo et al. 2015	*				60	*	*	*	*	
5	Lee.et al 2015	*				45,65 and 80	*	*	*	*	
6	Ou 2012	*				50,60,70 and 100	*	*	*		
7	Ezeldin et al. 1992	*				60,75 and 100	*		*	*	
8	Fanella and Antoine 1985	*				47,83,and 100	*		*		
				*		100 and 250		*	*	*	
9	Oliveira et al. 2010	*				64	*		*	*	
10	Poon et al. 2004	*				60	*			*	
				*		60 and 360	*			*	
11	Bhargava et al. 2006	*				60	*	*	*	*	
12	Neves and Almeida 2005	*				55 and 80	*	*	*	*	
13	Lin and Hsu 1994	*				60	*	*	*		
14	Ayub et al. 2015				*	1389		*		*	
15	Bencardino et al. 2007	*				40	*	*		*	
16	Dhakal et al. 2005	*				47, 64, 83 and 100	*	*	*		
17	Altun et al. 2006	*				80	*		*		
18	Ünal et al. 2007	*				60 and 80	*		*		
19	Srikar et al. 2016			*		35	*		*		
20	Şahmaran et al. 2011		*			308		*		*	

Table 3-8 mentions some details as Type, aspect ratio, the volume of fraction and compressive strength of Fiber. A total of 20 kinds of research

consisting of over 250 data points using steel, PVA, polypropylene, and basalt fibers were collected for both FRC and FRCC mixtures. The length and volume fractions of fiber ranged from 0.20 in (5 mm) to 2.36 in (60 mm) and 0.1% to as high as 3.0%, respectively. The concrete compressive strengths were between 2,900 psi (20 MPa) and 17,400 psi (120 MPa).

4 Chapter 4 Theoretical Analytical

4.1 Theoretical determining for compression stress block

To determine the stress block in the compression part, it should be obtained from stress-strain curves in compression. From 250-points database from previous research that explained the stress-strain curves in compression for different types of fiber and volume fraction for both FRC and FRCC, it was easy to determine the stress block through determining the parameters study. These parameters depended on yield strain, ultimate strain, and elastic modulus. This dissertation used the Sukawang equation to determine the elastic modules for FRC and FRCC.

4.1.1 Yield Strain

The yield point represents the end of the elastic range of behavior. This behavior is represented by the elastic modulus. The elastic modulus is the slope of stress-strain relationship that it is the triangle shape.

In ACI 544 the yield compressive strength for FRC is adopted as:

$$\sigma_{cy} = 0.85 f_c' \qquad \textit{Equation 4-1}$$

Therefore*;*

$$\varepsilon_{cy} = \frac{0.85 f_c'}{E_c} \qquad \textit{Equation 4-2}$$

$$\varepsilon_{cy} = \frac{0.85 f_c'}{4700\sqrt{f_c'}} \qquad \textit{Equation 4-3}$$

Then

$$\varepsilon_{cy} = 0.00018\sqrt{f_c'} \text{ (MPa)}$$

$$\varepsilon_{cy} = 0.000015\sqrt{f_c'} \text{ (Psi)}$$

Equation 4-4

The new equation depends on the concept of elastic behavior that the yield strain is equal to the slope of the yield strength- elastic modules of the stress-strain curve, as shown in Figure 4.1. The equation below determines the yield strain for FRC by determining factor α to account for the influence of additional fibers in concrete.

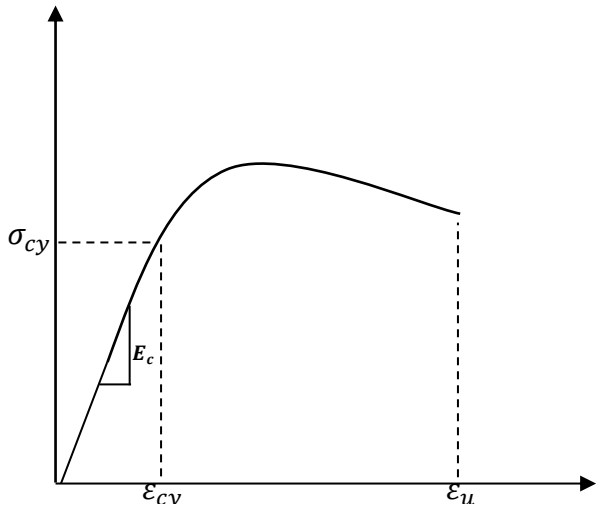

Figure 4-1: Yield strain for FRC.

$$\varepsilon_{cy} = \frac{\alpha . f_c'}{E_c}$$

Equation 4-5

This research adopted the Suksawang 2018 equation for elastic modulus of FRC and FRCC.

4.1.2 Ultimate Strain

An elastic-perfectly plastic model defines the compression model. Since the compressive behavior of FRC will not vary significantly from that of normal concrete or concrete without fibers, the same concept can be used for FRC in compression. Some data indicate 0.003 may be conservative. Williamson (1973) and Pearlman (1979) suggest the ultimate strain for steel fiber concrete is 0.0033, and Swamy and Al-Ta'an (1981) suggest 0.0035. Hassoun and Sahebjam (1985) suggest a failure strain of 0.0035 for concrete with 1.0 percent steel fibers and 0.004 for 1 to 3 percent fibers based on a study of plastic hinges (Ahmad et al., 1988).

According to the RILEM model16, the ultimate compressive strain ε_{cu} is limited to 0.0035, which is the lower bound value of typical SFRC (Soranakom and Mobasher, 2009). The value of ultimate strain is taken as 0.0035, instead of 0.003 recommended in ACI 363R-92 and ACI 318-14, based on the results of compressive strain corresponding to the maximum compressive strength. Canadian standard CSA and European standard Eurocode 2 also suggest the value of ultimate strain as 0.0035. It has been reported that fiber-RC can sustain a strain value of 0.005–0.006 at failure, and the corresponding failure stress improves to $0.9f_c'$ from $0.85f_c'$, where f_c' is the cylinder strength (Lim et al. 1987). Accordingly, the maximum design flexural stress of fiber-RC can be taken as $0.5f_c'$ by applying a

partial safety factor of 1.5, and the corresponding ultimate strain can be taken as 0.004 (Singh, 2014).

Based on the experimental work and the other researcher's database, this dissertation will check a volume fraction of fiber affected by the ultimate strain. The value for the ultimate strain was chosen as a lower bound on the test data that will be given the safer design for FRC.

4.1.3 Model Analysis

The proposed relationships also validated and confirmed for fiber reinforced concrete compressive strengths up to 18 ksi using statistical and parametric analyses. For design purposes, however, the following additional assumptions are introduced to simplify the problem with little loss of accuracy. There are three types of stress block in the compression part. The traditional type of stress block that is used in design and analysis reinforced concrete in ACI code is rectangular. Also, the trapezoid shape is used for design and analysis fiber reinforced concrete that is adopted by ACI 544. The third type of stress block is triangular. In this research, it passed the rectangular and trapezoid stress block. However, it did not use the triangular stress block because of a constant of a center of gravity which did not appear sufficient for FRC.

Based on the researches in the literature, the rectangular stress block parameters also decrease as the concrete compressive strength increases.

4.1.3.1 Rectangular Stress Block

Emperger first proposed the theory of equivalent rectangular stress distribution and it was modified by **Whitney** for application to Ultimate Strength Design (USD). Simplicity stress block replaces the actual curve stress shape. Stress block appears to be entirely satisfactory and gives the most straightforward possible mathematical solution that would provide roughly the same 1) area and 2) center of gravity.

Since the assumed compressive stress distribution has no exact theoretical basis, the stress block parameters (K_1, K_2, and K_3) and coefficients for ACI rectangular stress block (α1 and β1)must be determined experimentally.

The stress-strain relationships were selected to derive the coefficients K_1 and K_2. Since the proposed compressive stress-strain model for the ascending branch is an indefinite integral, the area under the curve and the centroid of the area for all types of FRC up to the ultimate compressive strain $\varepsilon_{Ult.}$is estimated with the help of trapezoidal rule. The centroid of the area relative to extreme fiber strain yielded coefficientK_2. The coefficient K_1 was determined such that the area of the compressive stress-strain relationship was set equal to an equivalent rectangular stress distribution over the entire compressive zone. The estimated areas were under the curve and the centroid of areas for all FRC, using experimental results and proposed compressive stress-strain relationships.

The K_1 and K_2 values can be obtained from the equilibrium of the external and internal forces, as follows:

$$K_2 = \varepsilon_{Ult.} - \frac{Moment\ under\ stress\ strain\ curves\ to\ netural\ axies}{Area\ under\ stress\ strain\ curves} \qquad \textit{Equation 4-6}$$

$$K_1 = \frac{Area\ under\ stress\ strain\ curves}{\varepsilon_{Ult.}} \qquad \textit{Equation 4-7}$$

The proposed rectangular of compressive stress block is defined by a width equal to $\alpha f c'$ and depth as $\beta.\varepsilon_u$, as done in ACI 318-14. The proposed rectangular compressive stress block is shown in Figure 4.2.

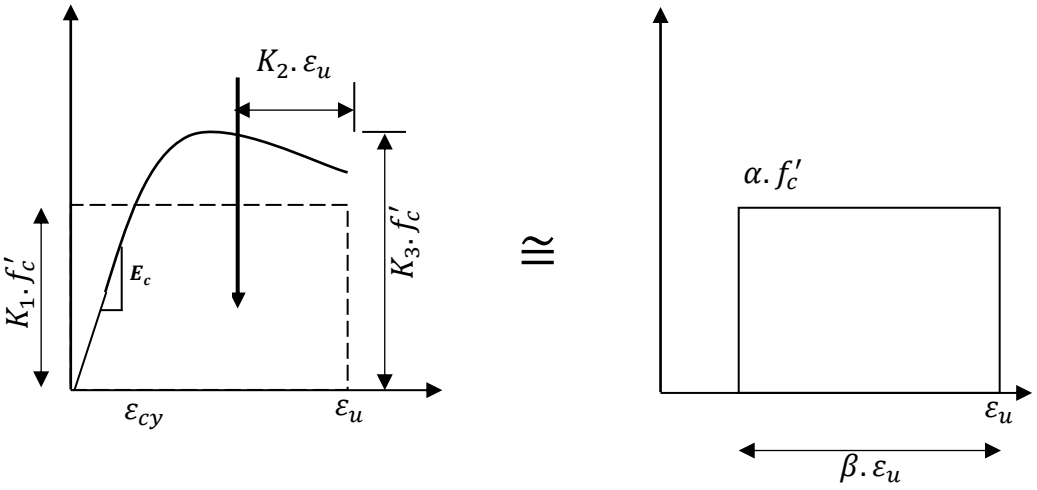

Figure 4-2: Rectangular stress block for proposal model.

Based on the other researcher's database, a volume fraction of fiber affected β. The value for $\beta_1$was chosen as a lower bound on the test data. The

internal moment arm of the compression force in the concrete at the centroid axis of a rectangular is $\left(\varepsilon_{Ult.} - \frac{\beta_1.\varepsilon_{Ult.}}{2}\right)$. If β_1 is too small, the moment arm will be too large, and the moment capacity will be overestimated. This error is already corrected by using the lower bound of the ultimate strain that will be led to decrease the moment arm.

Based on the other researcher's database, a volume fraction of fiber affected $\propto$. The value for $\propto$ was chosen as a lower bound on the test data so that it will give a safer design for FRC.

To the derivations for neutral axis depth ratio k, normalized moment m, and normalized curvature ϕ, it important to know the stress block parameters for each stage of compression behavior of FRC. Therefore this dissertation determined the stress block parameters for four ranges of applied top compressive strain $\varepsilon_c < \varepsilon_{cy}$, $\varepsilon_c = \varepsilon_{cy}$, $\varepsilon_{cy} < \varepsilon_c < \varepsilon_{Ult.}$, and $\varepsilon_c = \varepsilon_{Ult.}$. The location of the neutral axis parameter k is derived by solving the equilibrium of internal forces. The moment was computed by taking the force of the neutral axis, while the curvature is obtained by dividing top compressive strain with the depth of neutral axis.

4.1.3.2 Trapezoid Stress Block

An idealized constitutive model has been assumed for concrete in this study, as shown in Figure 4-3 to simplify equations. In this model, a bilinear elastic-perfectly plastic stress-strain response has been assumed in compression

where the linear portion of response terminates at a yield point (∝fc', ε_{cy}) and remains constant at compressive yield stress until the ultimate compressive strain $\varepsilon_{Ult.}$, see equation below. The concrete constitutive model has been assumed as a bilinear elastic-perfectly plastic stress-strain response in compression.

$$f_c = \begin{cases} E.\varepsilon_c & for \quad 0 < \varepsilon_c < \varepsilon_{cy} \\ \propto.f_c' & for \quad \varepsilon_{cy} \le \varepsilon_c \le \varepsilon_{ult} \end{cases} \qquad \textit{Equation 4-8}$$

To the derivations for neutral axis depth ratio k, normalized moment m, and normalized curvatureϕ in the trapezoid stress block.

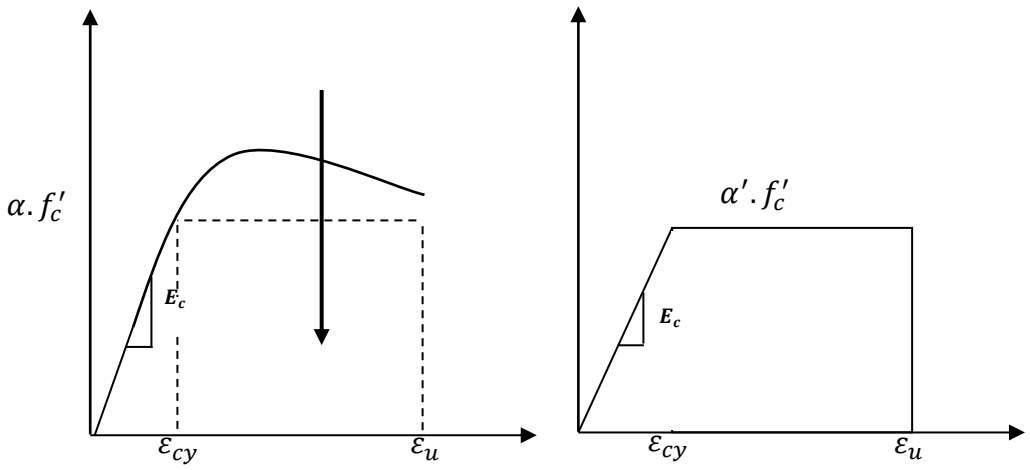

Figure 4-3: Rectangular stress block for proposal model.

4.2 Compression vs. Tension Modulus

Much of the research assumes that the elastic modulus in the tension test for the concrete material is the same of elastic modulus in the compression test. That is

accurate for concrete without fiber due to homogeneous in concrete material. Occasionally in FRC, the elastic modulus in the tension test for the concrete material is not the same as the elastic modulus in the compression test (Naaman et al., 1992).

There are four reasons for these differences between the tension and compression test results, as follows:

First, the tension specimens are sometimes not fully homogeneous especially when lower volume fractions of fiber due to orientation and distribution of fiber. Second, many researchers explain that fiber does not affect compression strength; on the contrary, tension strength fibers were aligned primarily parallel to the direction of loading, whereas the fibers in the compression specimens were aligned randomly in the direction of loading. Third, another reason is the difference in specimen size, shape, and testing configurations (Naaman et al., 1992). Fourth, the nonlinear behavior of the concrete will result in different values of elastic modulus depending on the stress range (Naaman et al., 1992).

Therefore, the design of FRC should also be pointed out of these differences between the tension and compression test results.

A simplified design equation of FRC was made by determining the factor (γ) that normalized elastic modulus by divideding the elastic modulus of compression by the elastic modulus of tension.

So,

$$\gamma = \frac{E_c}{E_t} \qquad \textit{Equation 4-9}$$

E_c = Elastic modules in compression (= $\frac{f_c}{\varepsilon_c}$),

E_t = Elastic modules in tension(= $\frac{f_t}{\varepsilon_t}$).

Flexural Stress (f_t): The maximum stress of the test specimen occurs at the midpoint of a simple beam supported at two points and loaded at the midpoint.

$$\sigma_f = \frac{PL}{bd^2} \qquad \textit{Equation 4-10}$$

Where:

f_t = stress in the outer fibers at the midpoint, MPa (psi),

P = load that at a given point on the load-deflection curve, N (lbf),

L = support span, mm (in.),

b = width of beam tested, mm (in.), and

d = depth of beam tested, mm (in.).

Flexural Strain (ε_t)*:* the change in the length of an element of the test specimen at midspan of the bottom beam, where the maximum strain occurs. ASTMD790, ε_t= strain in the outer surface, mm/mm (in./in.),

$$\varepsilon_f = \frac{6Dd}{L^2} \qquad \textit{Equation 4-11}$$

D = maximum deflection of the midspan of the beam, mm (in.),

Elastic modulus considers the slope of the stress-strain curve within the elastic limit. It is calculated by drawing a tangent to the steepest initial straight-line portion of the load-deflection curve and using Eq6 in 12.5.1 (for highly anisotropic composites, see Note 9). ASTMD790

$$E_t = \frac{PL^3}{6bd^2D}$$ *Equation 4-12*

Where:

E_t = modulus of elasticity in bending, MPa (psi),

4.3 Theoretical determination for tension stress block

To determine the stress block in the tension part, it should be obtained on stress-strain curves in tension. The flexural strength test and direct tensile strength test give a good view of the behavior of softening and hardening deflection and softening and hardening strain. Experimental studies of others research have been performed on FRC and FRCC and showed that the residual flexural strength is typically between twice its residual tensile strength (Vandewalle 2003) (Naaman 2007). For this reason, the residual flexural strength cannot be a substitute for residual tensile strength in design FRC and FRCC, for the post-crack tensile strengths are required for design purposes. Because of elastic behavior, the first crack strength can be determined from both the flexural strength test and the direct tensile strength test.

Stress block was evaluated by using 21 case studies from experimental work and around 250 curves from the flexural test, in addition to more than150 curves of tensile test for different types of fiber and volume fraction for both FRC and FRCC. This data analysis used four steps to achieve a good model for stress block. The first step was to determine the stress-strain curves from a flexural test of experimental work. The second step was to evaluate the parameters study of stress block. These parameters are a first crack strength, first crack strain, the elastic modulus in tension, and ultimate strain. The third step was evaluated in the analysis model. The last steps were evaluated in the design model.

4.3.1 Determine the stress-strain curves from a flexural test of experimental work

By getting the load-strain curves and load-deflection curves results as explained in Chapter 3, then the tension theoretical is determined as three regions.

1- The first region is design and analysis FRC & FRCC before /and at first Crack, explained by an elastic modulus E and first cracking (ε_{cr}).

2- The second region is design and analysis FRC & FRCC after cracking in tension and before cracking in compression, defined by strains at compression yield (ε_{cy}) and tensile strength which is used to simulate the behavior of the softening and hardening strains.

3- The third region in the tensile model is design and analysis FRC & FRCC after cracking in tension and compression, defined by strains at

compression yield (ε_{cy}) and tensile strength which is used to simulate the behavior of softening and hardening strains, in addition to the ultimate tensile strain level of ε_{tu}.

After that, the first step is to determine the neutral axis through the result of strain in fiber compression and strain in fiber tension for each region.

The second step determines the tension stress at any point f_{ti} that was by equal to the moment of resistance to tension stress block of elastic and tension stress block of plastic.

The third step determines compression stress for each region by balancing the force for the stress-strain curve in compression part with force for the stress-strain curve in tension part.

The fourth step determines the bending moment for each region by multiplying the force for the stress-strain curve in the compression part by the distance from the resultant of force between compression part and tension part.

Moreover, this dissertation is the development of the material models by the following assumptions:

4- linear strain distribution across the depth

5- Ignor shear deformations,

6- The tension failure first, and

7- Three stages of stress distribution across the cross section at tensile strain: $\boldsymbol{\varepsilon_t < \varepsilon_{cr}}$, $\boldsymbol{\varepsilon_c < \varepsilon_{cy}}$, $\boldsymbol{\varepsilon_t > \varepsilon_{cr}, \varepsilon_c \leq \varepsilon_{cy}}$ and $\boldsymbol{\varepsilon_t > \varepsilon_{cr}, \varepsilon_c > \varepsilon_{cy}}$.

4.3.1.1 Stress-strain curves of FRC & FRCC before and at first crack: ($\boldsymbol{\varepsilon_t < \varepsilon_{cr}}$, $\boldsymbol{\varepsilon_c < \varepsilon_{cy}}$)

As mentioned above, the elastic modulus may be different in compression than in the tension part. Therefore, when determining the neutral axis, it must the in the view the variations between the elastic modulus.

To determine the neutral axis by equilibrium, the force for the stress-strain curve in the compression part with force for the stress-strain curve in tension part.

$$\frac{\varepsilon_c}{\varepsilon_c + \varepsilon_t} f_c = \frac{\varepsilon_t}{\varepsilon_c + \varepsilon_t} f_t \qquad \textit{Equation 4-13}$$

$$\therefore \frac{f_t}{f_c} = \frac{\varepsilon_c}{\varepsilon_t}$$

So,

ε_c: Strain in compression.

ε_t: Strain in tension.

f_c: Stress in compression

f_t: Stress in tension before crack or (f_{cr}) stress at first crack.

$$f_t = \frac{P.L}{b.h^2} \qquad \textit{Equation 4-14}$$

P=load before crack or at first crack, L=span length, b=beam width, and h=beam depth.

For $E_c = E_t$

$$\varepsilon_c = \varepsilon_t, f_c = f_t, and\ \gamma = 1.0$$

For $E_c \neq E_t$

$$\gamma = \frac{f_c . \varepsilon_t}{f_t . \varepsilon_c} \qquad \textit{Equation 4-15}$$

From equilibrium the force for the stress-strain curve in the compression part with force for the stress-strain curve in the tension part, see Figure 4-4.

$$\frac{f_t}{f_c} = \frac{\varepsilon_c}{\varepsilon_t} \qquad \textit{Equation 4-16}$$

Therefore,

$$\gamma = \frac{{\varepsilon_t}^2}{{\varepsilon_c}^2} \qquad \textit{Equation 4-17}$$

Strain in compression is

$$\varepsilon_c = \frac{\varepsilon_t}{\sqrt{\gamma}} \qquad \textit{Equation 4-18}$$

Stress in compression is

$$f_c = \sqrt{\gamma} \cdot f_t \qquad \textit{Equation 4-19}$$

Neutral axis is

$$N.A = k \cdot h \qquad \textit{Equation 4-20}$$

$$k = \frac{1}{1+\sqrt{\gamma}} \qquad \textit{Equation 4-21}$$

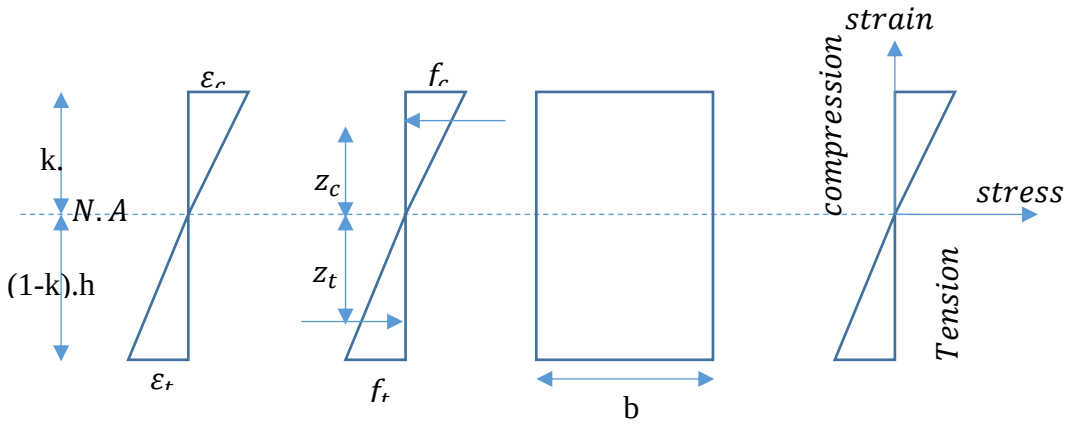

Figure 4-4: stress block and strain distributions for elastic stage.

Strain for compression and tension at any point was determined as:

$$\varepsilon_c = \frac{\sqrt{\gamma}.f_t}{E_c} \qquad \textit{Equation 4-22}$$

$$\varepsilon_t = \frac{\gamma.f_t}{E_c} \qquad \textit{Equation 4-23}$$

Bending moment was determined as:

$$M_b = \frac{(1-k)h^2 b}{3} f_t \qquad \textit{Equation 4-24}$$

4.3.1.2 Stress-strain curves of FRC & FRCC after cracking in tension before cracking in compression: ($\boldsymbol{\varepsilon_t > \varepsilon_{cr}, \varepsilon_c \leq \varepsilon_{cy}}$)

Figure 4-5 explained stress block and strain distributions after cracking for FRC and FRCC.

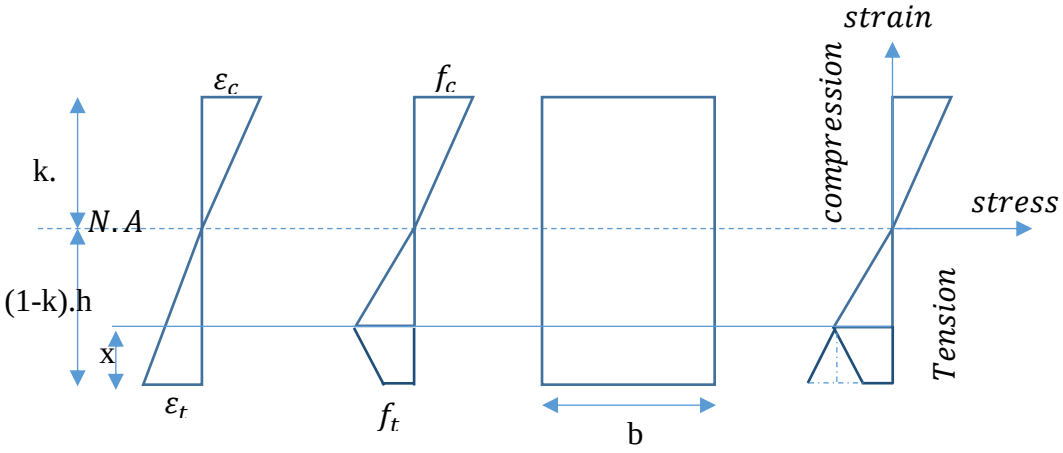

Figure 4-5: stress block and strain distributions after cracking in tension.

To change the load to stress for all points in the curves by following the procedure below:

1- Determine N.A or K

$$K_i = \frac{\varepsilon_{c_i}}{\varepsilon_{c_i} + \varepsilon_{t_i}} \qquad \textit{Equation 4-25}$$

2- Determine the stress as equal to the moment of resistance to tension stress block of elastic and tension stress block of plastic because they can carry the same load.

To determine the tension stress at any point f_{ti} that was by balancing the moment of resistance to tension stress block of elastic and tension stress block of plastic.

1- For trapezoid stress block:

The tensile strength in the cracked part for FRC, as shown in Figure 4-6 and 4-7, can be evaluated for the case where the moment of resistance of tensile strength in the cracked part is equal to the moment of resistance of flexural tensile strength.

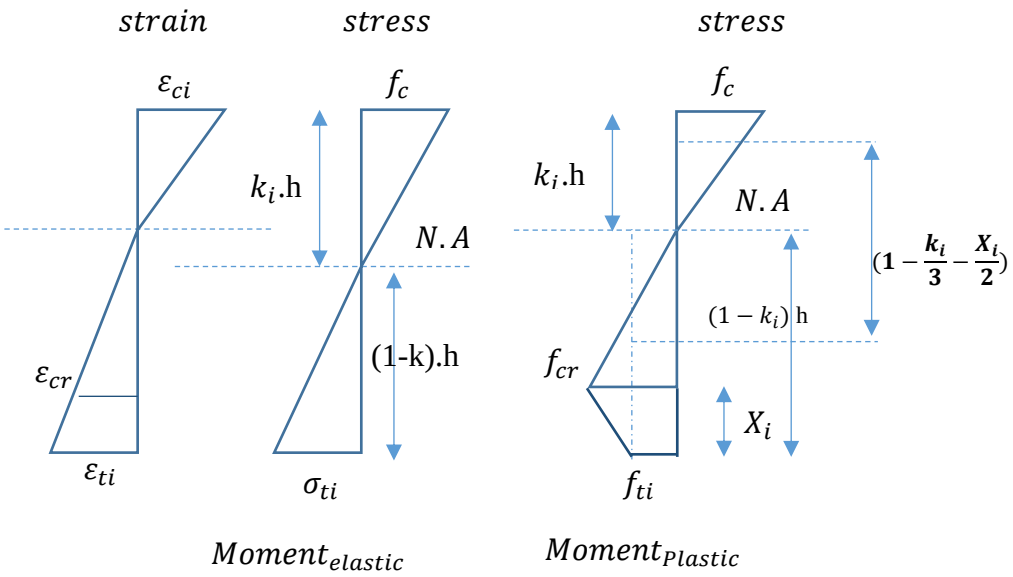

Figure 4-6: trapezoid stress block and strain distributions after cracking in tension (softening behavior).

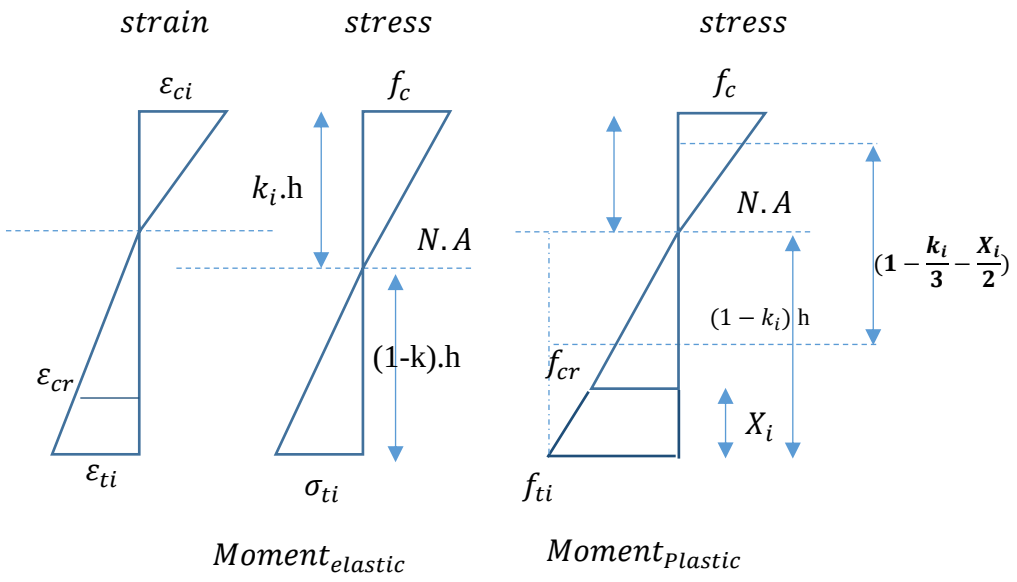

Figure 4-7: trapezoid stress block and strain distributions after cracking in tension (hardening behavior).

$$X_i = \frac{\varepsilon_{t(i-1)}}{\varepsilon_{t(i-1)} + \varepsilon_{t(i)}}(1 - k_{(i)}) \qquad \textit{Equation 4-26}$$

$$Moment_{elastic} = Moment_{Plastic} \qquad \textit{Equation 4-27}$$

$$\frac{\sigma_{ti}(1-k_i)h^2}{3} = f_{ti}X_i h^2(1 - \frac{k_i}{3} - \frac{X_i}{2}) \qquad \textit{Equation 4-28}$$

$\therefore$

$$f_{ti} = \frac{2\sigma_{ti}(1-k_i)}{X_i(6-2k_i-3X_i)} \qquad \textit{Equation 4-29}$$

$$f_{ci} = \frac{2X}{k_i} f_{ti} \qquad \textit{Equation 4-30}$$

Bending moment was determined as:

$$M_b = \frac{(6-2k_i-3X_i)X_i h^2 b}{6} f_{ti} \qquad \textit{Equation 4-31}$$

2- For rectangular stress block:

The tensile strength in the cracked part for FRC, as shown in Figure 4-8, can be evaluated for the case where the moment of resistance of tensile strength in the cracked part is equal to the moment of resistance of flexural tensile strength.

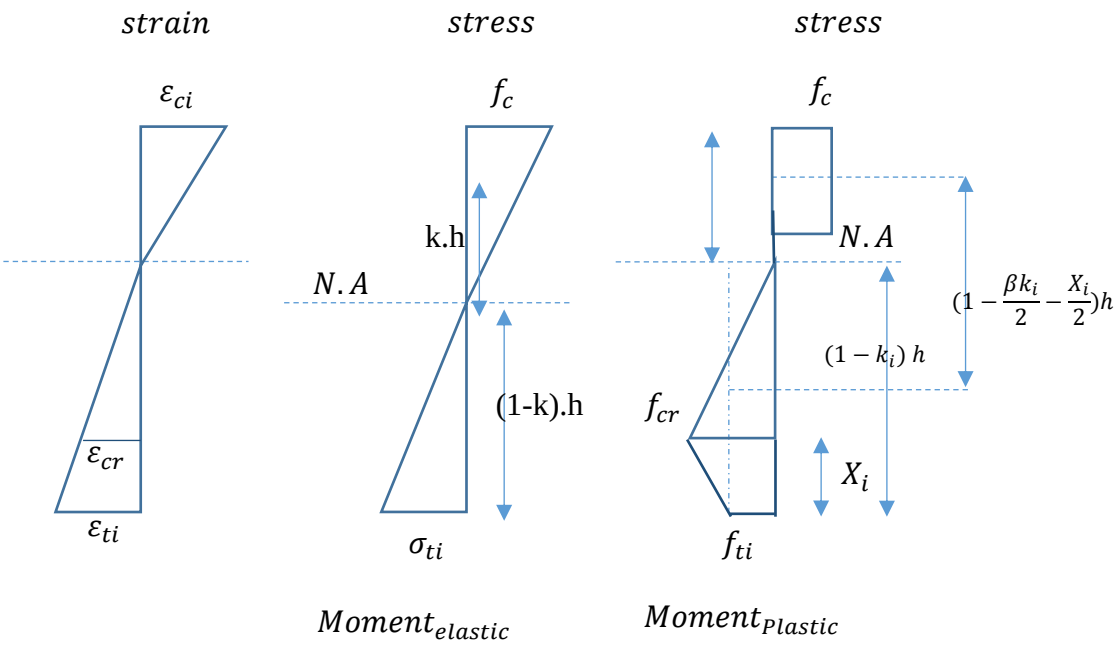

Figure 4-8: rectangular stress block and strain distributions after cracking in tension.

$$Moment_{elastic} = Moment_{Plastic}$$

$$\frac{\sigma_{ti}(1-K)h^2}{3} = f_{ti}X_i h^2\left(1-\frac{\beta k_i}{2}-\frac{X_i}{2}\right) \qquad \textit{Equation 4-32}$$

$$\therefore f_{ti} = \frac{\sigma_{ti}(1-K)}{3X_i(1-\frac{\beta k_i}{2}-\frac{X_i}{2})} \qquad \textit{Equation 4-33}$$

$$f_{ci} = \frac{X}{\beta k_i} f_{ti} \qquad \textit{Equation 4-34}$$

The bending moment was determined as:

$$M_b = \frac{(1-2.(\beta k_i - X_i)).X_i h^2 b}{2} f_{ti} \qquad \textit{Equation 4-35}$$

4.3.1.3 Stress-strain curves of FRC & FRCC after cracking in tension after cracking in compression: ($\boldsymbol{\varepsilon_t > \varepsilon_{cr}, \varepsilon_c > \varepsilon_{cy}}$*)*

To change the load to stress for all points in the curves following the procedure below:

1- Determine N.A or K

$$K_i = \frac{\varepsilon_{c_i}}{\varepsilon_{c_i} + \varepsilon_{t_i}}$$

2- Determine the stress as equilibrium the moment of resistance to the tension stress block of elastic and tension stress block of plastic because they can carry the same load.

To determine the tension stress at any point f_{ti} by making equal to the moment of resistance to the tension stress block of elastic and tension stress block of plastic.

(a) For trapezoid stress block:

The tensile strength in the cracked part for FRC, as shown in Figure 4-9, can be evaluated for the case where the moment of resistance of tensile strength in the cracked part is equal to the moment of resistance of flexural tensile strength.

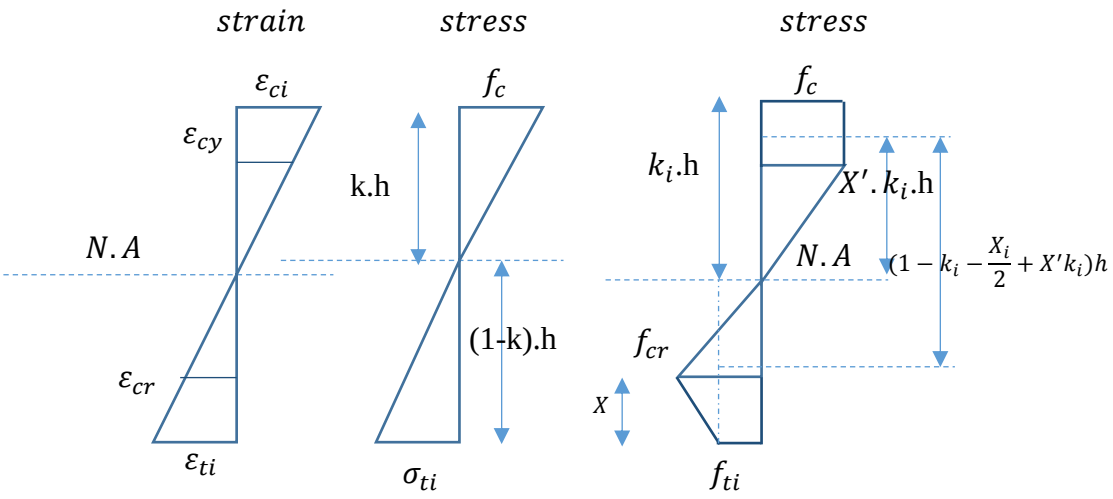

Figure 4-9: trapezoid stress block and strain distributions after cracking in tension and compression.

$$X_i = \frac{\varepsilon_{t(i-1)}}{\varepsilon_{t(i-1)} + \varepsilon_{t(i)}}(1 - k_{(i)}) \qquad \textit{Equation 4-36}$$

$$X' = \frac{3 - (\frac{\varepsilon_{cy}}{\varepsilon_{ci}})^2}{6 - 3.(\frac{\varepsilon_{cy}}{\varepsilon_{ci}})} \qquad \textit{Equation 4-37}$$

So,

$$Moment_{elastic} = Moment_{Plastic}$$

Therefore;

$$\frac{\sigma_{ti}(1-K)h^2}{3} = f_{ti}X_i h^2(1-k_i-\frac{X_i}{2}+X'.k_i) \qquad \textit{Equation 4-38}$$

$$\therefore f_{ti} = \frac{\sigma_{ti}(1-K)}{3X_i(1-\frac{X_i}{2}+(X'-1)k_i)} \qquad \textit{Equation 4-39}$$

$$f_{ci} = \frac{X.\varepsilon_{ci}}{(\varepsilon_{ci}-\varepsilon_{cy}).k_i} f_{ti} \qquad \textit{Equation 4-40}$$

The bending moment was determined as:

$$M_b = (1-k_i-\frac{X_i}{2}+X^{'})X_i h^2 b f_{ti} \qquad \textit{Equation 4-41}$$

(b) For rectangular stress block:

The tensile strength in the cracked part for FRC, as shown in Figure 4-10, can be evaluated for the case where the moment of resistance of tensile strength in the cracked part is equal to the moment of resistance of flexural tensile strength.

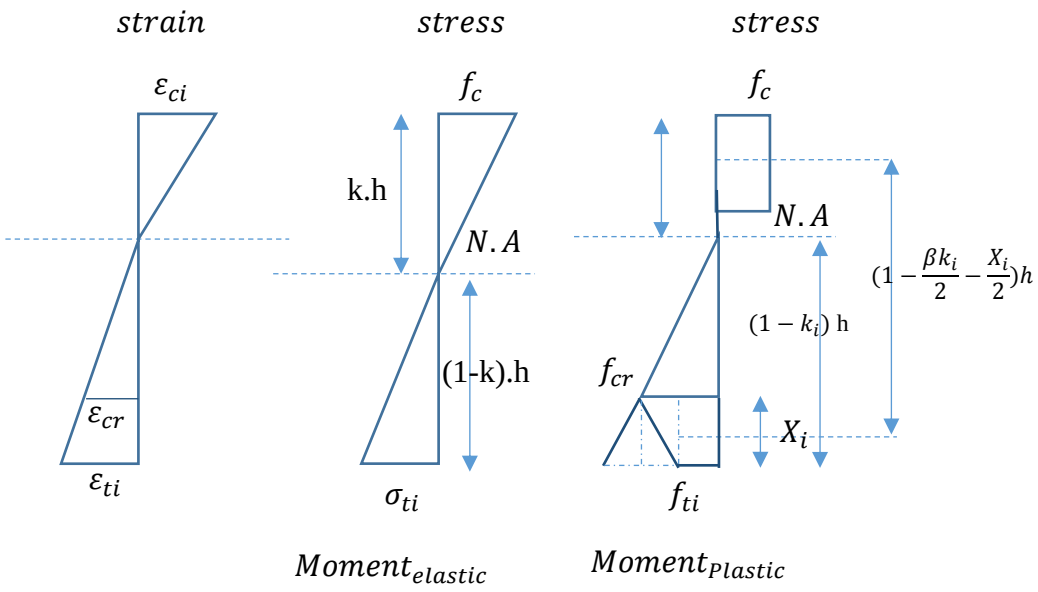

Figure 4-10: rectangular stress block and strain distributions after cracking in tension and compression.

$$Moment_{elastic} = Moment_{Plastic}$$

$$\frac{\sigma_{ti}(1-K)h^2}{3} = f_{ti}X_i h^2(1-\frac{\beta_1 k_i}{2}-\frac{X_i}{2}) \qquad \textit{Equation 4-42}$$

$$\therefore f_{ti} = \frac{\sigma_{ti}(1-K)}{3X_i(1-\frac{\beta_1 k_i}{2}-\frac{X_i}{2})} \qquad \textit{Equation 4-43}$$

$$f_{ci} = \frac{X}{\beta k_i} f_{ti} \qquad \textit{Equation 4-44}$$

The bending moment was determined as:

$$M_b = \frac{(1-2.(\beta k_i - X_i)).X_i h^2 b}{2} f_{ti} \qquad \textit{Equation 4-45}$$

4.3.2 Evaluate the parameters study of stress block.

These parameters are a first crack strength, first crack strain, the elastic modulus in tension, and ultimate strain.

4.3.2.1 First crack strength f_{cr}

According to ASTMC 1018, a first crack point on the load-deflection curve at which the form of the curve first becomes nonlinear. Naamen explained the concept of a first crack point is a first visible cracking point that deviates from linearity "percolated" as detected along the initial ascending portion of the stress-strain curve for the structural tensile member (Shi et al., 2008). As explained above, the first crack strength can be determine from both flexural strength test and direct tensile strength test because of elastic behavior or its stage. Therefore, more than 250 point data used to evaluate the first crack strength.

The new empirical relations developed the ACI 318 equation by a multiple factor λ:

$$f_{cr} = 7.5\,\lambda f_c'^{0.5} \qquad (psi) \qquad \textit{Equation 4-46}$$

Where f_r is a flexural strength; and f_c' is a compressive strength.

In order to further evaluate the deviation between experimental data points and prediction curves, integral absolute error (IAE) is employed, which is written:

$$IAE = \sum \frac{[(Q_i - P_i)^2]^{0.5}}{\sum Q_i} \times 100 \qquad \textit{Equation 4-47}$$

Where Q_i is the experimental result; P_i is the prediction result.

4.3.2.2 First crack strain ε_{cr}

At first crack strain point, the plastic stage of behavior starts. This behavior is represented by the point of submission in tensile. A new equation for first crack strain was developed to account for the influence of additional fibers in concrete. According to the ACI 544 requirement, the first crack strain was 0.000118.

4.3.2.3 Elastic modulus in tension

Elastic modulus in tension is the slope of stress-strain relationship that it is the triangle shape. The new equation can be calculated from Hooke's law that the elastic modulus in tension is equal to the slope of the first crack strength- a first crack strain of the stress-strain curve in the tension, as shown in Figure 4.1.

$$E_t = \frac{f_{cr}}{\varepsilon_{cr}} \qquad \textit{Equation 4-48}$$

4.3.2.4 Ultimate strain $\varepsilon_{ult.}$

According to Rilem 162 and ACI 544, the ultimate strain is 0.025. This limitation depend on steel fiber, without taking into consideration the volume fraction and the geometric of fiber. Therefore, it is necessary to include the volume fraction and the geometric of fiber in the calculation of the ultimate strain to reach a more comprehensive and safe model for the designer. The tensile responses terminate at the normalized ultimate tensile strain α_2.

$$\varepsilon_{Ult.} = \alpha_2 \varepsilon_{cr} \qquad \textit{Equation 4-49}$$

4.3.3 Statistical indicators

In order to further evaluate the deviation between experimental data points and prediction curves, the statistical indicators are employed. The statistical

indicators of the model and data are coefficients of variation ($C.O.V$), the mean square error (M.S.E), and the mean deviation (S.D) to indicate systematic overestimation or underestimation of a given model.

The 45-degree line represent a perfect correlation between the calculated and measured for the model. Data points above this line represent non-conservative deviations of the model equation, while the data points below this line represent conservative deviations. To better understand the variability between the calculated and measured results, a coefficient of variation (C.O.V) is used and also illustrated in the Figures for each equation. The C.O.V was computed by dividing the standard deviation (σ) by the mean (μ), as follows:

$$\mu = \frac{\sum_{i=1}^{n} E_{ci}}{n} \qquad \textit{Equation 4-50}$$

$$C.O.V = \frac{\sqrt{\frac{1}{n-1}\sum_{i=1}^{n}(E_{cpi} - E_{ci})^2}}{\mu} \qquad \textit{Equation 4-51}$$

To further examine the accuracy of these equations, other statistical indicators were also used in the evaluation, including the mean square error and mean deviation. Both of these statistical indicators provide a better mean to assess the quality and dispersion of the equation in predicting the model. The mean square error and mean deviation are calculated as follows:

$$Mean\ Square\ Error = \sqrt{\frac{1}{n-1}\sum_{i=1}^{n}(\frac{E_{cpi} - E_{ci}}{E_{ci}} \times 100)^2} \qquad \textit{Equation 4-52}$$

$$Mean\ Deviation = \frac{1}{n}\sum_{i=1}^{n}\frac{E_{cpi}}{E_{ci}} \qquad Equation\ 4\text{-}53$$

4.4 Analysis and design of new model of FRC and FRCC

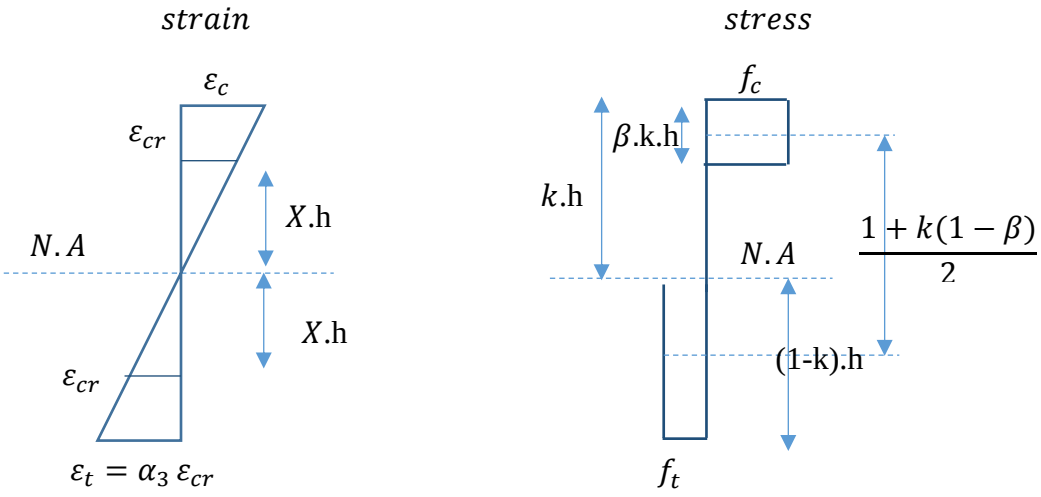

Figure 4-11: rectangular stress block in flexure for analysis model.

In this model, the FRC and FRCC in the compression zone is represented by a rectangular and trapezoid stress block according to FRC and FRCC compression stress block, that was explained above in section 4.1, and the FRC and FRCC in tension is assumed to have a rectangular stress block with an average uniform stress σ_p; refer to Figure 4-11.

According to ACI 544.4R,2018 and Rilem TC 162-TDF, 2003, from the experiments, it has been found that the compression part depth in the beam (neutral axis) was 10% from the total depth of the beam. They show that the compressive strength of FRC and FRCC is higher than tensile strength after cracking and the

depth of compression part in bending is very small compared with the depth of beams (Naaman, 2007). Therefore, the ultimate tensile strength can be taken at 0.35 times its residual flexural strength. In addition, because the depth of compression is small, and the difference between the value of this depth has no significant effect on the fore and moment; therefore, this research takes the compression part depth in the beam (neutral axis) (k) at the ultimate stage equal to 10% from the total depth of the beam.

Assumption:

1- Elastic stage in compression is therefore $\alpha = \frac{E_c\,\varepsilon_c}{f_c'}$.

2- The design moment capacity of FRC and FRCC $\emptyset M_n$ should be greater than the factored moment M_u applied to the member. ACI 544.4R-18. $\emptyset M_n > M_u$.

3- Assume K=0.1

4.4.1 Rectangular stress block stress in compression and tension

4.4.1.1 Analysis FRC and FRCC:

$$\varepsilon_t = \varepsilon_{Ult.} = \alpha_2 \varepsilon_{cr} \qquad \textit{Equation 4-54}$$

In Figure; we assumed that $E_c = E_t$, from strain distribution;

In the tension part, we can determine the depth of first crack strain by

$$\frac{\alpha_2\,\varepsilon_{cr}}{0.9\,h} = \frac{\varepsilon_{cr}}{X\,h} \qquad \textit{Equation 4-55}$$

$$X = \frac{0.9}{\alpha_2} \qquad \textit{Equation 4-56}$$

In the compression part, we can determine the compression strain by

$$\frac{\varepsilon_c}{0.1\,h} = \frac{\varepsilon_{cr}}{X\,h} \qquad \textit{Equation 4-57}$$

$$\varepsilon_c = \frac{0.1\varepsilon_{cr}}{\frac{0.9}{\alpha_2}} \qquad \textit{Equation 4-58}$$

Therefore;

$$\varepsilon_c = \frac{\alpha_2\,\varepsilon_{cr}}{9} \qquad \textit{Equation 4-59}$$

To determine the nominal bending resistance of FRC and FRCC by

$$M_n = Force\ \times lever\ arm = \alpha\, f_c'\, \beta k\, h^2 b\left(1 - \frac{1-k}{2} - \frac{\beta k}{2}\right) \qquad \textit{Equation 4-60}$$

Therefore;

$$M_n = \frac{\alpha\, f_c^{'}\, \beta k\, h^2 b}{2}\left(1 + (1-\beta)k\right) \qquad \textit{Equation 4-61}$$

The design moment capacity of FRC and FRCC $\emptyset M_n$ should be greater than the factored moment M_u applied to the member (ACI 544.4R-18).

$$\emptyset M_n > M_u \qquad \textit{Equation 4-62}$$

The reduction factor ∅ depends on the type of the member, and its failure mode should be determined based on ACI 318 or other building codes and is typically between 0.65 and 0.9 for flexural members (ACI 544.4R-18). These ∅ factors may require adjustments to satisfy with FRC and FRCC members for compression-controlled and tension-controlled failure modes. For FRC members without continuous support such as beams, suspended slabs, and precast, lower values of factors should be used. For FRC members with continuous support, such as slabs-on-ground and shotcrete, higher values of o factors may be used. ACI 544.4R-18.

4.4.1.2 Design FRC and FRCC:

From force equilibrium:

$$\alpha\, f_c'\, \beta k h = f_t\, (1 - k) h \qquad \textit{Equation 4-63}$$

$$\alpha = \frac{f_t\,(1-k)}{f_c'\,\beta k} \qquad \textit{Equation 4-64}$$

$$\alpha = \frac{9\,f_t}{f_c'\,\beta} \qquad \textit{Equation 4-65}$$

From FRC and FRCC compression stress blocks which are explained above in section 4.1; it will assume that $\varepsilon_c < \varepsilon_y$; and

$$\alpha = \frac{E_c\,\varepsilon_c}{f_c'} \qquad \textit{Equation 4-66}$$

$$\frac{E_c\,\varepsilon_c}{f_c'} = \frac{9\,f_t}{\beta\,f_c'} \qquad \textit{Equation 4-67}$$

$$\varepsilon_c = \frac{9\,f_t}{\beta\,E_c} \qquad \textit{Equation 4-68}$$

In Figure, we assumed that $E_c = E_t$, from strain distribution;

In the tension part, we can determine the depth of the first crack strain by

$$\frac{\alpha_2\,\varepsilon_{cr}}{0.9\,h} = \frac{\varepsilon_{cr}}{X\,h} \qquad \textit{Equation 4-69}$$

$$X = \frac{0.9}{\alpha_2} \qquad \textit{Equation 4-70}$$

In the compression part, we can determine the compression strain by

$$\frac{\varepsilon_c}{0.1\,h} = \frac{\varepsilon_{cr}}{X\,h} \qquad \textit{Equation 4-71}$$

$$\varepsilon_c = \frac{0.1\varepsilon_{cr}}{\frac{0.9}{\alpha_2}} \qquad \textit{Equation 4-72}$$

Therefore;

$$\varepsilon_c = \frac{\alpha_2\, \varepsilon_{cr}}{9} \qquad \textit{Equation 4-73}$$

$$\frac{\alpha_2\, \varepsilon_{cr}}{9} = \frac{9\, f_t}{\beta\, E_c} \qquad \textit{Equation 4-74}$$

$$\alpha_2 = 81 \frac{f_t}{\varepsilon_{cr}\, \beta\, E_c} \qquad \textit{Equation 4-75}$$

To determine the nominal bending resistance of FRC and FRCC by

$$M_n = Force \times lever\ arm = f_t(1-k)h^2 b(k - \frac{1-k}{2} - \frac{\beta k}{2}) \qquad \textit{Equation 4-76}$$

$$M_n = \frac{(1-k)h^2 b(1+(1-\beta)k) f_t}{2} \qquad \textit{Equation 4-77}$$

The design moment capacity of FRC and FRCC $\emptyset M_n$ should be greater than the factored moment M_u applied to the member (ACI 544.4R-18).

$$\emptyset M_n > M_u$$

$$\emptyset \frac{(1-k)h^2 b(1+(1-\beta)k) f_t}{2} > M_u \qquad \textit{Equation 4-78}$$

$$f_t > \frac{2\, M_u}{\emptyset\, (1-k)h^2 b(1+(1-\beta)k)} \qquad \textit{Equation 4-79}$$

Because $\alpha_2 = 81 \frac{f_t}{\varepsilon_{cr}\,\beta\,E_c}$

$$f_t = \frac{\alpha_2\,\varepsilon_{cr}\,\beta\,E_c}{81} \qquad \textit{Equation 4-80}$$

Therefore;

$$\frac{\alpha_2\,\varepsilon_{cr}\,\beta\,E_c}{81} > \frac{2\,M_u}{\emptyset\,(1-k)h^2 b(1+(1-\beta)k)} \qquad \textit{Equation 4-81}$$

$$\therefore\ \alpha_2 > \frac{162\,M_u}{\emptyset\,(1-k)h^2 b(1+(1-\beta)k)\varepsilon_{cr}\,\beta\,E_c} \qquad \textit{Equation 4-82}$$

So,

M_u: factored moment applied to the member $(N.mm)$

$f_c' : compressive\ strength\ of\ cylinder\ (N/mm^2)$

$h: depth\ of\ beam\ (mm);\ b: width\ of\ beam\ (mm);\ l_f : fiber\ length\ (mm)$

From equilibrium Force:

$$f_t = \frac{\alpha\,f_c'\,\beta k}{(1-k)} \qquad \textit{Equation 4-83}$$

4.4.2 Trapezoid stress block stress in compression and rectangular stress block stress tension.

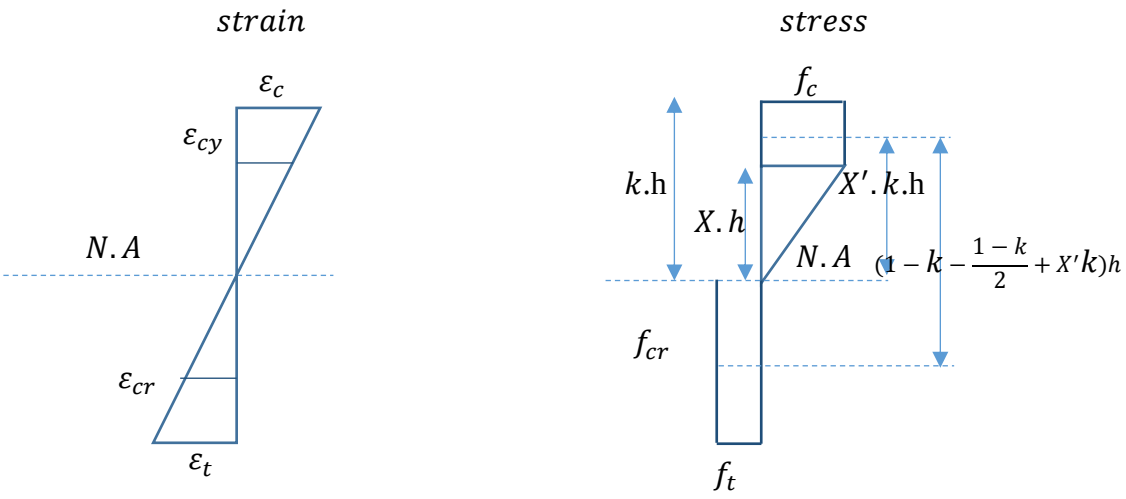

Figure 4-12: trapezoid stress block in flexure for design model.

4.4.2.1 Analysis FRC and FRCC:

$$\varepsilon_t = \varepsilon_{Ult.} = \alpha_2 \varepsilon_{cr} \qquad \textit{Equation 4-84}$$

In Figure 4-12, we assumed that $E_c = E_t$, from strain distribution;

In the tension part, we can determine the depth of the first crack strain by

$$\frac{\alpha_2\, \varepsilon_{cr}}{0.9\, h} = \frac{\varepsilon_{cr}}{X\, h} \qquad \textit{Equation 4-85}$$

$$X = \frac{0.9}{\alpha_2} \qquad \textit{Equation 4-86}$$

In the compression part, we can determine the compression strain by

$$\frac{\varepsilon_c}{0.1\,h} = \frac{\varepsilon_{cr}}{X\,h} \qquad \textit{Equation 4-87}$$

$$\varepsilon_c = \frac{0.1\varepsilon_{cr}}{\frac{0.9}{\alpha_2}} \qquad \textit{Equation 4-88}$$

Therefore;

$$\varepsilon_c = \frac{\alpha_2\,\varepsilon_{cr}}{9} \qquad \textit{Equation 4-89}$$

To determine the nominal bending resistance of FRC and FRCC by

$$M_n = Force\ \times lever\ arm = \alpha\, f_c^{'}\, \beta k\, h^2 b(1 - k - \frac{1-k}{2} + X^{'}k)h \qquad \textit{Equation 4-90}$$

Therefore;

$$M_n = \frac{\alpha\, f_c^{'}\, \beta k\, h^2 b}{2}\,(1 + (2X^{'} - 1)k) \qquad \textit{Equation 4-91}$$

The design moment capacity of FRC and FRCC $\emptyset M_n$ should be greater than the factored moment M_u applied to the member (ACI 544.4R-18).

$$\emptyset M_n > M_u$$

4.4.2.2 Design FRC and FRCC:

From force equilibrium:

$$\frac{\alpha\, f_c' h\,(2k - x)}{2} = f_t\,(1 - k)h \qquad \textit{Equation 4-92}$$

$$\alpha = 2\,\frac{f_t\,(1-k)}{f_c'\,(2k-x)} \qquad \textit{Equation 4-93}$$

$$\alpha = \frac{1.8\,f_t}{f_c'\,(0.2-x)} \qquad \textit{Equation 4-94}$$

From FRC and FRCC compression stress blocks which are explained above in section 4.1, it will assume that $\varepsilon_c < \varepsilon_y$; and

$$\alpha = \frac{E_c\,\varepsilon_c}{f_c'} \qquad \textit{Equation 4-95}$$

$$\frac{E_c\,\varepsilon_c}{f_c'} = \frac{1.8\,f_t}{f_c'\,(0.2-x)} \qquad \textit{Equation 4-96}$$

$$\varepsilon_c = \frac{1.8\,f_t}{(0.2-x)E_c} \qquad \textit{Equation 4-97}$$

In Figure, we assumed that $E_c = E_t$, from the strain distribution;

In the tension part, we can determine the depth of the first crack strain by

$$\frac{\alpha_2\,\varepsilon_{cr}}{0.9\,h} = \frac{\varepsilon_{cr}}{X\,h} \qquad \textit{Equation 4-98}$$

$$X = \frac{0.9}{\alpha_2} \qquad \textit{Equation 4-99}$$

In the compression part, we can determine the compression strain by

$$\frac{\varepsilon_c}{0.1\,h} = \frac{\varepsilon_{cr}}{X\,h} \qquad \textit{Equation 4-100}$$

$$\varepsilon_c = \frac{0.1\varepsilon_{cr}}{\frac{0.9}{\alpha_2}} \qquad \textit{Equation 4-101}$$

Therefore;

$$\varepsilon_c = \frac{\alpha_2\, \varepsilon_{cr}}{9} \qquad \textit{Equation 4-102}$$

$$\frac{\alpha_2\, \varepsilon_{cr}}{9} = \frac{1.8\, f_t}{(0.2 - x)E_c} \qquad \textit{Equation 4-103}$$

$$\alpha_2 = \frac{16.2\, f_t}{(0.2 - x)E_c\varepsilon_{cr}} \qquad \textit{Equation 4-104}$$

To determine the nominal bending resistance of FRC and FRCC by

$$M_n = Force \times lever\ arm = \alpha\, f_c^{'}\, \beta k\, h^2 b(1 - k - \frac{1-k}{2} + X^{'}k)h \qquad \textit{Equation 4-105}$$

Therefore;

$$M_n = \frac{\alpha\, f_c^{'}\, \beta k\, h^2 b}{2}\, (1 + (2X^{'} - 1)k) \qquad \textit{Equation 4-106}$$

The design moment capacity of FRC and FRCC $\emptyset M_n$ should be greater than the factored moment M_u applied to the member (ACI 544.4R-18).

$$\emptyset M_n > M_u$$

$$\emptyset \frac{\alpha\, f_c'\, \beta k\, h^2 b}{2}\, (1 + (2X^{'} - 1)k) > M_u \qquad \textit{Equation 4-107}$$

$$f_t > \frac{2\, M_u}{\emptyset\, \alpha\, f_c'\, \beta k\, h^2 b(1 + (2X^{'} - 1)k)} \qquad \textit{Equation 4-108}$$

Because

$$\alpha_2 = \frac{16.2\, f_t}{(0.2 - x) E_c \varepsilon_{cr}} \qquad \textit{Equation 4-109}$$

$$f_t = \frac{\alpha_2\, \varepsilon_{cr}\, (0.2 - x)\, E_c}{16.2} \qquad \textit{Equation 4-110}$$

Therefore;

$$\frac{\alpha_2\, \varepsilon_{cr}\, (0.2 - x)\, E_c}{16.2} > \frac{2\, M_u}{\emptyset\, \alpha\, f_c'\, \beta k\, h^2 b (1 + (2x' - 1)k)} \qquad \textit{Equation 4-111}$$

$$\therefore\ \alpha_2 > \frac{32.4\, M_u}{\emptyset\, \alpha\, f_c'\, \beta k\, h^2 b (1 + (2x' - 1)k)(0.2 - x)\ \varepsilon_{cr}\ E_c} \qquad \textit{Equation 4-112}$$

5 Chapter 5 Results and Discussion

This section provides critical reviews of the design and analysis of FRC and FRCC methods for some codes and recommendations in Chapter 2.

Based on the test results of this dissertation combined with the database in Chapter 3, either new relationships or currently used relationships with some modifications are proposed to define the characteristics of FRC and FRCC for parameters of study in compressive and tension parts of structures' members. The results of this disseretation combined with the available database are used to recommend revisions for the ACI-544 to extend the current limitation of types of concrete and volume fractions.

The proposal methods and study parameters' relationships are also validated and confirmed for FRC and FRCC by using statistical and parametric analyses.

5.1 Determining for compression stress block

As mentioned in Chapter 4, this dissertation used 250 point-database from the previous 24 research papers that explained the stress-strain curves in compression for different types of fiber and volume fraction for both FRC and FRCC. The first step was to determine the parameters study of stress block that depends on yield strain, ultimate strain, and elastic modulus. In this dissertation determined yield strain equation and limit number for ultimate strain, and also, used the Sukawang equation to determine the elastic modulus for FRC and FRCC.

The second step was to compare the new model with ACI 318, ACI 544, and Rilem, in addition to other models of researchers.

5.1.1 Yield strain

A new equation for yield strain was developed by modifying the ACI 544 and Rilem equations to account for the influence of additional fibers in concrete.

$$\sigma_{cy} = \alpha . f_c' \qquad \textit{Equation 5-1}$$

$$\varepsilon_{cy} = \frac{\sigma_{cy}}{E_c} \qquad \textit{Equation 5-2}$$

$$\varepsilon_{cy} = \frac{\alpha . f_c'}{E_c}$$

$$\alpha = \begin{cases} 0.85 & for\ f_c' < 69\ Mpa\ (10000\ Psi) \\ 1 & for\ f_c' \geq 69\ Mpa\ (10000\ Psi) \end{cases}$$

As mention above, this research adopted the Suksawang 2018 equation for elastic modulus of FRC and FRCC.

$$\varepsilon_{cy} = \frac{\alpha}{4700\ \lambda_{V_f}} \sqrt{f_c'} \ldots (\mathrm{N/mm^2}) \qquad \textit{Equation 5-3}$$

$$\varepsilon_{cy} = \frac{\alpha}{57000\ \lambda_{V_f}} \sqrt{f_c'} \ldots (\mathrm{Ib/in^2})$$

In ACI 544 the yield compressive strength for FRC is adopted as:

$$\varepsilon_{cy} = 0.00018 \sqrt{f_c'} \ldots (\mathrm{N/mm^2}) \qquad \textit{Equation 5-4}$$

$$\varepsilon_{cy} = 0.000015\sqrt{f_c'} \ldots (\mathrm{Ib/in^2})$$

In this research, a volume fraction of fiber did not affect yield strength. The significant impact on yield strength was a compressive strength. For normal strength $f_c' < 69\ Mpa$, the yield strength is $0.85f_c'$. For high strength $f_c' \geq 69\ Mpa$, the yield strength is roughly f_c' because the shape of the ascending branch of the stress-strain relationship becomes more linear and steeper, and the slope of the descending part also becomes steeper. The general shape of the stress-strain relationship becomes more likely to be a triangle.

Figures. 5-1 and 5-2 illustrate the comparison between the calculated and measured yield strain using the proposed equation. It is determined that the C.O.V. of the proposed equation is 18.81%, while the C.O.V. of the ACI 544 is 27.90%. ACI 544 provides the best correlation between the calculated and measured yield strain with mean square error and mean deviation of 20.10 and 0.89, respectively. Thus, the new equation provides a good prediction of the yield strain with mean square error and mean deviation of 18.48% and 0.99, respectively.

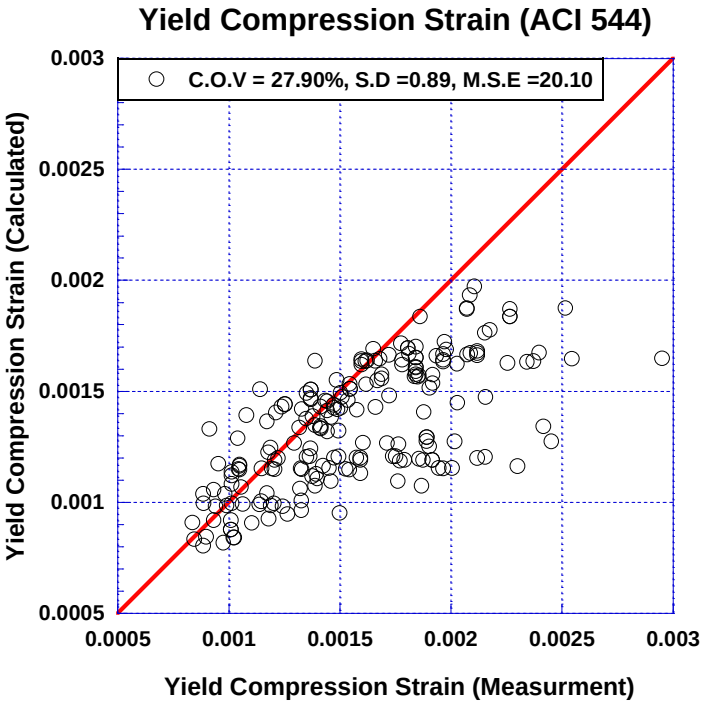

Figure 5-1: Comparison of calculated and measurement of yield strain for ACI 544.

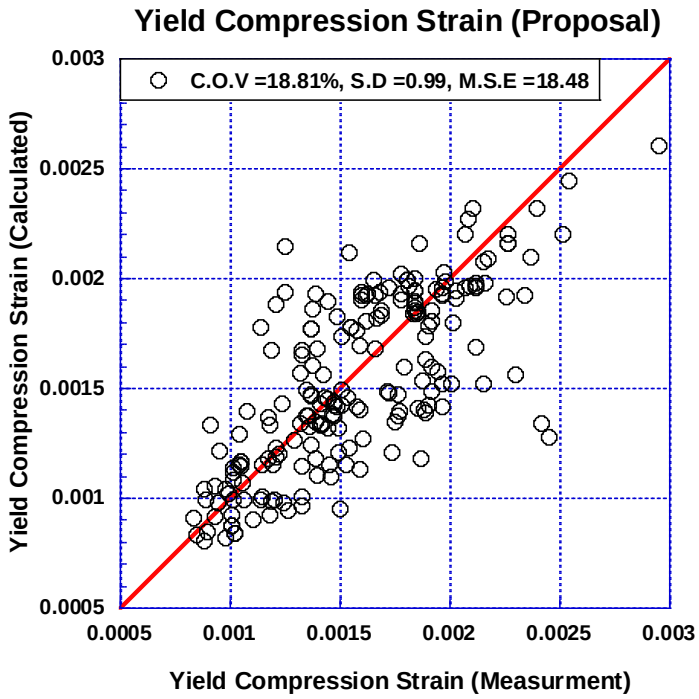

Figure 5-2: Comparison of calculated and measurement of yield strain for proposal model.

5.1.2 Ultimate Strain

Based on the other researcher's database, a volume fraction of fiber affected the ultimate strain. There is no significant trend of an ultimate compressive strain of FRC and FRCC as compressive strength increases. The ultimate strain at the extreme concrete compression fiber is taken to be 0.0035 for volume fraction less than 1%, and 0.005 for volume fraction more than or equal 1%. The value for ultimate strain was chosen as a lower bound on the test data, as indicated by the line in Figures 5-3 and 5-4. It will be given the safer design for FRC.

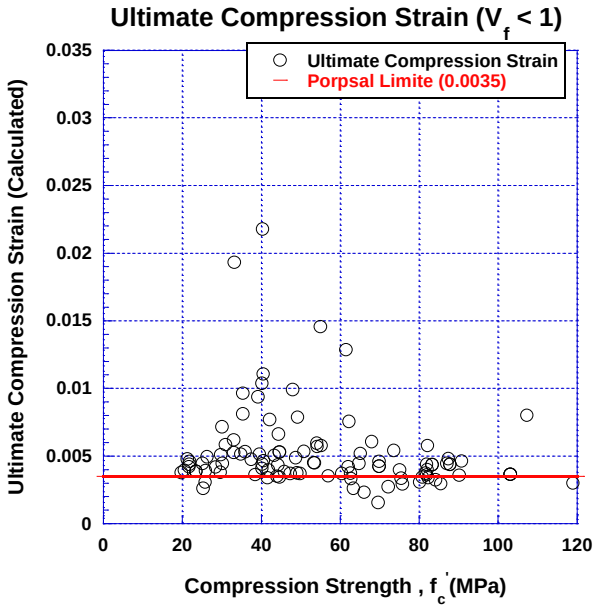

Figure 5-3: Ultimate compression strain for the volume fraction of fiber less than 1%.

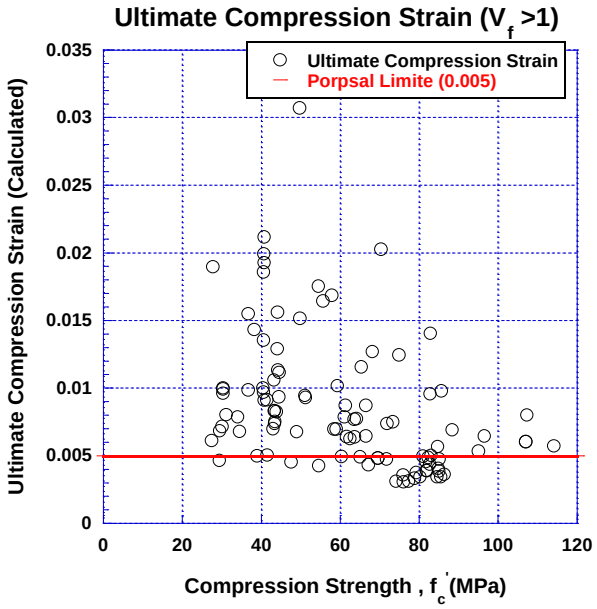

Figure 5-4: Ultimate compression strain for the volume fraction of fiber more than 1%.

5.1.3 Model Analysis

As mentioned in Chapter 4, the purpose of modeling compression block is to simplify the problem with little loss of accuracy. In this research, it passed the rectangular and trapezoid stress block.

5.1.3.1 Rectangular Stress Block

Simplicity stress block replaces the actual curve stress shape by using the theory of equivalent rectangular stress distribution and is modified by Whitney for application to Ultimate Strength Design (USD). This theory appears in Stress block to be entirely satisfactory and gives the most straightforward possible mathematical solution that would provide roughly the same area and center of gravity. As discussed earlier in Chapter 4, to achieve this proposed solution it was determined the K_1, K_2 and K_3 in addition to α and β all FRC, using 250 databases of experimental results and other researchers. Based on the literature, coefficient K_3 is assumed equal to1.0.

The K_1 values can be obtained from dividing the area under stress-strain curves for FRC and FRCC in compression to natural axis depth, as follows:

$$K_1 = \frac{Area\ under\ stress - strain\ curves}{\varepsilon_{Ult.} f_c^{'}} \qquad \textit{Equation 5-5}$$

Figure 5-5 illustrate the effect of volume fraction of fiber on K_1 $for\ V_f \geq 1\%\ and\ V_f < 1\%, respectivaly.$

For volume fraction less than 1, it clear from the Figure 5-5 that in general K_1 value decreases with an increase in concrete strength, but it becomes approximately a constant for concrete strength greater than about 55.2 MPa and less than 27.6 MPa. This behavior is exactly the same as plain concrete as ACI code equation. But this behavior will be different for $f_c' \geq 69\ Mpa$ because the curves become more linear and steeper. The proposal model for K_1suggested using same values of ACI-318 as the lower bound for $V_f < 1\%$ and for $f_c' < 69\ Mpa$, while for $f_c' \geq 69\ Mpa\ K_1\ is\ 0.65$, as shown:

$$K_1 = \begin{cases} 0.723 & , f_c' \leq 27.6\ Mpa \\ 0.553 & , f_c' \geq 55.2\ Mpa \\ 0.525 - 0.00362 f_c' & , 27.6 < f_c' < 55.2\ Mpa \end{cases} \qquad \textit{Equation 5-6}$$

From the Figure 5-5 for the volume fraction more than 1, K_1 the value may be observed that becomes approximately a constant value is 0.75.

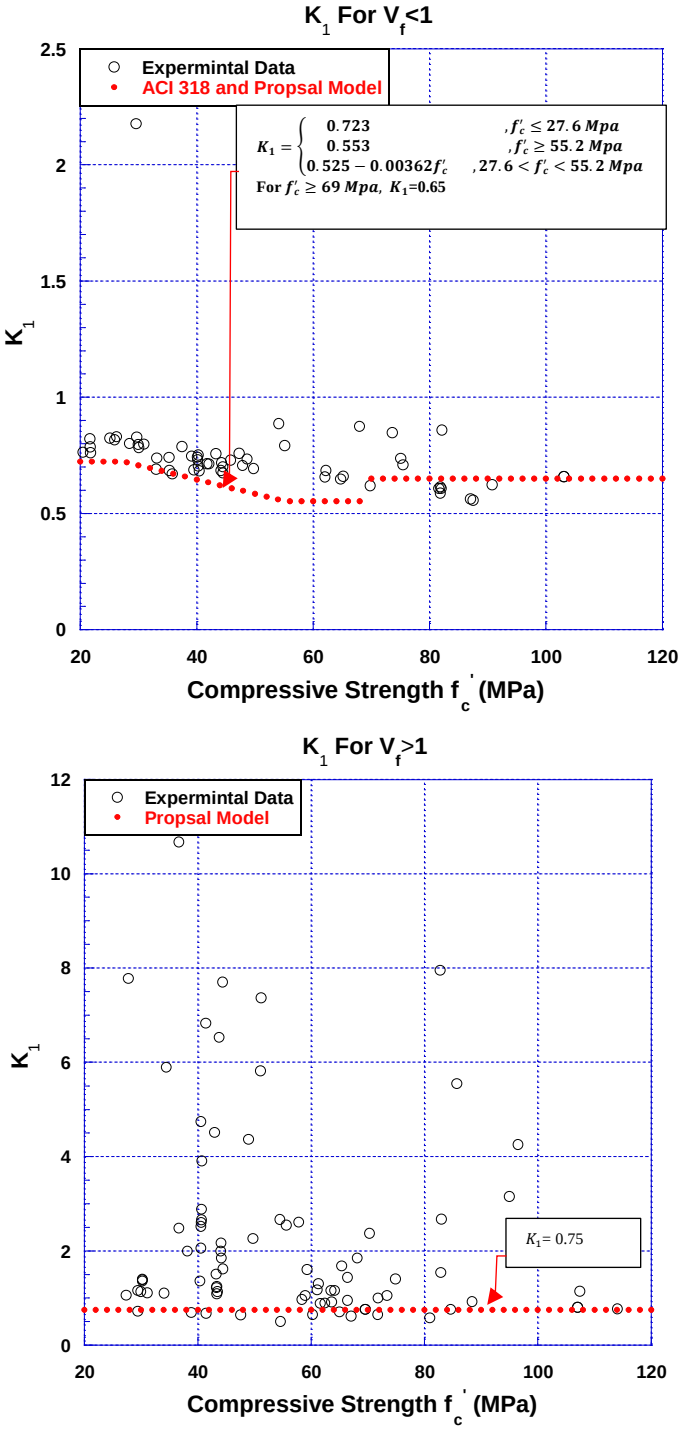

Figure 5-5: K1 values of FRC for the volume fraction of fiber less and more than 1%.

The K_2 values can be obtained from the equilibrium of the external and internal forces, as follows:

$$K_2 = 1 - \frac{Moment\ under\ stress\ strain\ curves\ to\ netural\ axies}{Area\ under\ stress\ strain\ curves.\varepsilon_{Ult.}} \qquad \textit{Equation 5-7}$$

The value of K_2 obtained from the database, plotted in Figure 5-6, shows a similar trend as K_1. For volume fraction less than 1, it is clear from the Figure 5-6 that in general K_2 value decreases with an increase in concrete strength, but becomes approximately a constant for concrete strength greater than about 55.2 MPa and less than 27.6 MPa. The proposed model for K_2suggested using the same value of ACI-318 for $V_f < 1\%$ depending on the database, as explained below:

$$K_2 = \begin{cases} 0.425 & , f_c' \leq 27.6\ Mpa \\ 0.325 & , f_c' \geq 55.2\ Mpa \\ 0.525 - 0.00362 f_c' & , 27.6 < f_c' < 55.2\ Mpa \end{cases} \qquad \textit{Equation 5-8}$$

From Figure 5-6 that $V_f \geq 1\%$, K_2 value may be observed that becomes approximately a constant value suggested *0.375.*

Figure 5-6 illustrate the effect of volume fraction of fiber on $K_2\ for\ V_f \geq 1\%\ and\ V_f < 1\%\ , respectivaly.$

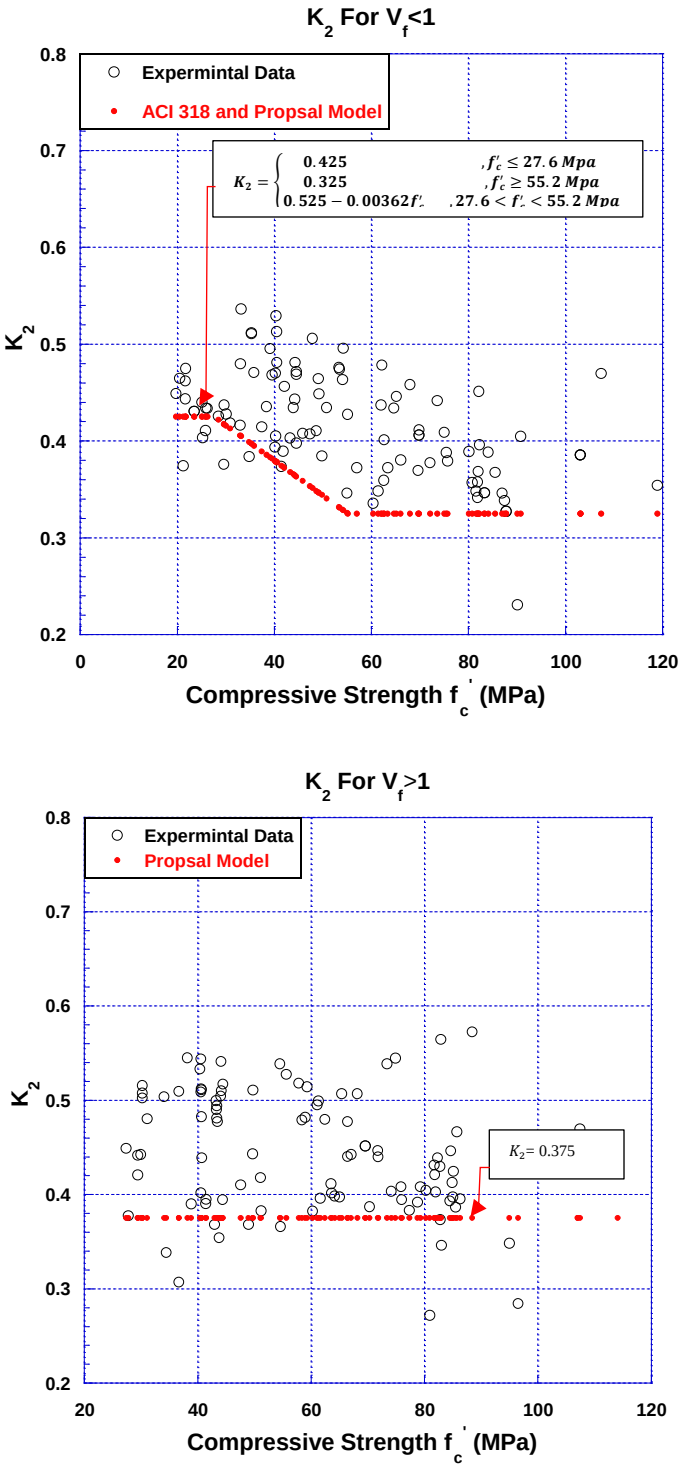

Figure 5-6: K2 values of FRC for the volume fraction of fiber less and more than 1%.

As explained in Chapter 4, the proposed rectangular compressive stress block as shown in the Figure 5-7 is defined by a width equal to $\alpha fc'$ and depth as $\beta.\varepsilon_u$, as done in ACI 318-14.

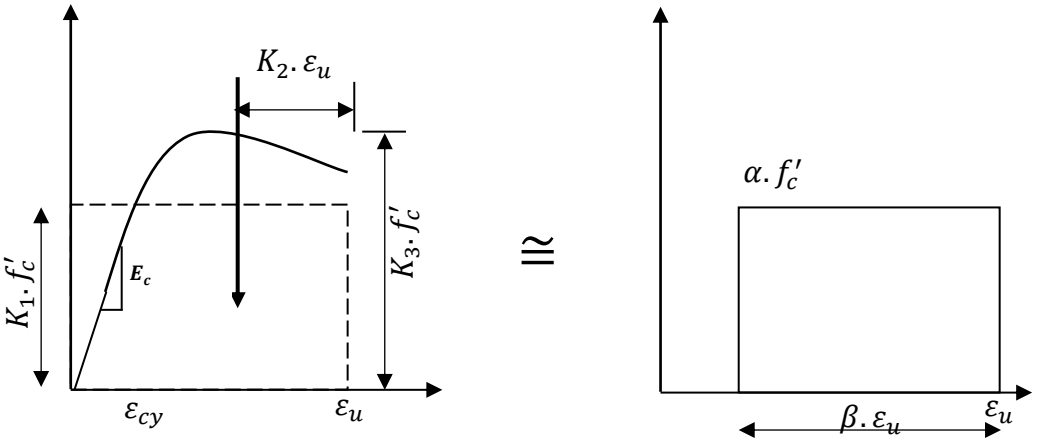

Figure 5-7: Rectangular stress block for proposal model.

For $\varepsilon_c \leq \varepsilon_{cy}$, the shape of stress-strain curves becomes more likely to be a triangle. Therefore, the center of gravity of curves in distance of 0.33 from neutral of axis then led to $\beta \cong 0.65$.

Based on the database, the ultimate stage ($\varepsilon_c = \varepsilon_{Ult.}$) of β affected a volume fraction of fiber. The value of β used in the ACI 318 represents the lower bound on the test data for FRC and FRCC with compressive strength from 20 to 120 MPa. From Figure 5-8 it clear that behavior of $\beta\ parameter$ decreases with an increase in concrete strength, but becomes approximately a constant for concrete strength greater than about 55.2 MPa and less than 27.6 MPa. Therefore, the β for

FRC and FRCC with $V_f < 1\%$ will be the same the ACI 318 Code value "β_1" *that is as following:*

$$\beta_1 = \begin{cases} 0.85 & , f_c' \leq 27.6\ Mpa \\ 0.65 & , f_c' \geq 55.2\ Mpa \\ 1.05 - 0.00725 f_c' & , 27.6 < f_c' < 55.2\ Mpa \end{cases} \qquad \textit{Equation 5-9}$$

While for $\varepsilon_{cy} < \varepsilon_c < \varepsilon_{Ult.}$, it used an interpolation method to find values between a pair of β data points, as shown below:

$$\beta = \begin{cases} 0.65 + \dfrac{\varepsilon_c - \varepsilon_{cy}}{\varepsilon_{Ult.} - \varepsilon_{cy}} \left(\beta_1^{***} - 0.65\right) & for\ V_f < 1\% \\ 0.65 + 0.1 \dfrac{\varepsilon_c - \varepsilon_{cy}}{\varepsilon_{Ult.} - \varepsilon_{cy}} & for\ V_f \geq 1\% \end{cases} \qquad \textit{Equation 5-10}$$

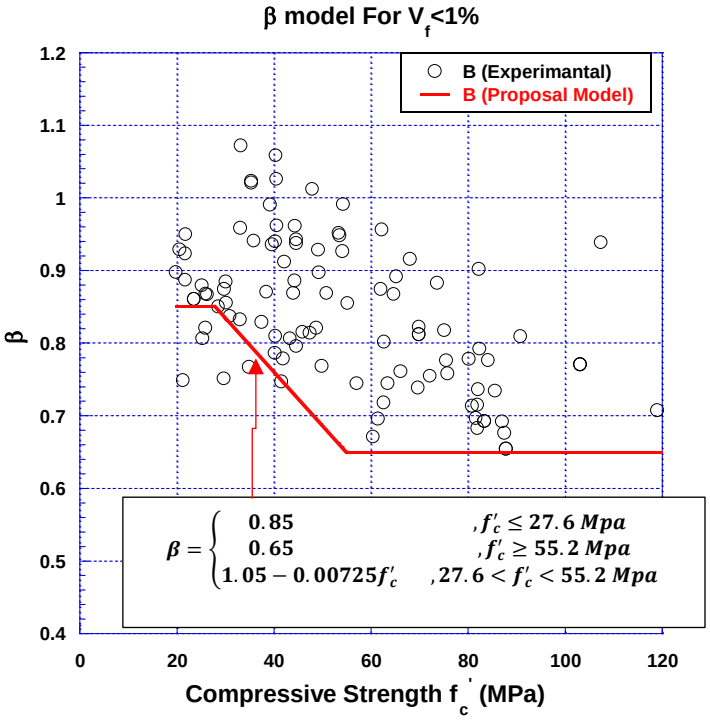

Figure 5-8: B for the volume fraction of fiber less than 1%.

From figure 5-9 that $V_f \geq 1\%$, β value may be observed that becomes approximately a constant value suggested 0.75.

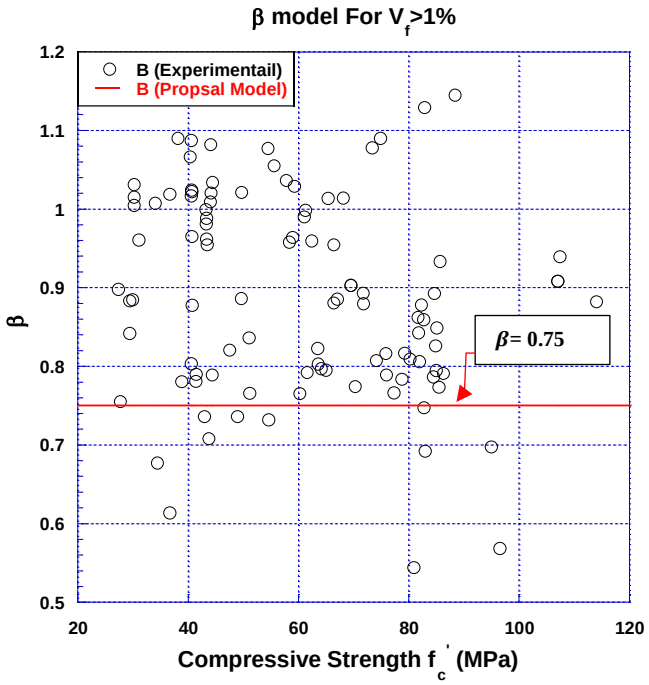

Figure 5-9: B for the volume fraction of fiber more than 1%.

For $\varepsilon_c \leq \varepsilon_{cy}$, $\propto$ parameter is taken depending on the Hook's Law; therefore, by using the yield strain equation, it can determine the $\propto$, as below:

$$\propto = \frac{E.\varepsilon_c}{f_c'} \leq 0.85 \qquad \textit{Equation 5-11}$$

Based on the database, the ultimate stage ($\varepsilon_c = \varepsilon_{Ult.}$) and ($\varepsilon_{cy} < \varepsilon_c < \varepsilon_{Ult.}$) of $\propto$ is affected by a factor volume fraction of fiber. For volume fraction less than 1%, $\propto$ of fiber reinforced concrete for ultimate design is taken to be 0.85 as same of ACI 318, while $\propto = 1$ for $f_c' \geq 69\ Mpa$,see Figure 5-10.

For volume fraction more than or equal to 1% see Figure 5-11. The value for $\propto$ was chosen as a lower bound on the test data with a value of $\propto = 1.$, as indicated by the line in Figures 5-10 and 5-11. It will be given the safer design for FRC.

For a rectangular section, Table 5-1 shows the summary of four ranges of applied top compressive strain $\varepsilon_c < \varepsilon_{cy}$, $\varepsilon_c = \varepsilon_{cy}$, $\varepsilon_{cy} < \varepsilon_c < \varepsilon_{Ult.}$,and $\varepsilon_c = \varepsilon_{Ult.}$.

Table 5-1: Parameters of rectangular stress block for proposal model.

Stress Block Parameter	α	β
$\varepsilon_c < \varepsilon_{cy}$	$\frac{E.\varepsilon_c}{f_c'} \leq 0.85$*	0.65
$\varepsilon_c = \varepsilon_{cy}$	0.85*	
$\varepsilon_{cy} < \varepsilon_c < \varepsilon_{Ult.}$	0.85* $for\ V_f < 1\%$ 1 $for\ V_f \geq 1\%$	$0.65+\frac{\varepsilon_c-\varepsilon_{cy}}{\varepsilon_{Ult.}-\varepsilon_{cy}}(\beta_1{}^{***} - 0.65)$ $for\ V_f < 1\%$ $0.65+0.1\frac{\varepsilon_c-\varepsilon_{cy}}{\varepsilon_{Ult.}-\varepsilon_{cy}}$ $for\ V_f \geq 1\%$
$\varepsilon_c = \varepsilon_{Ult.}$**		$\beta_1{}^{***}$ $for\ V_f < 1\%$ 0.75 $for\ V_f \geq 1\%$

* $for\ f_c' \geq 69\ Mpa\ \alpha = 1$

** $\varepsilon_{Ult.} = 0.0035\ and\ 0.005\ for\ V_f < 1\%\ and\ V_f \geq 1\%$, *respectively.*

*** β_1 *is same ACI 318 Code.*

From the results above, it is clear that the stress blocks of FRC and FRCC are affected by the limitation of V_f=1 that is manifested by each of parameter of

$\beta, \alpha, \varepsilon_{cy}$ and $\varepsilon_{Ult.}$. In addition, the high strength $f_c' \geq 69\ Mpa$ also affects on these parameters.

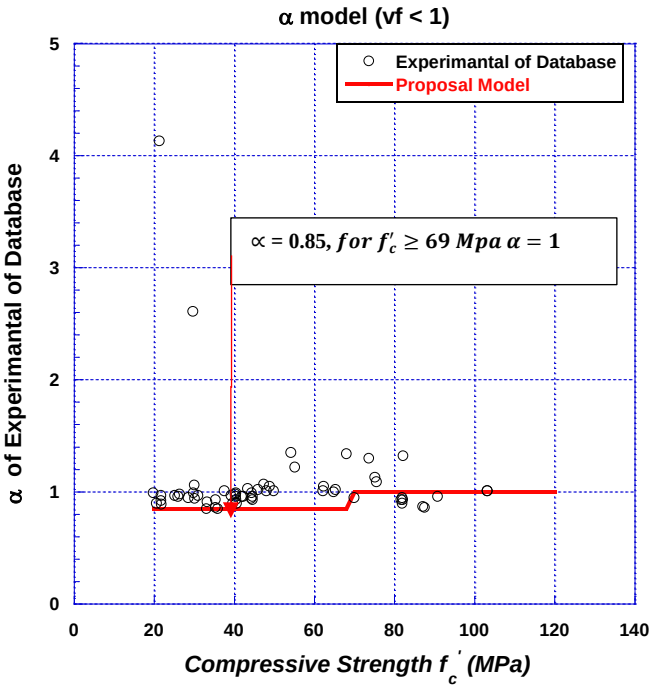

Figure 5-10: ∝ for the volume fraction of fiber less than 1%.

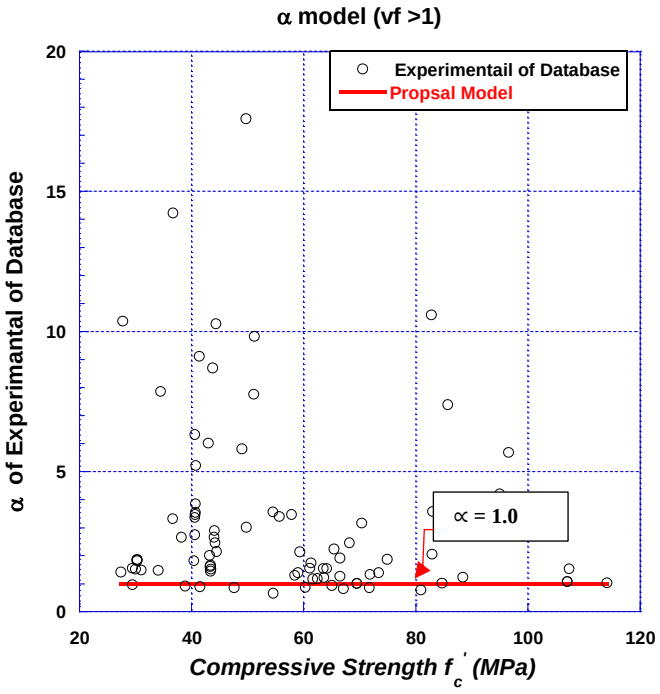

Figure 5-11: ∝ for the volume fraction of fiber more than 1%.

5.1.3.2 Trapezoid Stress Block

An idealized constitutive model, a bilinear elastic-perfectly plastic stress-strain response has been assumed in compression where the linear portion of response terminates at yield point (∝fc',ε_{cy}) and remains constant at compressive yield stress until the ultimate compressive strain $\varepsilon_{Ult.}$, see Figure 5-12.

$$f_c = \begin{cases} E.\varepsilon_c & for \quad 0 < \varepsilon_c < \varepsilon_{cy} \\ \propto . f_c' & for \quad \varepsilon_{cy} \le \varepsilon_c \le \varepsilon_{ult} \end{cases} \qquad \textit{Equation 5-12}$$

$$so, \quad \alpha = 0.85 \ for \ f_c' < 69\ Mpa$$
$$\alpha = 1.0 \ for \ f_c' \ge 69\ Mpa$$

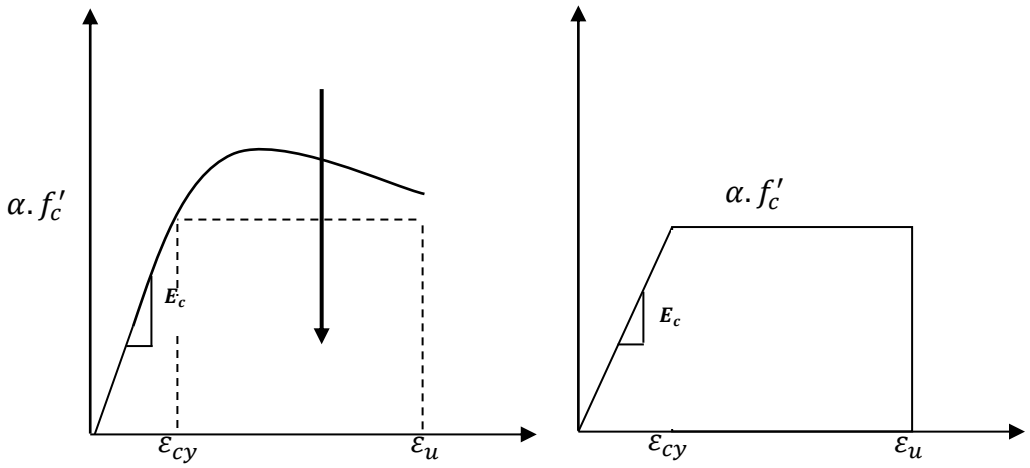

Figure 5-12: Trapezoid stress block for proposal model.

As mentioned above in the rectangular stress block section, for $\varepsilon_c \leq \varepsilon_{cy}$, $\propto$ parameter depends on the Hook's Law; therefore, by using the yield strain equation we can determine the $\propto$, as shown in Figure 5-13.

$$\propto = \frac{E . \varepsilon_c}{f_c'} \leq 0.85 \qquad \textit{Equation 5-13}$$

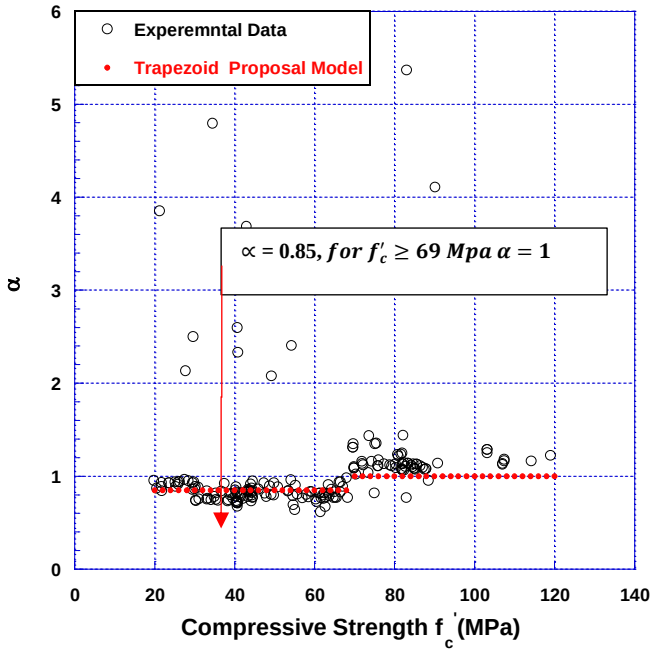

Figure 5-13: ∝ for the trapezoid Stress Block.

Table 5-2 shows four ranges of applied top compressive strains: $\varepsilon_c < \varepsilon_{cy}$, $\varepsilon_c = \varepsilon_{cy}$, $\varepsilon_{cy} < \varepsilon_c < \varepsilon_{Ult.}$, and $\varepsilon_c = \varepsilon_{Ult.}$.

Table 5-2: Parameters of trapezoid stress block for proposal model.

Stress Block Parameter	α
$\varepsilon_c < \varepsilon_{cy}$	$\frac{E.\varepsilon_c}{f_c'} \leq 0.85$*
$\varepsilon_c = \varepsilon_{cy}$	0.85*
$\varepsilon_{cy} < \varepsilon_c < \varepsilon_{Ult.}$	
$\varepsilon_c = \varepsilon_{Ult.}$**	

$* \; for \; f_c^{'} \geq 69 \; Mpa \; \alpha = 1$,

** $\varepsilon_{Ult.} = 0.0035 \; and \; 0.005 \; for \; V_f < 1\% \;\; and \; V_f \geq 1\%$, *respectively.*

*5.1.3.3 Database of **stress** block Parameters*

Six stress block design codes were used to evaluate their accuracy with the 250 points of the database obtained from the previous studies. Table 5-3 summarizes all the stress block model and their parameters. All codes depend on the rectangular stress block to design the FRC except ACI 544, which depends on the trapezoid stress block in the design.

Table 5-3: Database for stress block models.

Reference	α	β	ε_u
LRFD (2004) and ACI 318 (2005)	0.85	$0.85\text{-}0.008(f_c' - 30)$ $0.85 \geq \beta_1 \geq 0.65$	0.003
NZS 3101 (2006)	$0.85 - 0.004(f_c' - 55)$ $0.85 \geq \alpha_1 \geq 0.75$	$0.85\text{-}0.008(f_c' - 30)$ $0.85 \geq \beta_1 \geq 0.65$	0.003
CSA A23.3 (2004)	$0.85 - 0.0015f_c' \geq 0.67$	$0.97 - 0.0025f_c' \geq 0.67$	0.0035
CEB-FIB Model Code (1990)	$0.85\left(1 - \frac{f_c'}{250}\right)$	1	$0.004 - 0.002\frac{f_c'}{100}$
Eurocode2 (2004)	$0.85\left(1 - \frac{f_c' - 50}{200}\right)$ $50 \leq f_c' \leq 90$	$0.8\left(1 - \frac{f_c' - 50}{320}\right)$ $50 \leq f_c' \leq 90$	$0.0026 - 0.035\left(\frac{90 - f_c'}{100}\right)^4$ $50 \leq f_c' \leq 90$
ACI 544	0.85	-	0.0035

To be entirely satisfactory give and to the most straightforward possible mathematical solution for the proposal model of Stress block, we determined the area and center of gravity of stress block for the proposed model and the codes model and compared it with the experimental data of the database.

To determine the area of rectangular stress block of the proposal model and the codes model by:

$$Area\ under\ curves = \propto f_c' \beta \varepsilon_{ult} \qquad \textit{Equation 5-14}$$

While the area for trapezoid stress block of the proposal model and the codes model is

$$Area\ under\ curves = \frac{\propto f_c' \beta}{2} (2\varepsilon_{ult} - \varepsilon_{cy}) \qquad \textit{Equation 5-15}$$

The behavior and parameters value of Basalt fiber in stress-strain curves are more likely in the plain concrete. The suggestion model for Basalt FRC and FRCC used ACI 318 Codes Model is the best representative to determine the area under stress-strain curves for lower bound of database. For ACI 544 Model, it awards more accuracy but it is considered as overestimated because it does not take into account the lower bound of data, see Figure 5-14.

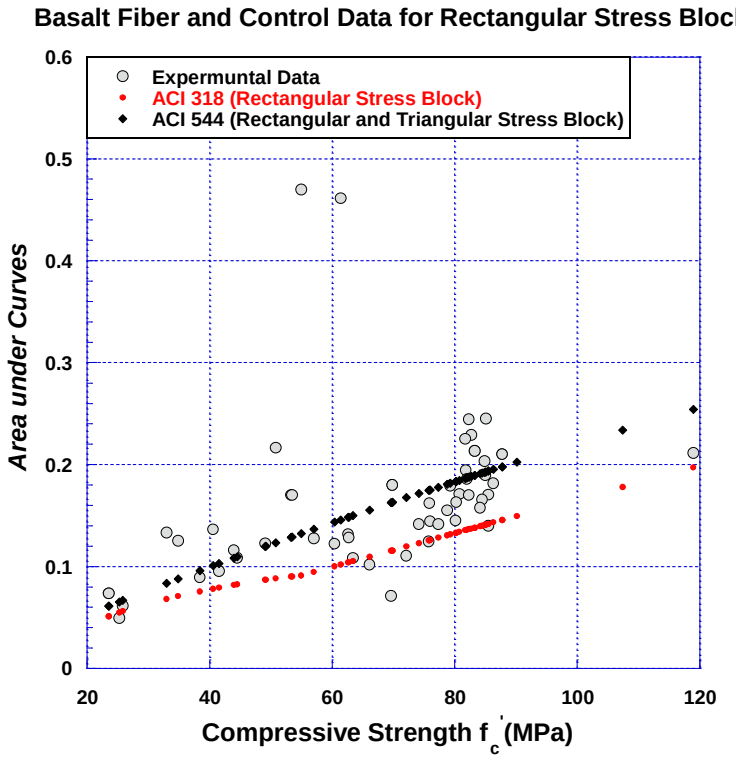

Figure 5-14: ACI 318 code and ACI 544 area with the compressive strength for Basalt fibers.

For basalt FRC and FRCC, it is clear from Figure 5-14 that in general K_2 is closest to the pain concrete value that decreases with an increase in concrete strength, but becomes approximately a constant for concrete strength greater than about 55.2 MPa and less than 27.6 MPa, as shown in Figure 5-15, as explained below:

$$K_2 = \begin{cases} 0.425 & , f_c' \leq 27.6\ Mpa \\ 0.325 & , f_c' \geq 55.2\ Mpa \\ 0.525 - 0.00362 f_c' & , 27.6 < f_c' < 55.2\ Mpa \end{cases} \qquad \textit{Equation 5-16}$$

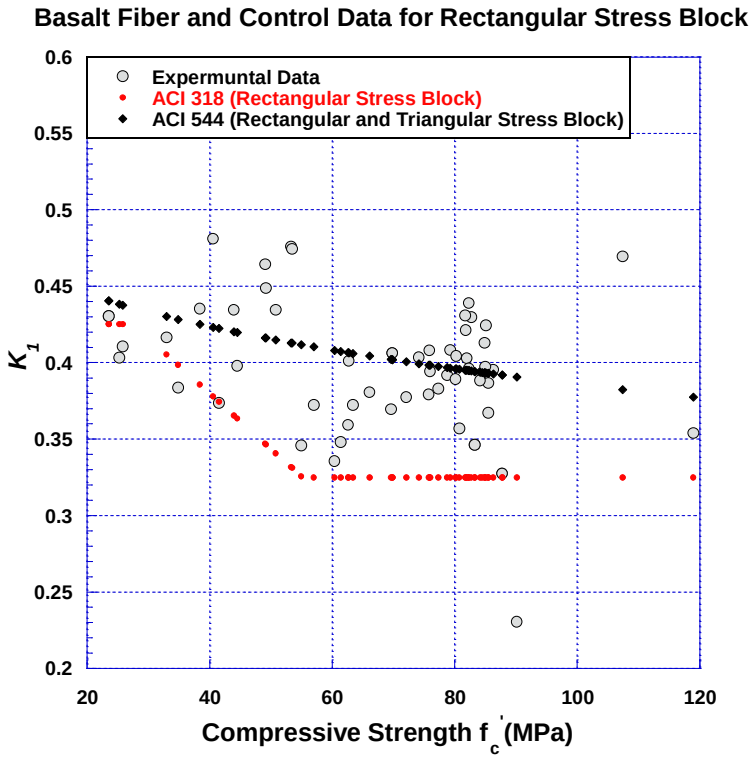

Figure 5-15: ACI 318 code and ACI 544 K1 with the compressive strength for Basalt fibers.

For other types of fibers, such as PVA, steel and synthetic fibers, the area under stress-strain curves that determine stress block depend on the volume fraction of fiber. For rectangular stress blocks, the proposed model takes the lower bound of the data, according to the requirement of designers for more safety.

Despite other stress block codes underestimating of the lower bound, the difference is not significant between the proposed model and other codes. In volume fraction less than 1, the six stress blocks codes are similar of proposal model for compressive strength less than 40 MPa, except for the CSA A233 (1994). For other codes, the difference compared to the proposed model is clear as underestimated of the lower bound of data above the compressive strength of 40

MPa. The Eurocode 2 (CEN, 2004) and CEB-FIB model code (1990) show the evaluation for an area of data for stress block almost twice the lower bound. Therefore, the other codes, except for the CSA A233 (1994), do not give the good evaluation for compressive strength of more than 40 MPa, due to neglecting the effect of fiber.

Figures 5-16 to 5-20 show the kinds of the database the area of stress block for the proposal model and the codes model with the compressive strength for volume fraction less than 1.0.

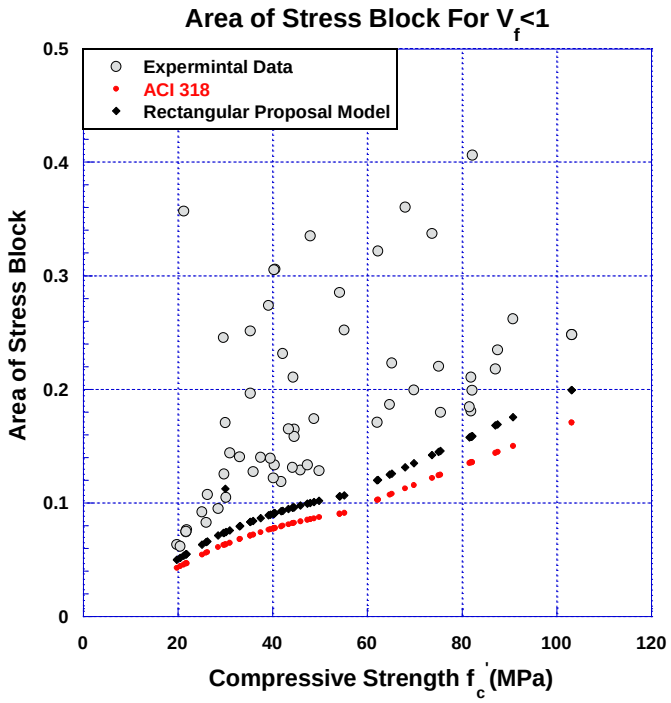

Figure 5-16: ACI 318 code area with the compressive strength for volume fraction less than 1.0.

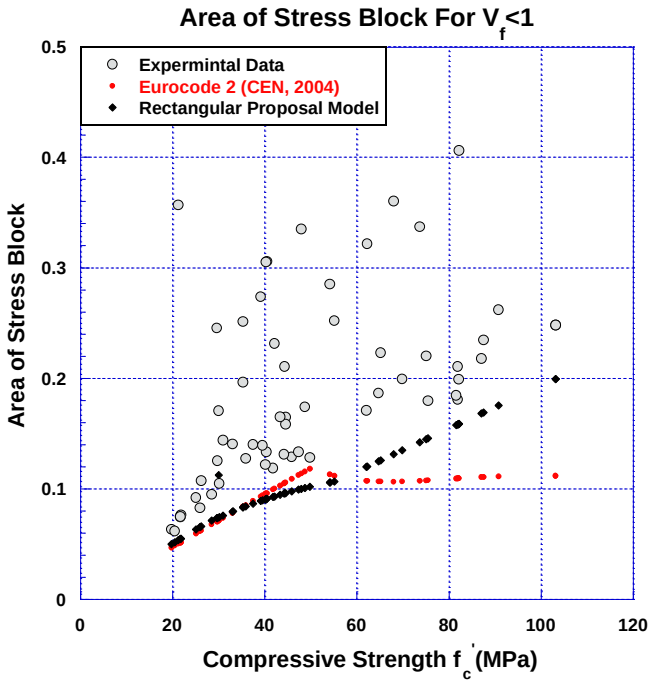

Figure 5-17: Eurocode area with the compressive strength for volume fraction less than 1.0.

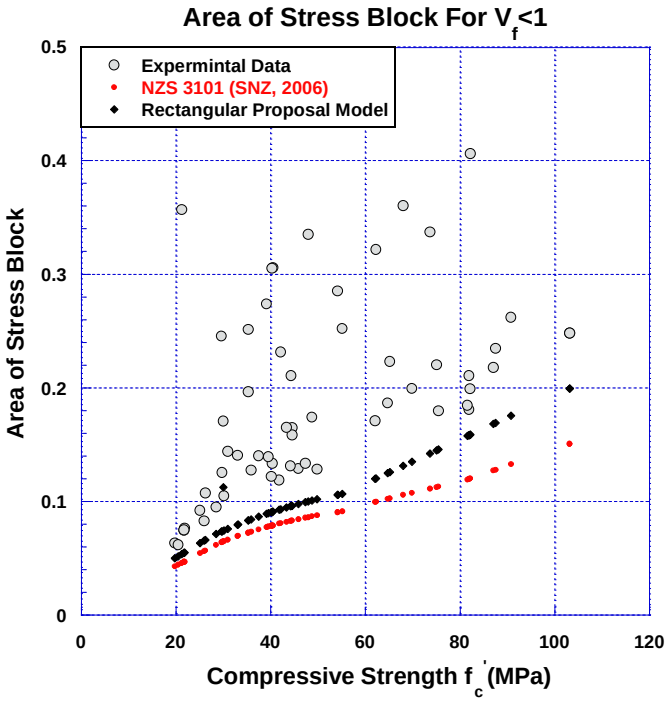

Figure 5-18: NZS 3101 code area with the compressive strength for volume fraction less than 1.0.

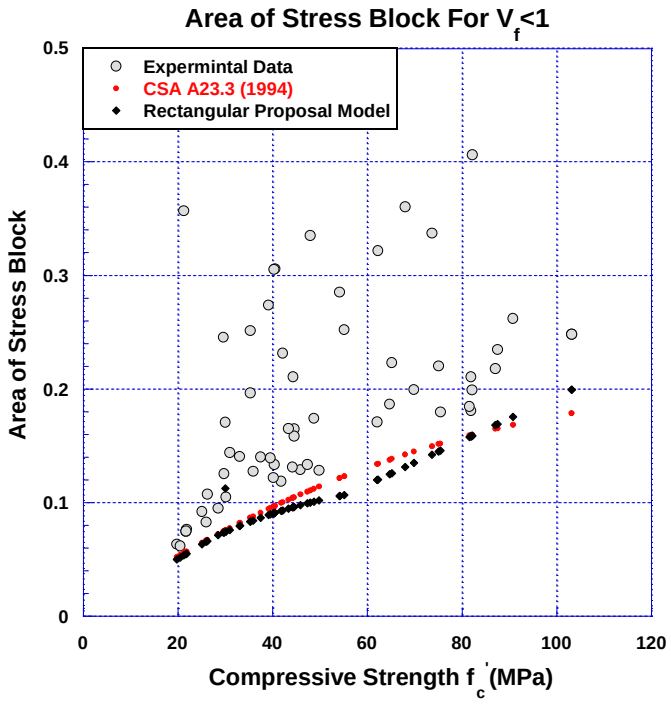

Figure 5-19: CSA code area with the compressive strength for volume fraction less than 1.0.

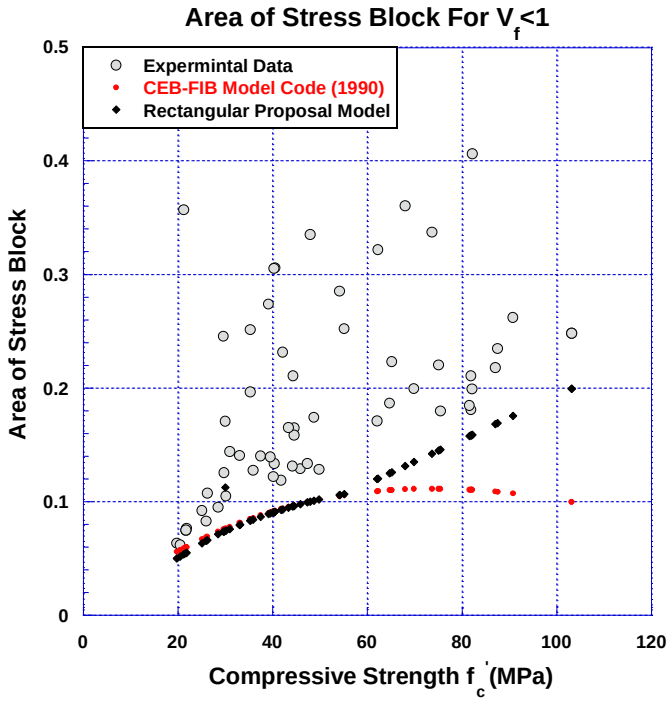

Figure 5-20: FIB Model code area with the compressive strength for volume fraction less than 1.0.

For volume fraction less than 1, it is clear from Figures 5-21 to 5-25 that the proposed model for K_2 is closest to the ACI 318 and NZS 3101 models by taking in view the lower bound of the database. The CEB-FIB model code depends on the higher bound that causes an overestimation in compressive force and an underestimation in moment capacity. The Eurocode 2 model heads to the lower bound of the database, in contrast to CSA A233 that takes the average database.

The value of K_2 decreases with an increase in concrete strength, but becomes approximately a constant for concrete strength greater than about 55.2 MPa and less than 27.6 MPa. The proposed model for K_2 uses the same values of ACI-318, as explained below:

$$K_2 = \begin{cases} 0.425 & , f_c' \leq 27.6\ Mpa \\ 0.325 & , f_c' \geq 55.2\ Mpa \\ 0.525 - 0.00362 f_c' & , 27.6 < f_c' < 55.2\ Mpa \end{cases} \quad \textit{Equation 5-17}$$

Figures 5-21 to 5-25 show the kinds of the database the center of gravity of stress block for the proposal model and the codes model with the compressive strength for volume fraction less than 1.0.

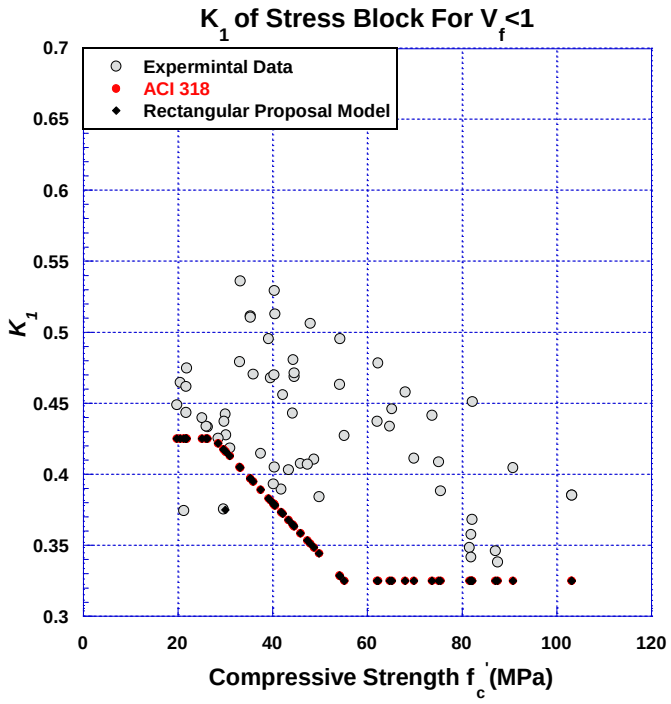

Figure 5-21: ACI 318 code K2 with the compressive strength for volume fraction less than 1.0.

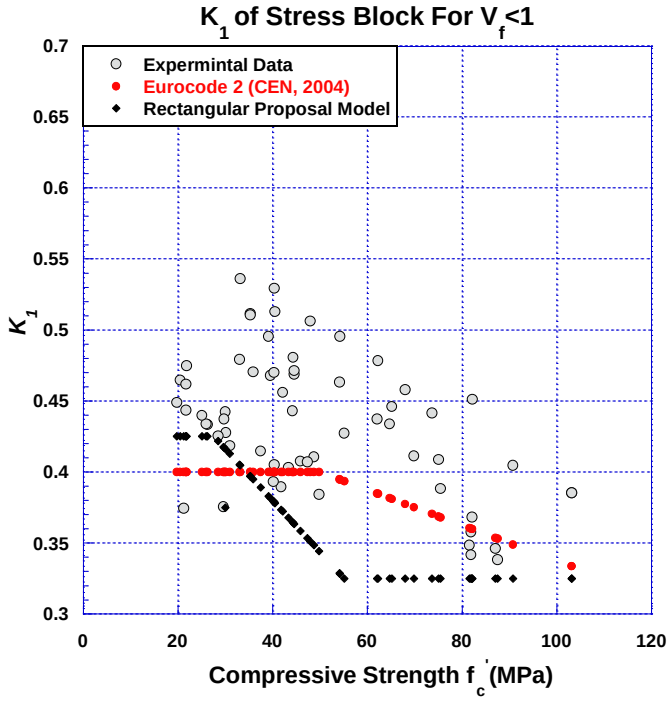

Figure 5-22: Eurocode K2 with the compressive strength for volume fraction less than 1.0.

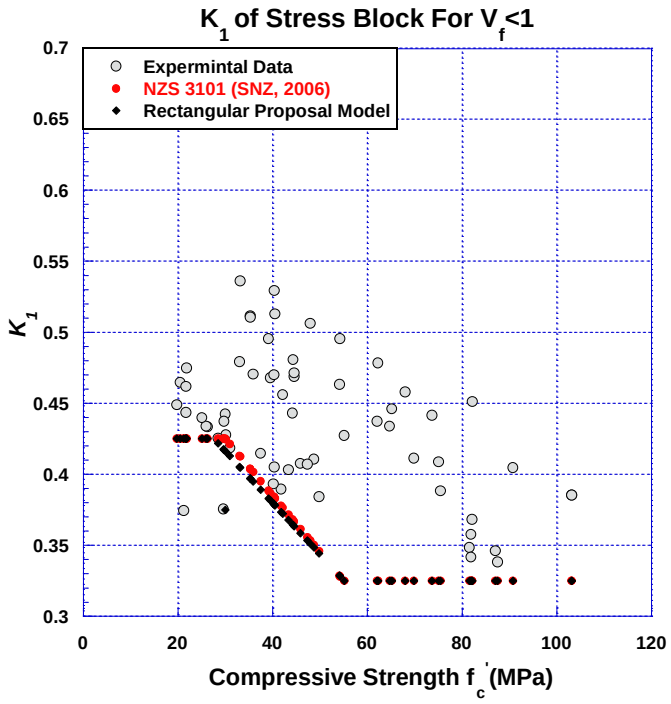

Figure 5-23: NZS 3101 code K2 with the compressive strength for volume fraction less than 1.0.

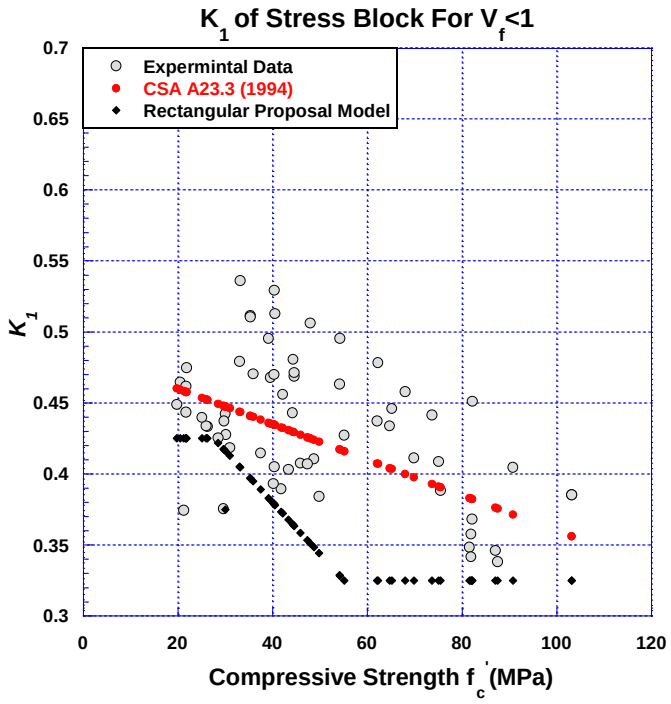

Figure 5-24: CSA code K2 with the compressive strength for volume fraction less than 1.0.

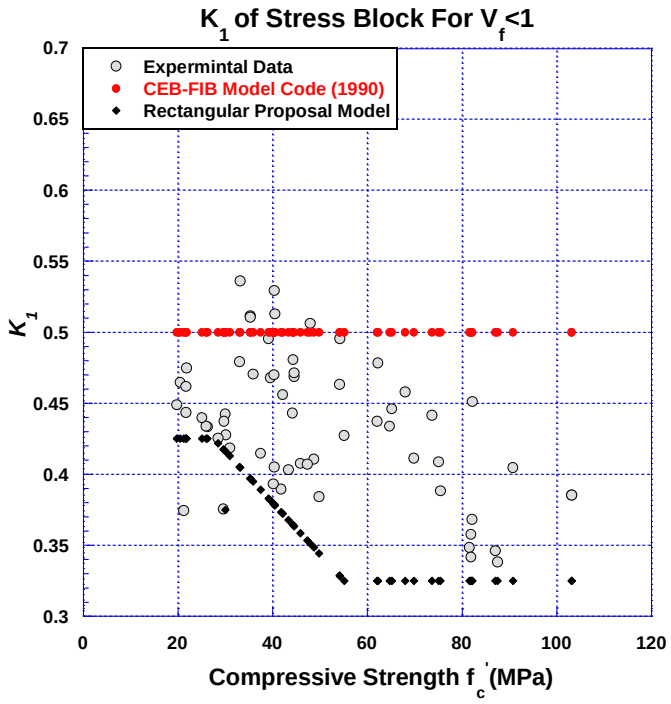

Figure 5-25: FIB Model code K2 with the compressive strength for volume fraction less than 1.0.

Figures 5-26 to 5-30 show the kinds of the database the area of stress block for the proposal model and the codes model with the compressive strength for volume fraction more than 1.0.

In volume fraction more than 1, it is clear that the difference of the six stress blocks codes on the proposed model, underestimated the lower bound of data. As result, it shows the evaluation for an area of data for another stress block more than twice underestimated the lower bound. Therefore, the other codes do not give a good evaluation for compressive strength, due to neglecting the effect of fiber.

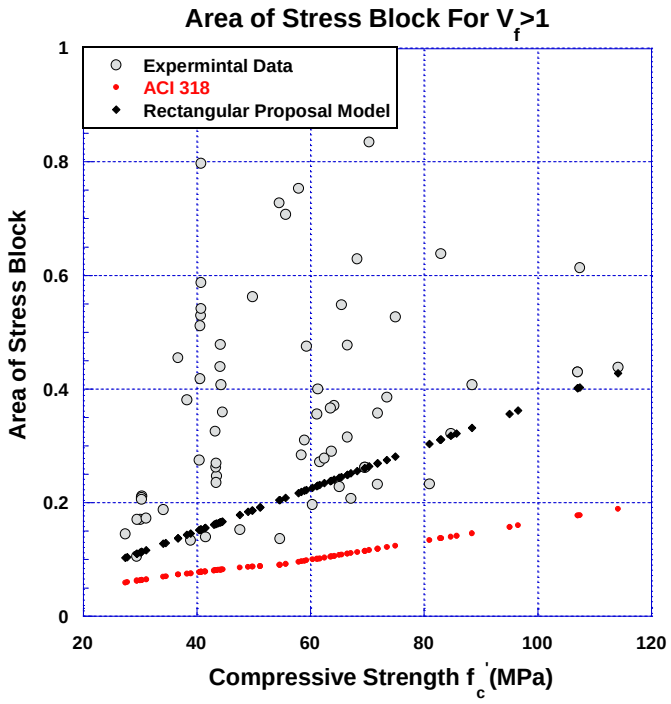

Figure 5-26: ACI 318 code area with the compressive strength for volume fraction more than 1.0.

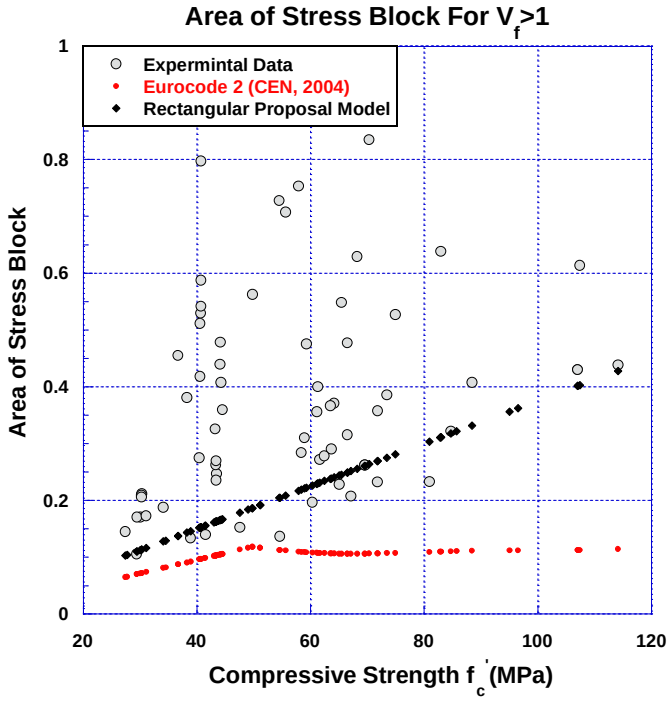

Figure 5-27: Eurocode area with the compressive strength for volume fraction more than 1.0.

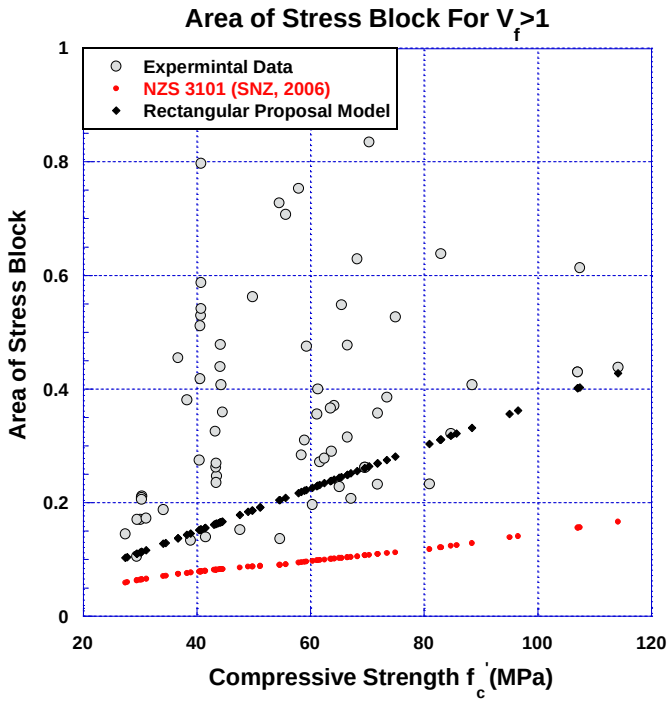

Figure 5-28: NZS 3101 code area with the compressive strength for volume fraction more than 1.0

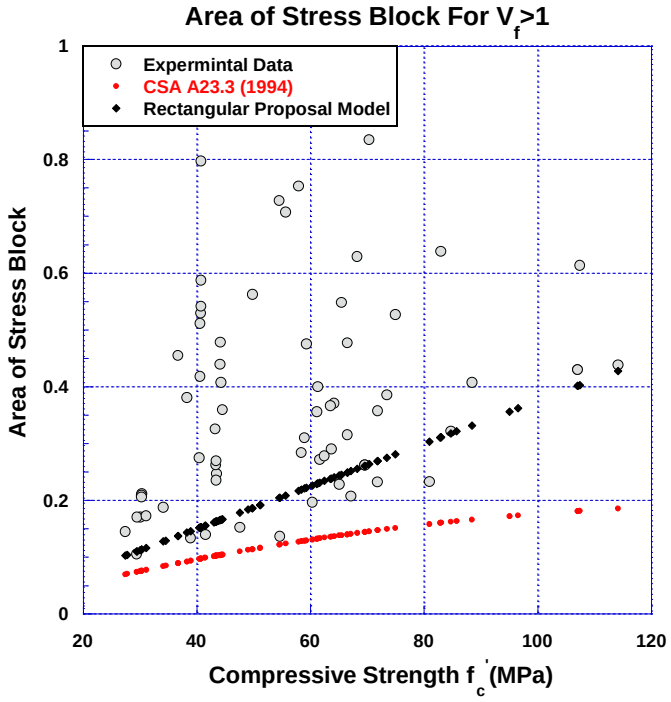

Figure 5-29: CSA code area with the compressive strength for volume fraction more than 1.0.

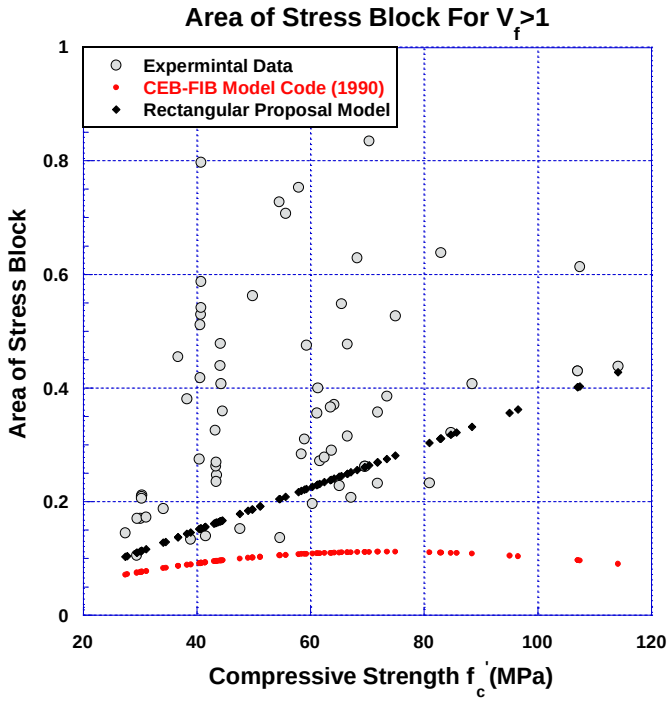

Figure 5-30: FIB Model code area with the compressive strength for volume fraction more than 1.0.

As explained above, the results show that $V_f \geq 1\%$, K_2 is 0.375, toke as a constant value in a lower bound of database. It is clear from Figures 5-31 to 5-35 that the proposed model for K_2 is closest to ACI 318, and, NZS 3101 models decrease with compressive strength until 57 MPa, then they become be constants. The CEB-FIB model code depends on the higher bound that causes an overestimation of compressive force and underestimated the moment capacity. The Eurocode 2 model heads to the lower bound of the database, in contrast to CSA A233 which takes the average database.

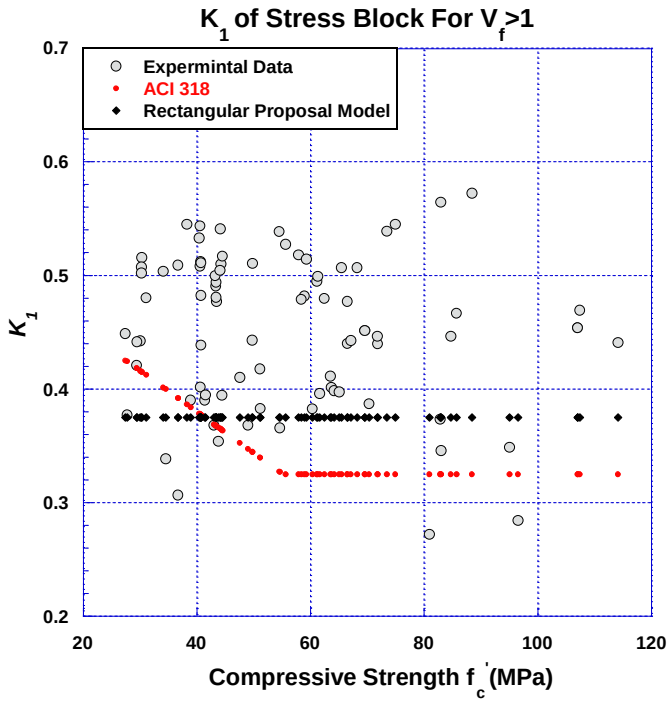

Figure 5-31: ACI 318 code K2 with the compressive strength for volume fraction more than 1.0.

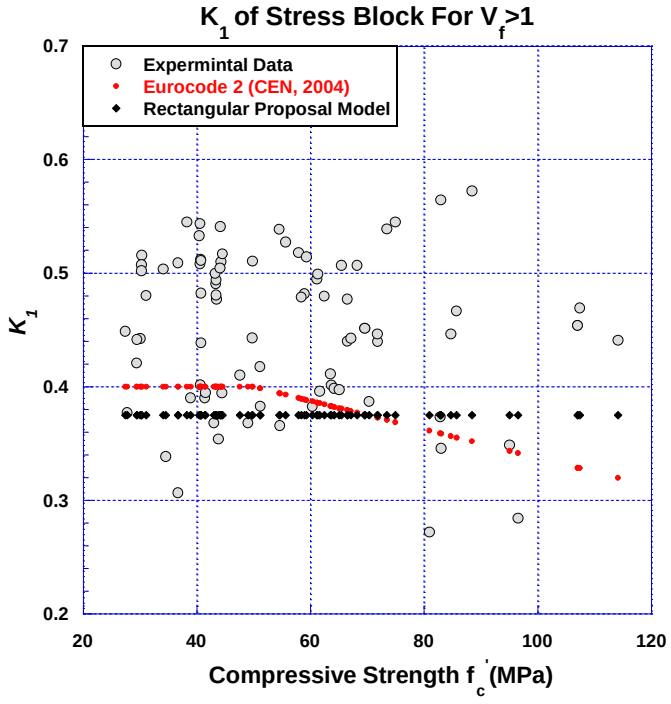

Figure 5-32: Eurocode K2 with the compressive strength for volume fraction more than 1.0.

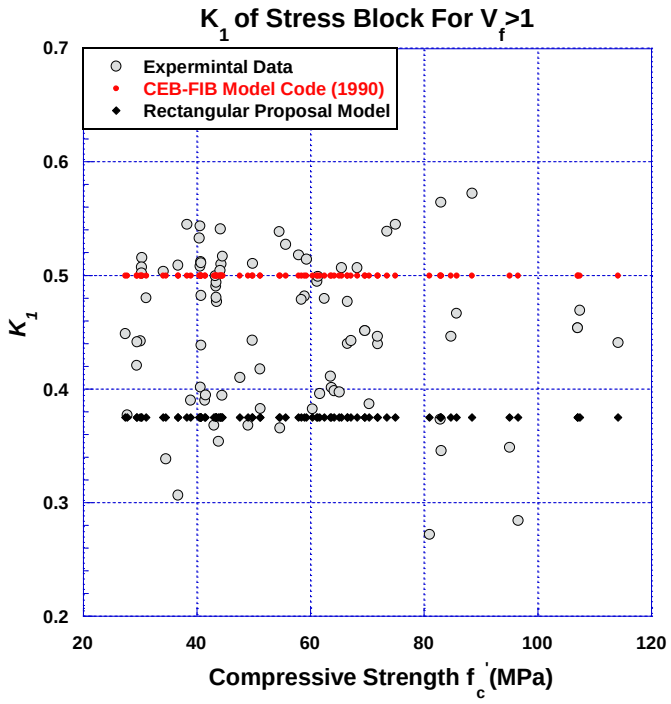

Figure 5-33: FIB Model code K2 with the compressive strength for volume fraction more than 1.0.

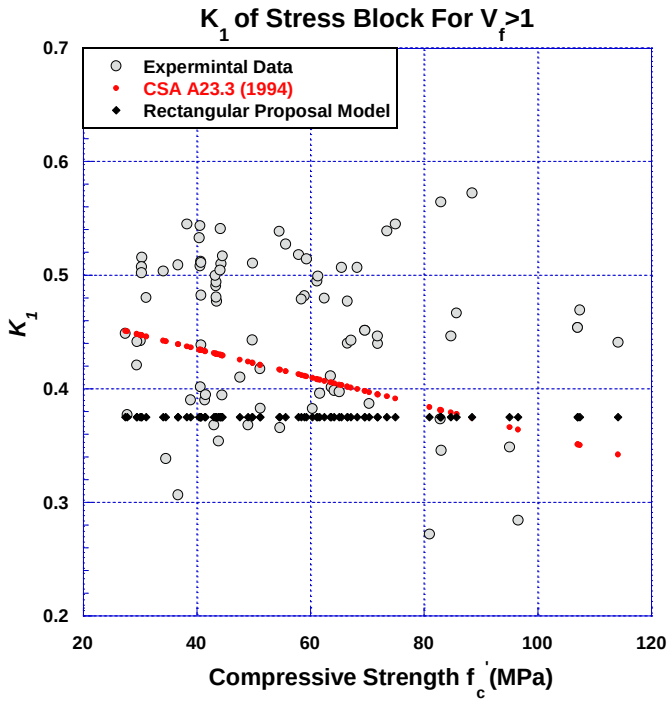

Figure 5-34: CSA code K2 with the compressive strength for volume fraction more than 1.0.

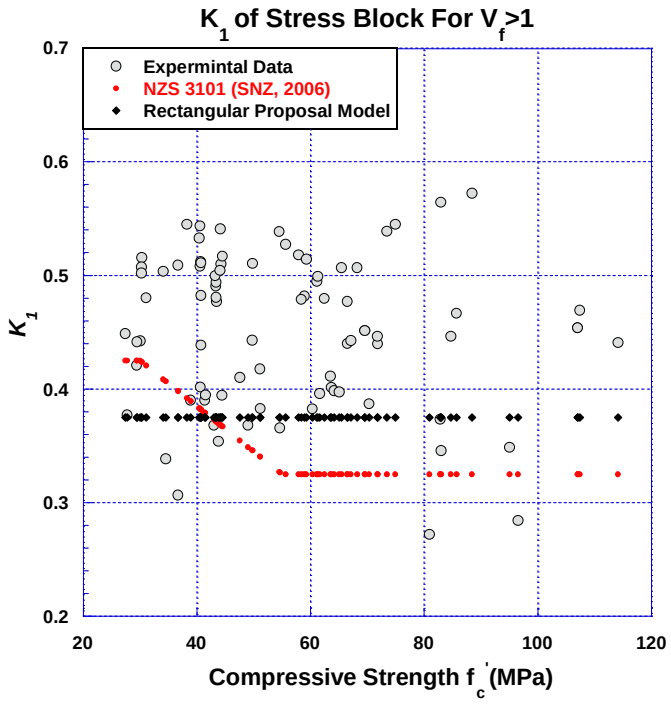

Figure 5-35: NZS 3101 code K2 with the compressive strength for volume fraction more than 1.0.

For trapezoid stress blocks, the proposed model is the same as the rectangular process which takes the lower bound of the data of area under stress-strain curves according to the requirement of designer for more safety. In volume fraction less than 1, the ACI 544 the stress block code is similar to the proposed model for compressive strength less than 69 MPa. While, for compressive strength more than 69 MPa, the ACI 544 underestimation of the lower bound of data. Despite that, the different is not big significant between the proposed and the ACI 544 model, see Figure 5-36.

For K_2 value, ACI 544 stress block code is similar to the proposed model for compressive strength less than 69 MPa. While, for compressive strength more than 69 MPa, ACI 544 is overestimated the lower bound of data, see Figure 5-37.

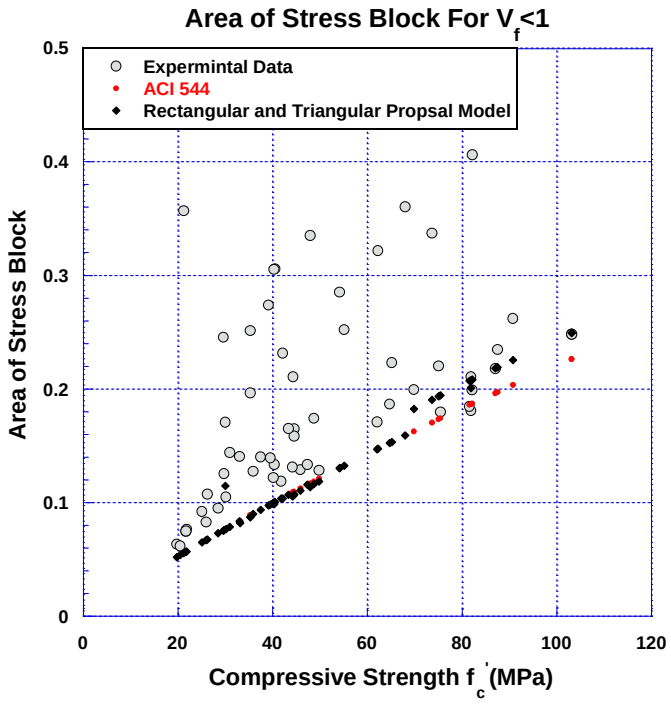

Figure 5-36: ACI 544 and proposal model area with the compressive strength for volume fraction < 1.0.

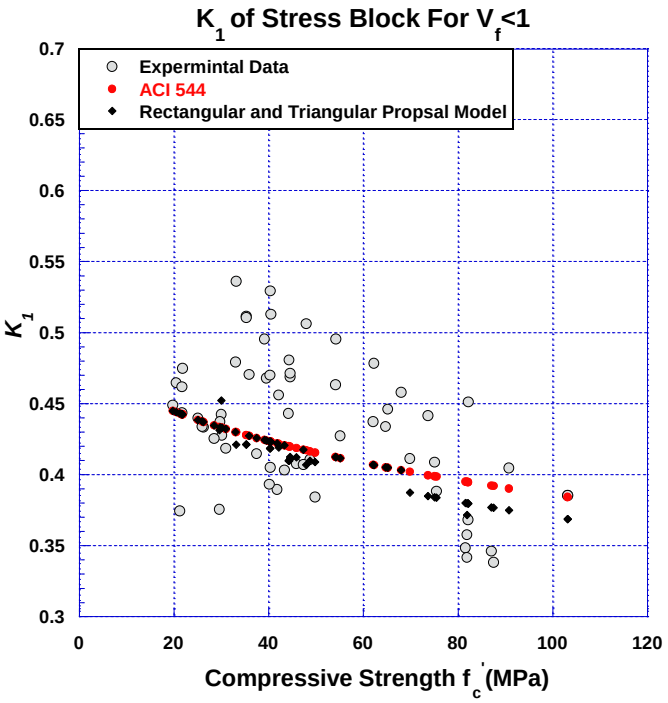

Figure 5-37: ACI 544 and proposal model K2 with the compressive strength for volume fraction < 1.0.

In volume fraction more than 1, ACI 544 shows the evaluation for an area of data for stress block more than twice the lower bound, see Figure 5-38. Therefore the other codes do not give a good evaluation due to neglecting the effect of fiber.

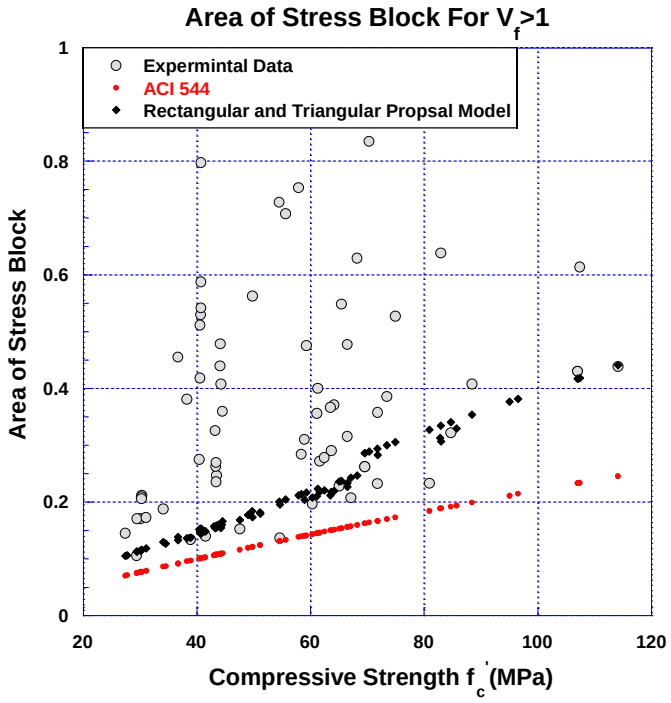

Figure 5-38: ACI 544 and proposal model area with the compressive strength for volume fraction > 1.0.

For K_2 value, ACI 544 stress block code is in the lower bound of the database while the proposal model is close to the average of database, as shown in Figure 5-39.

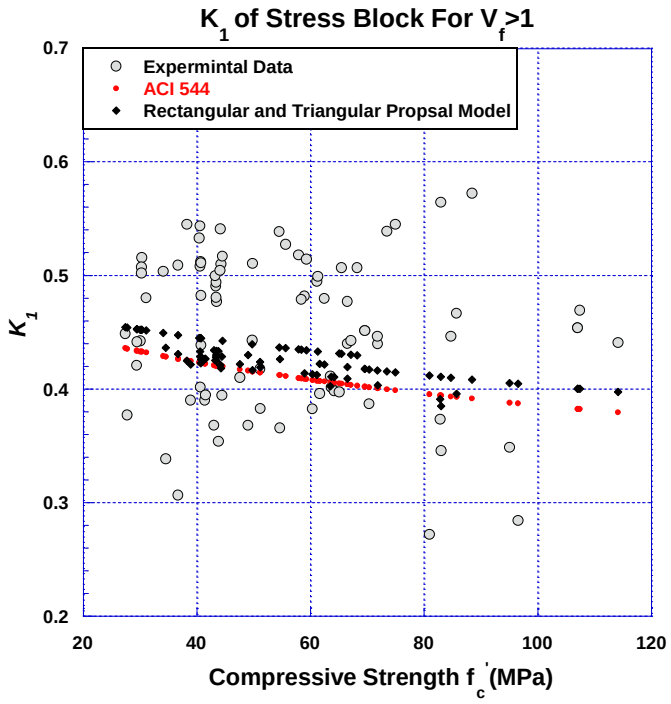

Figure 5-39: ACI 544 and proposal model K2 with the compressive strength for volume fraction > 1.0.

As shown in the Figures 5-40 and 5-41, the difference is clear between the rectangular and trapezoid of the area of stress blocks in volume fraction less than 1 for compressive strength more than 40 MPa. The rectangular stress block is underestimated in the database and also easy for a designer to use. For volume fraction more than 1, the rectangular and trapezoid area of stress blocks are almost identical. For K_2 value as shown in Figure 5-42 and 5-43, the rectangular stress block is in the lower bound of the database while the trapezoid of stress block model is close to the average of the database. Therefore, it will be using in the new design and analysis proposed model.

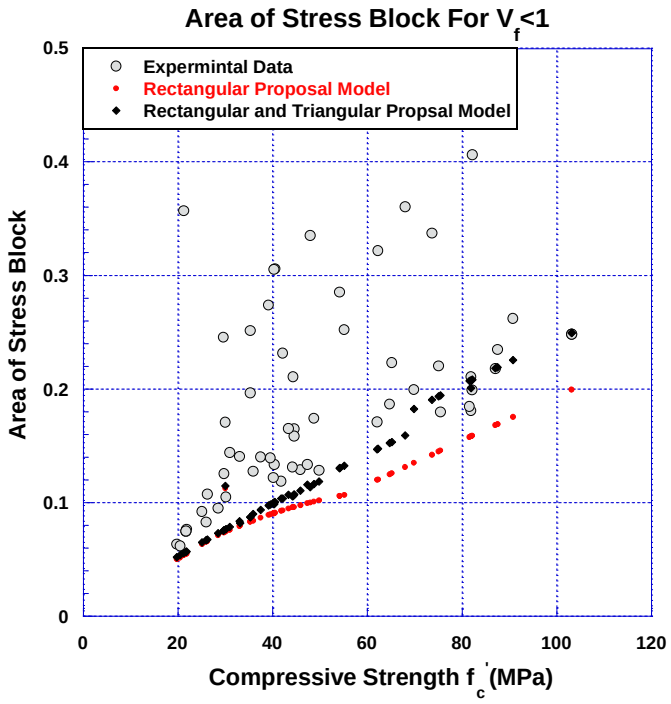

Figure 5-40: rectangular and trapezoid proposal model area with the compressive strength for Vf < 1.0.

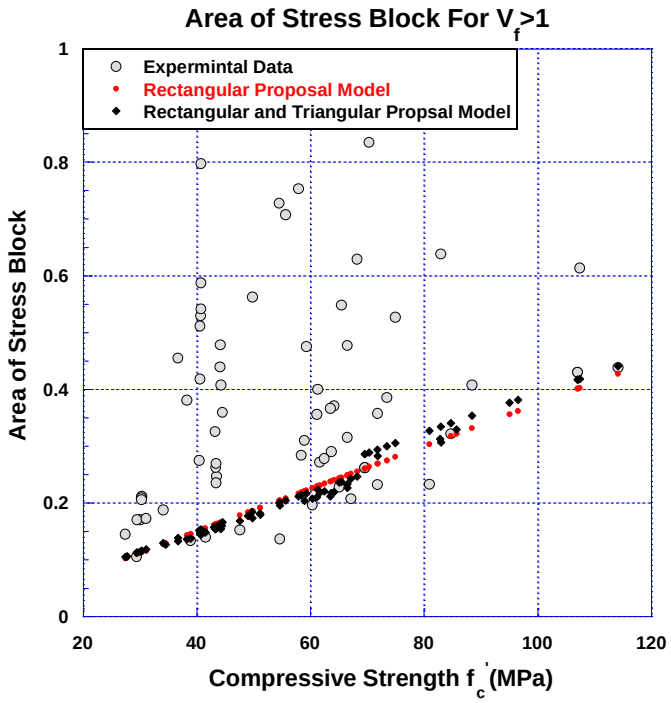

Figure 5-41: rectangular and trapezoid proposal model area with the compressive strength for Vf > 1.0.

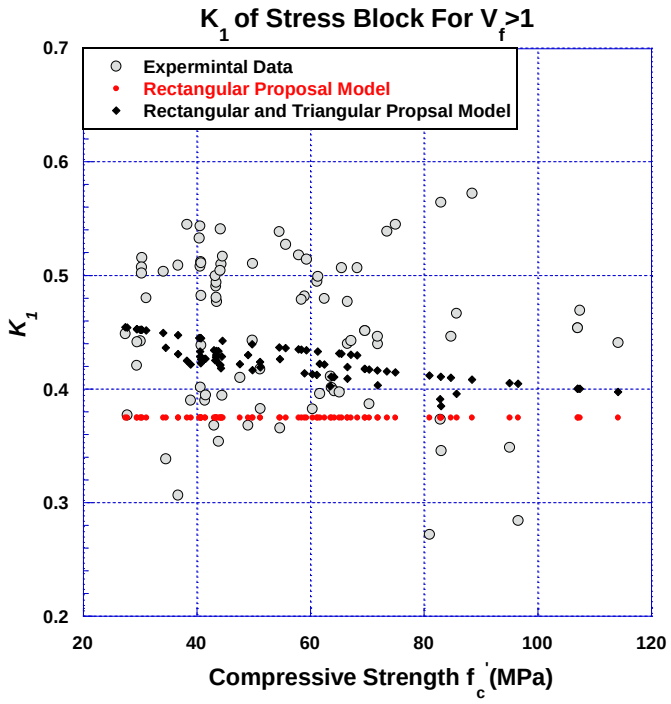

Figure 5-42: rectangular and trapezoid proposal model K2 with the compressive strength for Vf < 1.0.

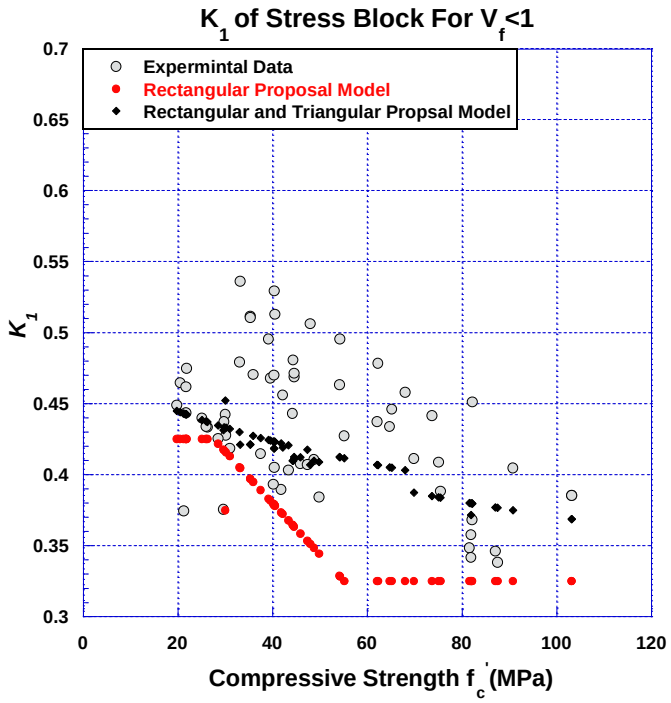

Figure 5-43: rectangular and trapezoid proposal model K2 with the compressive strength for Vf >1.0.

5.2 Theoretical determining for tension stress block

As explained in Chapter 4, the flexural strength test and direct tensile strength test give a good idea of the behavior of softening and hardening deflection and softening and hardening strain. There are four steps to achieve a good model for stress block.

1- The first step is to determine the stress-strain curves from a flexural test of experimental work.

2- The second step is evaluating the parameters study of stress block. These parameters are a first crack strength, first crack strain, the elastic modulus in tension and ultimate strain.

3- The third step is evaluated in the analysis model.

4- The last steps are evaluated in the design model.

5.2.1 Determine the stress-strain curves from a flexural test of experimental work

21 case studies of experimental work from the flexural test for different types of fiber and volume fraction for both FRC and FRCC were stress-strain evaluated by getting the load-strain curves results and compression and tension fiber strain. Thus, explained in Chapter 3, the tension theoretically is determined as three regions.

Table 5-4 showed the stress and strain of FRC and FRCC in five points in its curves, so $fcr\ and\ \varepsilon cr$ explain the stress and strain of the first crack point, and $flop\ and\ \varepsilon lop$ are the stress and strain of the first stress peak point in the curve

after the first crack. $fmin\ and\ \varepsilon min$ are the stress and strain of minimum stress point in the curve after first crack, and $fmax\ and\ \varepsilon max$ are the stress and strain of maximum stress points in the curve after the first crack. Last, $fult\ and\ \varepsilon ul$ are the stress and strain of ultimate strain that are the last points in the curve.

Table 5-4: the stress and strain of FRC and FRCC in five points in its curves.

$Fiber\ types$	$V_f\%$	fcr	εcr	$flop$	εlop	$fmin$	εmin	$fmax$	εmax	$fult$	εult
control	0	485.8293	0.000865	485.8293	0.000865	-	-	-	-	394.9235	0.002716
steel	0.5	374.0189	0.000292	438.7756	0.000752	-	-	374.2347	0.056769	334.0934	0.196358
	0.8	410.4155	0.000241	478.9828	0.001158	-	-	584.8864	0.032807	456.4182	0.192174
pva240	0.5	440.327	0.00022	373.0426	0.000908	-	-	-	-	199.959	0.009162
	0.8	506.1325	0.000308	399.1572	0.001817	-	-	-	-	281.0046	0.007919
pva150	0.5	463.8163	0.000285	508.8692	0.000475	-	-	-	-	183.9841	0.013641
	0.8	456.5112	0.000558	536.0151	0.001034	-	-	-	-	241.5012	0.011733
Polypropylene	0.5	360.5973	0.000238	431.0277	0.000821	21.69776	0.059867	48.93478	0.197441	48.78742	0.197644
	0.8	358.7407	0.000399	446.0325	0.000928	33.02051	0.033182	71.63661	0.144148	69.86513	0.14801
Polyefilen	0.5	464.8116	0.000257	-	-	-	-	559.7956	0.000258	123.5849	0.012085
	0.8	457.2269	0.000193	-	-	-	-	254.476	0.11406	148.5439	0.151376
control	0	426.2154	0.000932	426.2154	0.000932	-	-	-	-	421.1239	0.00129
steel	1.5	368.1942	0.000593	455.6503	0.001165	-	-	598.9056	0.023959	519.3117	0.19386
	2	642.4857	0.001787	-	-	-	-	1018.965	595.012	725.1223	402.7067
pva240	1.5	442.0967	0.000661	316.5854	0.0008	-	-	615.0705	0.014495	615.736	0.024532
	2	448.2691	0.000467	290.4337	0.000573	-	-	615.736	0.024532	278.8811	0.067207
pva150	1.5	342.9837	0.000335	448.7389	0.028413	-	-	-	-	299.8249	0.102647
	2	393.0865	0.000506	-	-	-	-	452.4299	0.030523	307.687	0.081178
Polypropylene	1.5	270.4055	0.000338	273.095	0.001163	126.4405	0.031145	105.6892	0.194457	104.106	0.20866
	2	288.6389	0.000376	359.7556	0.000695	126.3204	0.015332	138.2896	0.19631	135.4491	0.20755
Basalt	2	408.7276	0.000552	362.491	0.001071	-	-	363.456	0.001178	334.7673	0.001835

5.2.2 Evaluated the parameters study of stress block.

These parameters are a first crack strength, first crack strain, the elastic modulus in tension, and ultimate strain.

5.2.2.1 First crack strength f_{cr}

According to ASTMC 1018, and Naamen, the first crack strength can be determined from both flexural strength test and direct tensile strength test because of the elastic behavior or its stage. Therefore, more than 250 data points were used to evaluate the first crack strength.

The new empirical relations developed the ACI 318 equation by multiple factor λ:

$$f_{cr} = 7.5\,\lambda f_c'^{0.5} \quad (psi) \qquad \textit{Equation 5-18}$$

As a result, in Figure 5-44, the data show that two behaviors for λ factor depend on the length of the fiber before and after $l_f = 10\ mm$. From the results,it is clear that the average λ data for $(l_f) < 10\ mm$ is 1, while the lower bound for this data is 0.75. for $(l_f) \geq 10\ mm$. The λ data representive as a liner equation starts from 0.42 at $l_f = 10\ mm$ to 1.6 at $l_f = 60\ mm$, while for lower bound of the database the difference decreases 0.3 from the value of the a liner equation of avearge data.

To summarize the results of the λ factors proposal for 250 databases as below,

$$\lambda = \begin{cases} 1.0, & for\ concrete\ without\ fiber \\ 1.0, & for\ FRC\ and\ FRCC\ with\ fiber\ length\ (l_f) < 10\ mm \\ 0.02\ l_f + 0.4, & for\ FRC\ and\ FRCC\ with\ fiber\ length\ (l_f)\ \geq 10\ mm \end{cases}$$

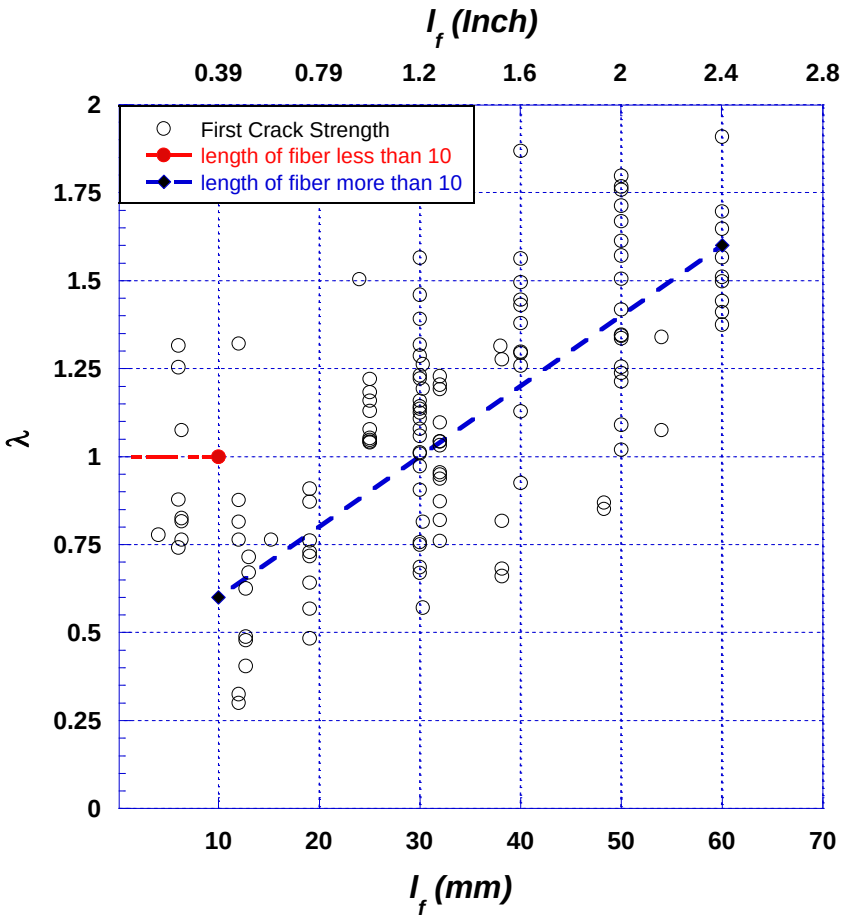

Figure 5-44: λ factor with the length of the fiber (average of the data).

For design purposes, λ will be the lower bound of data to be more satisfied; therefore, λ will be equal to λ_{min}, see Figure 5-45.

$$\lambda_{min} = \begin{cases} 1.0, & for\ concrete\ without\ fiber \\ 0.75, & for\ FRC\ and\ FRCC\ with\ fiber\ length\ (l_f) < 10\ mm \\ 0.02\ l_f + 0.1\ \leq 1.3, & for\ FRC\ and\ FRCC\ with\ fiber\ length\ (l_f)\ \geq 10\ mm \end{cases}$$

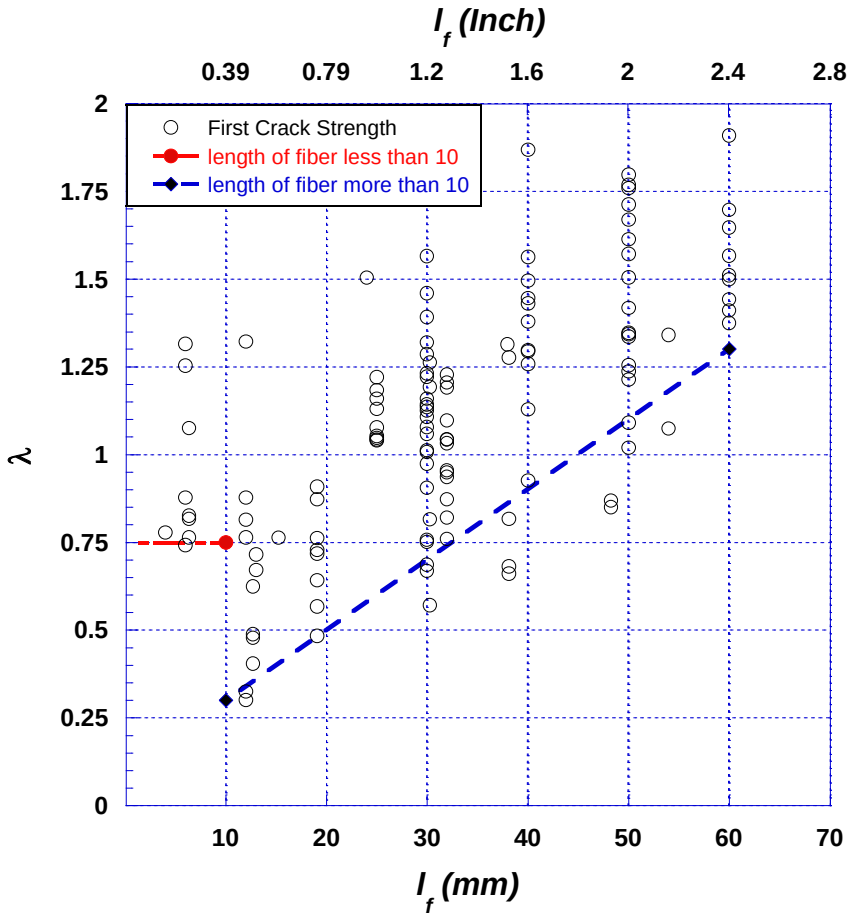

Figure 5-45: λ factor with the length of the fiber (lower bound of the data).

5.2.2.2 First crack strain ε_{cr}

According to the 150 data point, a new equation for first crack strain was developed to account for the influence of additional fibers in concrete for FRC and FRCC. The new equation below depends on the lower bound of data. Apparently, the new equation does not depend on the volume of fraction and types of fiber.

$$\varepsilon_{cr} = \frac{0.008}{f_c'} \geq 0.0001, \quad for\ f_c'\ in\ Mpa \qquad \textit{Equation 5-19}$$

$$\varepsilon_{cr} = \frac{1.12}{f_c'} \geq 0.0001, \quad for\ f_c'\ in\ psi$$

From the Figure 5-46, it is clear the first crack strain decreases with the increase in compressive strength.

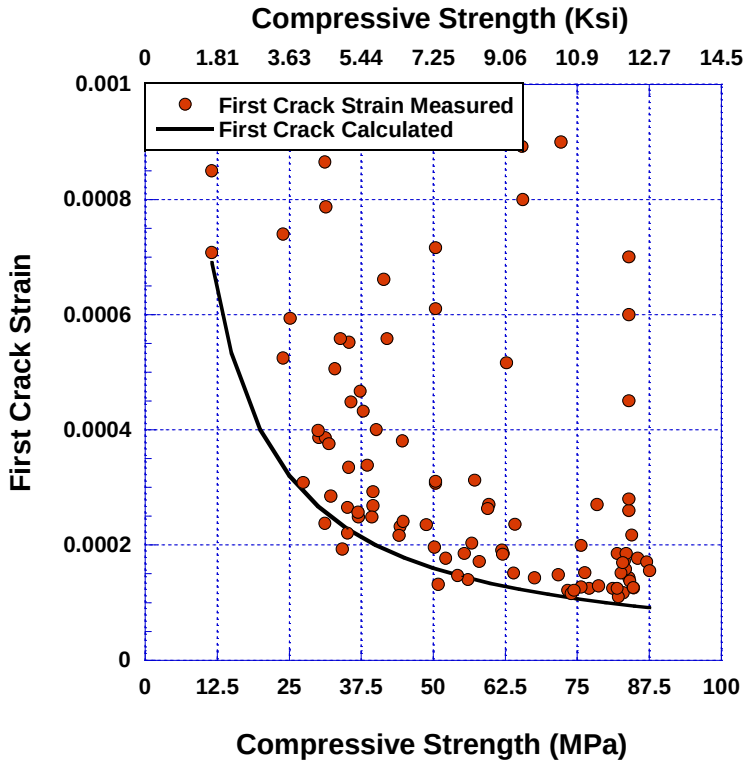

Figure 5-46: first crack strain with compressive strength of FRC and FRCC.

5.2.2.3 Elastic modulus in tension

As explained in Chapter 4, the new equation can be calculated from Hooke's law that states that the elastic modulus in tension is equal to the slope of the first crack strength to first crack strain of the stress-strain curve in tension.

$$E_t = \frac{f_{cr}}{\varepsilon_{cr}} \qquad \textit{Equation 5-20}$$

Therefore;

$$E_t = 77.5\ \lambda\ {f_c'}^{1.5}, \quad Mpa$$
$$E_t = 6.7\ \lambda\ {f_c'}^{1.5}, \quad psi$$

Equation 5-21

And $\gamma\ factore\ is$

$$\gamma = \frac{E_c}{E_t} = \frac{4700\ \lambda_{V_f}\sqrt{f_c'}}{77.5\ \lambda\ {f_c'}^{1.5}} = \frac{60.65\ \lambda_{V_f}}{\lambda\ f_c'}, \quad for\ f_c'\ in\ Mpa$$
$$\gamma = \frac{E_c}{E_t} = \frac{57000\ \lambda_{V_f}\sqrt{f_c'}}{6.7\ \lambda\ {f_c'}^{1.5}} = \frac{850.75\ \lambda_{V_f}}{\lambda\ f_c'}, \quad for\ f_c'\ in\ psi$$

Equation 5-22

Also, the neutral axis of FRC and FRCC

$$K_{(Elastic)} = \frac{1}{1+\sqrt{\gamma}}$$

Equation 5-23

$$N.A_{\ (Elastic)} = K_{(Elastic)}h$$

Equation 5-24

From the 250 database, the Figure 5-47 illustrates that the neutral axis of FRC and FRCC decreases with the increasing of compressive strength.

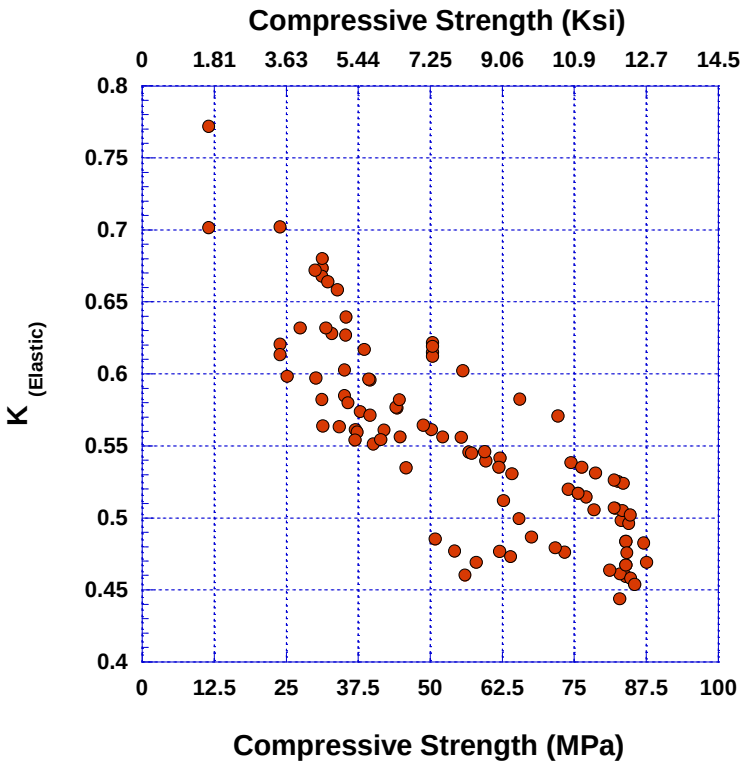

Figure 5-47: elastic modulus in tension of FRC and FRCC.

5.2.2.4 Ultimate strain $\varepsilon_{ult.}$

The new equation for ultimate strain in tension depends on the types of fiber taking into consideration the volume fraction and the geometric of fiber. Therefore, including the volume fraction and the geometric of fiber in the calculation of the ultimate strain is done in order to reach a more comprehensive and safe model for the designer. The tensile responses terminate at the normalized ultimate tensile strain α_2, as shown below.

$$\varepsilon_{Ult.} = \alpha_2 \varepsilon_{cr} \qquad \textit{Equation 5-25}$$

Table 5-5 explains the α_2 factor for three groups of fiber: PVA, steel, and synthetic fiber. This factor depends on the volume of fraction and length of the fiber.

Table 5-5: α_2 factor of FRC and FRCC for different types of fibers.

α_2	
Synthetic Fiber	$1.25\ V_f l_f$
PVA Fiber	$0.85\ V_f l_f$
Steel Fiber	$1.85 V_f l_f - 48, \leq 10$

The method that adopts to evaluating this factor is a lower bound of the database. Figure 5-48 illustrate that value of α_2 factor of synthetic fiber is so high, due to the high ultimate strain to first crack strain ratio. That was caused by the behavior of synthetic fiber that allowed to high ultimate strain of concrete after first crack. As explained above, this model depends on the lower bound of data.

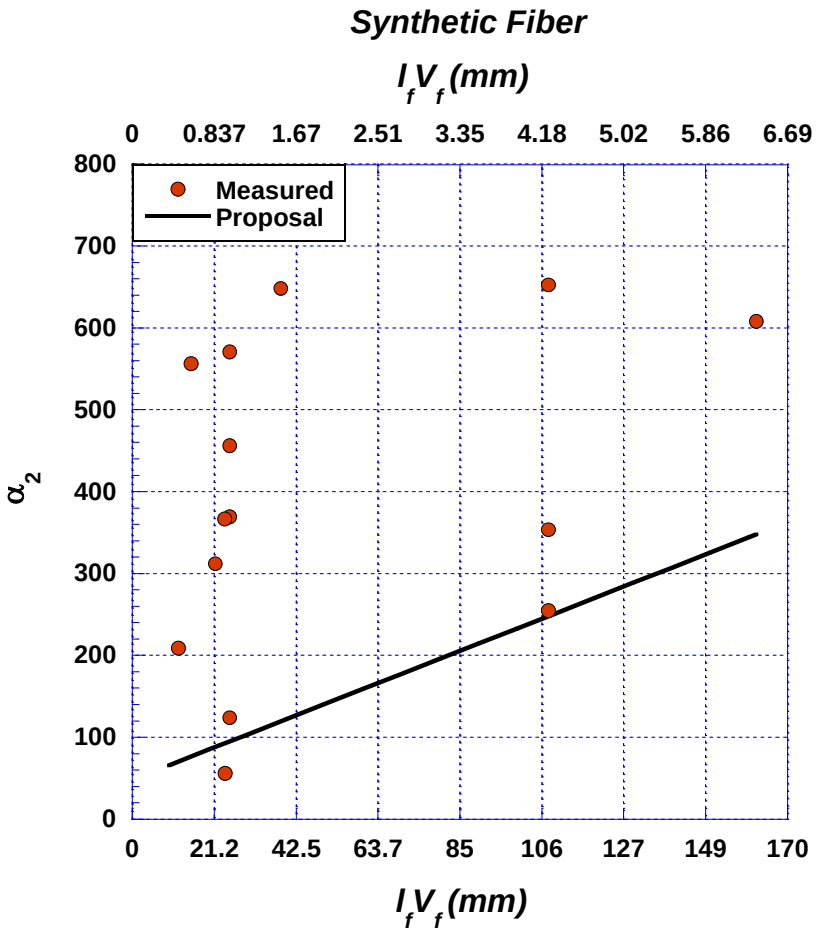

Figure 5-48: α_2 factor used the lower bound of data of synthetic fiber.

For PVA fiber, by the same concept of synthetic fiber, the equation of α_2 factor used the lower bound of data, see Figure 5-49. The results show the PVA has lower ultimate strain than synthetic and steel fibers, despite having higher strength because the PVA fiber characteristic is micro-fiber.

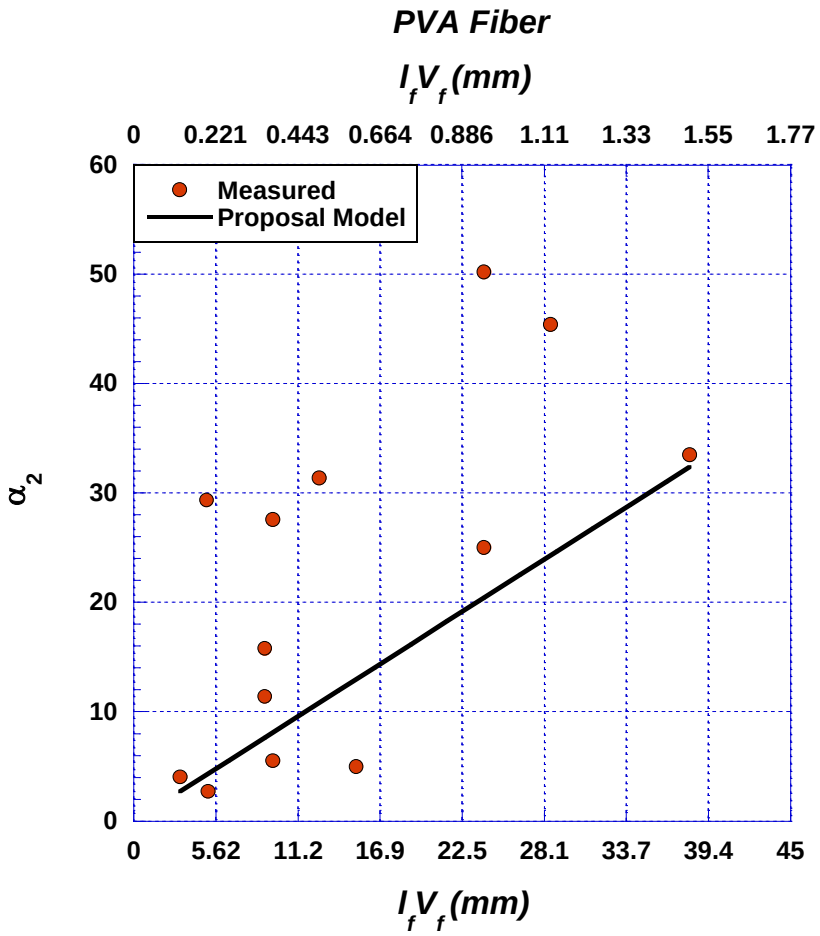

Figure 5-49: α_2 factor used the lower bound of data of PVA fiber.

Also steel fiber, the equation of α_2 factor used the lower bound of data. The results show the steel fiber has lower ultimate strain than synthetic fiber and higher than PVA fiber.

It is clear that α_2 factor of the steel fiber has two behaviors that depend on V_f, as shown in Figure 5-50. For $V_f l_f < 30\ mm$, the α_2 factor of the steel fiber is constant value =10 mm. For $V_f l_f \geq 30\ mm$, the α_2 factor of the steel fiber increases with the increase of $V_f l_f$.

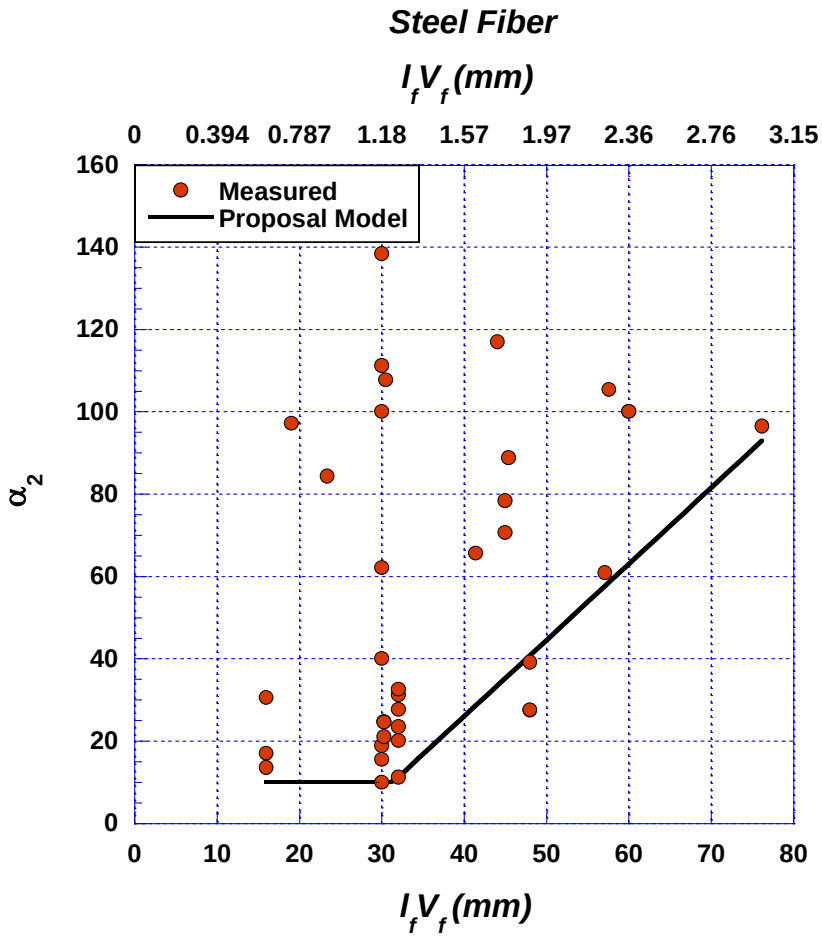

Figure 5-50: α_2 factor used the lower bound of data of steel fiber.

As shown in Figure 5-51, this model will lead to the best safe design and an easier process method for the designers.

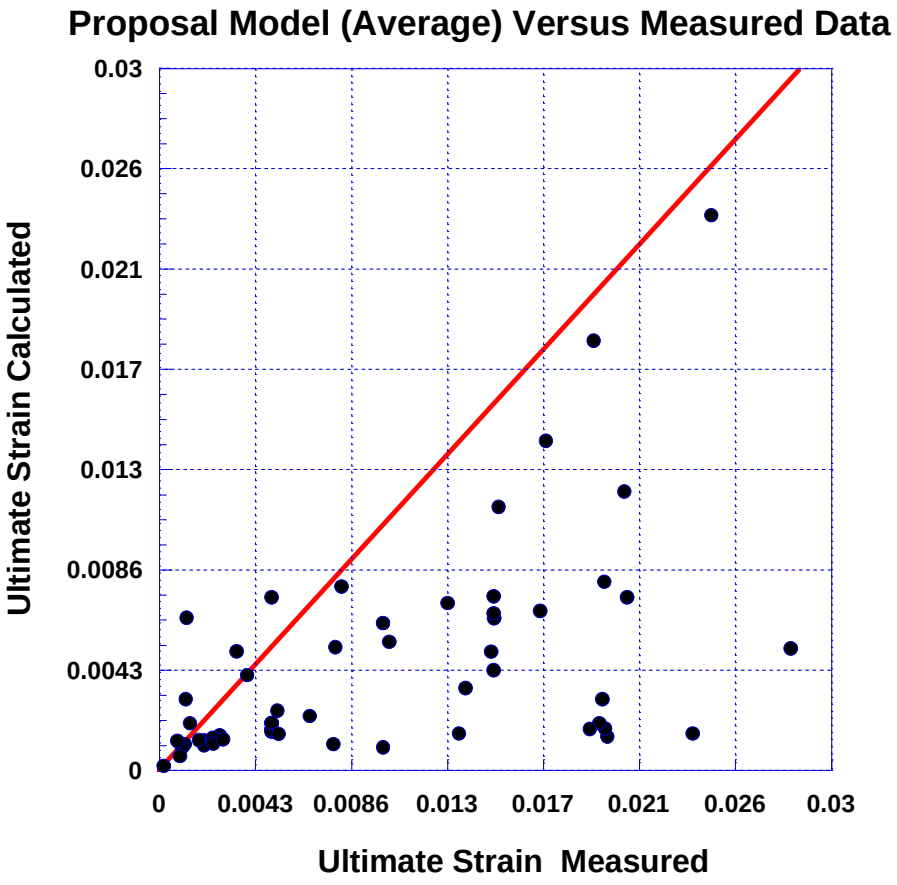

Figure 5-51: ultimate strain of FRC and FRCC in tension.

5.3 Analysis and design of new model of FRC and FRCC for the ultimate stage

According to results of compression, stress block explains that the FRC and FRCC in compression zone are represented by a rectangular stress block due to underestimation of the database and also because it is easy for a designer to use. Also, the FRC and FRCC in tension is assumed to have a rectangular stress block with an average uniform stress σ_p, referring to Figure 5-52.

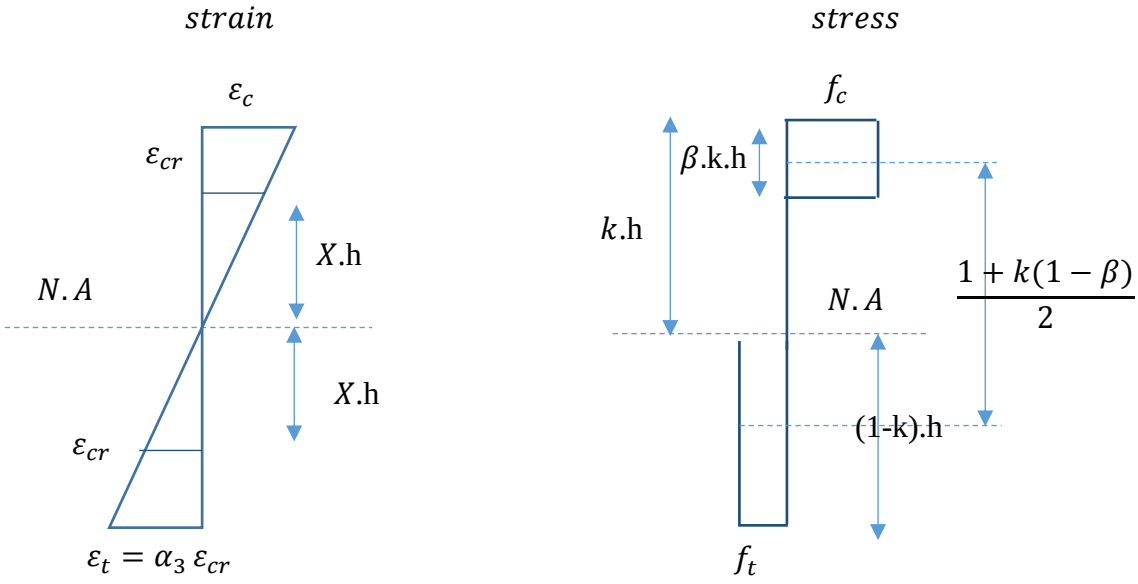

Figure 5-52: stress block in flexural.

Assumption:

As explained in Chapter 2 and 4, ACI 544.4R, 2018 and Rilem TC 162-TDF, 2003, found that the compression part depth in the beam (neutral axis) was 10% from the total depth of the beam. Therefore, neutral axis (k) at ultimate stage

is equal to 10% from the total depth of the beam. Therefore, summary of the assumption of this model follows below:

4- Elastic stage in compression, therefore $\alpha = \frac{E_c\, \varepsilon_c}{f_c'}$.

5- The design moment capacity of FRC and FRCC $\emptyset M_n$ should be greater than the factored moment M_u applied to the member. ACI 544.4R-18. $\emptyset M_n > M_u$.

6- Assume K=0.1

5.3.1 Analysis FRC and FRCC:

Figure 5-53 explained that stress block in flexure for analysis model.

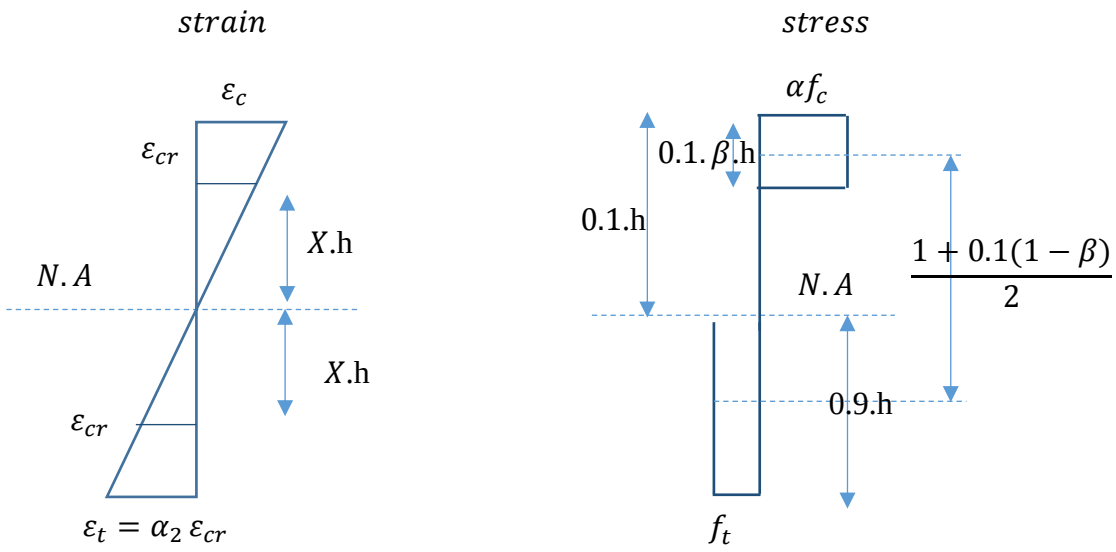

Figure 5-53: stress block in flexure for analysis model.

The first step is to determine the first crack strain in tension by the proposal equation below;

$$\varepsilon_{cr} = \frac{0.008}{f_c'} \geq 0.0001, \quad for\ f_c'\ in\ Mpa \qquad \textit{Equation 5-26}$$

Then determine the α_2 factor of ultimate strain in tension depending on the length and volume fraction of fiber, see Table 5-6.

$$\varepsilon_t = \varepsilon_{Ult.} = \alpha_2 \varepsilon_{cr} \qquad \textit{Equation 5-27}$$

In the tension part, we can determine the depth of first crack strain by

$$\frac{\alpha_2\,\varepsilon_{cr}}{0.9\,h} = \frac{\varepsilon_{cr}}{X\,h}$$

$$X = \frac{0.9}{\alpha_2} \qquad \textit{Equation 5-28}$$

In the compression part, we can determine the compression strain by

$$\frac{\varepsilon_c}{0.1\,h} = \frac{\varepsilon_{cr}}{X\,h}$$

$$\varepsilon_c = \frac{0.1\varepsilon_{cr}}{\frac{0.9}{\alpha_2}} \qquad \textit{Equation 5-29}$$

Therefore;

$$\varepsilon_c = \frac{\alpha_2\,\varepsilon_{cr}}{9} \qquad \textit{Equation 5-30}$$

After determiningε_c, it is easy to evaluate $\alpha\ and\ \beta$, depending on the rectangular stress block parameters.

Then determine the arm is

$$\text{arm} = \frac{1 + 0.1(1-\beta)}{2} = \frac{1.1 - 0.1\beta}{2}\,h \qquad \textit{Equation 5-31}$$

, and force is

$$F = 0.1\alpha\,f_c^{'}\,\beta\,hb \qquad \textit{Equation 5-32}$$

To determine the nominal bending resistance of FRC and FRCC by

$$M_n = Force\ \times lever\ arm = 0.1\alpha\,f_c'\,\beta\,h^2 b(1 - \frac{1-0.1}{2} - \frac{0.1\beta}{2}) \qquad \textit{Equation 5-33}$$

Therefore;

$$M_n = \frac{\alpha\, f_c'\, h^2 b}{2}(0.11 - 0.01\beta)\beta \qquad \textit{Equation 5-34}$$

The **analysis moment capacity** of FRC and FRCC $\emptyset M_n$ should be lower than the factored moment M_u applied to the member.

$$\boldsymbol{\emptyset M_n < M_u}$$

As explained in Chapter4, the reduction factor $\emptyset$ depends on the type of the member, and its failure mode should be determined based on ACI 318 or other building codes and is typically between 0.65 and 0.9 for flexural members.

Figures 5-54 to 5-60 illustrated the $\emptyset$ factor with the moment. For $\emptyset = 1$, it is clear that the model provides internal moment less than the external moment for analysis of FRC and FRCC; therefore, it has more safety, but is overestimated. As shown in the Figures 5-55 to 5-57 when the value$\emptyset$ were 0.9, 0.85, and 0.75there were some data that became underestimated. For $\emptyset$ are 0.5, 0.65, and 0.7, there was much of the value of moment overestimated that it is not safety. Therefore, this model adopts the $\emptyset$ is 0.75 because of the safety, despite a very small amount of data that has been overestimated.

Figure 5-61 explains the comparison of the moment of the proposed model with a moment of the ACI 544 model. It is clear that the proposed model is safer and more accurate than the ACI 544 model because the ACI 544 model has overestimated moment value for more than 3.5 Kn.m.

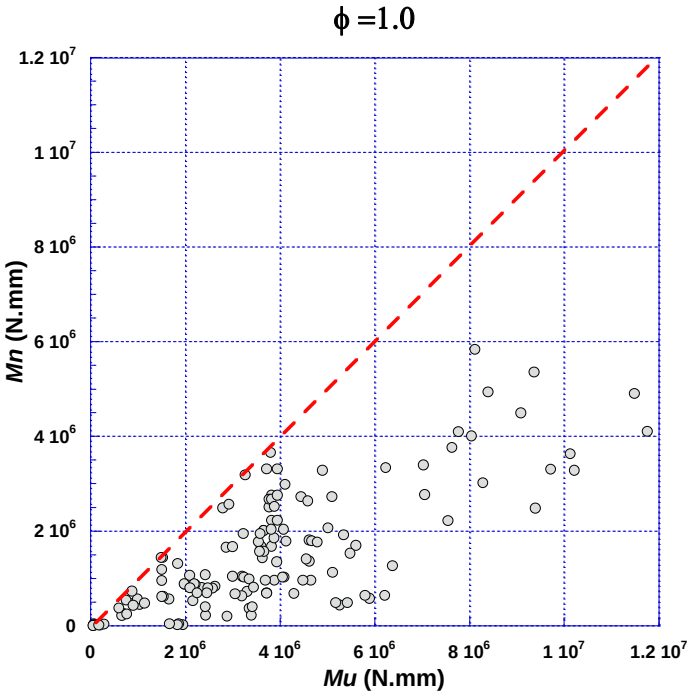

Figure 5-54: internal moment vs. the external moment for analysis of FRC and FRCC with Ø=1.

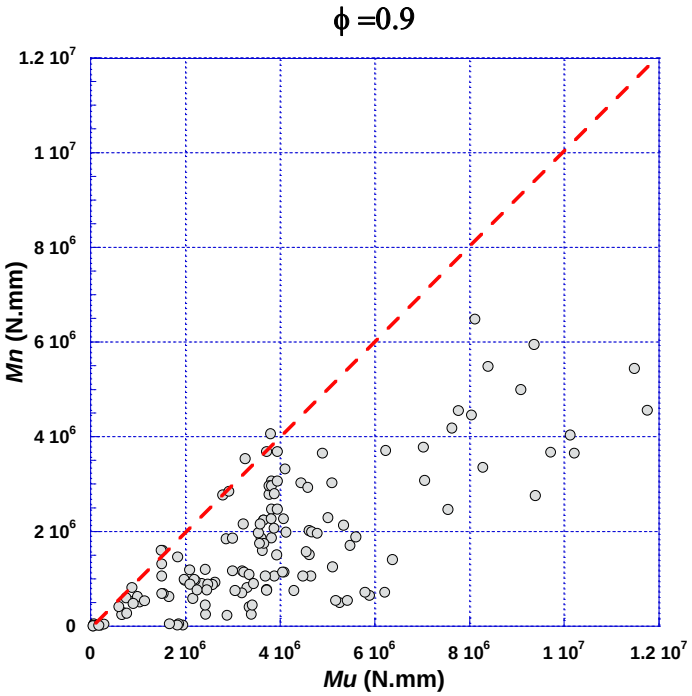

Figure 5-55: internal moment vs. the external moment for analysis of FRC and FRCC with Ø=0.9.

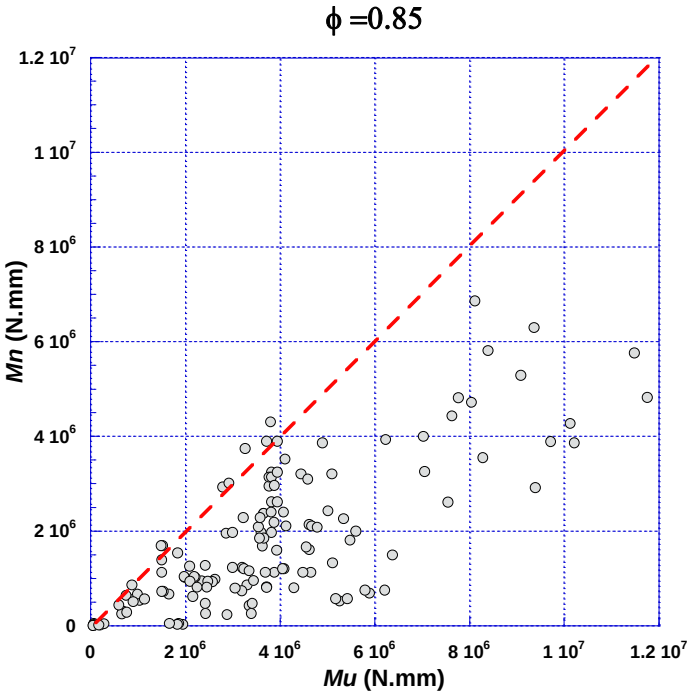

Figure 5-56: internal moment vs. the external moment for analysis of FRC and FRCC with Ø=0.85.

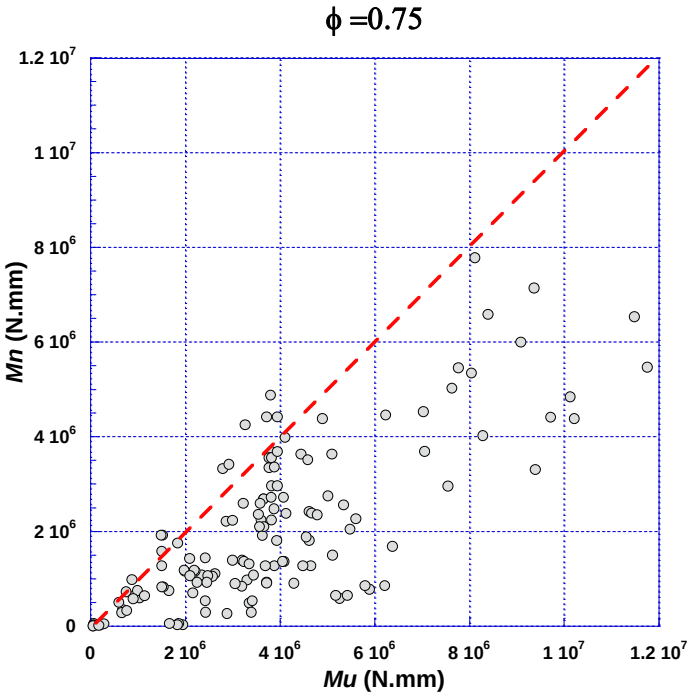

Figure 5-57: internal moment vs. the external moment for analysis of FRC and FRCC with Ø=0.75.

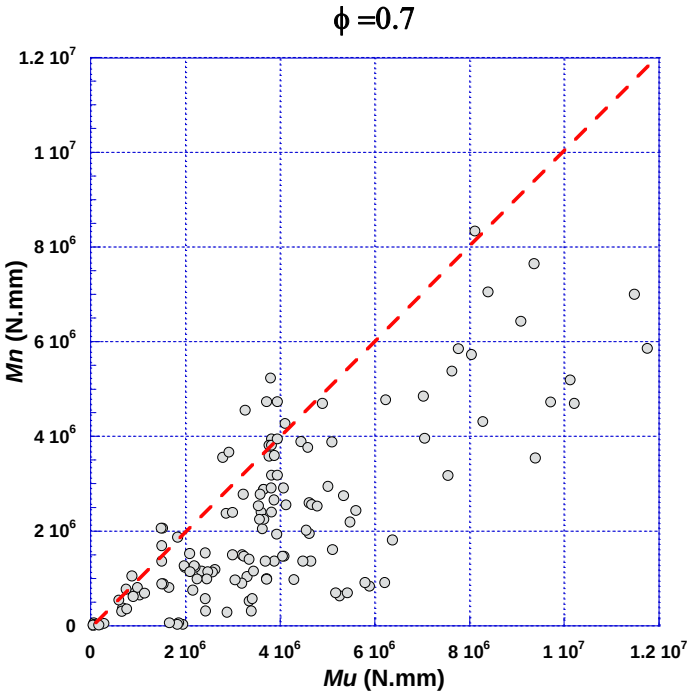

Figure 5-58: internal moment vs. the external moment for analysis of FRC and FRCC with Ø=0.7.

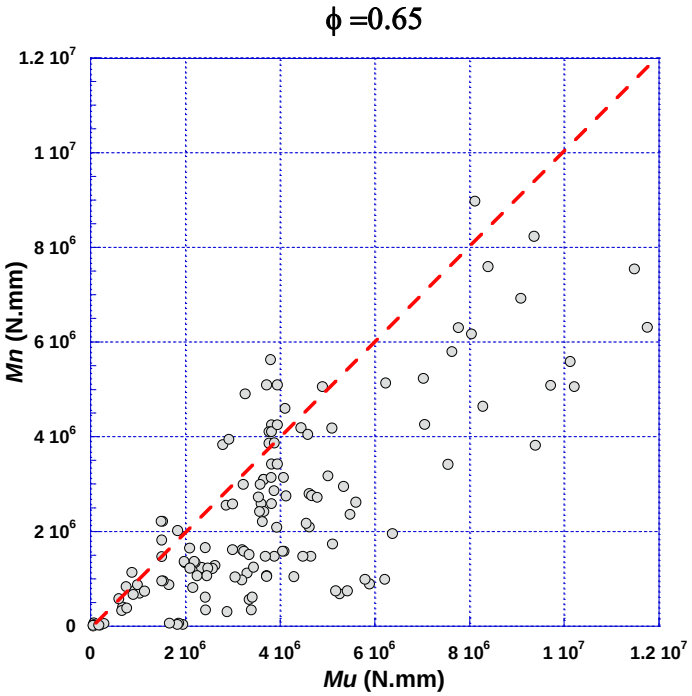

Figure 5-59: internal moment vs. the external moment for analysis of FRC and FRCC with Ø=0.65.

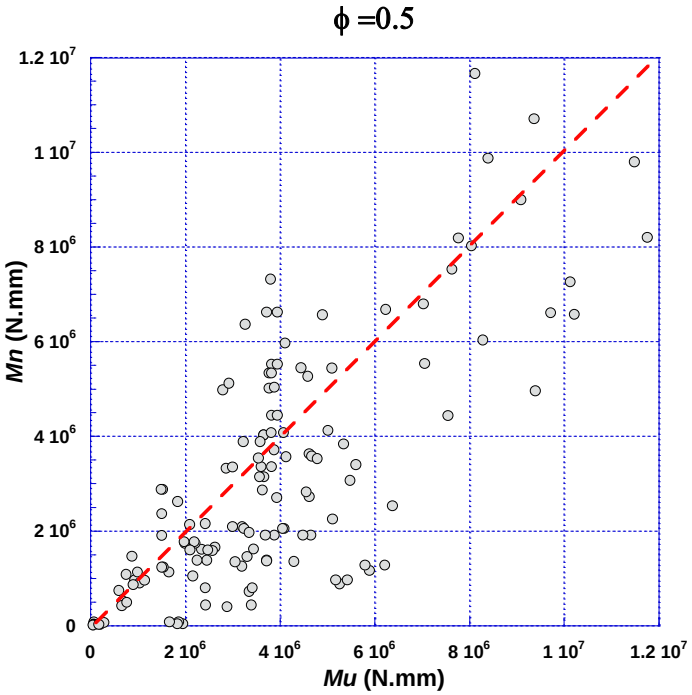

Figure 5-60: internal moment vs. the external moment for analysis of FRC and FRCC with Ø=0.5.

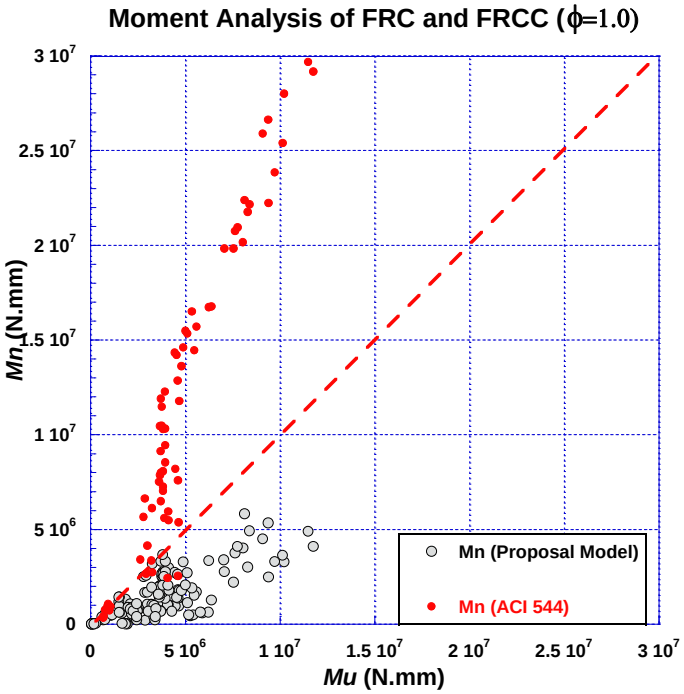

Figure 5-61: moment of proposal model vs. a moment of ACI 544 model.

5.3.2 Design FRC and FRCC:

Figure 5-62 explained stress block in flexure for design model for FRC and FRCC.

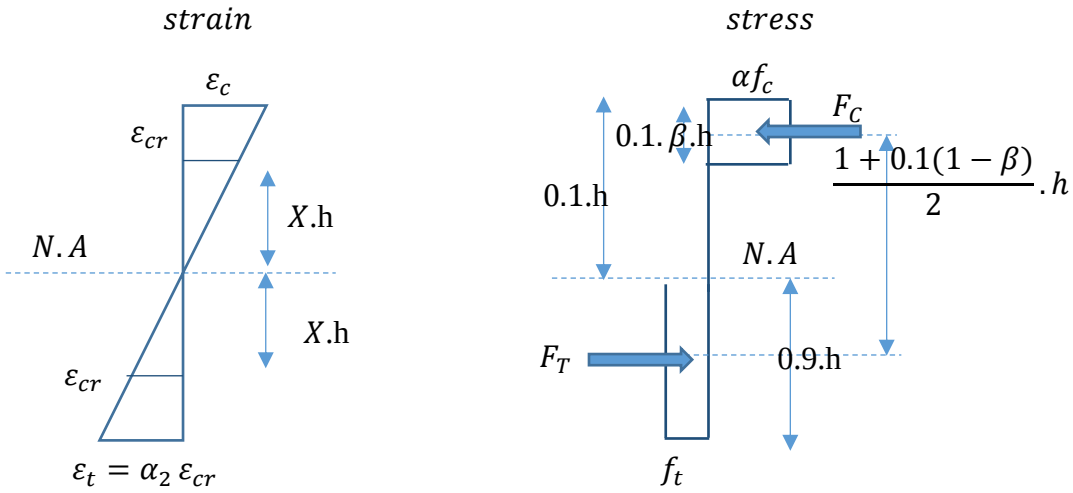

Figure 5-62: stress block in flexure for design model.

From force equilibrium:

$$F_T = F_C$$

$$0.1\alpha\, f_c'\, \beta h = 0.9 f_t\, h \qquad \textit{Equation 5-35}$$

$$\alpha = \frac{9 f_t}{f_c'\, \beta} \qquad \textit{Equation 5-36}$$

From FRC and FRCC compression stress block explained above in section 4.1, it will assume that $\varepsilon_c < \varepsilon_y$; therefore the β =0.65 and

$$\alpha = \frac{E_c\, \varepsilon_c}{f_c'} \leq 0.85 \qquad \textit{Equation 5-37}$$

$$\frac{E_c\,\varepsilon_c}{f_c'} = \frac{9\,f_t}{0.65\,f_c'} \qquad \textit{Equation 5-38}$$

$$\varepsilon_c = 13.85\,\frac{f_t}{E_c} \qquad \textit{Equation 5-39}$$

In Figure 5-62, we assumed that $E_c = E_t$, from strain distribution;

In the tension part, we can determine the depth of first crack strain by determining the first crack strain in tension by the proposed equation below;

$$\varepsilon_{cr} = \frac{0.008}{f_c'} \geq 0.0001, \quad for\ f_c'\ in\ Mpa \qquad \textit{Equation 5-40}$$

Then determine the α_2 factor of ultimate strain in tension, depending on the length and volume fraction of fiber, see Table 5-6.

$$\varepsilon_t = \varepsilon_{Ult.} = \alpha_2 \varepsilon_{cr}$$

$$\frac{\alpha_2\,\varepsilon_{cr}}{0.9\,h} = \frac{\varepsilon_{cr}}{X\,h} \qquad \textit{Equation 5-41}$$

$$X = \frac{0.9}{\alpha_2}$$

In the compression part, we can determine the compression strain by

$$\frac{\varepsilon_c}{0.1\,h} = \frac{\varepsilon_{cr}}{X\,h}$$

$$\varepsilon_c = \frac{0.1\varepsilon_{cr}}{\frac{0.9}{\alpha_2}} \qquad \textit{Equation 5-42}$$

Therefore;

$$\varepsilon_c = \frac{\alpha_2\, \varepsilon_{cr}}{9}$$

Equation 5-43

$$\frac{\alpha_2\, \varepsilon_{cr}}{9} = 13.85\frac{f_t}{E_c}$$

$$\alpha_2 = 124.6\frac{f_t}{\varepsilon_{cr}\, E_c}$$

$$\alpha_2 = 124.6\frac{f_t}{\frac{0.008}{f_c^{'}}\, .4700\sqrt{f_c^{'}}}$$

Equation 5-44

Because that first crack strain for FRC and FRCC is $\varepsilon_{cr} = \frac{0.008}{f_c^{'}} \geq 0.001$, and the elastic modulus for FRC and FRCC is $E_c = 4700\ \lambda_{V_f}\sqrt{f_c'}$, this design model assumed $\lambda_{V_f} = 1$

$$\alpha_2 = 3.32\, f_t\sqrt{f_c^{'}}$$

Equation 5-45

Then determine the arm is

$$\text{arm} = \frac{1 + 0.1(1-\beta)}{2}\text{h} = \frac{1.1 - 0.1\beta}{2}h$$

Equation 5-46

, and force is

$$F = f_t(1 - 0.1)hb$$

Equation 5-47

To determine the nominal bending resistance of FRC and FRCC, $k_{Ult.} = 0.1$ and β=0.65, by

$$M_n = Force \times lever\ arm = f_t(1-0.1)h^2 b\frac{1.1-0.1\beta}{2} \quad \textit{Equation 5-48}$$

So,

$$M_n = \frac{0.9h^2 b(1.035)f_t}{2} \quad \textit{Equation 5-49}$$

$$M_n = 0.465\ h^2 b f_t$$

The design moment capacity of FRC and FRCC $\emptyset M_n$ should be greater than the factored moment M_u applied to the member (ACI 544.4R-18).

$$\emptyset M_n > M_u \quad \textit{Equation 5-50}$$

$$0.465\emptyset\ h^2 b f_t > M_u$$

$$f_t > \frac{M_u}{0.465\emptyset\ h^2 b} \quad \textit{Equation 5-51}$$

Because $\alpha_2 = 3.32.f_t\sqrt{f_c^{'}}$

$$f_t = \frac{\alpha_2}{3.32\sqrt{f_c^{'}}} \quad \textit{Equation 5-52}$$

Therefore;

$$\frac{\alpha_2}{3.32\sqrt{f_c'}} > \frac{M_u}{0.465\emptyset\, h^2 b}$$

Equation 5-53

$$\therefore\ \alpha_2 > 7.14\,\frac{M_u\sqrt{f_c'}}{\emptyset\, h^2 b}$$

For Synthetic,

$$V_f > 5.712\,\frac{M_u\sqrt{f_c'}}{\emptyset\, h^2 b\, l_f}$$

Equation 5-54

For PVA,

$$V_f > 8.4\,\frac{M_u\sqrt{f_c'}}{\emptyset\, h^2 b\, l_f} \geq \frac{31.35}{l_f}$$

Equation 5-55

For steel,

$$V_f > \left(\frac{3.86\, M_u\sqrt{f_c'}}{\emptyset\, h^2 b\, l_f} + \frac{25.95}{l_f}\right)$$

Equation 5-56

From equilibrium Force:

$$f_t = \frac{\alpha\, f_c'\, \beta k}{(1-k)}$$

Equation 5-57

From equilibrium Moment:

$$f_t = \frac{2M_n}{(1-k)h^2 b(1+(1-\beta)k)} \qquad \textit{Equation 5-58}$$

Then,

$$\frac{\alpha\, f_c'\, \beta k}{(1-k)} = \frac{2M_n}{(1-k)h^2 b(1+(1-\beta)k)} \qquad \textit{Equation 5-59}$$

$$\alpha = \frac{2M_n}{h^2 b(1+(1-\beta)k) f_c'\, \beta k} \qquad \textit{Equation 5-60}$$

Figure 5-63 explain the majority of the design volume fraction for proposal more than the measurement volume fraction for the database. According to the database, this model work for volume fraction ≤ 2.

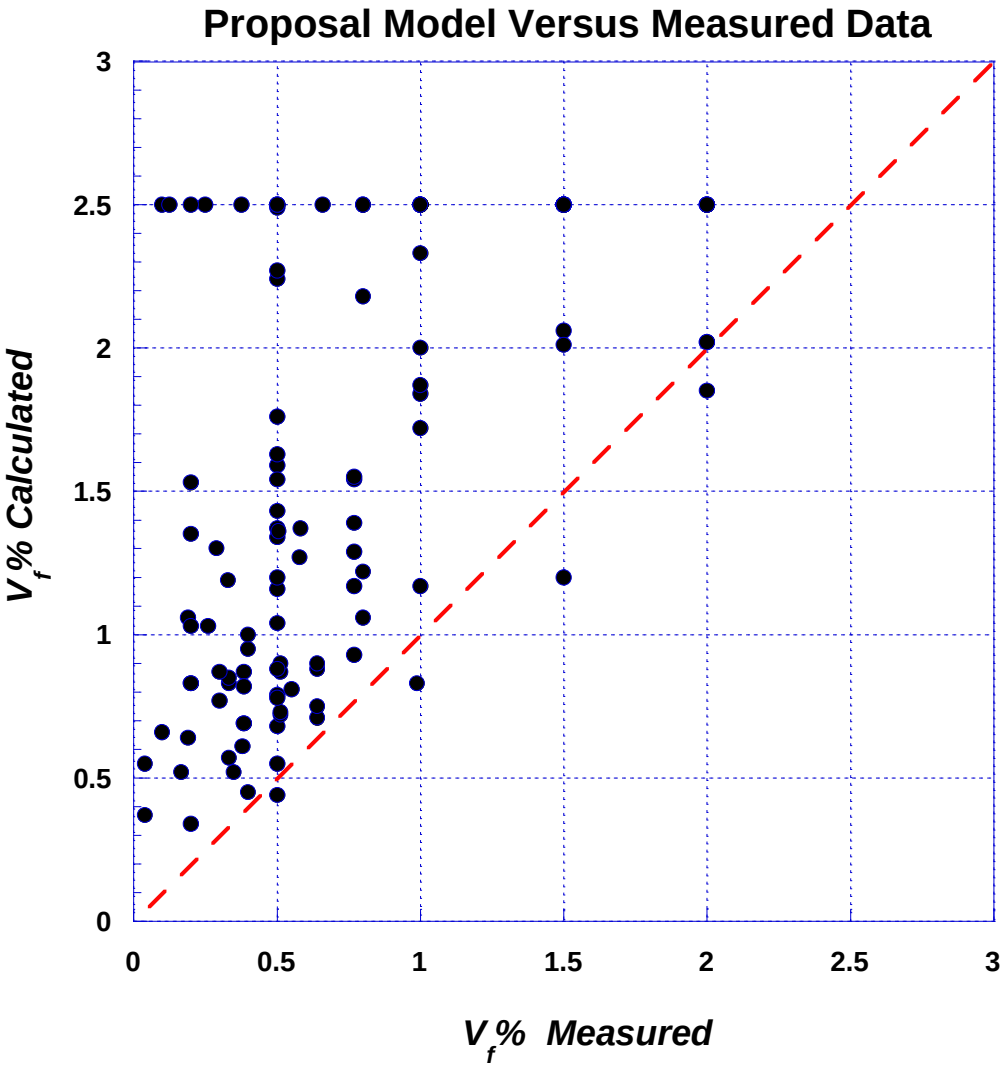

Figure 5-63: proposal volume fraction vs. the measurement volume fraction.

5.3.3 The critical volume fraction of Fiber Reinforced Concrete

To see how much the concrete needs to be reinforce, it necessary to know the external moment and the internal moment for FRC and FRCC. As explained above, the behavior of FRC and FRCC, is rare for two ways.

The first way is improving the concrete to carry more load after the first crack occurs, and that is called strain hardening. This behavior led to multi-cracks and improved the concrete to resist more external moment in addition to increasing the modulus of rupture. The second way is not carrying more load, but improving the concrete to resist more external moments and that is called strain softening. Therefore, it is necessary for the desinger to know what kind of behavior is appropriate for each design, and then can clearly the desinger estimate the volume fraction of the requirement of each behavior, as explained below.

5.3.3.1 The critical volume fraction of fiber for strain-softening (deflection-softening and hardening) response

In case of strain softening, the internal moment that is provided by FRC and FRCC to resist the external moment should be more than the first crack moment, as shown below.

$$M_n \geq M_{cr} \qquad \textit{Equation 5-61}$$

So,

$$\frac{M_n}{M_{cr}} \geq 1 \qquad \textit{Equation 5-62}$$

As explained in Chapter 4 and sections 5.3.a and 5.3.b, the first crack and internal FRC and FRCC moment are:

$$M_{cr} = \frac{f_{cr} b h^2}{12 K_{elastic}} \qquad \textit{Equation 5-63}$$

$$M_n = \frac{\alpha\, f_c^{'}\, h^2 b}{2}(0.11 - 0.01\beta)\beta \qquad \textit{Equation 5-64}$$

So,

$$K_{(Elastic)} = \frac{1}{1+\sqrt{\gamma}} \qquad \textit{Equation 5-65}$$

Therefore,

$$\frac{12\alpha\, f_c^{'}\, h^2 b(0.11 - 0.01\beta)\beta K_{elastic}}{2 f_{cr} b h^2} \geq 1$$

$$\frac{6\alpha\, f_c^{'}\,(0.11 - 0.01\beta)\beta K_{elastic}}{f_{cr}} \geq 1 \qquad \textit{Equation 5-66}$$

In section (5.2.2. a) the first crack strength is:

$$f_{cr} = 0.62\,\lambda {f_c'}^{0.5} \qquad \textit{Equation 5-67}$$

Therefore,

$$\frac{6\alpha\, f_c^{'}\,(0.11-0.01\beta)\beta}{0.62\,(1+\sqrt{\gamma})\lambda\sqrt{f_c^{'}}} \geq 1 \qquad \textit{Equation 5-68}$$

And,

$$\alpha \geq \frac{0.62\,(1+\sqrt{\gamma})\lambda}{6\,(0.11-0.01\beta)\beta\sqrt{f_c'}} \qquad \textit{Equation 5-69}$$

$$\frac{E_c\,\frac{\alpha_2\,\varepsilon_{cr}}{9}}{f_c'} \geq \frac{0.62\,(1+\sqrt{\gamma})\lambda}{6\,(0.11-0.01\beta)\beta\sqrt{f_c'}} \qquad \textit{Equation 5-70}$$

In the end, α_2 factor is:

$$\alpha_2 \geq \frac{0.93\,(1+\sqrt{\gamma})\lambda\sqrt{f_c^{'}}}{(0.11-0.01\beta)\beta E_c\varepsilon_{cr}} \qquad \textit{Equation 5-71}$$

As explained in section 5.2.2.d, Table 5-6 shows the α_2 factor with three groups of fiber.

For Synthetic Fiber:

$$V_{f(min)} \geq \frac{0.75\,(1+\sqrt{\gamma})\lambda\sqrt{f_c'}}{(0.11-0.01\beta)\beta E_c\varepsilon_{cr}l_f} \qquad \textit{Equation 5-72}$$

For PVA Fiber:

$$V_{f(min)} \geq \frac{1.1\,(1+\sqrt{\gamma})\lambda\sqrt{f_c'}}{(0.11-0.01\beta)\beta E_c\varepsilon_{cr}l_f} \qquad \textit{Equation 5-73}$$

For Steel Fiber:

$$V_{f(min)} \geq \frac{0.5\,(1+\sqrt{\gamma})\lambda\sqrt{f_c'}}{(0.11-0.01\beta)\beta E_c\varepsilon_{cr}l_f} + \frac{26}{l_f} \qquad \textit{Equation 5-74}$$

For more safety, assume $\beta = 0.65$, $\lambda$and λ_{V_f}=1; therefore the equation above can be rewritten as follows:

For Synthetic Fiber is:

$$V_{f(min)} \geq \frac{0.11(7.8 + \sqrt{f_c'})\sqrt{f_c'}}{l_f} \qquad \textit{Equation 5-75}$$

For PVA Fiber is:

$$V_{f(min)} \geq \frac{0.16(7.8 + \sqrt{f_c'})\sqrt{f_c'}}{l_f} \qquad \textit{Equation 5-76}$$

For Steel Fiber is:

$$V_{f(min)} \geq \frac{0.075\left(7.8 + \sqrt{f_c'}\right)\sqrt{f_c'} + 26}{l_f} \qquad \textit{Equation 5-77}$$

5.3.3.2 The critical volume fraction of fiber for Strain-hardening response

In the case of strain hardening for FRC and FRCC, the strength of tension is defined for stress block model as a constant value. FRC and FRCC strength in tension should be more than the first crack strength, as shown below.

$$\frac{f_t}{f_{cr}} \geq 1 \qquad \textit{Equation 5-78}$$

In section 5.2.2..a, the first crack strength is:

$$f_{cr} = 0.62\,\lambda {f_c'}^{0.5} \qquad \textit{Equation 5-79}$$

In section 5.3.b, the FRC and FRCC strength in tension is:

$$f_t = \frac{\alpha\, f_c'\, \beta k}{(1-k)} \qquad \textit{Equation 5-80}$$

Therefore,

$$\frac{\dfrac{\alpha\, f_c^{'}\, \beta k}{(1-k)}}{0.62\,\lambda\sqrt{f_c^{'}}} \geq 1 \qquad \textit{Equation 5-81}$$

So, the α factor is:

$$\alpha \geq \frac{5.58\lambda}{\beta\,\sqrt{f_c'}} \qquad \textit{Equation 5-82}$$

$$\alpha = \frac{E_c\,\varepsilon_c}{f_c'} \leq 0.85$$

Then,

$$\frac{E_c\,\dfrac{\alpha_2\,\varepsilon_{cr}}{9}}{f_c'} \geq \frac{5.58\lambda}{\beta\,\sqrt{f_c'}} \qquad \textit{Equation 5-83}$$

In the end, α_2 factor is:

$$\alpha_2 \geq \frac{50.22\sqrt{f_c^{'}}}{\beta E_c \varepsilon_{cr}} \qquad \textit{Equation 5-84}$$

$$\alpha_2 \geq \frac{1.34\lambda f_c^{'}}{\beta\lambda_f}$$

As explained in section 5.2.2.d, Table 5-6 shows the α_2 factor with three groups of fiber.

For Synthetic Fiber is:

$$V_{f(min)} \geq \frac{1.1 f_c'}{\beta \lambda_f l_f} \qquad \textit{Equation 5-85}$$

For PVA Fiber is:

$$V_{f(min)} \geq \frac{1.6 f_c'}{\beta \lambda_f l_f} \qquad \textit{Equation 5-86}$$

For Steel Fiber is:

$$V_{f(min)} \geq \frac{0.7 f_c'}{\beta \lambda_f l_f} + \frac{26}{l_f} \qquad \textit{Equation 5-87}$$

For more safety, assume $\lambda = 1$ and $\beta = 0.65$; therefore the equation above can be rewritten as follows;

For Synthetic Fiber is:

$$V_{f(min)} \geq \frac{1.64 f_c'}{l_f} \qquad \textit{Equation 5-88}$$

For PVA Fiber is:

$$V_{f(min)} \geq \frac{2.4 f_c'}{l_f} \qquad \textit{Equation 5-89}$$

For Steel Fiber is:

$$V_{f(min)} \geq \frac{1.11 f_c' + 26}{l_f} \qquad \textit{Equation 5-90}$$

5.3.4 Summary of Analysis of New Model of FRC and FRCC for ultimate stage

1- The results of compression stress block explains that the FRC and FRCC in compression zone is represented by a rectangular stress block due to an underestimation of databases and also because it is easy for designers to use. Also, the FRC and FRCC in tension is assumed to have a rectangular stress block with an average uniform stress σ_p.

2- Assumption**:** As explained in Chapters 2 and 4, ACI 544.4R, 2018 and Rilem TC 162-TDF, 2003, it has been found that the compression part depth in the beam (neutral axis) was 10% from the total depth of the beam. Therefore, the neutral axis (k) at the ultimate stage is equal to 10% from the total depth of the beam. Therefore, it a summary of the assumption of this model, follows below:

a. Elastic stage in compression therefore $\alpha = \frac{E_c\, \varepsilon_c}{f_c'}$.

b. Assume K=0.1

3- The first step is to determine the first crack strain in tension by the proposal equation below;

$$\varepsilon_{cr} = \frac{0.008}{f_c'} \geq 0.0001, \quad for\ f_c'\ in\ Mpa$$

4- Then determine the α_2 factor of ultimate strain in tension, depending on the length and volume fraction of fiber, see Table 5-6.

$$\varepsilon_t = \varepsilon_{Ult.} = \alpha_2 \varepsilon_{cr}$$

$$\varepsilon_c = \frac{\varepsilon_t}{9} = \frac{\alpha_2\, \varepsilon_{cr}}{9}$$

5- After determining ε_c, it is easy to evaluate $\alpha\ and\ \beta$ depending on the rectangular stress block parameters, see Table 5-1.

6- For a rectangular section, Table 3 shows the summary of four ranges of applied top compressive strain $\varepsilon_c < \varepsilon_{cy}$, $\varepsilon_c = \varepsilon_{cy}$, $\varepsilon_{cy} < \varepsilon_c < \varepsilon_{Ult.}$,and $\varepsilon_c = \varepsilon_{Ult.}$.

$$\varepsilon_{cy} = \frac{\alpha}{4700\, \lambda_{V_f}} \sqrt{f'_c} \ldots (\mathrm{N/mm^2})$$

$$\varepsilon_{cy} = \frac{\alpha}{57000\, \lambda_{V_f}} \sqrt{f'_c} \ldots (\mathrm{Ib/in^2})$$

7- To determine the nominal bending resistance of FRC and FRCC by

$$M_n = \frac{\alpha\, f'_c\, h^2 b}{2} (0.11 - 0.01\beta)\beta$$

8- The **analysis moment capacity** of FRC and FRCC $\emptyset M_n$ should be lower than the factored moment M_u applied to the member.

$$\boldsymbol{\emptyset M_n < M_u}$$

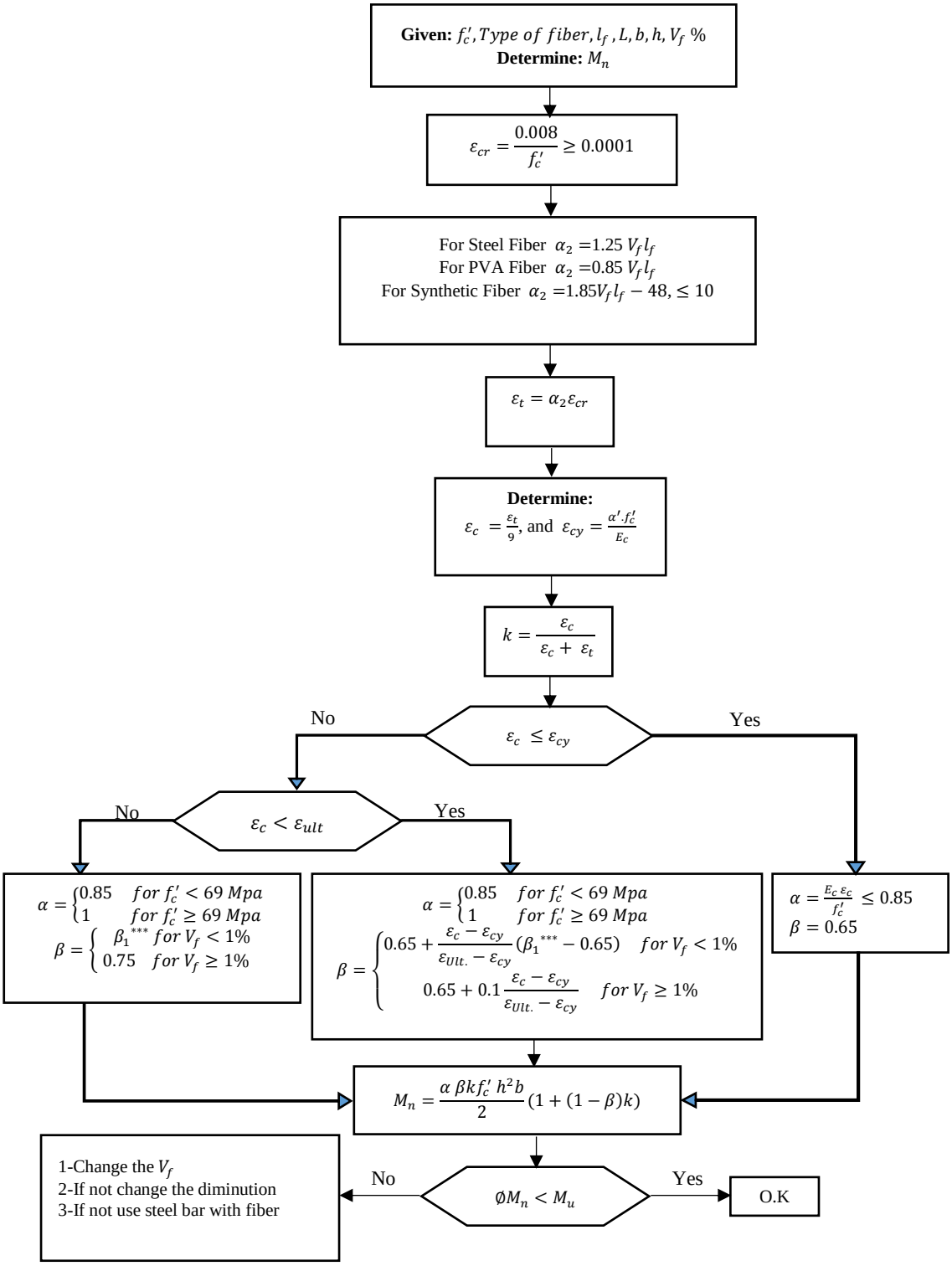

Flowchart 1: Analysis of fiber reinforced concrete and fiber reinforced cement concrete.

5.3.5 Summary of Design New Model of FRC and FRCC for ultimate stage

1. The design moment capacity of FRC and FRCC $\emptyset M_n$ should be greater than the factored moment M_u applied to the member. ACI 544.4R-18. $\emptyset M_n > M_u$.
2. As explained in Chapter4, the reduction factor $\emptyset$ depends on the type of the member and its failure mode, and should be determined based on ACI 318 or other building codes, and is typically between 0.65 and 0.9 for flexural members.
3. Determine:

    a. $f_{cr} = 0.62\ \lambda\sqrt{f_c'} \qquad (Mpa)$

$$\lambda = \begin{cases} 1.0, & for\ concrete\ without\ fiber \\ 0.75, & for\ FRC\ and\ FRCC\ with\ fiber\ length\ (l_f) < 10\ mm \\ 0.02\ l_f + 0.1\ \leq 1.3, & for\ FRC\ and\ FRCC\ with\ fiber\ length\ (l_f)\ \geq 10\ mm \end{cases}$$

    b. $\varepsilon_{cr} = \frac{0.008}{f_c'} \geq 0.0001, \quad for\ f_c'\ in\ Mpa$

    c. $E_t = 77.5\ \lambda\ {f_c'}^{1.5}, \qquad Mpa$

    d. $E_c = 4700\ \sqrt{f_c'},\ Mpa$

    e. $\gamma = \frac{E_c}{E_t}$

    f. $K_{(Elastic)} = \frac{1}{1+\sqrt{\gamma}}$

    g. $detrmine\ M_{cr}$

$$M_{cr} = \frac{f_{cr} b h^2}{12\ K_{(Elastic)}}$$

    h. If $\emptyset M_{cr} > M_u$, then O.K there is no need to adding fiber.

i. If $\emptyset M_{cr} < M_u$, then add fiber.

4. Determine the volume fraction of fiber by assuming the N.A for ultimate stage 0.1h and the compression part in elastic stage (β=0.65)

j. For steel,

$$V_f > 5.712 \frac{M_u \sqrt{f_c'}}{\emptyset\, h^2 b\, l_f}$$

k. For PVA,

$$V_f > 8.4 \frac{M_u \sqrt{f_c'}}{\emptyset\, h^2 b\, l_f} \geq \frac{31.35}{l_f}$$

l. For Synthetic,

$$V_f > \left(\frac{3.86\, M_u \sqrt{f_c'}}{\emptyset\, h^2 b\, l_f} + \frac{25.95}{l_f}\right)$$

5. Determine ultimate strain in compression.

$$\varepsilon_c = \frac{29.729 M_u}{\emptyset h^2 b E_c}$$

Check the assumption:

a) Check Strain and N.A

1- If $\varepsilon_c \leq \varepsilon_{cy}\ then\ OK$

$$\varepsilon_{cy} = \frac{\alpha'.f_c'}{E_c}$$

$$\alpha' = \begin{cases} 0.85 & for\ f_c' < 69\ Mpa\ (10000\ Psi) \\ 1 & for\ f_c' \geq 69\ Mpa\ (10000\ Psi) \end{cases}$$

Then determine

1) $\alpha = \frac{E_c\,\varepsilon_c}{f_c'} \leq 0.85$

2) $\beta = 0.65$. then determine

3) $k = \frac{\varepsilon_c}{\varepsilon_c + \varepsilon_t}$, So, $\varepsilon_t = \alpha_2 \varepsilon_{cr}$

2- If $\varepsilon_c > \varepsilon_{cy}$ *and* $\varepsilon_c < \varepsilon_{ult}$ *then*

Then determine

$$\alpha = \begin{cases} 0.85 & for\ f_c^{'} < 69\ Mpa\ (10000\ Psi) \\ 1 & for\ f_c^{'} \geq 69\ Mpa\ (10000\ Psi) \end{cases}$$

And

$$\beta = \begin{cases} 0.65 + \dfrac{\varepsilon_c - \varepsilon_{cy}}{\varepsilon_{Ult.} - \varepsilon_{cy}}(\beta_1{}^{***} - 0.65) & for\ V_f < 1\% \\ 0.65 + 0.1\dfrac{\varepsilon_c - \varepsilon_{cy}}{\varepsilon_{Ult.} - \varepsilon_{cy}} & for\ V_f \geq 1\% \end{cases}$$

So, $\varepsilon_{Ult.} = 0.0035\ and\ 0.005\ for\ V_f < 1\%\ \ and\ V_f \geq 1\%$,

respectively

β_1 *is same ACI 318 Code*

After that determine ε_c again

$$\varepsilon_c = \frac{2M_u}{\emptyset h^2 b(1 + (1-\beta)k)E_c\,\beta k}$$

Then determine $k = \frac{\varepsilon_c}{\varepsilon_c + \varepsilon_t}$

6. The critical volume fraction of fiber for strain-softening (hardening deflection) response. In the case of the strain of softening, the internal moment that is provided by FRC and FRCC to resist the external moment should be more than the first crack moment, as below.
7. For more safety, assume $\beta = 0.65$, $\lambda$and λ_{V_f}=1; therefore the equation above can be rewritten as below;
8. For Synthetic Fiber is:

$$V_{f(min)} \geq \frac{0.11(7.8 + \sqrt{f_c'})\sqrt{f_c'}}{l_f}$$

For PVA Fiber is:

$$V_{f(min)} \geq \frac{0.16(7.8 + \sqrt{f_c'})\sqrt{f_c'}}{l_f}$$

For Steel Fiber is:

$$V_{f(min)} \geq \frac{0.075\left(7.8 + \sqrt{f_c'}\right)\sqrt{f_c'} + 26}{l_f}$$

9. The critical volume fraction of fiber for Strain-hardening response. In the case of the strain hardening for FRC and FRCC, the strength of tension is defined for stress block model as a constant value. FRC and FRCC strength in tension should be more than the first crack strength, as below. For more safety assume λ =1 and $\beta = 0.65$; therefore the equation above can be rewritten as below;

For Synthetic Fiber is:

$$V_{f(min)} \geq \frac{1.64 f_c'}{l_f}$$

For PVA Fiber is:

$$V_{f(min)} \geq \frac{2.4 f_c'}{l_f}$$

For Steel Fiber is:

$$V_{f(min)} \geq \frac{1.11 f_c' + 26}{l_f}$$

b) Determine flexural stress and moment

$$f_t = \frac{\alpha\, f_c'\, \beta k}{(1-k)}$$

$$M_n = \frac{(1-k)h^2 b(1+(1-\beta)k) f_t}{2}$$

If $\emptyset M_n \geq M_u$ then Ok.

If $\emptyset M_n < M_u$ then Ok.

1- Change the V_f

2- If not change the diminution

3- If not use steel bar with fiber

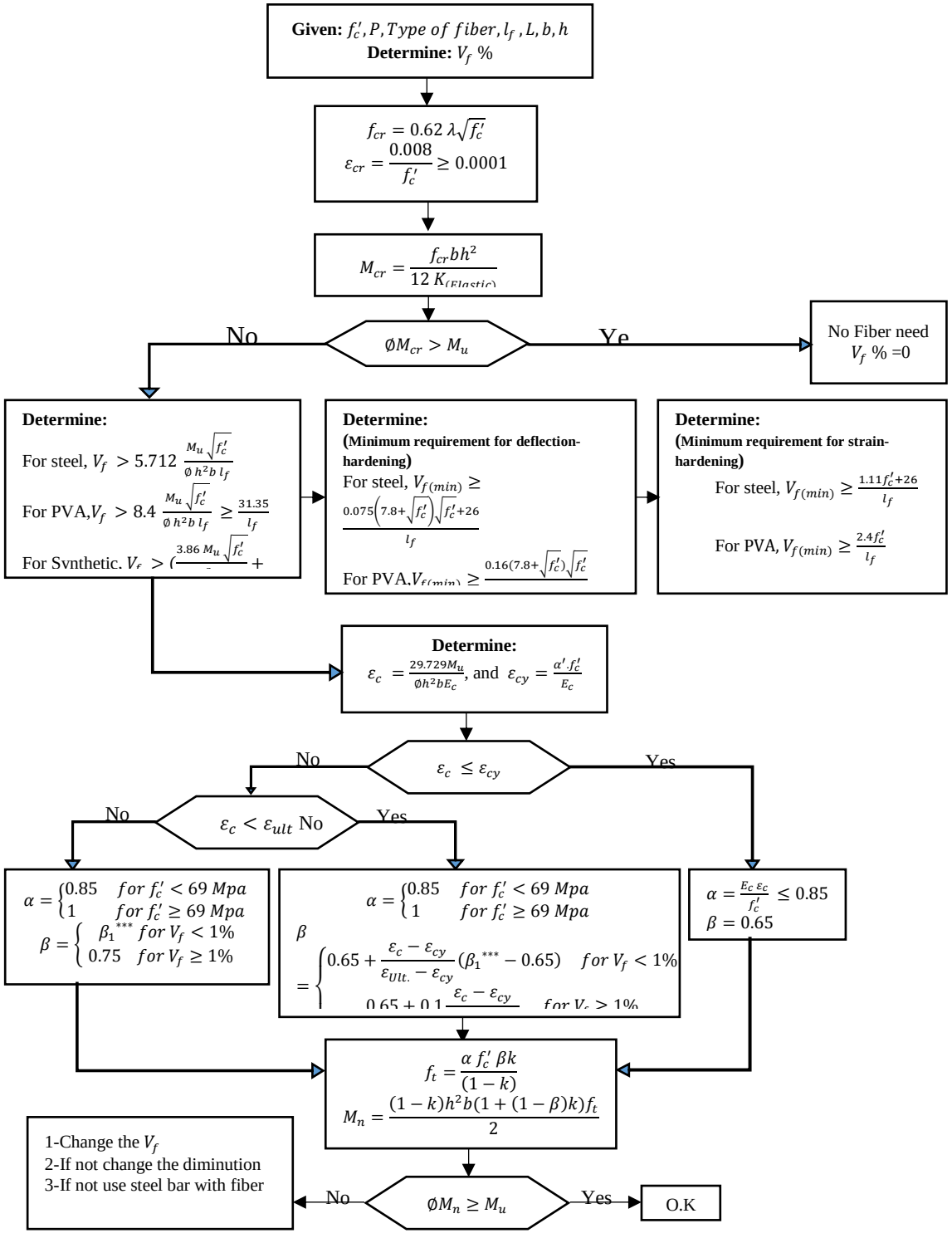

Flowchart 2: Design of fiber reinforced concrete and fiber reinforced cement concrete.

6 Chapter 6 Conclusion and Recommendation

6.1 Conclusions

As fibers improve behaviors in tension, it is necessary to include this effect in design methods or code. The aim with the work was to deepen the knowledge parameters of study for fiber reinforced concrete and, if possible, to find a method to predict the stress blocks of compression and tension in the ultimate limit state.

To accomplish this, commonly used test methods to characterize FRC and FRCC were investigated in detail, using a cylinder compression test, flexural test, and direct tensile test to assess their usefulness in verifying design assumptions.

Experimental results of this research, combined with other researches in the literature, were analytically evaluated using statistical analysis. These analyses were used to evaluate the validity of the provisions of codes and researches.

The conclusions presented in this dissertation are based on the experiments, 1,120 points of the database of other studies, and investigations carried out on the FRC and FRCC for three groups of fibers (steel, PVA, basalt and synthetic fiber with volume fraction ranging from 0 to 2%.

The following conclusions are based on the results obtained from this dissertation and database of others researches on the development of a model to predict the stress block of FRC and FRCC to evaluate the moment capacity. That was further illustrated by the classification of this thesis into four parts: stress block

in compression, stress block in tension, analysis, and design of the new model for the ultimate stage.

6.1.1 Determining for compression stress block

Based on the experiment in this dissertation and 250- stress-strain curves of the database for other studies investigations, compression stress block and its parameters was evaluated as rectangular and trapezoid stress block.

For rectangular and trapezoid stress block, the behavior and parameters value of Basalt fiber in stress-strain curves are similar to the behavior of plain concrete. K_2 is closest for the plain concrete value that decreases with an increase in concrete strength, but becomes approximately a constant for concrete strength greater than about 55.2 MPa and less than 27.6 MPa. The suggested model for Basalt FRC and FRCC is ACI 318 Codes Model, which is the best representative to determine the area under stress-strain curves for a lower bond of the database.

For other types of fibers such as PVA, steel and synthetic fibers, the area under stress-strain curves that determine stress block depend on the volume fraction of fiber. For rectangular stress blocks, the proposal model takes the lower bond of the data according to the requirement of designer for more safety.

1- A new equation for yield strain was developed by modifying the ACI 544 and Rilem equations to account for the influence of additional fibers in concrete. It was observed that the new equation depends on the compressive strength.

2- This research adopted the Suksawang 2018 equation for elastic modulus of FRC and FRCC that depend on the types of mix and volume fraction of fiber.

3- There is no significant trend of an ultimate compressive strain of FRC and FRCC as compressive strength increases. Based on the other researchers' database, a volume fraction of fiber affected the ultimate strain. The ultimate strain at the extreme concrete compression fiber is taken to be 0.0035 for volume fraction of less than 1%, and 0.005 for volume fraction more than or equal to 1%.

4- For volume fraction less than 1, it was found that in general K_1 value decreases with an increase in concrete strength, but becomes approximately a constant for concrete strength greater than about 55.2 MPa and less than 27.6 MPa. This behavior is exactly the same as plain concrete as ACI code equation, but this behavior will change after $f_c' \geq 69\ Mpa$ because the curves become more linear and steeper. The proposal model for K_1suggested using the same values of ACI-318 as lower bond for $V_f <$ 1% and for $f_c' < 69\ Mpa$, and for $f_c' \geq 69\ Mpa\ K_1\ is\ 0.65$. With a volume fraction of more than 1, K_1 the value is observed tto become approximately a constant value is 0.75.

5- The value of K_2 obtained from the database indicate that similar trend as K_1. For volume fraction less than 1, it was found that in general K_2 value

decreases with an increase in concrete strength, but becomes approximately a constant for concrete strength greater than about 55.2 MPa and less than 27.6 MPa. The proposal model for K_2suggests using the same values of ACI-318 for $V_f < 1\%$ depend on the database. For $V_f \geq 1\%$, K_2 the value may be observed to become approximately a constant value, suggested 0.375.

6- As explained in chapter 4, the proposed rectangular compressive stress block is defined by a width equal to $\alpha f c'$ and depth as $\beta . \varepsilon_u$, as done in ACI 318-14. For β parameter is:

   a. For $\varepsilon_c \leq \varepsilon_{cy}$, the shape of stress-strain curves becomes more likely to be a triangle. Therefore, the center of gravity of curves in distance 0.33 of neutral of axis then led to $\beta \cong 0.65$.

   b. Based on the database, the ultimate stage ($\varepsilon_c = \varepsilon_{Ult.}$) of β affected a volume fraction of fiber. The value of β used in the ACI 318 represents the lower bound on the test data for FRC and FRCC with compressive strength from 20 to 120 MPa. It was found that behavior of $\beta\ parameter$ decreases with an increase in concrete strength, but becomes approximately a constant for concrete strength greater than about 55.2 MPa and less than 27.6 MPa. Therefore, the β for FRC and FRCC with $V_f < 1\%$ will be the same as the ACI 318 Code value.

c. While for $\varepsilon_{cy} < \varepsilon_c < \varepsilon_{Ult.}$, an interpolation method was used to find values between a pair of β data points.

7- For $\propto$ parameter of rectangular compressive stress block is:

a. For $\varepsilon_c \leq \varepsilon_{cy}$, the $\propto$ parameter is taken depending on the Hook's Law; therefore, using the yield strain equation can determine the $\propto$.

b. Based on the database, the ultimate stage ($\varepsilon_c = \varepsilon_{Ult.}$) and ($\varepsilon_{cy} < \varepsilon_c < \varepsilon_{Ult.}$) of $\propto$ affected by a factor a volume fraction of fiber. $\propto$ of fiber reinforced concrete for ultimate design is taken to be 0.85, the same as the $\propto$ of ACI 318 for the volume fraction of less than 1%, and 1 for $f_c' \geq 69\ Mpa$, $\propto = 1$.

c. For volume fraction more than or equal 1%, the value for $\propto$ was chosen as a lower bound on the test data with a value of $\propto = 1$. It will be safer.

8- Form the results in chapter 5, the stress block of FRC and FRCC in compression are affected by the limitation of V_f=1 that is manifested by each of β, α, ε_{cy} and $\varepsilon_{Ult.}$ parameters. In addition, the high strength $f_c' \geq 69\ Mpa$ is also affected on these parameters.

For trapezoid stress block, An idealized constitutive model, a bilinear elastic-perfectly plastic stress-strain response has been assumed in compression where the linear portion of response terminates at a yield point ($\propto$fc',ε_{cy}) and remains constant at compressive yield stress until the ultimate compressive strain $\varepsilon_{Ult.}$. $\propto$ of fiber

reinforced concrete for ultimate design is taken to be 0.85 that same the $\propto$ of ACI 544 for volume fraction less than 1%, and 1 for $f_c' \geq 69\ Mpa$, $\propto = 1$.

Six stress block design codes were used to evaluate their accuracy with the 250 points of the database obtained from the previous studies. All codes depend on the rectangular stress block to design the FRC, except ACI 544, which depends on the trapezoid stress block in the design.

1- For rectangular stress block codes:

   a. In volume fraction less than 1, the six stress blocks codes are similar to the proposed model when compressive strength less than 40 MPa. Therefore, for volume fraction less than 1 and compressive strength is more than 40 MPa, there was small different between the proposal model and other codes. For other codes, the difference on the proposed model is underestimated of the lower bond of data after the compressive strength of 40 MPa. The Eurocode 2 (CEN, 2004) and CEB-FIB model code (1990) shows the evaluation for an area of data for stress block almost twice the lower bond. Therefore the other codes except for the CSA A233 (1994), it does not give an acceptable evaluation for compressive strength of more than 40 MPa due to neglecting the effect of fiber.

b. For volume fraction less than 1, the proposed model for K_2 is closest to ACI 318 and NZS 3101 models by taken viewing the lower bond of the database. While the CEB-FIB model code depends on the higher bond that causes overestimation in compressive force and underestimation in moment capacity. The Eurocode 2 model is heading to the lower bond of the database in contrast to CSA A233 that takes the average database. In volume fraction of more than 1, the difference of the six stress blocks codes on the proposal model, so they underestimated the lower bond of data.

c. As a result, the evaluation for an area of data for another stress block models more than twice underestimated of the lower bond of the database. Therefore the other codes, do not give the accurate evaluate for compressive strength due to neglecting the effect of fiber. The proposed model for K_2 is closest to ACI 318 and NZS 3101 models decrease with compressive strength until 57 MPa, then remain constant. While the CEB-FIB model code is dependent on the higher bond that causes overestimation in compressive force and underestimation in moment capacity. The Eurocode 2 model is heading to the lower bond of the database in contrast to the CSA A233 that take the average database.

2- For trapezoid stress blocks code, the ACI 544 that is depending on the trapezoid stress block in the design.

   a. For the volume fraction more than 1, has more accuracy but for safety reasons, the designer should recognize that it is overestimated because it does not take into account the lower bond of data. In volume fraction less than 1, the ACI 544 stress block code is similar to the proposed model for compressive strength less than 69 MPa, while for compressive strength more than 69 MPa, ACI 544 is underestimated to the lower bond of data. Despite that, the difference is not significant between the proposal and the ACI 544 model.

   b. For the volume fraction of less than 1, K_2 value of the ACI 544 stress block code is similar of proposal model for compressive strength less than 69 MPa, while for compressive strength more than 69 MPa, the ACI 544 is overestimated to lower bond of data. The volume fraction of more than 1, the ACI 544 shows the evaluation for an area of data for stress block more than twice the lower bond. Therefore the other codes, do not give an accurate evaluation due to neglecting the effect of fiber. For K_2 value, the ACI 544 stress block code ranks in the lower bond of

the database while proposal model is nearer the average of the database.

3- As shown in results in chapter 5, there is a small difference between the rectangular and trapezoid of the area of stress blocks.

   a. The rectangular stress block is underestimated of the database and also more comfortable for a designer to use. For volume fraction of more than 1, the rectangular and trapezoid area of stress blocks are almost matches. For K_2 value, the rectangular of stress block is in lower bond of the database while the trapezoid of the stress block model is nearer the average of the database.

   b. Therefore, it will be used in the new design and analysis proposal model.

6.1.2 Theoretical determination for tension stress block

1- More than 250 points data are used to evaluate the first crack strength. The new empirical relations developed ACI 318 equation by multiple factor λ. The average λ data for $(l_f) < 10\ mm$ is 1, while the lower bond for this data is 0.75. for $(l_f) \geq 10\ mm$. the λ data representive as a liner equation start from 0.42 at $l_f = 10\ mm$ to 1.6 at $l_f = 60\ mm$, while the lower bond of the database the decreaseses 0.3 from the value of the a liner equation of

average data. For design purpose λ will be the lower bond of data to be more satisfied.

2- According to the 150 data point, the new equation of first crack strain depends on the lower bond of data. Apparently, the new equation does not depend on the volume of fraction and types of fiber. The first crack strain decreases with increasing compressive strength.

3- As explained in chapter 4, the new equation of elastic modulus in tension can be calculated from Hooke's law of elastic modulus in tension.

4- The new equation for ultimate strain in tension depends on the types of fiber which take into consideration the volume fraction and the geometric of fiber. The tensile responses terminate at the normalized ultimate tensile strain α_2. The method adopted for evaluating this factor is a lower bond of the database.

    a. In the values of α_2 the factor of synthetic fiber is so high because of the high ultimate strain of first crack strain. That was caused by the behavior of synthetic fiber that allowed the high ultimate strain of concrete after the first crack. As explained above, this model depends on the lower bond of data.

    b. Using the same concept of synthetic fiber, the PVA has lower ultimate strain than synthetic and steel fiber regardless of has higher strength because of the PVA fiber has characteristics of micro-fiber.

c. For steel fiber, also in the equation of α_2 the factor used the lower bond of data. The results show that steel fiber has lower ultimate strain than synthetic fiber and higher than PVA fiber. α_2 the factor of the steel fiber has two behaviors depending on $V_f \; and \; l_f$. For $V_f l_f <$ 30 mm, the α_2 the factor of the steel fiber is constant value =10 mm. where $V_f l_f \geq 30 \; mm$, The α_2 the factor of the steel fiber is increases by $V_f l_f$.

6.1.3 Analysis of the New Model of FRC and FRCC for the ultimate stage

According to the results of compression, the rectangular stress block of the FRC and FRCC in compression zone is an underestimation of the database and easier designer use. Also, the FRC and FRCC in tension is assumed to have a rectangular stress block with an average uniform stress σ_p. It was assumed that the compression part depth in the beam (neutral axis) was 10% from the total depth of the beam depending on the assumption in the literature review. Therefore, the conclusions of this research can be summarized, as follows:

9- The value∅ were 0.9, 0.85, and 0.75. Where ∅ was 0.9, all data became underestimated. Where∅, it was 0.5, 0.65, and 0.7, the value of moment was so overestimated that the results were unsafe. Therefore, this model adopts the ∅ is 0.75 because of the safety although very little data has been overestimated.

10- Concerning the comparing moment of the proposal model with a moment of ACI 544 model. It has clear that the proposed model is more safety and accuracy than ACI 544 model because the ACI 544 model has overestimated the moment value by more than 3.5 Kn.m.

6.1.4 Design of New Model of FRC and FRCC for the ultimate stage

1- As explained in chapter4, the reduction factor ∅ depends on the type of the member, and its failure mode should be determined based on ACI 318 or other building codes and is typically between 0.65 and 0.9 for flexural members.

2- The majority of the design volume fraction for the proposal is more than the measurement volume fraction for the database. According to the database, this model works with a volume fraction ≤ 2.

It is necessary for the designer to know what kind of behavior is appropriate for each design. The designer can then precisly to estimate the volume fraction of the requirement of each behavior as will be explained below. The volume fraction of fiber was critical for a strain-softening (hardening deflection) response. In the case of the strain of softening, the internal moment that provided by FRC and FRCC to resistance the external moment more than the first crack moment. In addition to that, the critical volume fraction of fiber aws critical for strain-hardening response. In the case of the strain hardening for FRC and FRCC, the

strength of tension is defined for stress block model as a constant value. FRC and FRCC strength in tension is more than the first crack strength.

Table 6-1 Summary of the new proposal equations in this dissertation including compressive and tension part and design and analysis equations.

Table 6-1: the new proposal equations in this dissertation.

<table>
<tr><th>#</th><th></th><th>Equations</th></tr>
<tr><td>1</td><td>Yield strain in compression</td><td>$\varepsilon_{cy} = \frac{\alpha . f_c'}{E_c}$,
$\alpha = \begin{cases} 0.85 & for\ f_c' < 69\ Mpa\ (10000\ Psi) \\ 1 & for\ f_c' \geq 69\ Mpa\ (10000\ Psi) \end{cases}$</td></tr>
<tr><td>2</td><td>K_1 factor for stress block in compression</td><td>$K_1 = \begin{cases} 0.723 & , f_c' \leq 27.6\ Mpa \\ 0.553 & , f_c' \geq 55.2\ Mpa \\ 0.525 - 0.00362 f_c' & , 27.6 < f_c' < 55.2\ Mpa \end{cases}$, for $V_f < 1\%$
K_1= 0.75 for $V_f \geq 1\%$</td></tr>
<tr><td>3</td><td>K_2 factor for stress block in compression</td><td>$K_2 = \begin{cases} 0.425 & , f_c' \leq 27.6\ Mpa \\ 0.325 & , f_c' \geq 55.2\ Mpa \\ 0.525 - 0.00362 f_c' & , 27.6 < f_c' < 55.2\ Mpa \end{cases}$, for $V_f < 1\%$
K_1= 0.375 for $V_f \geq 1\%$</td></tr>
<tr><td>4</td><td>Ultimate strain in compression</td><td>$\varepsilon_{Ult.} = 0.0035\ \ for\ V_f < 1\%$
$\varepsilon_{Ult.} = 0.005\ for\ V_f \geq 1\%$,</td></tr>
<tr><td>5</td><td>B factor for rectangular stress block in compression</td><td>
<table>
<tr><th>Stress Block Parameter</th><th>β</th></tr>
<tr><td>$\varepsilon_c < \varepsilon_{cy}$</td><td rowspan="2">0.65</td></tr>
<tr><td>$\varepsilon_c = \varepsilon_{cy}$</td></tr>
<tr><td>$\varepsilon_{cy} < \varepsilon_c < \varepsilon_{Ult.}$</td><td>$0.65 + \frac{\varepsilon_c - \varepsilon_{cy}}{\varepsilon_{Ult.} - \varepsilon_{cy}} (\beta_1^{***} - 0.65)$ $for\ V_f < 1\%$
$0.65 + 0.1 \frac{\varepsilon_c - \varepsilon_{cy}}{\varepsilon_{Ult.} - \varepsilon_{cy}}$ $for\ V_f \geq 1\%$</td></tr>
<tr><td>$\varepsilon_c = \varepsilon_{Ult.}$**</td><td>$\beta_1^{***}$ $for\ V_f < 1\%$
0.75 $for\ V_f \geq 1\%$</td></tr>
<tr><td colspan="2">** $\varepsilon_{Ult.} = 0.0035$ and $0.005\ for\ V_f < 1\%$ and $V_f \geq 1\%$, respectively.
*** β_1 is same ACI 318 Code.</td></tr>
</table>
</td></tr>
<tr><td>6</td><td>α factor for rectangular stress block in compression</td><td>
<table>
<tr><th>Stress Block Parameter</th><th>α</th></tr>
<tr><td>$\varepsilon_c < \varepsilon_{cy}$</td><td>$\frac{E . \varepsilon_c}{f_c'} \leq 0.85$*</td></tr>
<tr><td>$\varepsilon_c = \varepsilon_{cy}$</td><td>0.85*</td></tr>
<tr><td>$\varepsilon_{cy} < \varepsilon_c < \varepsilon_{Ult.}$</td><td>0.85* $for\ V_f < 1\%$</td></tr>
<tr><td>$\varepsilon_c = \varepsilon_{Ult.}$**</td><td>1 $for\ V_f \geq 1\%$</td></tr>
<tr><td colspan="2">* $for\ f_c' \geq 69\ Mpa\ \alpha = 1$
** $\varepsilon_{Ult.} = 0.0035$ and $0.005\ for\ V_f < 1\%$ and $V_f \geq 1\%$, respectively.</td></tr>
</table>
</td></tr>
<tr><td>7</td><td>α factor for trapezoid stress block in compression</td><td>
<table>
<tr><th>Stress Block Parameter</th><th>α</th></tr>
<tr><td>$\varepsilon_c < \varepsilon_{cy}$</td><td>$\frac{E . \varepsilon_c}{f_c'} \leq 0.85$*</td></tr>
<tr><td>$\varepsilon_c = \varepsilon_{cy}$</td><td rowspan="3">0.85*</td></tr>
<tr><td>$\varepsilon_{cy} < \varepsilon_c < \varepsilon_{Ult.}$</td></tr>
<tr><td>$\varepsilon_c = \varepsilon_{Ult.}$**</td></tr>
<tr><td colspan="2">* $for\ f_c' \geq 69\ Mpa\ \alpha = 1$
** $\varepsilon_{Ult.} = 0.0035$ and $0.005\ for\ V_f < 1\%$ and $V_f \geq 1\%$, respectively.</td></tr>
</table>
</td></tr>
</table>

Table 6-1: (continued)

8	First crack strength in tension	$f_{cr} = 0.62\,\lambda {f_c'}^{0.5} \quad (Mpa)$ $\lambda = \begin{cases} 1.0, & for\ concrete\ without\ fiber \\ 1.0, & for\ FRC\ and\ FRCC\ with\ fiber\ length\ (l_f) < 10\ mm \\ 0.02\,l_f + 0.4, & for\ FRC\ and\ FRCC\ with\ fiber\ length\ (l_f) \geq 10\ mm \end{cases}$ $\lambda_{min} = \begin{cases} 1.0, & for\ concrete\ without\ fiber \\ 0.75, & for\ FRC\ and\ FRCC\ with\ fiber\ length\ (l_f) < 10\ mm \\ 0.02\,l_f + 0.1 \leq 1.3, & for\ FRC\ and\ FRCC\ with\ fiber\ length\ (l_f) \geq 10\ mm \end{cases}$
9	First crack strain in tension	$\varepsilon_{cr} = \frac{0.008}{f_c'} \geq 0.0001, \quad for\ f_c'\ in\ Mpa$
10	Elastic modulus in tension	$E_t = 77.5\,\lambda\, {f_c'}^{1.5}, \quad Mpa$
11	Neutral axis for elastic stage in tension	$N.A_{(Elastic)} = K_{(Elastic)}h$ $K_{(Elastic)} = \frac{1}{1+\sqrt{\gamma}}$ $\gamma = \frac{60.65\,\lambda_{V_f}}{\lambda\, f_c'}, \quad for\ f_c'\ in\ Mpa$
12	Ultimate strain in tension	$\varepsilon_{Ult.} = \alpha_2 \varepsilon_{cr}$ α_2: Synthetic Fiber: $1.25\,V_f l_f$; PVA Fiber: $0.85\,V_f l_f$; Steel Fiber: $1.85 V_f l_f - 48, \leq 10$
13	Moment capacity for analysis and design model	$M_n = \frac{\alpha\, f_c'\, h^2 b}{2}(0.11 - 0.01\beta)\beta$
14	Tension strength for analysis and design model	$f_t = \frac{\alpha\, f_c'\, \beta k}{(1-k)}$
15	Volume fraction equation of fiber for the design model	For steel, $V_f > 5.712\,\frac{M_u\sqrt{f_c'}}{\emptyset\, h^2 b\, l_f}$ For PVA, $V_f > 8.4\,\frac{M_u\sqrt{f_c'}}{\emptyset\, h^2 b\, l_f} \geq \frac{31.35}{l_f}$ For Synthetic, $V_f > (\frac{3.86\,M_u\sqrt{f_c'}}{\emptyset\, h^2 b\, l_f} + \frac{25.95}{l_f})$
16	Volume fraction equation of fiber for the design model **(a Minimum requirement for deflection-hardening)**	For steel, $V_{f(min)} \geq \frac{0.075\left(7.8+\sqrt{f_c'}\right)\sqrt{f_c'}+26}{l_f}$ For PVA, $V_{f(min)} \geq \frac{0.16(7.8+\sqrt{f_c'})\sqrt{f_c'}}{l_f}$ For Synthetic, $V_{f(min)} \geq \frac{0.11(7.8+\sqrt{f_c'})\sqrt{f_c'}}{l_f}$
17	Volume fraction equation of fiber for the design model **(a Minimum requirement for strain-hardening)**	For steel, $V_{f(min)} \geq \frac{1.11 f_c'+26}{l_f}$ For PVA, $V_{f(min)} \geq \frac{2.4 f_c'}{l_f}$ For Synthetic, $V_{f(min)} \geq \frac{1.64 f_c'}{l_f}$

6.2 Recommendation:

Some of the key topics which could be studied in the future are classified in two axes: database and modeling.

An investigation of the size of beams for FRC and FRC is warranted due to the difference of orientation and distribution behavior of fiber with size changing.

In order to avoid the limitation of design arising from the lack of some data in FRC and FRCC, an investigation on adding more data collection is highly recommended. An investigation on data of stress-strain in tension part, including the effect of the length, type of mix, and volume of the fraction for some types of fiber on the first crack strain, post crack stress, and ultimate strain is recommended. That is also in line with the perspective of the inclusiveness in design.

Studies on the long-term durability properties of FRC and FRCC should be carried out.

It is important to check the results obtained in experimental work and database by analytical analysis as well as in FEM analysis. It is also important to prove the validity of the assumptions of FEM analysis for proposal model and an investigation to determine the effects of various size of beams. Also, the stress-strain relationship response obtained from the FEA models can be compared with the experimental results, and thus these models can be further refined to reduce the dissimilarity, if any, between the FEA results and the experimental results.

Additional research work to study the shear behavior of FRC with the new model is necessary.

Further research is needed on the influence of elevated temperature on the analysis and design of FRC and FRCC.

7 References

1. AASHTO LRFD Bridge Design Specifications, Third Edition including 2005 and 2006 Interim Revisions, American Association of State Highway and Transportation Officials, Washington DC, 2004.

2. Abbas, Usama. "Materials development of steel-and basalt fiber-reinforced concretes." Master's thesis, Institutt for konstruksjonsteknikk, 2013.

3. Abbass, W., Khan, M. I., & Mourad, S. (2018). Evaluation of mechanical properties of steel fiber reinforced concrete with different strengths of concrete. Construction and Building Materials, 168, 556-569.

4. ACI (American Concrete Institute) (2014) ACI 318M-08: Building code requirements for reinforced concrete and commentary. ACI, Farmington Hills, MI.

5. ACI Committee 363. State-of-the-art report on high strength concrete (ACI 363R-92). Farmington Hills, MI: American Concrete Institute; 1992, 23 pp.

6. ACI Committee, American Concrete Institute, and International Organization for Standardization. "Building code requirements for structural concrete (ACI 318-14) and commentary." American Concrete Institute, 2014.

7. Ahmad, Shuaib H., Charles H. Henager Sr, M. Arockiasamy, P. N. Balaguru, Claire Ball, Hiram P. Ball Jr, Gordon B. Batson et al. "Design Considerations for Steel Fiber Reinforced Concrete." (1988).

8. Ahmed, S. F. U., & Maalej, M. (2009). Tensile strain hardening behaviour of hybrid steel-polyethylene fibre reinforced cementitious composites. Construction and Building Materials, 23(1), 96-106.

9. Altun, Fatih, Tefaruk Haktanir, and Kamura Ari. "Effects of steel fiber addition on mechanical properties of concrete and RC beams." Construction and Building Materials 21, no. 3 (2007): 654-661.

10. Altun, Fatih, Tefaruk Haktanir, and Kamuran Ari. "Experimental investigation of steel fiber reinforced concrete box beams under bending." Materials and structures 39, no. 4 (2006): 491-499.

11. American Concrete Institute, Detroit, MI, 1978, pp. 161–185.

12. American Society for Testing Materials. "Standard Test Method for Compressive Strength of Cylindrical Concrete Specimens." Philadelphia, PA, USA: American Society for Testing and Materials, 2015.

13. Antona, Bruno, and Richard Johansson. "Crack Control of Concrete Structures Subjected to Restraint Forces, Influence of Fibre Reinforcement." (2011).

14. AS3600-06, Australian Standard for Concrete Structures, Australia, 2006.

15. ASTM C 143/C 143M, Standard test method for slump of hydraulic cement concrete, in: Annual Book of ASTM Standards, vol. 04.02, American Society for Testing and Materials, Philadelphia, 2002.

16. ASTM C192/C192M. "Standard Practice for Making and Curing Concrete Test Specimens in the Laboratory." (2000).

17. ASTM C469 “Standard test method for static modulus of elasticity and Poisson’s ratio of concrete in compression” West Conshohocken: American Society for Testing and Materials (2001).

18. ASTM International. (2003). “Standard test method for density of hydraulic cement.” ASTM C 188–195, West Conshohocken, Pa.

19. Aviram, Ady, Bozidar Stojadinovic, and Gustavo J. Parra-Montesinos. "High-performance fiber-reinforced concrete bridge columns under bidirectional cyclic loading." ACI Structural Journal 111, no. 2 (2014): 303.

20. Ayub, T., Khan, S. U., & Shafiq, N. (2018). Flexural Modelling and Finite Element Analysis of FRC Beams Reinforced with PVA and Basalt Fibres and Their Validation. Advances in Civil Engineering, 2018.

21. Ayub, Tehmina, Nasir Shafiq, and Sadaqat Ullah Khan. "Compressive stress-strain behavior of HSFRC reinforced with basalt fibers." Journal of Materials in Civil Engineering 28, no. 4 (2015): 06015014.

22. Banthia, N., Trottier, J. F., Wood, D., & Beaupre, D. (1992). Influence of fiber geometry in steel fiber reinforced dry-mix shotcrete. Concrete International, 14(5), 24-28.

23. Barsby, Christopher L. "Toughness based analysis and design of fiber reinforced concrete." Master's thesis, Arizona State University, 2011.

24. Bastien-Masse, Malena, Emmanuel Denarié, and Eugen Brühwiler. "Effect of fiber orientation on the in-plane tensile response of UHPFRC reinforcement layers." Cement and Concrete Composites 67 (2016): 111-125.

25. Bei-Xing, L. I., Ming-xiang, C., Fang, C., & Lu-ping, L. (2004). The mechanical properties of polypropylene fiber reinforced concrete. Journal of Wuhan University of Technology-Mater. Sci. Ed., 19(3), 68-71.

26. Bencardino, F., L. Rizzuti, and G. Spadea. "Experimental tests v/s theoretical modeling for FRC in compression." In Proc., 6th Int. Conf. on Fracture Mechanics of Concrete and Concrete Structures—FraMCoS-6, Catania, Italy, vol. 3, pp. 1473-1480. 2007.

27. Bhargava, Pradeep, Umesh K. Sharma, and Surendra K. Kaushik. "Compressive stress-strain behavior of small-scale steel fibre reinforced high strength concrete cylinders." Journal of advanced concrete technology 4, no. 1 (2006): 109-121.

28. Caglar N., Demir A., Ozturk H., Akkaya A., "A simple formulation for effective flexural stiffness of circular reinforced concrete columns", Engineering Applications of Artificial Intelligence, 2015, 38(2015)79–87.

29. Canadian Highway Bridge Design Code, CSA S6 2001, Canadian Standards Association, Rexdale, Ontario, 2001.

30. Carnovale, D. J. (2013). Behaviour and analysis of steel and macro-synthetic fibre reinforced concrete subjected to reversed cyclic loading: a pilot investigation (Doctoral dissertation).

31. CEB/FIP Model MC90, Committee Euro International de Beton, Bulletind' Information Nos. 195 and 196, Lausanne, Mar. 1990, 348pp.

32. CEN (European Committee for Standardization) (2004) Eurocode 2: Design of concrete structures: Part 1–1: General rules and rules for buildings. CEN, Brussels.

33. Charron, J-P., F. Duchesneau, and B. Massicotte. "Static and dynamic behavior of hybrid precast bridge parapet made of ultra-high performance

fiber reinforced concrete." In High Performance Fiber Reinforced Cement Composites 6, pp. 405-412. Springer, Dordrecht, 2012.

34. Choun, Y. S., & Park, H. K. (2015). Containment performance evaluation of prestressed concrete containment vessels with fiber reinforcement. Nuclear Engineering and Technology, 47(7), 884-894.

35. Code, CEB-FIP Model. "Model code for concrete structures." Bulletin D'Information 117-E (1990).

36. Concrete," Douglas McHenry International Symposium on Concrete Structures, ACI Publication SP-55,

37. Craig, R. J. "Flexural behavior and design of reinforced fiber concrete members." Special Publication 105 (1987): 517-564.

38. CSA A23.3 1994, Canadian Standards Association, Design of Concrete Structures, Rexdale, Ontario, 1994, pp.199.

39. Dhakal, R. P., C. Wang, and J. B. Mander. "Behavior of steel fibre reinforced concrete in compression." (2005).

40. Eurocode 2 (EC2) Design of Concrete Structures, UK, 2004.

41. Ezeldin, A. Samer, and Perumalsamy N. Balaguru. "Normal-and high-strength fiber-reinforced concrete under compression." Journal of materials in civil engineering 4, no. 4 (1992): 415-429.

42. Fanella, David A., and Antoine E. Naaman. "Stress-strain properties of fiber reinforced mortar in compression." Journal of The American Concrete Institute 82, no. 4 (1985): 475-483.

43. fib (2010): Model code 2010, first complete draft, bulletin 55, vol. 1

44. fib (2010): Model code 2010, first complete draft, bulletin 56, vol. 2

45. Grzybowski, Miroslaw, and Surendra P. Shah. "Shrinkage cracking of fiber reinforced concrete." Materials Journal 87, no. 2 (1990): 138-148.

46. Han, Y. J., Oh, S. K., & Kim, B. (2017). Effect of Load Transfer Section to Toughness for Steel Fiber-Reinforced Concrete. Applied Sciences, 7(6), 549.

47. Hassoun, M. N., and Sahebjam, K., May 1985, “Plastic Hinge in Two-Span Reinforced Concrete Beams Containing Steel Fibers,” Proceedings, Canadian Society for Civil Engineering, Montreal, pp. 119-139.

48. Henager, Charles H., and Terrence J. Doherty. "Analysis of reinforced fibrous concrete beams." Journal of the Structural Division 102, no. ASCE# 11847 (1976).

49. Hillerborg, Arne. "Analysis of fracture by means of the fictitious crack model, particularly for fibre reinforced concrete." International Journal of Cement Composites 2, no. 4 (1980): 177-184.

50. Hsie, M., Tu, C., & Song, P. S. (2008). Mechanical properties of polypropylene hybrid fiber-reinforced concrete. Materials Science and Engineering: A, 494(1-2), 153-157.

51. Hsu, Lin Showmay, and ChengTzu Thomas Hsu. "Stress-strain behavior of steel-fiber high-strength concrete under compression." Structural Journal 91, no. 4 (1994): 448-457.

52. http://ourancientworld.com/Settlement.aspx?id=703

53. Islam, GM Sadiqul, and Sristi Das Gupta. "Evaluating plastic shrinkage and permeability of polypropylene fiber reinforced concrete." International Journal of Sustainable Built Environment (2016).

54. Jamsawang, P., Voottipruex, P., & Horpibulsuk, S. (2014). Flexural strength characteristics of compacted cement-polypropylene fiber sand. Journal of Materials in Civil Engineering, 27(9), 04014243.

55. Jansson, Anette. "Fibres in reinforced concrete structures-analysis, experiments, and design." (2008).

56. Jiang, Liying. "Strain-hardening behavior of fiber reinforced concrete." In Masters Abstracts International, vol. 47, no. 03. 2003.

57. joo Kim, D., Naaman, A. E., & El-Tawil, S. (2008). Comparative flexural behavior of four fiber reinforced cementitious composites. Cement and concrete Composites, 30(10), 917-928.

58. Kanda, T., & Li, V. C. (2006). Practical design criteria for saturated pseudo strain hardening behavior in ECC. Journal of advanced concrete technology, 4(1), 59-72.

59. Kanda, T., Li, V. C., & Hamada, T. (1998). Material design and development of high-ductility composite reinforced with short random polyvinyl alcohol fiber.

60. Kim, D. J., Naaman, A. E., & El-Tawil, S. (2010, May). Correlation between tensile and bending behavior of FRC composites with scale effect. In Proceedings of FraMCoS-7, 7th international conference on fracture mechanics of concrete and concrete structures. Jeju Island, South Korea.

61. Kim, D., Naaman, A. E., & El-Tawil, S. (2008). High tensile strength strain-hardening FRC composites with less than 2% fiber content. In Proceedings of second international symposium on ultra high performance concrete, Kassel, Germany (pp. 169-176).

62. Korea Concrete Institute, Concrete Design Code and Commentary, Kimoondang Publishing Company, Seoul, Republic of Korea, 2007.

63. Lee, Jae-Hoon, and Hyeok-Soo Son. "Failure and strength of high-strength concrete columns subjected to eccentric loads." ACI Structural Journal 97, no. 1 (2000): 75-85.

64. Lee, Seong-Cheol, Joung-Hwan Oh, and Jae-Yeol Cho. "Compressive behavior of fiber-reinforced concrete with end-hooked steel fibers." Materials 8, no. 4 (2015): 1442-1458.

65. Li, V. C., Mishra, D. K., & Wu, H. C. (1995). Matrix design for pseudo-strain-hardening fibre reinforced cementitious composites. Materials and Structures, 28(10), 586-595.

66. Li, Victor C. "Large volume, high-performance applications of fibers in civil engineering." Journal of Applied Polymer Science 83, no. 3 (2002): 660-686.

67. Liao, W. C., Chao, S. H., Park, S. Y., & Naaman, A. E. (2006). Self-Consolidating High Performance Fiber Reinforced Concrete (SCHPFRC)–Preliminary Investigation. Report No. UMCEE 06, 2.

68. Lim, T.-Y., Paramasivam, P., and Lee, S.-L. (1987). “Behavior of reinforced steel-fiber-concrete beams in flexure.” J. Struct. Eng., 10.1061/(ASCE) 0733-9445(1987)113:12(2439), 2439–2458.

69. Löfgren, Ingemar. Fibre-reinforced Concrete for Industrial Construction--a fracture mechanics approach to material testing and structural analysis. Chalmers University of Technology, 2005.

70. Mansur, M. A., M. S. Chin, and T. H. Wee. "Flexural behavior of high-strength concrete beams." Structural Journal 94, no. 6 (1997): 663-674.

71. MARTÍNEZ, DAVID MARTÍNEZ. "Analysis of Fibre-reinforced Concrete Elements." Moment (kN· m) 12, no. 14: 16.

72. Martínez, David Martínez. "Bending with σ-ε and σ-w approach." (2006).

73. Massicotte, Bruno, Anne Bélanger, and K. Moffatt. "Analysis and design of SFRC bridge decks." In Fifth International RILEM Symposium on Fibre-Reinforced Concrete (FRC), pp. 263-272. RILEM Publications SARL, 2000.

74. Meng, Y., Chengkui, H., & Jizhong, W. (2006). Characteristics of stress-strain curve of high strength steel fiber reinforced concrete under uniaxial tension. Journal of Wuhan University of Technology-Mater. Sci. Ed., 21(3), 132-137.

75. Mertol, Halit Cenan. "Behavior of high-strength concrete members subjected to combined flexure and axial compression loadings." (2006).

76. Mobasher, B., Bakhshi, M., & Barsby, C. (2014). Backcalculation of residual tensile strength of regular and high performance fiber reinforced concrete from flexural tests. Construction and Building Materials, 70, 243-253.

77. Moffatt, K., and B. Massicotte. "107. Design of continuous SFRC bridge decks for serviceability criteria." In 6th International RILEM Symposium on Fibre Reinforced Concretes, pp. 1173-1182. RILEM Publications SARL, 2004.

78. Naaman, A. E. "Deflection-Softening and Deflection-Hardening FRC Composites: Characterization and Modeling." Special Publication 248 (2007): 53-66.

79. Naaman, Antoine E., Duane Otter, and Husamuddin Najm. "Elastic modulus of SIFCON in tension and compression." Materials Journal 88, no. 6 (1992): 603-613.

80. Neves, Rui D., and JCO Fernandes De Almeida. "Compressive behaviour of steel fibre reinforced concrete." Structural concrete 6, no. 1 (2005): 1-8.

81. New Zealand Concrete Structures Standards (NZS 3101), New Zealand Standards, 1995.

82. Norwegian Standard, N. S. "3473." Design of Concrete Structures. Norwegian Council for Building Standardization, Oslo, Norway (1992).

83. Noushini, A., Vessalas, K., & Samali, B. (2014). Static mechanical properties of polyvinyl alcohol fibre reinforced concrete (PVA-FRC). Magazine of Concrete Research, 66(9), 465-483.

84. Oliveira Júnior, Luiz Álvaro de, Vanessa Elizabeth dos Santos Borges, Alice Ribeiro Danin, Daiane Vitória Ramos Machado, Daniel de Lima Araújo, El Debs, Mounir Khalil, and Paulo Fernando Rodrigues. "Stress-strain curves for steel fiber-reinforced concrete in compression." Matéria (Rio de Janeiro) 15, no. 2 (2010): 260-266.

85. Ou, Yu-Chen, Mu-Sen Tsai, Kuang-Yen Liu, and Kuo-Chun Chang. "Compressive behavior of steel-fiber-reinforced concrete with a high reinforcing index." Journal of Materials in Civil Engineering 24, no. 2 (2011): 207-215.

86. Paul H. Kaar, Norman W. Hanson, and H. T. Capell, "Stress-Strain Characteristics of High Strength

87. Pearlman, S. L., Apr. 1979, "Flexural Performance of Reinforced Steel Fiber Concrete Beams," MS thesis, Carnegie-Mellon University, Pittsburgh.

88. Pliya, P., Beaucour, A. L., & Noumowé, A. (2011). Contribution of cocktail of polypropylene and steel fibres in improving the behaviour of high strength concrete subjected to high temperature. Construction and Building Materials, 25(4), 1926-1934.

89. Poon, C. S., Z. H. Shui, and L. Lam. "Compressive behavior of fiber reinforced high-performance concrete subjected to elevated temperatures." Cement and Concrete Research 34, no. 12 (2004): 2215-2222.

90. Resplendino, Jacques, and François Toulemonde. Designing and Building with UHPFRC. John Wiley & Sons, 2013.

91. Roesler, J. R., Bordelon, A. C., Ioannides, A., Beyer, M., & Wang, D. (2008). Design and concrete material requirements for ultra-thin whitetopping. Illinois Center for Transportation.

92. Şahmaran, Mustafa, Erdoğan Özbay, Hasan E. Yücel, Mohamed Lachemi, and Victor C. Li. "Effect of fly ash and PVA fiber on microstructural damage and residual properties of engineered cementitious composites exposed to high temperatures." Journal of Materials in Civil Engineering 23, no. 12 (2011): 1735-1745.

93. Said, S. H., Razak, H. A., & Othman, I. (2015). Flexural behavior of engineered cementitious composite (ECC) slabs with polyvinyl alcohol fibers. Construction and building materials, 75, 176-188.

94. Sasmal, S., & Avinash, G. (2016). Investigations on mechanical performance of cementitious composites micro-engineered with poly vinyl alcohol fibers. Construction and Building Materials, 128, 136-147.

95. Shi, Caijun, and Yi-Lung Mo, eds. High-performance construction materials: science and applications. Vol. 1. World scientific, 2008.

96. Singh, Harvinder. "Flexural modeling of steel fiber-reinforced concrete members: analytical investigations." Practice Periodical on Structural Design and Construction 20, no. 4 (2014).

97. SNZ (Standards New Zealand) (2006) NZS 3101: Concrete structures standard: Part 1: The design of concrete structures. SNZ, Wellington.

98. Soranakom, Chote, and Barzin Mobasher. "Flexural Design of Fiber-Reinforced Concrete." ACI Materials Journal 106, no. 5 (2009).

99. Soutsos, M. N., Le, T. T., & Lampropoulos, A. P. (2012). Flexural performance of fibre reinforced concrete made with steel and synthetic fibres. Construction and building materials, 36, 704-710.

100. Srikar, G., G. Anand, and S. Suriya Prakash. "A study on residual compression behavior of structural fiber reinforced concrete exposed to moderate temperature using digital image correlation." international journal of concrete structures and materials 10, no. 1 (2016): 75-85.

101. Standard specification for concrete aggregates, ASTM C 33, American Society for Testing and Materials, ASTM specification, Philadelphia; 1999.

102. Swamy, R. N.; Al-Ta-an, S. A.; and Ali, Sami A. R., Aug. 1979, “Steel Fibers for Controlling Cracking and Deflection,” Concrete International: Design & Construction, V. 1, No. 8, pp. 41-49.

103. Ünal, Osman, Fuat Demir, and Tayfun Uygunoğlu. "Fuzzy logic approach to predict stress-strain curves of steel fiber-reinforced concrete in compression." Building and environment 42, no. 10 (2007): 3589-3595.

104. Van Zijl, G. P. A. G., and P. B. K. Mbewe. "Flexural modeling of steel fibre-reinforced concrete beams with and without steel bars." Engineering Structures 53 (2013): 52-62.

105. Vandewalle, Lucie, D. Nemegeer, L. Balazs, and Marco di Prisco. "Final recommendations of RILEM TC 162-TDF: test and design methods for steel fibre reinforced concrete sigma-epsilon design method." Materials and Structures 36, no. 262 (2003): 560-567.

106. Vandewalle, Lucie. "RILEM TC162-TDF: Test and Design Methods for Steel Fibre Reinforced Concrete: sigma-epsilon Design Methdos," Technical Recommendation"." Materials and Structures 33 (2000): 75-81.

107. Wang, Y., Li, V. C., & Backer, S. (1990). Experimental Determination of Tensile Behavior of Fiber. ACI Materials Journal, 87(5).

108. Whitney, Charles S. "Design of reinforced concrete members under flexure or combined flexure and direct compression." In Journal Proceedings, vol. 33, no. 3, pp. 483-498. 1937.

109. Wight, James K. and James Grierson MacGregor "Reinforced concrete Mechanics and design." SIXTH EDITION Upper Saddle River, NJ: Prentice Hall, 2009.

110. Williamson, G. R., Dec. 1973,"Compression Characteristics and Structural Beam Design Analysis of Steel Fiber Reinforced Concrete," Technical Report No. M-62, U.S. Army Construction Engineering Research Laboratory, Champaign.

111. Yang, Keun-Hyeok. "Tests on Concrete Reinforced with Hybrid or Monolithic Steel and Polyvinyl Alcohol Fibers." ACI Materials Journal 108, no. 6 (2011).

112. Yazdani, Nur, Lisa Spainhour, and Saif Haroon. Application of fiber reinforced concrete in the end zones of precast prestressed bridge girders. No. Final Report, 2002.

113. Yi, Seong-Tae, Jang-Ho Jay Kim, and Jin-Keun Kim. "Effect of specimen sizes on ACI rectangular stress block for concrete flexural members." ACI Structural Journal 99, no. 5 (2002): 701-708.

114. Yoo, Doo-Yeol, Young-Soo Yoon, and Nemkumar Banthia. "Predicting the post-cracking behavior of normal and high-strength steel-fiber-reinforced concrete beams." Construction and Building Materials 93 (2015): 477-485.